Author: Hannah Louisa Scheicher

Combination of LiDAR and Sentinel data for wall-to-wall vegetation parameter assessment in the National Park Kalkalpen

Master´s thesis

submitted in fulfillment of the requirements for the

Master of Science

in **Applied Physical Geography and Mountain Research**

at the University of Graz

Faculty of Environmental, Regional and Educational Sciences

Supervisor and Reviewer:
Manuela Hirschmugl, Ass.-Prof. Dr.rer.nat.
Department of Geography and Regional Science

2024

Acknowledgement

I would like to sincerely thank everyone who supported me during the process of writing my master thesis.

First and foremost I would like to thank Ass.-Prof. Dr.rer.nat. Manuela Hirschmugl for the professional support, the motivation, and the numerous suggestions, without which writing my thesis in this form would not have been possible.

Thanks also go to my family and my boyfriend for emotionally supporting me through my studies.

And also, many thanks to my friends proofreading my work.

You all have been so very patient.

.

Hannah Scheicher

München 07.04.2024

Abstract

Forest ecosystems play an important role in preserving biodiversity, providing ecoservices and storing carbon. Monitoring vegetation parameters such as vertical forest structure or aboveground biomass can provide important information about the forest conditions. LiDAR has been proven to be a powerful tool for estimating the canopy height and additional vegetation parameters. This thesis compares the accuracy of spaceborne Global Ecosystem Dynamics Investigation (GEDI) LiDAR data and airborne laser scanning (ALS) data when modelling wall-to-wall vegetation parameters for an area with difficult topographic terrain and a complex vegetation structure in the Austrian Alps. The chosen vegetation parameters are the mean and maximum vegetation height, the Foliage Height Diversity (FHD) and the Above ground Biomass Density (AGBD). Their datasets are combined with different combinations of Sentinel-1 VV/ VH backscatter, Sentinel-1 textural metrics, Sentinel-2 multispectral bands and Sentinel-2 derived vegetation indices. The machine learning algorithm Random Forest (RF) is utilized to model wall-to-wall regressions with a 10x10 m resolution. Two different forms of sampling are employed: cells of a fishnet grid placed over the study area and the GEDI plots. Regressions are calculated based on ALS data provided in the sampled fishnet grid cells and GEDI plots, that are then validated with the ALS data. Regressions modelled that are based on GEDI data are validated with the help of ALS data or through a cross-validation using the GEDI data. An assessment is made, which Sentinel variables contribute the most to the prediction of the different vegetation parameters. The red band as well as vegetation indices calculated with red edge bands achieve the highest feature importance when calculating the mean vegetation height and the AGBD. The green band and the first vegetation red edge band contribute the most when calculating the maximum vegetation height and the FHD. For the FHD the red band also makes a noticeable contribution. Neither Sentinel-1 backscatter, or texture variables were strongly correlated to any of the vegetation parameters. Nevertheless, the mean and standard deviation texture variables show in part a high feature importance, improving the accuracy of the regressions. Comparing the RMSE and MAE values, the accuracy of regressions trained and validated with ALS data is similar to the accuracy of regressions trained and validated with GEDI data. Though it is noticeable that the R^2 values of the regressions trained and validated with GEDI are lower compared to all other regressions. Generally, regressions based on GEDI data possess a much smaller value range compared to regressions based on ALS data. However, the models utilizing GEDI data manage to reproduce the pattern of the horizontal value distribution of all four vegetation parameters. Leading to the conclusion that GEDI is a viable option when assessing vegetation parameters for inaccessible and challenging areas.

Zusammenfassung

Waldökosysteme spielen eine zentrale Rolle für den Erhalt der biologischen Vielfalt, die Bereitstellung von Ökoystemdienstleistungen und die Speicherung von Kohlenstoff. Die Erfassung von Vegetationsparametern, wie der vertikalen Waldstruktur oder der Biomasse kann Auskunft geben über den Zustand der jeweiligen Waldfläche. LiDAR hat sich als leistungsstarkes Werkzeug zur Schätzung der Kronenhöhe und weiterer Vegetationsparameter etabliert. Diese Arbeit untersucht die Stärken und Schwächen weltraumbasierter LiDAR-Daten des Global Ecosystem Dynamics Investigation (GEDI) im Vergleich zu flugzeugbasierten Laserscanning-Daten (ALS) bei der Modellierung flächendeckender Vegetationsparameter für ein Untersuchungsgebiet mit anspruchsvoller Topographie und komplexer Vegetationsstrukur innerhalb der österreichischen Alpen. Hierfür werden die vier Parameter mittlere und maximale Vegetationshöhe, die Foliage Height Diversity (FHD) und die Abovegroung Biomass Density (AGBD) gewählt. Im Anschluss werden die Datensätze der vier Vegetationsparameter mit Sentinel-1 VV/VH Backscatter, Sentinel-1 basierten Texturmetriken, multispektralen Sentinel-2 Bändern und Sentinel-2 basierten Vegetationsindizes kombiniert. Der maschinelle Lernalgorithmus Random Forest (RF) wird verwendet, um flächendeckende Regressionen mit einer räumlichen Auflösung von 10x10 m zu modellieren. Als Sampling Formen werden sowohl die GEDI Plots, als auch die Zellen eines über dem Untersuchungsgebiet platzierten Netzgitters verwendet. Der ALS Trainingsdatensatz wird in Form von Netzgitterzellen oder GEDI Plots bereitgestellt und die daraus berechneten Regressionen wiederum mit dem ALS Datensatz validiert. Mit GEDI Daten modellierte Regressionen, werden entweder durch die ALS Daten oder mithilfe einer Kreuzvalidierung durch die GEDI Daten validiert. Bedeutsame Sentinel Variablen für die Modellierung der mittleren Vegetationshöhe und der AGBD sind hierbei das rote multispektral Band und mit „red edge“ multispektral Bändern berechnete Vegetationsindizes. Das grüne multispektral Band und das „first red edge“ multispektral Band tragen am meisten zur Berechnung der maximalen Vegetationshöhe und der FHD bei. Auch ist das rote multispektral Band bedeutsam für die Berechnung der FHD. Des Weiteren tragen die Sentinel-1 Texturmetriken merklich zur Modellierung der Parameter bei, trotzdem sie nur sehr schwach mit diesen korrelieren. Die Güte der Regressionen wird anhand des RMSE, MAE und R^2 verglichen. RMSE und MAE Werte von Regressionen, welche mit GEDI Daten trainiert und validiert werden, sind vergleichbar mit Regressionen, welche mit ALS Daten trainiert und validiert werden. Jedoch fallen die R^2-Werte der mit GEDI Daten trainierten und validierten Regressionen im Vergleich zu allen anderen Regressionen niedriger aus. Allgemein lässt sich beobachten, dass Regressionen welche auf GEDI Daten basieren über eine deutlich begrenztere Werteskala verfügen. Modellen, welche GEDI Daten verwenden, gelingt es

jedoch, das Muster der horizontalen Werteverteilung aller vier Vegetationsparameter zu reproduzieren. GEDI kann somit als angemessene Option bei der Erfassung und Modellierung von Vegetationsparametern in unzugänglichen und anspruchsvollen Gebieten gewertet werden.

Table of Contents

I. List of Figures

II. List of Tables

III. List of Equations

IV. List of Abbrevations

4 Orbits	–	RF model utilizing the variable combination of all Sentinel-2 variables and the averaged variables for all four Sentinel-1 Orbits (ASC146, ASC44, DSC22, DSC95) to calculate the regressions for the vegetation parameters
AGB	–	Aboveground Biomass
AGBD	–	Aboveground Biomass Density
All bands	–	RF model utilizing the variable combination of all Sentinel-1 and -2 variables to calculate the regressions for the vegetation parameters
ALS	–	Airborne Laser Scanning
ALS FHD	–	Foliage Height Diversity based on the airborne laser scanning data
ALS max	–	Maximum vegetation height based on the airborne laser scanning data
ALS mean	–	Mean vegetation height based on the airborne laser scanning data
ASC	–	Ascending
ATLAS	–	Advanced Topographic Laser Altimeter System
B2	–	Sentinel-2 blue band
B3	–	Sentinel-2 green band
B4	–	Sentinel-2 red band
B5	–	Sentinel-2 first vegetation red edge band
B6	–	Sentinel-2 second vegetation red edge band
B7	–	Sentinel-2 third vegetation red edge band
B8	–	Sentinel-2 NIR band
B8a	–	Sentinel-2 narrow NIR band
B11	–	Sentinel-2 SWIR-Cirrus band
B12	–	Sentinel-2 SWIR band
BCEF	–	Biomass Conversion and Expansion Factors
CCF	–	Canopy Cover Fraction
CHM	–	Canopy Height Model
DBH	–	Diameter at Breast Height
DL	–	Deep Learning
DLT	–	Dominant Leaf Type
DSC	–	Descending
DSM	–	Digital Surface Model
DTM	–	Digital Terrain Model
DVI	–	Difference Vegetation Index
EVI	–	Enhanced Vegetation Index

EVIRE1	–	Red Edge 1 Enhanced Vegetation Index
FHD	–	Foliage Height Diversity
(fishnet)	–	Models utilizing fishnet grid cells as training samples to calculate regressions
GEDI	–	Global Ecosystem Dynamics Investigation
GLAS	–	Geoscience Laser Altimeter System
GLCM	–	Gray level co-occurrence matrix
GNDVI	–	Green Normalized Difference Vegetation Index
Group A	–	Validating regression results with ALS data
Group B	–	Validating regression results with GEDI data
ICESat	–	Ice Cloud and Elevation Satellite
ISS	–	International Space Station
LAI	–	Leaf Area Index
LiDAR	–	Light Detection and Ranging
LPDAAC	–	Land Processes Distributed Active Archive Center
LTER	–	Long-Term Ecosystem Research
LVIS	–	Land Vegetation, and Ice Sensor
MAE	–	Mean Absolute Error
MSAVI	–	Modified Soil Adjusted Vegetation Index
MSAVI2	–	Modified Soil Adjusted Vegetation Index2
MSE	–	Mean Sqare Error
MSI	–	Moisture Stress Index
MSI	–	Multispectral Instrument
NC	–	RF model utilizing the variable combination comprised of the 10 variables with the best negative correlation (NC) to calculate the regressions for the vegetation parameters
NDII5	–	Normalized Difference Infrared Index – band 5
NDII7	–	Normalized Difference Infrared Index – band 7
nDSM	–	normalized Digital Surface Model
NDVI	–	Normalized Difference Vegetation Index
NDVI6	–	Normalized difference vegetation index with bands 4 and 6
NDVI7	–	Normalized difference vegetation index with bands 4 and 7
NDVI8a	–	Normalized difference vegetation index with bands 4 and 8a
NDWI	–	Normalized Difference Water Index
NIR	–	Near Infrared Radiation
NLVI	–	Non-linear vegetation index with bands 4 and 5

ORNL DAAC	–	Oak Ridge National Laboratory Distributed Active Archive Center
PAI	–	Plant Area Index
PAVD	–	Plant Area Volume Density
PC	–	RF model utilizing the variable combination comprised of the 10 variables with the best positive correlation (PC) to calculate the regressions for the vegetation parameters
(plots)	–	Models utilizing all GEDI plots as training samples to calculate regressions
PSRI	–	Plant Senescence Reflectance Index
R	–	Bravais-Pearson correlation coefficient
R^2	–	coefficient of determination (or multiple correlation coefficient)
Radar	–	Radio detecting and ranging
RF	–	Random Forest
RH	–	Relative Height
RH100	–	Relative Height at which 100% of the energy is returned
RH50	–	Relative Height at which 50% of the energy is returned
RMSE	–	Root Mean Square Error
RVI	–	Ratio vegetation index
S1	–	Sentinel-1
S2	–	Sentinel-2
S2REP	–	Sentinel-2 red edge position index
SAR	–	Synthetic Aperture Radar
SAVI	–	Soil Adjusted Vegetation Index
SDGs	–	Sustainable Development Goals
SWIR	–	short wave infra-red
TCB	–	Tasseled cap brightness
TCD	–	Tree Cover Density
TCW	–	Tasseled cap wetness
Top 10	–	RF model utilizing the variable combination comprised of the 10 variables with the best R^2 results to calculate the regressions for the vegetation parameters
VH	–	vertical-horizontal polarisation
VH/VV146	–	Sentinel-1 ascending orbit 146 with vertical-horizontal/-vertical polarisation
VH/VV22	–	Sentinel-1 descending orbit 22 with vertical-horizontal/-vertical polarisation
VH/VV44	–	Sentinel-1 ascending orbit 44 with vertical-horizontal/-vertical polarisation

VH/VV95	–	Sentinel-1 descending orbit 95 with vertical-horizontal/-vertical polarisation
VIs	–	Vegetation Indices
VV	–	vertical-vertical polarisation

1. Introduction

Forests can be referred to as ecosystems with global importance due to the various functions they fulfil. They are present in nearly all climate zones from tropical to boreal and montane regions and include riparian and coastal mangrove forests (Huete 2012, 513). 31% of dry land is forested, which amounts to 4.06 billion ha in total. A loss of 178 million ha of forest has been documented since 1990, with the highest annual rate of net forest loss in 2010 to 2020 happening in Africa, followed by South America (FAO 2020, XI). Forests are mentioned within the Sustainable Development Goals (SDGs) in relation to sustainable production and consumption, poverty alleviation, food security, biodiversity conservation and climate change. This is, because they significantly contribute to food security and livelihoods by providing many products and ecosystem services (FAO 2020, 13). The range of products from forests encompass timber, food, fodder, medicinal products, and fuelwood (FAO 2020, 109). It is estimated that most rural households in developing countries, and a large percentage of urban households, rely on forest products to meet some part of their food, nutritional, health and livelihood needs (Arnold et al. 2011, 259). Of the 115 leading food crops globally – representing 35% of global food production in total – ca. 75% benefit from pollination by animals, of which many inhabit woodlands (FAO 2022, 29). More than half of the world´s terrestrial taxa can be found within forests. Furthermore, forest habitats have the highest species diversity for many taxonomic groups including birds, invertebrates, and microbes (Lindenmayer et al. 2006, 434). Besides being a cradle for biological diversity, forests also fulfil a broad spectrum of other ecosystem functions, such as the supply of clean water and the protection of watersheds. Most of the world´s drinking water comes from catchments that are or would naturally be forested. There appears to be a clear link between forests and the quality of water coming out of a catchment. One reason for this is that most of the alternative land uses, such as agriculture, industry, and settlement, are very likely to increase the amounts of pollutants introduced into the water system. Another reason is the fact that forests contribute to the regulation of soil erosion and therefore decrease the sediment load. It appears that the undisturbed forest with its understory, leaf litter and organically enriched soil is the best land cover for minimizing erosion by water (Dudley & Stolton 2003, 11ff.). Furthermore, forests play an important part within the carbon cycle, emitting as well as storing CO_2. It is estimated that global forests were an average net carbon sink of -7.6 (+/-49) $GtCO_2e/yr$ over the years 2001 to 2019. This reflects a balance between the gross carbon removals of -15.6 (+/- 49) $GtCO_2$ e/yr and gross emissions from deforestation and other disturbances of 8.1 (+/- 2.5) $GtCO_2$ e/yr (Harris et al. 2021, 234). Even though 89 % of the global anthropogenic carbon emissions for the period 2012 to 2021 were caused by using fossil fuels, 11 % were still a result of land use, land-use change and

forestry. Hereby one of the main components was deforestation (Friedlingstein et al. 2022, 4829f.).

Regarding the fact, that forests can vary considerably in their characteristics, such as species composition, structure, and the extent of modification by humans and by non-human factors, simply estimating the forest area is an insufficient parameter. On its own, it will not be enough for identifying important trends and assessing progress towards a more sustainable forest management (FAO 2020, 27). Therefore, additional variables or parameters need to be monitored alongside the forest area. Traditional parameters for foresters to assess the current or prospective commercial value of forest stands and to plan thinning and cutting are the tree height, diameter at breast height (DBH) and the basal area. Complementary parameters are tree density and age. These parameters open up the possibility to build allometric relationships in order to estimate aboveground biomass (AGB) (Morin et al. 2019, 2). Other parameters of interest to management are for example biodiversity indicators, net and gross primary production (NPP/GPP) and the leaf area index (LAI) (Van Leeuwen & Nieuwenhuis 2010, 749). Tree height in particular is a very important structural measurement, since it is linked to other parameters like DBH, timber volume and biomass. Most of these variables can be measured on the ground by carrying out field inventories and observations. In many countries forest inventories are conducted on a national scale, to produce normalized and actualized data on a regular basis. The most representative forest inventory in Austria is carried out by the Federal Research Center for Forests (Bundesforschungszentrum für Wald – BFW) since 1961 on permanent test plots in periodic intervals of several years. In total the sample network is comprised of ~11000 sample areas (BFW 2022) each one 300 m^2 in size. Every year a sixth of all the sampling plots are reviewed (Hauk et al. 2016, 11). The resulting statistics provide useful information such as changes in the national forest estate and the main tree species distribution. However, this approach is not designed for mapping and carrying out precise estimates at a local scale. Furthermore, in-situ measurements are slow, costly and can only be done for small areas or on samples. To overcome the limitations and related uncertainties of these surveys, one area of improvement would be the additional use of airborne/spaceborne remote sensing instruments with the aim to generate better data (Morin et al. 2019, 2) and wall-to-wall information. It enables a rapid and cost-effective monitoring and change detection of large forest areas. This is highly relevant, since forest managers often lack accurate and up-to-date data (Atzberger et al. 2020, 109). Remote sensing in forest resource assessment provides three levels of information. First, the extent of the forest cover to assess its spatial and temporal dynamics. Second, the forest type (tree species) and on the third level remote sensing provides information about the biophysical and biochemical properties of the forest (Boyd & Danson 2005, 1). In this respect, it presents the chance to monitor plant phenology,

logging, pest and diseases, wildfires, storm damages, droughts, and water content through change detection (Atzberger et al. 2020, 22).

In general, there are two types of remote sensing techniques: passive and active. Passive sensing refers to sensors that detect or measure the reflected or emitted electromagnetic radiation from natural sources, an example is Sentinel-2. Active sensing comprises sensors that detect reflected responses from objected irradiated from artificially generated energy sources, such as photons in light detection and ranging (LiDAR) and microwave energy in radio detecting and ranging (Radar) sensors (Shugart et al. 2010, 21). A typical example for spaceborne LiDAR is the Global Ecosystem Dynamics Investigation (GEDI) sensor and for Radar is Sentinel-1.

Passive sensors are less sensitive to the vegetation structure, but more to the optical properties (in visible and infrared wavelengths) and moisture (in thermal and microwave wavelength) (Shugart et al. 2010, 21). One of the most widely used satellite products to characterize forests based on optical properties are spectral vegetation indices (VIs), in part to their simplicity and transparency. They provide the possibility to monitor forest states and canopy processes. Usually, they have the scientific requirement of contrasting an absorbing leaf spectral feature with a non-absorbing one. Primarily for the blue (470 nm) and red (670 nm) wavelengths of green leaves possess a very high absorption, whereas nearly all the Near Infrared Radiation (NIR) is reflected and transmitted in a manner dependent on leaf type, morphology, and cellular structure. Therefore, most VIs will combine a chlorophyll-absorbing spectral band in the red with a non-absorbing band in the NIR to depict canopy greenness or area-average canopy photosynthetic activity (Huete et al. 2014, 1ff.).

Active sensors measure reflection in one direction by penetrating the vegetation canopies, and hence are more sensitive to the arrangement of objects (structure) on their propagation pathway (Shugart et al. 2010, 21). LiDAR is a technique that utilizes lasers, usually in the NIR wavelengths, to actively transmit energy from a satellite or aircraft and then record the energy reflected back to the instrument at those same wavelengths (Goetz & Dubayah 2011, 231). The travel time of the pulse, from initiation until it returns to the sensor, provides a distance or range from the instrument to the object (Dubayah & Drake 2000, 44). This technology provides horizontal and vertical information at high spatial resolutions and vertical accuracies. Therefore, LiDAR data can deliver direct information about forest attributes such as the canopy height. This offers the opportunity to model the AGB and the canopy volume. Access to the vertical nature of forest ecosystems also offers new opportunities for enhanced forest monitoring, management, and planning (Lim et a. 2003, 88). Still there are several limitations when working with LiDAR data. Airborne LiDAR has very high operating costs. Due to the limited flying height, covering large areas is time-consuming and expensive. While spaceborne

LiDAR is less cost intensive and covers larger areas, it often does not provide wall-to-wall information.

The fusion of LiDAR data with multispectral data, vegetation spectral indices and Radar data has the potential to provide cost effective wall-to-wall information about vegetation height and structure. Furthermore, it can improve species-specific estimates of standing wood biomass, carbon stock assessments of tree stands and carbon accumulation through forest regrowth (Huete 2012, 5).

2. Research Questions

This thesis was conducted as part of the project GEDI-Sens a cooperation between the University of Graz and the institute Joanneum Research Graz. The thesis focusses on the assessment of wall-to-wall vegetation parameters by combining airborne and spaceborne LiDAR with Sentinel-1 (S1) and Sentinel-2 (S2) data, to answer the following research questions:

(1) Which S1 and S2 variables are best suited to estimate the vegetation parameters aboveground biomass density (AGBD), mean and maximum vegetation height and foliage height diversity (FHD) in combination with LiDAR data in an alpine forest?

(2) When utilizing LiDAR data in combination with S1 and S2 data for the assessment of wall-to-wall vegetation parameters, what qualitative differences can be detected between spaceborne and airborne LiDAR data?

3. State of the Art

3.1. LiDAR Data for Forest Parameter Estimation

LiDAR data can be used to derive digital elevation models, but it can also be used for the extraction of descriptive variables, related to urban or environmental mapping and forest management (García-Gutiérrez et al. 2015, 24).

LiDAR systems for forestry applications can be defined based on three characteristics:

(1) What they record: the range to the first or last return or fully digitize the return signal (full waveform).
(2) Size of the footprint: small (a few centimeters) or large (tens of meters).
(3) Sampling rate / scanning pattern.

Most commercial LiDAR systems are low-flying, small-footprint (5 to 30 centimeters in diameter) systems with high pulse rates (1 to 10 kHz) that record the range to the highest reflecting surface within the footprint. These systems do not create a full image, instead using many laser returns in close proximity to recreate a surface (Dubayah & Drake 2000, 44). Such small-footprint airborne LiDAR, sometimes referred to as airborne laser scanning (ALS) (see Figure 1), provide the best measurement accuracy of terrain elevation and vegetation heights, even on sloped terrain or for dense forests (Popescu et al. 2011, 2786). However, they also face some disadvantages concerning the mapping of forest structures. Due to their small beam, extensive flying is required to map large areas. Another problem for the small-footprint LiDAR is the frequent oversampling of tree crown shoulders and missing of treetops. Unless many shots are taken, the true canopy topography must be reconstructed statistically. Further, it is difficult to determine whether a shot has penetrated the canopy all the way to the ground, with a system that only records first or last returns, although there are also ALS systems that record the full waveform. As the canopy height is measured relative to the ground, accurate height determination is difficult, if the ground cannot be reconstructed or is erroneous (Dubayah & Drake 2000, 43).

In contrast, large-footprint systems have several advantages that help to avoid those problems. By enlarging the footprint to at least the average crown diameter of 10- to 25-meter, laser energy consistently reaches the ground even in dense forests. It eliminates the bias of small-footprint sensors that may miss the tops of trees. Furthermore, by covering a larger area, it reduces the costs of mapping large forest areas. Finally, large-footprint LiDAR systems digitize the entire return signal, thus providing a vertical distribution of intercepted surfaces (waveform) from the canopy to the ground (Dubayah & Drake 2000, 44). A downside is that the spatial resolution is a lot lower compared to the airborne LiDAR data. Also, large-footprint systems

such as GEDI often only take punctual recordings, not delivering wall-to-wall data (see Figure 1).

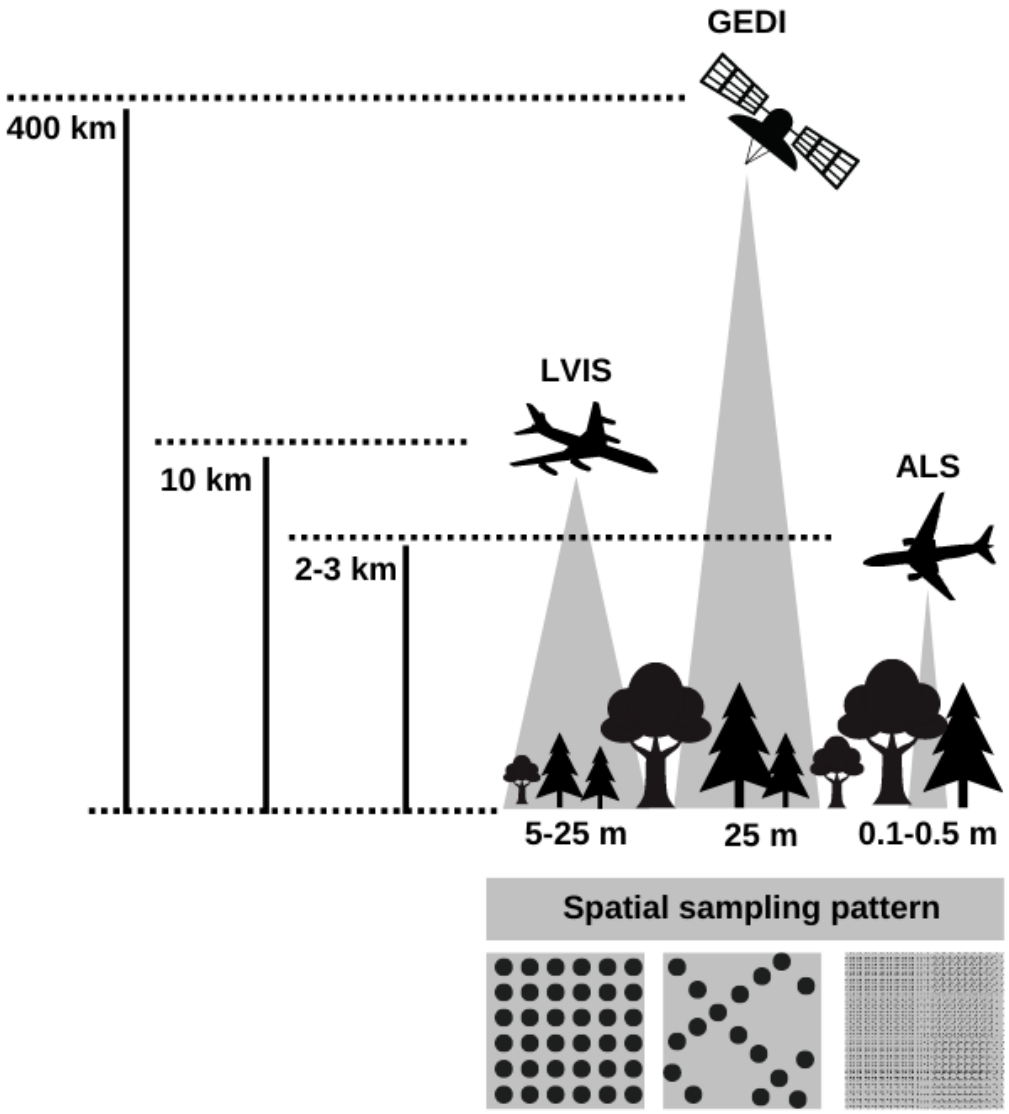

Figure 1: Field and LiDAR data of different scales and sampling patterns (after GEDI 2022a).

Small-footprint LiDAR sensors are mostly flown on airborne platforms, drones or operated on the ground. Large-footprint full-waveform LiDAR sensors are found mainly on spaceborne platforms, but can also be installed on airborne platforms, such as NASA's Land Vegetation, and Ice Sensor (LVIS) (Silva et al. 2018, 1) (see Figure 1). Operating since 2017, LVIS produces topographic maps and vertical height and structure measurements for vegetation and ice conditions (NASA 2021). The first spaceborne LiDAR instrument for continuous global observations of the earth was the Geoscience Laser Altimeter System (GLAS) sensor, launched aboard the Ice Cloud and Elevation Satellite (ICESat) spacecraft in 2003. The main task was the measurement of ice-sheet topography, but also cloud and atmospheric

properties, and the height and thickness of radiatively important cloud layers (NASA 2003). Following missions were the Cloud-Aerosol LiDAR and Infrared Pathfinder Satellite Observation (CALIPSO) in 2006, the Cloud-Aerosol Transport System (CATS-ISS) in 2015 and the Atmospheric Dynamics Mission (ADM-Aeolus) in 2018. These satellites were primarily designed for atmospheric measurements. The ICESat-2 satellite was launched in 2018 carrying the Advanced Topographic Laser Altimeter System (ATLAS) and the Global Positioning System Payload (GPSP) sensors. The ATLAS sensor is used to measure ice-surface heights but can also be applied for the detection of ground under dense canopy, the estimation of wall-to-wall AGB maps and generating vegetation cover and biomass in a dry land ecosystem (Fouladinejad et al. 2019, 408ff.).

Even though the ATLAS sensor's measurements allow vegetation analysis, the GEDI (see Figure 1) laser is the first spaceborne LiDAR instrument with the dedicated purpose of collecting information on the Earth's forests. The mission's goal is to characterize ecosystem structure and dynamics to enable improved quantification and understanding of the Earth's carbon cycle and biodiversity. Their LiDAR system has been installed on board the International Space Station (ISS) in December 2018 and started collecting scientific data in operational mode on March 25th, 2019 (GEDI 2022b) between 51.6°N and 51.6°S. The instrument, is a geodetic-class LiDAR system comprised of three neodymium-doped yttrium aluminum garnet (Nd:YAG) lasers that emit light at the wavelength 1064 nm. Two of the lasers run at full power, and one is split into two beams, producing a total of four beams. Beam Dithering Units (BDUs) rapidly change the deflection of the outgoing laser beams by 1.5 mrad, shifting them by 600 m on the ground. This results in eight ground tracks, four full power and four coverage laser tracks (see Figure 2). Each pulse send out by the lasers has the power of 10 mJ and a duration of 14 ns. Meaning that each laser fires 242 times per second, illuminating a spot, also called a footprint, on the earth's surface over which the 3D structure is measured. These footprints have an average diameter of 25 m and are separated by 60 m along the laser tracks (GEDI 2022c). LVIS data in combination with insitu biomass calculations and plot field inventory datasets were used for the calibration and validation of the GEDI LiDAR waveform simulator and data product algorithms, such as the biomass calculation (GEDI 2022d).

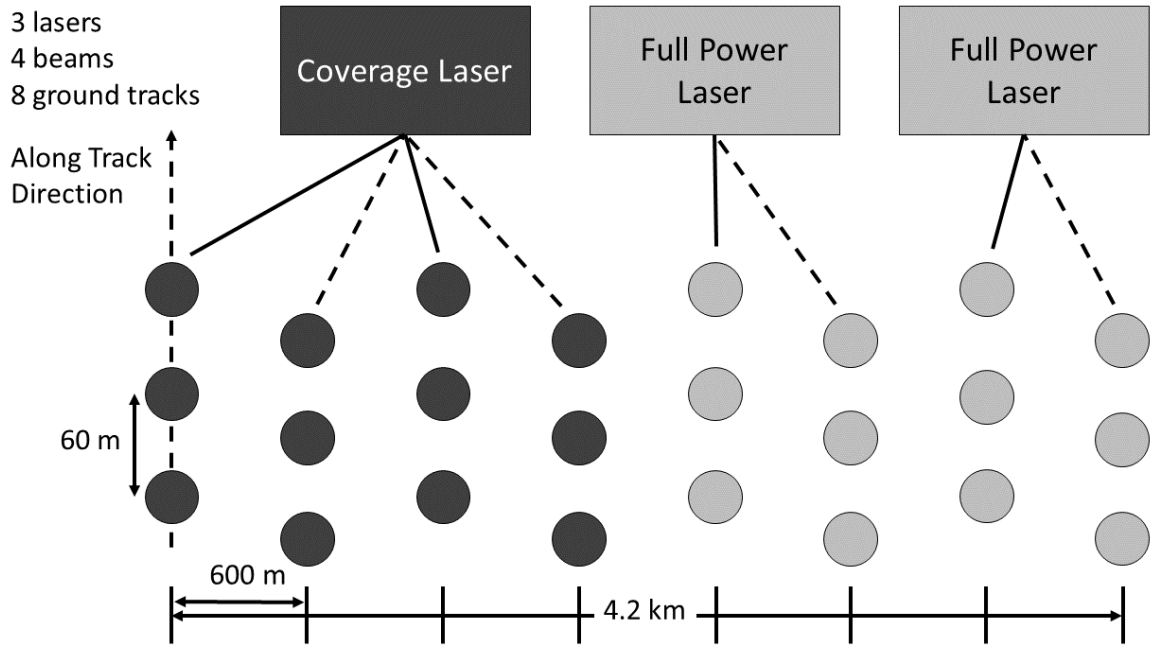

Figure 2: GEDI's ground sampling pattern (after GEDI 2022c)

3.2. Combining LiDAR Data with Multispectral and Radar Imagery

LiDAR can provide almost direct measurements of the tree height and the vertical forest structure (Lewis & Hancock 2007, 36). A limitation is often the availability of the data. The recording of airborne LiDAR is expensive and time consuming, therefore mostly done for small local areas. Also, due to this there are often large time gaps of several years between different recordings of the same area. Spaceborne LiDAR such as GEDI or ICESat-2 makes it possible to record information on a global level for shorter time intervals. But they do not provide wall-to-wall data (see chapter 3.1.). The combination of LiDAR with multispectral or radar imagery such as Sentinel or Landsat offers the possibility to translate punctual LiDAR recordings into wall-to-wall data.

The application of LiDAR data together with other satellite imagery to achieve a more complete picture on vegetation parameters has been around for a long time. Leckie (1990, 477) already suggested the fusion of airborne laser data with multispectral sensors in 1990. Hudak et al. published a study in 2002 describing how they estimated canopy height at locations unsampled by LiDAR, through the statistical and geostatistical relationships between airborne LiDAR data (Aeroscan) and Landsat Enhanced Thematic Mapper (ETM+).

As already mentioned, there are different sources providing LiDAR data. Pascual et al. (2010) tried to extrapolate airborne LiDAR height measurements across a broader landscape by combining them with Landsat 8 data. While Li et al. (2020) mapped the spatial pattern of the forest canopy height in a mountainous region utilizing ICESat-2 data in combination with S1,

S2 and Landsat 8 data. Verhelst et al. (2021) combined the GEDI Forest Height data and Sentinel-1 C-band GRD data acquired in both vertical-vertical (VV) and vertical-horizontal (VH) polarisation to create a remote sensing-based Forest/Non-Forest (FNF) mask. Even very accurate height differentiations based on GEDI data are possible, as demonstrated in the study of Di Tommaso et al. (2021). Hereby tall and short crops were meant to be mapped by combining GEDI L2A Elevation and Height Metrics data and S2 Level-2A data. The results show that GEDI data can distinguish tall crops (maize) from small crops with accuracies higher than 84%. Also, the random forest (RF) models trained on GEDI features (accuracy 82%) can be transferred much better than RF models trained on optical features (accuracy 64%) across regions spanning multiple continents. Furthermore, the study proofed, that GEDI data can generate training labels, that then enable wall-to-wall crop type mapping with optical imagery in the absence of other ground labels. But LiDAR not only provides information about the tree heights and therefore the canopy structure. A single equation for example can be used to relate the canopy structure to the above-ground biomass (Lefsky et al. 2002, 398). Zald et al. (2016) conducted a study predicting the forest structure and the AGB based on airborne LiDAR plots combined with Tasseled Cap indices and multi-temporal change metrics derived from Landsat TM/ETM based image composites. Vegetation parameters that were measured from LiDAR and used for the predictions were; the mean vegetation height (m), the standard deviation of vegetation height (m), the coefficient of variation of vegetation height (m), the 95th percentile of vegetation height (m), the percentage of first returns above 2m (%), the percentage of first returns above mean vegetation height (%), Lorey's tree height (m), basal area (m^2/ha), gross stem volume (m^3/ha) and the total aboveground biomass (kg/ha). Nandy et al. (2021) conducted a study aiming to map the forest canopy height by integrating ICESat-2 and Sentinel-1 data. Based on their results they investigate the effect of integrating forest canopy height information with Sentinel-2 Level 2A data-derived spectral variables on the prediction of spatial distribution of forest AGB.

A variation of variables can be used to predict the vegetation parameters. Li et al. (2020), as well as Nandy et al. (2021) and Vehelst et al. (2021) utilized the S1 backscattering coefficients for the VV and VH polarisation. Furthermore, texture features calculated from S1 imagery, such as mean, variance, homogeneity, contrast, dissimilarity, entropy, second moment and correlation can be employed (Nandy et al. 2021, Vehelst et al. 2021). One way to compute them is utilizing a gray level co-occurrence matrix (GLCM). The GLCM is one of the earliest techniques used for texture feature extraction and was proposed back in 1973 by Haralick et al. It is a square matrix *G* of order *N*, where the $(i, j)^{th}$ entry of *G* represents how often a pixel value known as the reference pixel with the intensity value *I* occurs in a specific relationship to a pixel value known as the neighbor pixel with the intensity value *j*. This method can reveal certain properties about the spatial distribution of the gray-levels in the texture image (Pathak

& Barooah 2013, 4207). The GLCM, combined with the original radar image, is one of the most trustworthy methods for improving the mapping accuracy for vegetation. Gašparović and Dobrinić (2020, 16) have found, that including the GLCM texture bands in their vegetation classifications, increased the overall accuracy by 19.38% compared to the classifications only using the VV and VH polarisation band.

Other variables are spectral bands as well as VIs derived from the multispectral imagery. One VIs that is very often employed is the normalized difference vegetation index (NDVI). A variation of this, when working with S2 data, can be the vegetation red edge NDVI utilized by Nandy et al. (2021), Li et al. (2020) or Chen et al. (2021). Further spectral variables found in other studies were the EVI and MSAVI in Li et al. (2020) or the CI, DVI, GNDVI, IRECI, MSI, NSII, NDWI, PSRI, RDVI, SAVI and STVI in Nandy et al. 2021).

Furthermore, one can achieve more complete data for the predictor variables by aggregating the imagery to spatiotemporal composites. Vehelst et al. (2021) calculated the temporal metrics (mean, median, minimum, maximum, 5^{th} percentile, 95^{th} percentile) for the S1 backscatter. Potapov et al. (2021) used global Landsat data to extrapolate GEDI footprint-level forest canopy height measurements and created a 30 m spatial resolution global forest canopy height map for the year 2019. The Landsat data was aggregated into 16-day composites using the observation quality layer to prioritize clear-sky images. Each of the 16 composites contains normalized surface reflectance values for blue, green, red, NIR, SWIR, brightness temperature, and the observation quality layer. A per-pixel machine-learning algorithm (regression tree) was used to predict forest height values from spatiotemporal multispectral Landsat data. The results were later on validated with the GEDI data and available airborne LiDAR data.

Furthermore, the quality of the estimated vegetation parameter values depends on the correlation of the input variables with the desired parameter. Pascual et al. (2010) used three Landsat ETM+ scenes. For each one several spectral indices were calculated; the NDVI, the normalized difference moisture index (NDMI) and the normalized burn ratio (NBR). Pearson and Spearman correlations were then calculated between the Landsat spectral indices and the LiDAR height measurements. Resulting in correlation coefficients R ranging from 0.64 to 0.73, 0.67 to 0.75 and 0.08 to 0.76 respectively. In the study by Chen et al. (2021) the forest stand volume is estimated by integrating the canopy cover and tree height values from GEDI Level 2B together with S1 Synthetic Aperture Radar (SAR), S2 Multispectral Instrument (MSI), and Advanced Land Observing Satellite (ALOS) digital surface model (DSM) imagery into a RF model. 53 remote sensing indices for volume extraction were selected in total, with 22, 26 and 5 indicators from SAR, MSI and DSM respectively. By carrying out a Pearson correlation analysis, 45 were found out to have a significant relationship with the stand volume and were selected as predictor variables. Comprising 16 variables from SAR, 25 from MSI and 4 from

DSM. For the SAR parameters the VV backscatters had positive correlations with the measured volume, but the overall influence of backscatter on stand volume mapping was marginal. Among 10 kinds of texture features from SAR, the GLCM mean of VV and contrast of VH were most related to the stand volume. The correlation analysis demonstrated that the texture characteristics of SAR imagery were much more beneficial to the volume estimation than the original backscatter. The study also concluded that the texture features from VV were more relevant to volume than those from VH. Of the 25 MSI predictor variables, B2, B3, B4, B5, B11, B12, TCW, and TWB were negatively related to volume, while the remaining 17 variables showed a positive correlation. Reflectance and spectral indices involved in featured red edge bands of S2 demonstrated a close connection to the measured volume. Overall MSI presented more sensitive variables for volume estimation than C band SAR. The DSM-based topographic indicators all had a strong positive influence on the growth of measured volume, except the SPI. The most important variables for volume modelling were H, S2REP, B12, PVI and S. In heterogeneous temperate forests canopy cover and tree height from LiDAR, topographic indices from L band in SAR, and spectral indices of red edge band from MSI are recommended for stand volume estimation. All in all, the VV texture characteristics of SAR, reflectance and spectral indices from MSI and DSM-derived elevation were comparatively important for volume mapping.

3.3. Vegetation Parameters

3.3.1. Vegetation Height

Tree height in particular is a very important structural measurement, since it is linked to other parameters like DBH, timber volume and biomass. It is also among the top thirty variables to monitor biodiversity from space, due to its capacity to provide information about the ecosystem structure (Skidmore et al. 2021, 901). Furthermore, the forest canopy height is a meaningful measurement concerning the forest vertical structure, that can be used to model the forest biomass (Hurtt et al. 2019, 5). It can be expected that the three-dimensional arrangement of individual trees has a profound effect on the ecosystem function and the carbon, water and nutrients cycle. The structure of a forest can be thought of as consequence of the statistical distribution of the sizes of trees over an area. Tree size is typically quantified as a DBH and its canopy or stem height. While tree height is a central feature in forestry yield tables for single species and even-aged forests, the predictive power of height can become weaker in mature or old-growth forests. In many cases, dominant trees do not show any noteworthy height growth and height may even decline in senescing but still dominant canopy trees. However, diameters continue to increase, adding to the biomass of trees (Shugart et al. 2010, 1ff.). Also,

the ability of height metrics form LiDAR data to estimate herbaceous biomass is limited (Li et al. 2017, 1).

3.3.2. Aboveground Biomass

Using allometric relationships between tree height and the crown diameter the volume or AGB can be predicted (Franklin 2001, 268). The AGB stands for the total mass of foliage and woody components of a vegetation canopy above the ground level. Normally 50% of the AGB is carbon, therefore AGB is also often referred to as aboveground carbon stock. Approximately 44 % of carbon within forests is found in the living biomass, 45 % is stored in the organic matter of the soil and the remaining carbon can be found in dead wood and litter (FAO 2020, XV). Even though the carbon pools of AGB can differ tremendously from those accumulated over much longer time periods in the underlying soils, the AGB is primarily impacted by disturbances, for example deforestation. Thus, it is an important variable concerning the reduction of emissions from land conversation (Goetz & Dubaya 2011, 233). Because of this the AGB has been identified by the Global Climate Observing System (GCOS) as one of the essential climate variables (ECVs) (Morin et al. 2019, 2). The carbon stocks of intact forests are more resilient to change than those in degraded or fragmented forests (Hicks et al. 2014, v).

3.3.3. Foliage Height Diversity

One important task for forestry is the conservation of biodiversity. Notably the vegetation structure has a strong local effect on this aspect, indicating that there is a relationship between the vegetations vertical complexity and biodiversity. One general hypothesis states that greater structural complexity creates more “niches” and therefore greater species diversity (Bergen et al. 2009, 2). To explain both the density and height distribution of foliage in a vegetation profile MacArthur & MacArthur introduced the FHD statistic in 1961 with following equation.

Equation 1: Foliage Height Diversity equation (MacArthur & MacArthur 1961, 594)

$$FHD = -\Sigma_i p_i{}^{*}\, ln(p_i)$$

P_i: vertical plant area index (PAI) profile in the i^{th} layer, summed over the number of layers

(MacArthur & MacArthur 1961, 594)

It can be said that “the more equal the proportion of vegetation coverage at every height, the higher the FHD value” (Hashimoto et al. 2004, 255) or “higher FHD values [are] often associated with multiple canopy layers” (Rishmawi et al. 2021, 442).

3.4. Correlation

The correlation analysis is concerned with measuring the strength of the relationship between variables. In contrast to regression analysis, correlation analysis does not require a distinction between a dependent and an independent variable (Bahrenberg et al. 2010, 197).
The mutual dependency of the two variables is questioned, and the result should allow a statement to be made about the strength and direction of the connection. The starting point for the correlation measurement is the covariance, which is normalized to produce the Bravais-Pearson correlation coefficient. The formula is as follows:

Equation 2: Bravais-Pearson correlation coefficient equation

$$r = \frac{n(\sum xy) - (\Sigma x)(\sum y)}{\sqrt{(n\sum x^2 - (\sum x)^2)(n\Sigma y^2 - (\Sigma y)^2)}}$$

n = number of values
x = x column
y = y column

(Emerson 2015, 242)

The correlation coefficient (R) according to Bravais-Pearson has - as normalized covariance – values between -1 and +1. They can be interpreted as following:

+1	if fully positive
-1	if fully negative
0	if there is no correlation.

Values located between the two extremes -1 and +1 can be interpreted by using the guide, that Evans (1996) suggested for the absolute values of R (see Table 1).

Table 1: R value guide according to Evans (1996)

R value guide	
R value	**Interpretation**
.00 - .19	very weak
.20 - .39	weak
.40 - .59	moderate
.60 - .79	strong
.80 - 1.0	very strong

Note that R measures the strength of the linear relationship. It is a measure that indicates whether and to what extent an imaginary straight line fits a point cloud (Zwerenz 2015, 214f.). While R is a measure of the relationship between two variables, the coefficient of determination R^2 (also called the multiple correlation coefficient) tells you how much variance is "explained" by the regression (Nagelkerke 1991, 691). It is therefore a measure of the *goodness-of-fit* of the statistical model, since it provides information about how well the straight line formed by the correlation corresponds to the measurements. It is calculated simply by squaring R. The determination coefficient is therefore always positive and assumes values between 0 and 1. These values are commonly stated as percentages from 0% to 100%. A R^2 close to 1 implies an almost perfect relationship between the model and the data, whereas a R^2 close to 0 implies that just fitting the mean is equivalent to the model fitted. But there are no set criteria what universally represents a "good" R^2 value. It is only possible to assess such a statistic via comparison with another predictive model (Saunders et al. 2012, 6830).

3.5. Random Forest

Complex ecological data requires flexible and robust analytical methods, which can deal with nonlinear relationships, high-order interactions, and missing values. García-Gutiérrez et al. (2015) compared several machine learning regression techniques for LiDAR-derived estimation of forest variables. Techniques they investigated were the classic multiple linear regression (MLR) methodology, artificial neural networks, support vector machines, nearest neighbour, and RF. The study concluded that the Support Vector Regression was statistically the most precise technique. Debastiani et al. (2019) also compared several machine-learning algorithms when evaluating the potential of C-band SAR data to estimate the AGBD in a high-biomass tropical ecosystem. These included multilayer perceptron, sequential minimal optimization regressor (SMOreg), robust regression, decision stump, RF, random tree, reduced error pruning tree (REP tree), M5Prime (M5P), instance-based k-nearest neighbors (IBk), K* instance-based learner (Kstar) and locally weighted learning (LWL). The best model

performance was achieved with the Random Tree algorithm. Other studies such as Hudak et al. (2008), Eskelson et al. (2009) and Vauhkonen et al. (2010) demonstrated that the RF approach generally resulted in better predictions compared to other imputation methods, when estimating plot-level stand volume, basal area and tree height. Latifi et al. (2010) and Stojanova et al. (2010) also demonstrated how ensembles such as RF could be used for biomass estimation, surpassing the classical stepwise regression.

The RF method is an extension of the classification and regression tree (CART) methods. Trees are able to explain the variation of a single response variable by repeatedly splitting the data into more homogenous groups, using combinations of explanatory variables that may be categorical (classification) and/or numeric (regression) (Breiman 2001, 5). Decision trees are reliable, simple models, that have the advantage of being able to work with a broad range of response types, can overcome missing values in explanatory and response variables and can deal with multi-output variables. To its disadvantage even small variations in the data can result in a different tree and the model can be prone to overfitting (Pekel 2020, 1113). To avoid these effects, RF grows and combines multiple decision trees to create a forest. The procedure used to create multiple versions of a predictor and use these to generate an aggregated predictor is called “bootstrap aggregating” or bagging (see Figure 3). The bootstrap method randomly performs row sampling and feature sampling from the dataset to form sample datasets for every model. The aggregation averages over the versions when predicting a numerical outcome and does a plurality vote when predicting a class (Breiman 1996, 123).

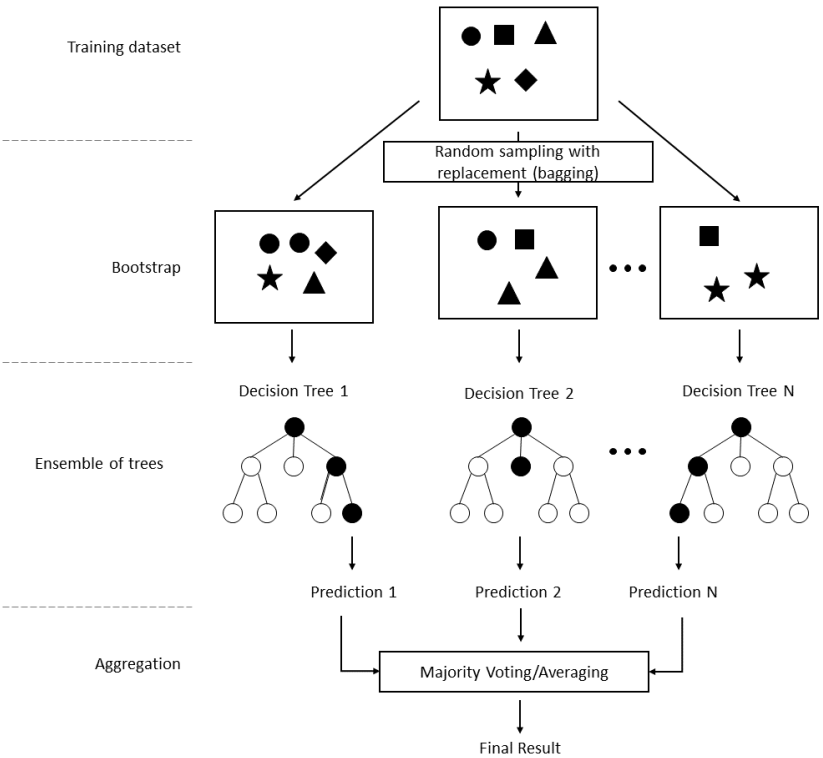

Figure 3: Random Tree Regression (according to Misra et al. (2019), Khan et al. (2021) and Galvão et al. (2020))

4. Study Area

To answer the research questions above, a part of the National Park Kalkalpen was selected as study area. The main reason for selecting this study area was to observe the quality of the assessment of vegetation parameters through the combination of LiDAR and Sentinel data in difficult mountainous terrain. The study area has a diverse and small structured topography, opening up the possibility to compare the goodness of GEDI compared to ALS in a complex terrain. It is characterized by steep slopes and a wide elevation amplitude. A height difference of 1260 m is covered, with the lowest elevation point at 524 m a.s.l. and the highest elevation point at 1784 m a.s.l., amounting to a median elevation of 1125 m a.s.l. Furthermore, an inclination of 0 to roughly 85° is covered, with the median inclination being 32° (see Figure 4). The National Park offers an extensive closed temperate montane forest area including old-growth beech forests, which are an approved UNESCO World Natural Heritage Site (see below). According to the CORINE Land Cover data from 2018 the research area consists to 19% out of broad-leaved forest, 27% are coniferous forest and mixed forest amounts to the biggest land cover class with 38%. The rest is covered with natural grasslands, moors and heathland (“alpine woodland”), transitional woodland-shrub and sparsely vegetated areas (see Figure 5). The available high resolution wall-to-wall ALS data from the year 2018 covers the center of the National Park and its extent determines the study area, which ultimately covers ~ 56 km^2. The area stretches from the peaks Hochsattel (1199m a.s.l), Brandleck (1725m a.s.l), Mayrwipfl (1736m a.s.l), Steyreck (1592m a.s.l) and the alpine pasture Blumauer Alm in the west to the peaks Falkenmauer (1294m a.s.l), Schwarzkogel (1333m a.s.l) and the stream Großer Bach in the east. Also, it includes the peaks Rotwagmauer (1191m a.s.l), Trampl (1424m a.s.l), Alpstein (1443 m a.s.l) and the alpine pasture Schaumbergalm in the north and the peaks Dürreneck (1271m a.s.l) and Hundseck (1259m a.s.l) in the south.

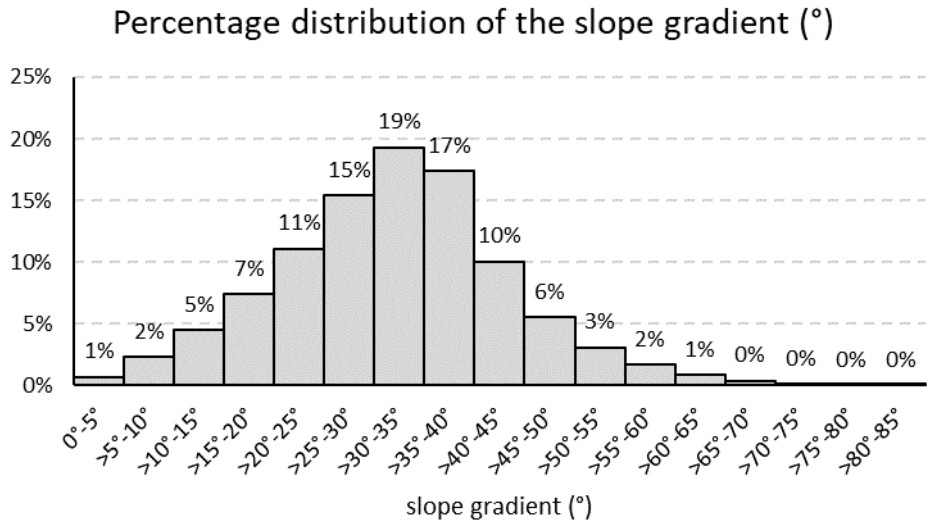

Figure 4: Distribution of the slope gradient (°) in percent across the study area

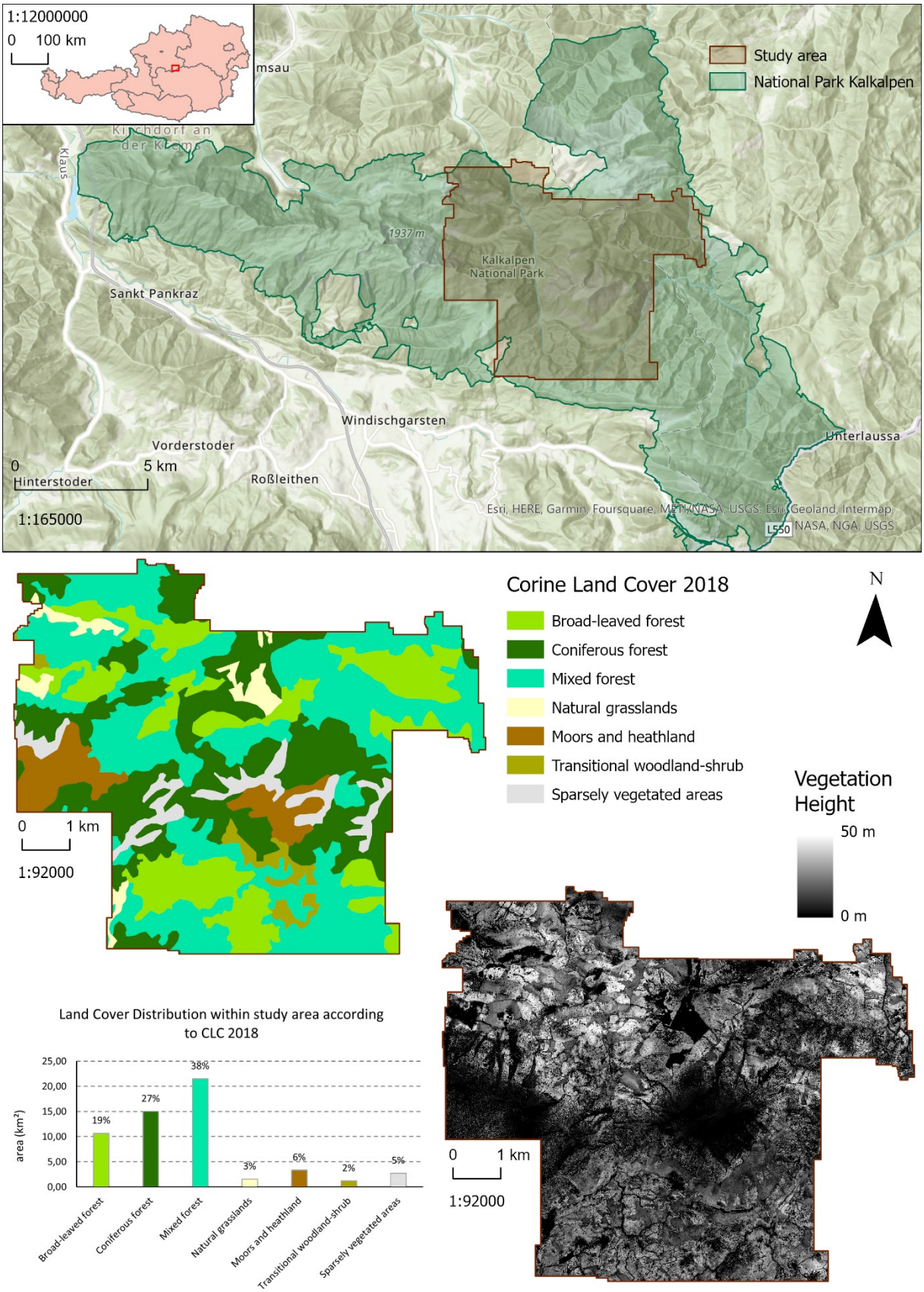

Figure 5: Overview of the study area within the National Park Kalkalpen. Top: Location; middle: Land cover distribution according to CLC 2018 and bottom right: vegetation height according to the normalized Digital Surface Model based on the ALS data

4.1. The National Park Kalkalpen

The National Park Kalkalpen was founded in the year 1997 on the 25th of July by the federal and state governments of Upper Austria covering an initial area of 16509 ha. During its existence the Park was constantly expanded and possesses now an area of 20856 ha (Nationalpark O. ö. Kalkalpen GmbH 2011a). 89% of the parks area are classified as nature zone, while 11% are defined as preservative zone. The area is divided into 81% forest, 8% coniferous shrub, 6% meadows and 5% rock and debris (Nationalpark O. ö. Kalkalpen GmbH 2011b). The Kalkalpen National Park is part of the Northern Limestone Alps. It is made up of two mountain ranges, the Reichraminger Hintergebirge and the Sengsengebirge. The Sengsengebirge, an outpost of the alpine Limestone Alps, with its approximately 20 kilometers long main ridge, reaches its highest elevation with the mountain Hoher Nock (1963 meters). The lowest point of the park, with 385 meters is located in the northern Reichraminger Hintergebirge (Nationalpark O. ö. Kalkalpen GmbH 2016, 18).

Of the six Austrian National Parks, the Kalkalpen National Park is described as the Forest National Park. It is one of the largest closed forest areas in Austria, that has been spared from fragmentation by traffic routes and settlements to this day (Nationalpark O. ö. Kalkalpen GmbH 2016, 18). A high biodiversity of tree species can be found, all in all 32 different species. For example: spruce, fir, larch, pine, beech, sycamore, rowan, etc. (Nationalpark O. ö. Kalkalpen GmbH 2011c), whereby the most prevalent tree species are fir with 44,5% and beech with 38,2% (Nationalpark O. ö. Kalkalpen GmbH 2020, 31). The most common forest type is the beech forest and the spruce-fir-beech forest (Nationalpark O. ö. Kalkalpen GmbH 2011d). Overall, 6 different beech forest communities are present in the protected region. This includes the Cyclamen beech forest, the Winter roses beech forest, the Woodruff beech forest, the Carbonate-Adenostyles-Spruce-Fir beech forest, the Loam-Spruce-Fir beech forest and the high montane-Carbonate beech forest. Especially notable is the Winter roses beech forest, or *Helleboro nigri-Fagetum*, which can be described as an endemic community for the north-eastern Limestone Alps (UNESCO). A quarter of the forests are older than 140 years, of these, 23% are older than 200 years and 5% are even older than 250 years. The oldest known beech in the National Park counts 548 years (Nationalpark O. ö. Kalkalpen GmbH 2022).

In the year 2017, 5250 ha of the beech forest in the Nationalpark Kalkalpen were declared part of the United Nations Educational, Scientific and Cultural Organization (UNESCO) world natural heritage site “Ancient and primeval beech forests of the Carpathians and other regions of Europe” together with the wilderness area Dürrenstein, whereby 246 ha of these 5250 ha are pristine primeval forest (Egelseer 2021, 27). The integrity of the UNESCO World Natural Heritage site in the Nationalpark Kalkalpen is proven by the closeness of the forests to nature, as 26% of the forests can be described as natural and 50% as near natural. Another important

aspect is the size of the nominated area. The National Park Kalkalpen is the largest connected protected area with a significantly high proportion of old beech stocks in the beech distribution area of the Alps (UNESCO). Up until now the National Park Kalkalpen and wilderness area Dürrenstein remain the only world natural heritage site within Austria (Egelseer 2021, 27).
An important aspect in protecting the European beech (Fagus sylvatica L.) is its endemic status within Europe. They can reach an average height of 20 to 35 m, with a maximum height of about 45 m. The maximum age is given at 200 to 300 years, with exceptional cases sometimes reaching an age of over 500 years. Concerning the soil trophy, vertical distribution and water balance the European beech is adapted to a very wide spectrum (Nationalpark O. ö. Kalkalpen GmbH 2016, 39). With its dense foliage and canopy shape the beech forest deeply influences the internal forest climate, by reducing the amount of light reaching the forest interior, and conditioning the soil formation, the regeneration cycles and the food chains. Within Europe this forest type plays a significant role in the maintenance of biodiversity, as they can offer a habitat for up to 10,000 different species. They are therefore among the most valuable terrestrial ecosystems in Europe (Jovanović et al. 2019, 16). Under natural conditions beech forests would be omnipresent in Central Europe. But due to the historical land development they had to give way to the land requirements for agriculture, industry and settlement activities. In Austria 12.3% of the forest area would be beech forest, while 29.6% would be spruce-fir-beech forest. However, forest inventories showed, that only 28% of potential beech forest habitat is covered with beech trees. Within Europe primeval beech forests have become very rare and inside Austria they only constitute to 0.7% of the forest area, which amounts to ~28138 ha (Nationalpark O. ö. Kalkalpen GmbH 2016, 43). Characteristic for an undisturbed beech forest is the uneven age structure, representing all development phases, from seedling to very old, senescent trees. This vertical diversification leads to the gap dynamics regeneration, where the mortality of canopy trees is prerequisite for the regeneration of beech. Together with dead wood, these gap dynamics create a complex, multi-layered stand structure, with natural species composition and ecological processes. Already the importance of preserving these forests for biodiversity conservation is well recognized (Jovanović et al. 2019, 17).

5. Data

Following the introductory remarks, different datasets are used to answer the research questions. As per definition, airborne and space-born LiDAR data are used in conjunction with wall-to-wall active and passive satellite data. Due to their availability and variations in quality the data used, is obtained from different years:

- ALS data acquired in 2018.
- GEDI data from 2019/2020.
- S1 Radar data from 2020.
- S2 optical satellite data from 2019.

5.1. LiDAR

For this study data based on small-footprint ALS and large-footprint GEDI was used. The AGBD values were solely based on the GEDI data, while the vegetation height and the FHD values were based on the ALS, as well as the GEDI data. Both datasets are explained in detail below.

5.1.1. ALS

The ALS data was acquired on the 21st of May 2018 using an ultra-light airplane at a cruising altitude of ~790 m above ground. The sensor is a RIEGL VQ580 with a point density of > 16 points/m^2. Additionally, approximately 4000 ha are covered by 50 flight lines. Direct georeferencing is done for ALS by using the GPS/IMU unit Navatel SPAN-FSAS (NovAtel Inc. 2016). Afterwards, the resulting data was existing data from a region-wide previous ALS campaign to ensure location accuracy. Based on the georeferenced point cloud, both a digital terrain model (DTM) as well as a DSM were processed at a resolution of 0.5 x 0.5 m per pixel. To determine the vegetation height above the mapped terrain surface, the DTM is subtracted from the DSM (Eysn et al. 2012, 767). The difference between the DTM and the DSM is known as the Canopy Height Model (CHM) or the normalized Digital Surface Model (nDSM) (Chen et al. 2006, 925). After the nDSM is calculated, outliers must be sorted out. All values that are less than 0 or greater than 50 are excluded. The latter value was chosen, because both beech and spruce can reach a maximum height between 40 to 50m (IVA 2016) and are the dominant tree species in the National Park Kalkalpen. Furthermore, the point density at the edges of the

study area was too low to generate reliable canopy height values, therefore these border areas were removed from the analysis.

5.1.2. GEDI

For this study the relative height (RH) metrics from GEDI Level 2A, the FHD based on the plant area index (PAI) from GEDI Level 2B and the AGBD from GEDI Level 4A were used.

The GEDI Level 2A Geolocated Elevation and Height Metrics product provides waveform interpretation and extracted products from each GEDI Level 1B received waveform. This includes the ground elevation, the canopy top height and the RH metrics. The methodology for generating these datasets is adapted from the LVIS algorithm (Dubayah et al. 2021a). This study uses the RH50 and the RH100 values representative for the mean and the maximum canopy height. Relative heights are defined as the distance between the elevations of detected ground return and the *n%* accumulated waveform energy, where *n* ranges from 1 to 100 (Wang et al. 2022, 975). RH100 for example stands for the relative height difference between the first and last mode, where the LiDAR pulse was reflected (Rishmawi et al. 2021, 4).

The GEDI Level 2B Canopy Cover and Vertical Profile Metrics product contains the canopy cover, the PAI, the Plant Area Volume Density (PAVD), and the FHD (Dubayah et al. 2021b). The FHD is a measurement for the complexity of the canopy structure. Higher FHD values are often associated with multiple canopy layers (Rishmawi et al. 2021, 5). It is hypothesized, that a greater structural complexity creates more niches and thus greater species diversity (Bergen et al. 2009, 2).

The GEDI Level 4A Footprint level AGBD product is the highest product level and represents the output of models. The vertical height profiles, derived from the L2A data waveform RH metrics, are put in relation to AGBD estimations from field inventories. These models are applied to the billions of GEDI profiles. Globally consistent measurements and algorithms help to overcome the uncertainties imposed by incomplete sampling and the use of different data sources and methods in different parts of the world (Dubayah et al. 2022).

The lower-level products (L2A & L2B) are received from NASA's Land Processes Distributed Active Archive Center (LPDAAC) and the higher level product (L4A) from the Oak Ridge National Laboratory Distributed Active Archive Center (ORNL DAAC).

5.2. Sentinel

S1 and S2 are the satellites of the European Space Agency (ESA), designed to deliver dense time series data and imagery for Europe's ambitious Earth Observation program Copernicus. S1 is an active Radar sensor, while S2 is an optical sensor covering 13 multispectral bands.

5.2.1. Sentinel-1

S1 is installed on two twin polar orbiting satellites, descending (DSC) and ascending (ASC), that are designed to provide spatial data for environment and security warranting, global economic and business growth. S1A was launched on the 3rd of April 2014 and S1B on the 25th of April 2016 (ESAa). Each satellite has a 12-day repeat cycle and 175 orbits per cycle. With both satellites operating, the repeat cycle is reduced to six days (ESAb). However, there was an anomaly of the power supply reported for S1B on the 23rd of December 2021. After several investigations, on August the 3rd, 2022, ESA announced that efforts to repair the failed C-band SAR sensor onboard the S1B satellite have not been successful, and the mission has therefore been terminated. This failure however did not affect the study.
The SAR instrument is the main instrument carried by the S1 spacecrafts (Bourbigot et al. 2016, 22). It is a type of active data collection, where a sensor produces its own energy and then records the amount of that energy reflected back after interacting with the earth. This allows S1 to collect imagery in all weather conditions and to operate day-and-night. Different wavelengths of SAR are categorized as bands, with letter designations such as X, C, L or P (Chan & Koo 2008, 28ff.) S1 operates in the C-Band with a frequency of 5.405 GHz a wavelength of 7.5 to 3.8 cm. The instrument supports operations in single polarisation (HH or VV) and dual polarisation (HH+HV or VV+VH). Whereby HH or VV means, that the signal transmits and receives in vertical or horizontal polarisation and VH for example means, that the signal transmits in vertical polarisation and receives in horizontal polarisation (Bourbigot et al. 2016, 22f.).

All available S1 images recorded in the year 2020 were used in this study. The earliest recording from the 2nd of January and the latest recording on the 21st of December. Images from four different orbits, two descending, two ascending, were selected. For each orbit the polarisation VV and VH was used. The orbit ASC146 provided 29 images, 28 images were available for ASC44, 33 images for DSC22 and 57 images for DSC95, which resulted in 147 images in total.

5.2.2. Sentinel-2

S2 sensors are installed on two identical satellites in the same orbit. S2A was launched on the 23rd of June 2015 and S2B was launched on the 7th of March 2017 (ESAc). Each satellite carries an innovative wide swath high-resolution multispectral imager with 13 spectral bands, an orbital swath width of 290 km and a revisit frequency of 5 days. The 13 spectral bands cover the visible, NIR and SWIR spectrum at different spatial resolutions at the ground ranging from 10 to 60 m (Drusch et al. 2012, 26).

This study uses S2A data and 10 of the available 13 bands (see Table 2). The 60 m bands (Band 1, Band 9, Band 10) were discarded. Due to difficult illumination and snow cover in winter, only images from the vegetation period (in this case between the 1st of June and the 30th of September) were used. All 24 images were recorded in the year 2019 with the earliest recording available on the 3rd of June 2019 and the latest recording on the 21st of September 2019. S2 data would also have been available for the year 2020, but of the 24 images recorded in the vegetation period 17 of the images had a cloud cover of more than 50%. Three so "severe", that the images were not available at all. The images of 2019 on the other hand only had a cloud cover over 50% for 13 of its available images. Therefore, the images from 2019 were selected, to provide a greater dataset.

Table 2: Sentinel-2A bands used for the study (ESAd)

	Single Bands Sentinel-2A					
Band Number	**Abbrevation**	Band Name	Sensor	Central wavelength (nm)	Bandwidth (nm)	Resolution (m)
Band 2	B2	Blue	MSI	492.7	65	10
Band 3	B3	Green	MSI	559.8	35	10
Band 4	B4	Red	MSI	664.6	30	10
Band 5	B5	Vegetation Red Edge	MSI	704.1	14	20
Band 6	B6	Vegetation Red Edge	MSI	740.5	14	20
Band 7	B7	Vegetation Red Edge	MSI	782.8	19	20
Band 8	B8	NIR	MSI	832.8	105	10
Band 8a	B8a	Narrow NIR	MSI	864.7	21	20
Band 11	B11	SWIR-Cirrus	MSI	1613.7	90	20
Band 12	B12	SWIR	MSI	2202.4	184	20

5.3. Reference Data

The ALS and GEDI data was utilized as reference data to train the RF model and to validate the regression results. Also, our results were compared to available forest inventory data (see chapter 5.3.1) and collected field data (see chapter 5.3.2). Furthermore, the influence of the study area characteristics was investigated. Hereby, the focus was on the slope inclination, the forest type and the canopy cover. The slope inclination is calculated, utilizing the acquired

DTM (NovAtel Inc. 2016). The forest type is based on the Dominant Leaf Type (DLT) (EEA 2020a) and the canopy cover on the Tree Cover Density (TCD) (EEA 2020b) of Copernicus. Both are available for the year 2018 with the resolution 10x10 m.

5.3.1. Forest Inventory Data

Zöbelboden covers a small, forested catchment (90 ha) of a karstic mountain range in the Northeast of the National Park Kalkalpen. It was established in 1992 as the only Integrated Monitoring station in Austria under the UN Convention on long-range transboundary air pollution and in 2006 it became part of the Long-Term Ecosystem Research (LTER) Austria. Monitoring and research are focusing on climate change effects on forest ecosystems, etc. (EAA 2022).

Data for the AGBD in g/m^2 was available for the year 2019 for the station 700 located in the sample area Intensive Plot 2 and station 2900 located in the sample area Intensive Plot 3. Both plots are located outside the study area (see Figure 6). Therefore, a comparison of the forest inventory measurements with the original ALS and GEDI data is not possible and only a comparison with the regression results is carried out. For each plot the available AGB measurements for each tree were transformed from g/m^2 to Mg/ha by multiplying the values with 100 and then summed up. Station 700 includes mostly beech trees, but also Norway spruce and could be, according to its tree composition, categorized as mixed forest. Station 2900 largely consists of Norway spruce and can therefore be labeled as coniferous forest. In total Station 700 can count 64 measured trees, on which the measured AGBD of 287.74 Mg/ha is based. Station 2900 contains a total number of 53 trees and an AGBD of 414.23 Mg/ha (see Table 3).

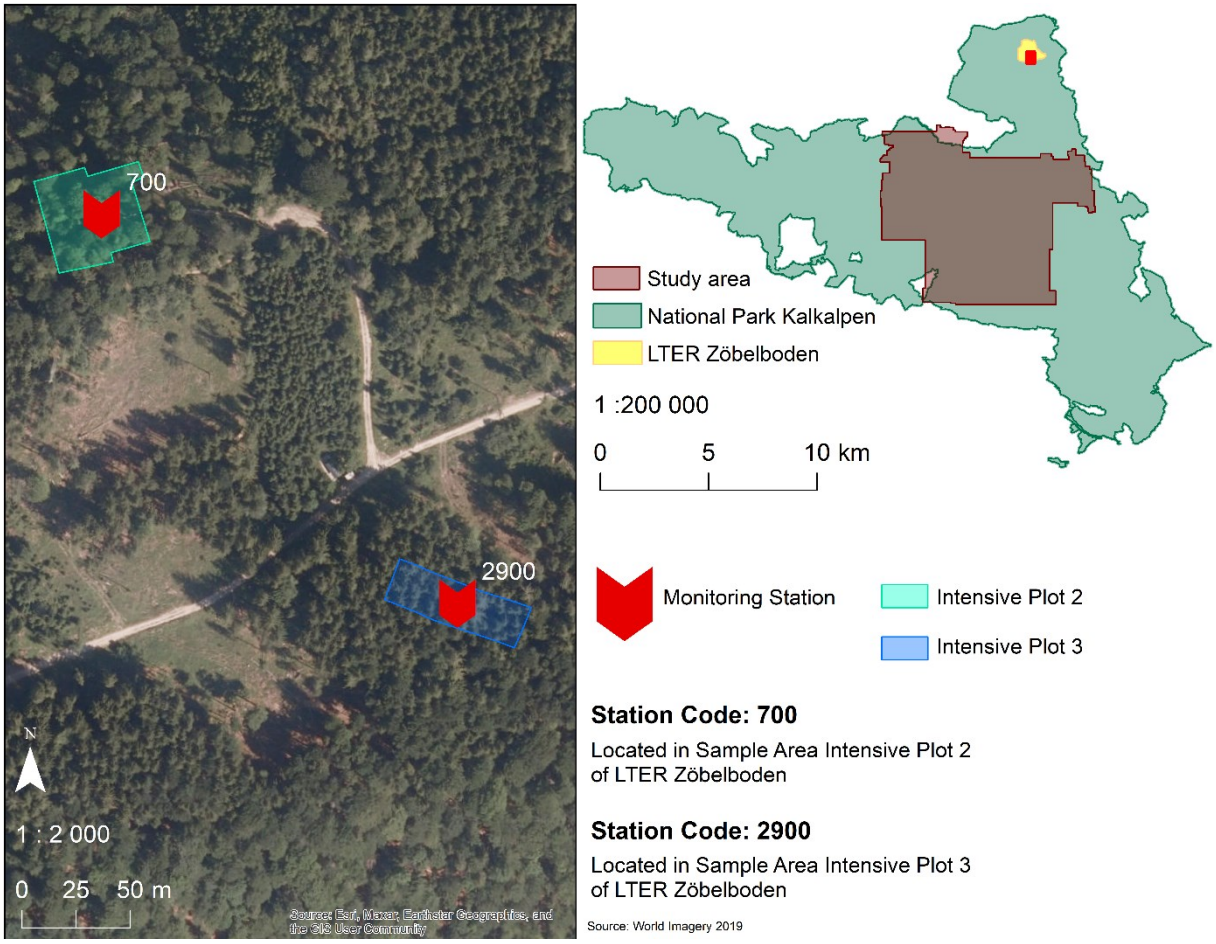

Figure 6: Field Inventory Data. Location of Station 700 and 2900

Table 3: Tree type distribution and AGBD (Mg/ha) values for station 700 and 2900

Station 700			
	Tree species	Number	AGBD (Mg/ha)
	beech	42	225.95
	norway spruce	14	33.86
	sycamore	7	26.37
	whitebeam	1	1.56
Total		**64**	**287.74**

Station 2900			
	Tree species	Number	AGBD (Mg/ha)
	beech	1	20.64
	european larch	6	86.65
	norway spruce	46	306.94
Total		**53**	**414.23**

5.3.2. Field Data

On the 20th of June 2022 several GEDI plots used for this study were visually addressed and documented via photography. The plots were selected according to their reachability (see Figure 7) and distributed from a height of 643 m up to 1249 m a.s.l. The slope gradient ranged from 17° to 42°. Several diverse forest types were covered in the field data plots for example: old growth forest; mixed forest; coniferous forest and broadleaved forest. The recordings of the plots and the associated ALS and GEDI values are given in Table 28. The main focus of the inspection was the inquiry of the type and the vertical structure of the forest.

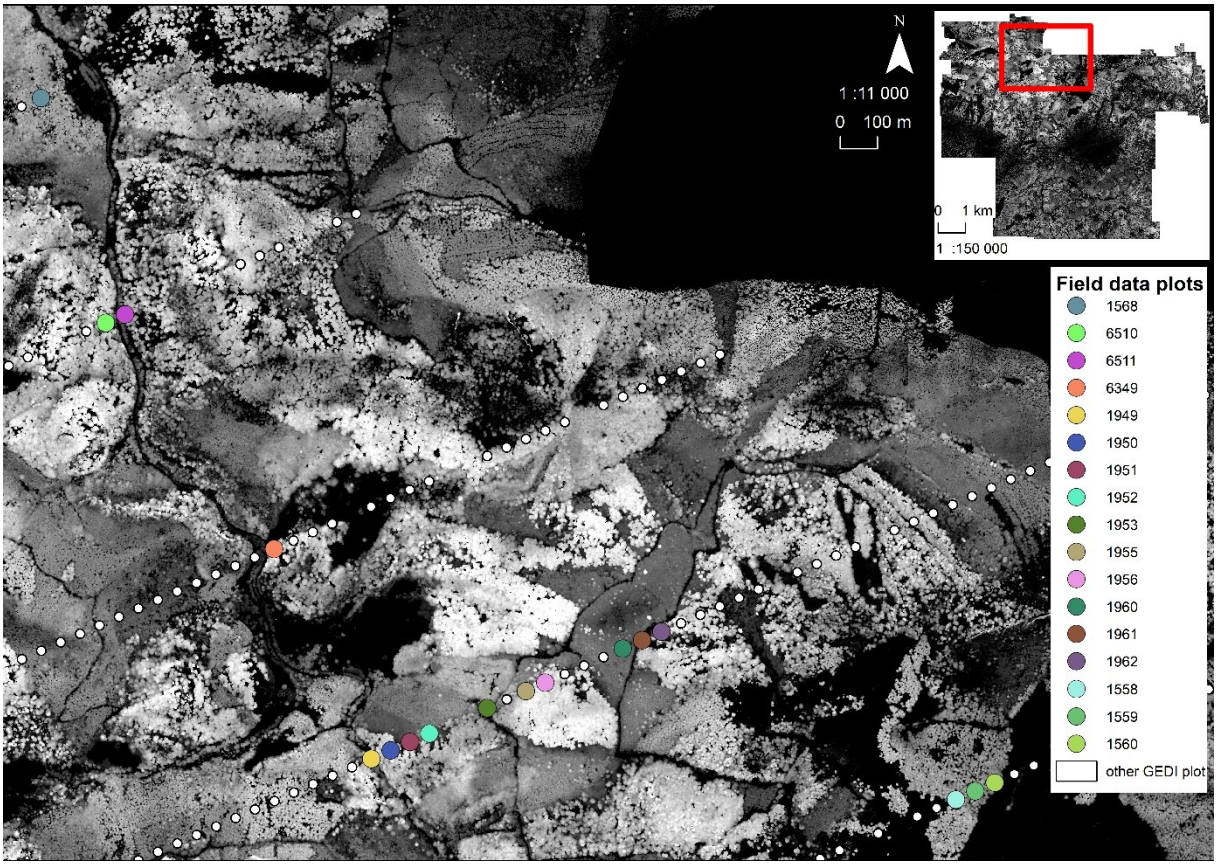

Figure 7: Field data plot distribution

6. Methods

6.1. Data Preprocessing

6.1.1. Removing Areas of Change and Subalpine Zones

As mentioned in chapter 5 the input data was recorded in different years. To avoid miscorrelations, changed areas had to be discarded from the analysis. Changes in the forest structure between 2019 and 2020 were visually detected, based on orthophotos from the year 2018 as reference data and World Imagery data available in ArcMap and ArcGIS Pro from the years 2019 and 2020. The change area amounted to 9.65 ha in total and was often the result of windbreak or bark beetle infestation. These change areas were later used to filter out GEDI plots, but also fishnet grids based on the ALS data.

Additionally, with the highest elevation point reaching 1784 m a.s.l., parts of the study area are located within the higher subalpine zone. This zone is characterized by loose groups of pine (Pinus cembra) and larch (Larix decidua) and shrublike mountain pine (Pinus mugo) (Kilian et al. 1994, 11). Differentiating between the coniferous shrub and the coniferous trees based alone on their spectral properties presents a challenge, due to similar morphological and anatomical needle characteristics (Rösch et al. 2022, 5). When modelling the vegetation parameters, large errors within these regions can therefore be expected. This was found in earlier calculations and therefore the higher subalpine zone was excluded from all calculations. Depending on the alpine region, the alpine height zones are located at different elevations. According to Kilian et al. (1994, 48) the National Park Kalkalpen is located in the “Northern Alps – eastern part” (Nördlichen Randalpen – Ostteil). Here the higher subalpine zone is positioned between an elevation of 1500 m a.s.l. and 2000 m a.s.l. Neither training, nor validation samples located above 1500 m a.s.l. are therefore utilized (see Figure 8).

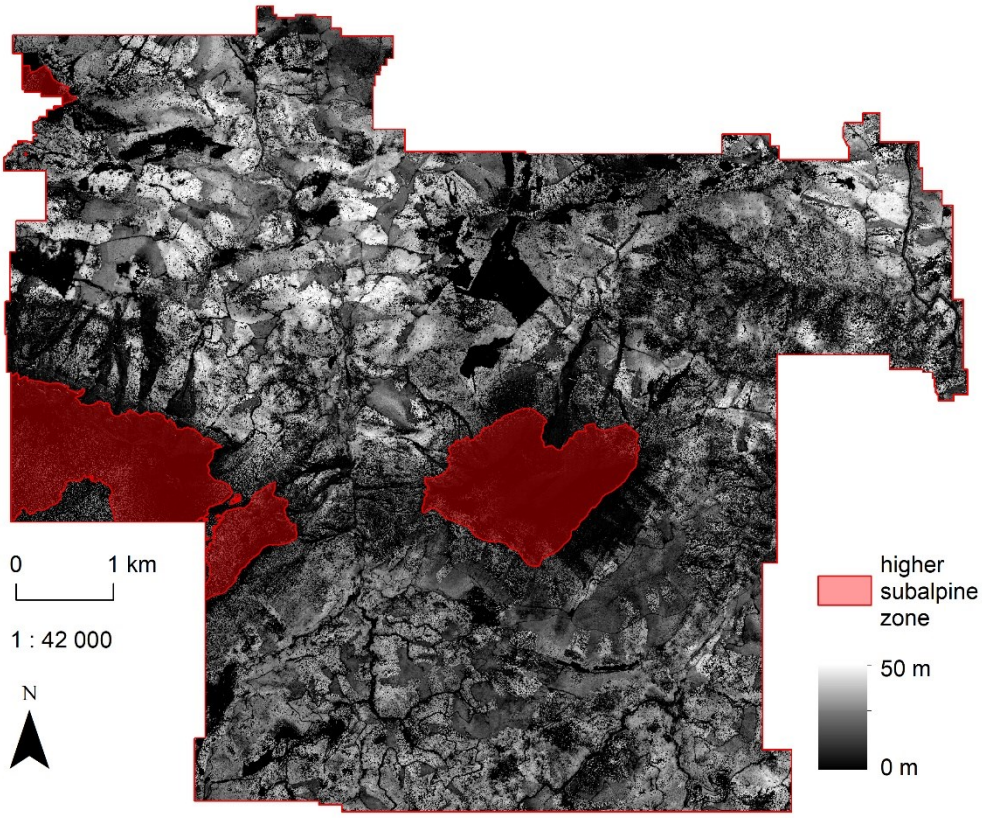

Figure 8: Higher subalpine zone in the study area National Park Kalkalpen

6.1.2. ALS

The ALS data is not only used for the training, but also for the validation of the regressions, which were calculated based on the Sentinel and the ALS or GEDI data. To be used for this purpose, the ALS nDSM is downscaled from the original spatial resolution of 0.5x0.5 m to a resolution of 10x10 m. It is important to ensure the positional accuracy of the new raster. In order to carry out further calculations, it is crucial that the pixel distribution of the resampled ALS raster is congruent with the Sentinel images. The ALS nDSM was therefore downscaled, using a fishnet grid shapefile, that was generated based on a Sentinel image. Within one grid 2000 pixels of the ALS nDSM are merged (see Figure 9). Figure 9 also includes the GEDI plots for comparison. For each grid both the statistical mean and the maximum of the ALS nDSM pixel values are calculated. The mean values are utilized as stand in for the mean vegetation height and the maximum values are used as the top or maximum vegetation height. Furthermore, the FHD is calculated based on the ALS data with the formula developed by MacArthur & MacArthur (1961, 594). In this case it was not possible to calculate the PAVD needed to compute the PAI, hence the amplitude per height layer is used as a substitute for the PAI. The vertical extent of each layer is set to 1 m. The FHD for the ALS data is then

calculated by using the discrete returns per height layer. This procedure is also described in the paper by Hirschmugl et al. (2023, 5).

Finally, areas intersecting with the forest change and the higher subalpine zone generated beforehand in chapter 6.1.1. are removed, resulting in a final fishnet grid shapefile, consisting of 508193 individual pixels, each one containing an ALS mean, max and FHD value. Based on this shapefile the correlation is calculated and the training and validation samples are generated.

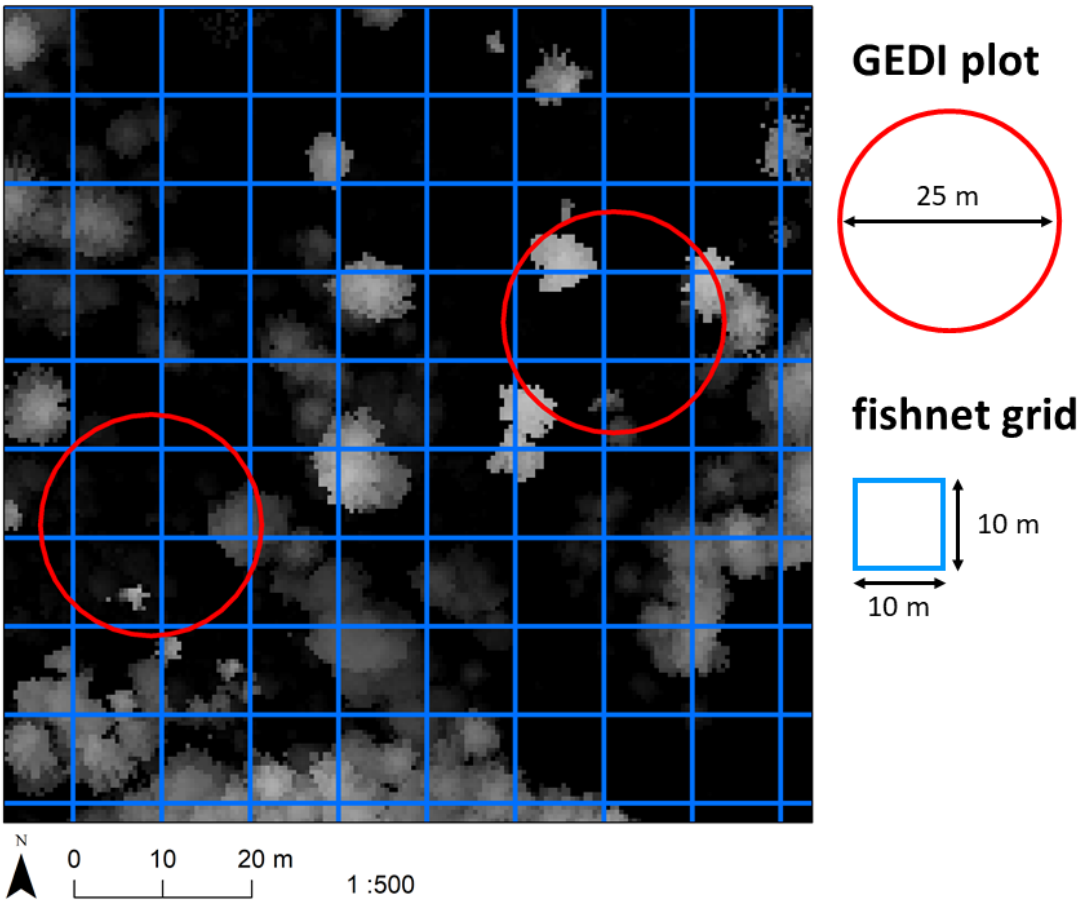

Figure 9: Comparison of fishnet grids and GEDI plots

6.1.3. GEDI

The GEDI products received from the LPDAAC and the ORNL DAAC are transformed into shapefiles. The 9065 footprints provided by the L2A product are then filtered according to certain parameters. These requirements are also listed in the paper of Hirschmugl et al. (2023, 5). For each applied filter the remaining footprints are given in brackets:

- Quality flag = 1; (4618)
- Waveforms with terrain height within accuracy limits. Due to the steep terrain, inaccuracies with regards to the terrain height occur. In order not to impact the analysis, these outliers (> 2*stdv) were discarded from further analysis; (4174)
- Acquisition during leaf-on season (June – October 2019 and 2020); (2911)
- Degrade flag = 0; (2911)
- Data overlapping the ALS coverage; (1734).
- Areas where no changes between 2018 and 2020 occurred (see chapter 6.1.1.); (1725)
- Footprints, where GEDI or ALS estimate heights above ground of 50 m or more are removed to account for artefacts (e.g. from birds); (1692)

After the L2A shapefile has been filtered all L2B and L4A plots that overlap with the L2A plots are selected to be used in this study. The resulting shapefile then contains the RH100, RH50, FHD and AGBD values. Furthermore, footprints located in the higher subalpine zone are later on excluded, resulting in a final set of **1156** plots in total.

6.1.4. Sentinel

All S1 as well as S2 tiles were preprocessed using the project partner Joanneum Research's software package IMPACT. This includes calculating the surface reflectance with Sen2Cor to correct the impact of the atmosphere and resampling all bands to the resolution 10x10m per pixel. Also, all bands were co-registered so that all pixels overlap. Clouds were filtered out with the so-called Function of mask (Fmask) algorithm and a topographic normalization was conducted with the Minnaert-correction in the IMPACT Tools. The Fmask was introduced by Zhu and Woodcock in 2012 for cloud and cloud shadow detection in satellite imagery (Zhu & Woodckock 2012, 83). Mainly used for Landsat imagery, it can also be applied to Sentinel data (Frantz et al. 2018, 480). Since this preprocessing was needed for several steps in the research project, this work was done only once for all data by Joanneum Research staff.

Several individual S2 images were disturbed by cloud cover, cloud shadow and haze, providing no information in the affected areas. To create homogenous and noise-free images, the S2 images, as well as the S1 images were temporally aggregated, and several spectral-temporal metrics were calculated (see Table 4). This compositing procedure combines the different

measurements of co-located pixels in different orbits of geometrically registered data together (Roy et al. 2010, 38). The calculated spectral-temporal metrics or temporal statistics are simply statistical metrics, that describe the distribution of a spectral band or index over a specified period of time (Pflugmacher et al. 2019, 588). This method has the advantage of substituting missing information by means of previous or subsequent recordings. It enables one to obtain more representative data.

The temporal statistics minimum, maximum, mean, median, standard deviation and variance were calculated for S2 as well as S1 in R. More information can be found in chapter 6.1.4.1. and chapter 6.1.4.2.

Table 4: Temporal Statistics Bands calculated for Sentinel-1 and Sentinel-2

Band Number	Temporal Statistics	Abbrevation
1	Minimum	min
2	Maximum	max
3	Mean	mean
4	Median	med
5	Standard Deviation	sd
6	Variance	var

6.1.4.1. Sentinel-1

Following the basic preprocessing, dedicated time series analysis was done to generate stacks of input data. The workflow is shown in Figure 10. Method A calculates for each of the four orbits (ASC146, ASC44, DSC95 and DSC22) and the two polarisations (VV and VH) six temporal statistics, based on all images available for the respective orbit and polarisation. Resulting in 48 temporal statistics bands. Method B only differentiates the images according to their polarisation. For each polarisation all orbits are combined. The calculated temporal statistics amount to 12 bands. This was done in order to investigate if the orbit of recording can also have an influence on the final result.

Furthermore, several GLCMs (see Chapter 3.2) were calculated based on the median temporal statistics band in ERDAS. For calculating the GLCM in ERDAS a square window the size of 5x5 pixel was chosen. The calculated nine texture bands are listed in Table 5. For method A for each orbit and polarisation the texture parameters were calculated based on the respective median temporal statistics band, resulting in 72 bands. Method B utilizes the median temporal statistics band for both polarisations, calculating 18 texture bands.

All bands calculated for method A amount to 120 bands in total and are later on employed for the regression variation *all bands*. In the end method B counts 30 bands in total, that are used for regression variation *4 Orbits*. More information can be found in chapter 6.4.2.

Table 5: Gray level co-occurrence matrix bands calculated based on the Temporal Statistics Median Band

Band Number	Gray level co-occurrence matrix (GLCM) band	Abbrevation
1	Contrast	con
2	Dissimilarity	dis
3	Homogenity	homo
4	Angular second moment	sec
5	Energy	eng
6	Entropy	ent
7	Correlation	cor
8	Mean	mean
9	Standard Deviation	sd

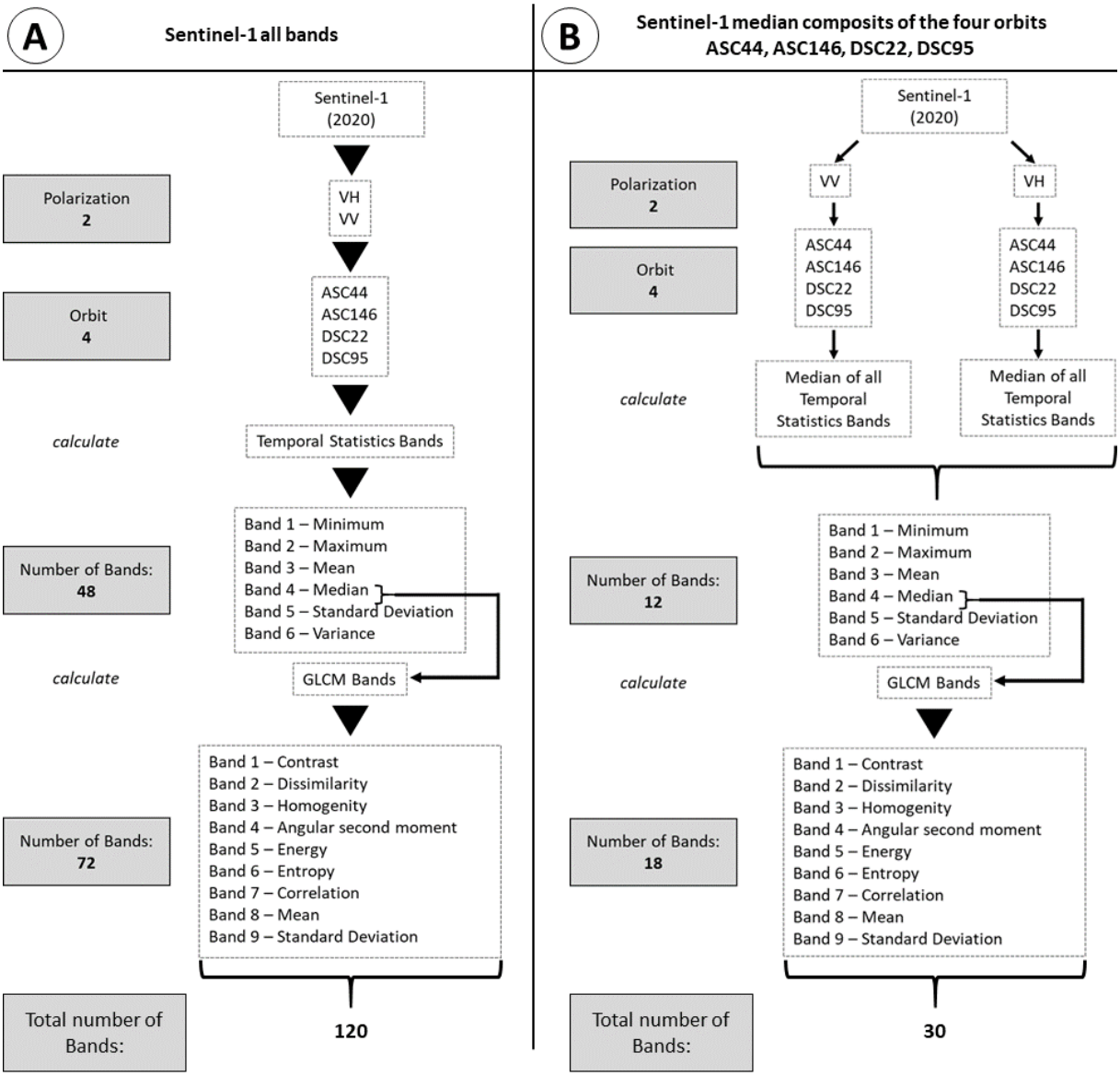

Figure 10: Workflow model - Sentinel-1 data preprocessing. Method A. using all bands; Method B. using the median composites of the four orbits ASC44, ASC146, DSC22 and DSC95

6.1.4.2. Sentinel-2

In the beginning, the temporal statistics for each of the ten spectral bands were calculated, using all 24 images recorded between the 3rd of June 2019 and the 21st of September 2019. Only images within the vegetation period were included in the analysis to avoid unwanted spectral response from snow or shadows occurring in winter. This step resulted in 60 temporal statistics bands. Furthermore, 21 VIs were calculated for each individual image with the IMPACT Tool (see Table 6). The indices were selected, according to the literature in chapter 3.2. (see Chen et a. 2021; Debastiani et al. 2019; Li et al. 2020; Nandy et al. 2021, Pereira-Pires 2021). Based on the 21 data templates for each VIs the temporal statistics were calculated, delivering 126 bands (see Figure 11). Thus 186 bands in total are available to analyze the correlation between S2 spectral characteristics and the vegetation parameters and to later on calculate the regressions.

Table 6: Indices calculated based on Sentinel-2

Sentinel-2 Indices		
Index	**Name**	**Formula**
DVI	Difference Vegetation Index	B8-B4
EVI	Enhanced Vegetation Index	2.5 * (B8a – B4)/(B8a + 6*B4 – 7.5 * B2 + 1)
EVIRE1	Red Edge 1 Enhanced Vegetation Index	2.5 * (B5 – B4)/(B5 + 6*B4 – 7.5 * B2 + 1)
GNDVI	Green Normalized Difference Vegetation Index	(B8 - B3)/(B8 + B3)
MSAVI	Modified Soil Adjusted Vegetation Index	((B8 - B4)*(1 + L))/(B8+B4+L)
MSAVI2	Modified Soil Adjusted Vegetation Index2	(2 * B8a + 1 -sqrt((2 * B8a + 1)2 – 8 * (B8a – B4))/2
MSI	Moisture Stress Index	B8/B11
NDII5	Normalized Difference Infrared Index – band5	(B5 - B11)/(B5+ B11)
NDII7	Normalized Difference Infrared Index – band7	(B7- B11)/(B7+ B11)
NDVI	Normalized Difference Vegetation Index	(B8 - B4)/(B8 + B4)
NDVI6	Normalized difference vegetation index with bands 4 and 6	(B6 - B4)/(B6 + B4)
NDVI7	Normalized difference vegetation index with bands 4 and 7	(B7 - B4)/(B7 + B4)
NDVI8a	Normalized difference vegetation index with bands 4 and 8a	(B8a - B4)/(B8a + B4)
NDWI	Normalized Difference Water Index	(B8 - B11)/(B8 + B11)
NLVI	Non-linear vegetation index with bands 4 and 5	$(B5^2 - B4)/(B5^2 + B4)$
PSRI	Plant Senescence Reflectance Index	(B4 - B3)/B8
RVI	Ratio vegetation index	B8/B4
S2REP	Sentinel-2 red edge position index	705 + 35 x [(B4 + B7)/2 – B5] x (B6 – B5)
SAVI	Soil Adjusted Vegetation Index	1.5 × (B8 - B4)/(B8 +B4 +0.5)
TCB	Tasseled cap brightness	0.3037 * B2 +0.2793 * B3 +0.4743 * B4 +0.5585 * B8 +0.5082 * B11 +0.1863 * B12
TCW	Tasseled cap wetness	0.1509 * B2 +0.1973 * B3 +0.3279 * B4 +0.3406 * B8 +0.7112 * B11 +0.4572 * B12

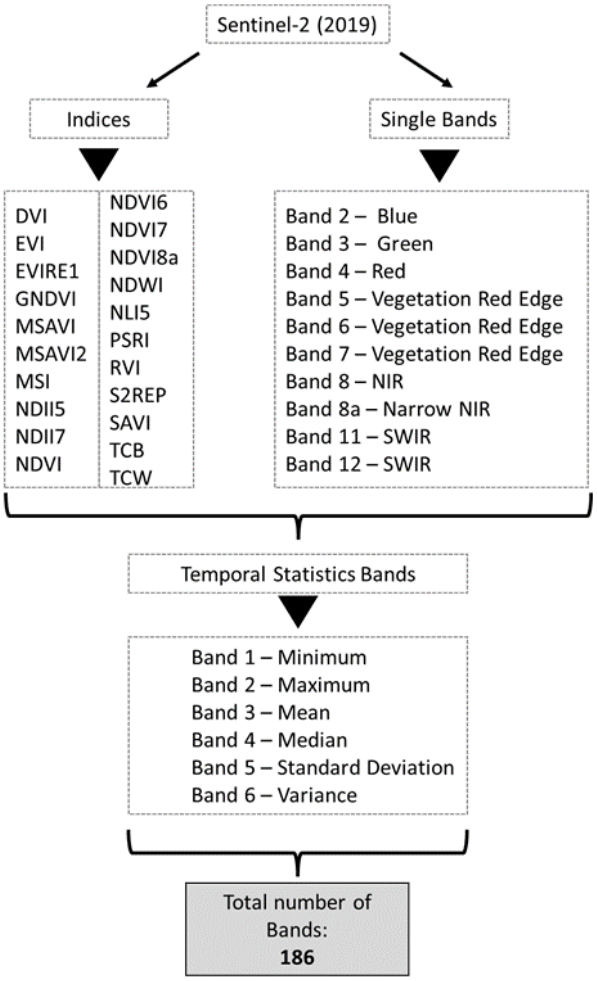

Figure 11: Workflow model - Sentinel-2 data preprocessing

6.2. Selection of Vegetation Parameters

6.2.1. Vegetation Height

In order to estimate which of the available GEDI RH values represents the maximum and mean vegetation height best, a correlation between the ALS and GEDI data was done. Hereby the correlation between the ALS maximum height and the GEDI values RH100, RH98, RH95 and RH90 is investigated, as well as between the ALS mean height and the GEDI values RH75, RH50 and RH25.

As can be seen by the result in Table 7, ALS mean, and ALS max show a positive correlation with all selected GEDI parameters. As expected, ALS max has the strongest correlation with RH100 and RH98 and ALS mean has the strongest correlation with RH50. Therefore, RH50 is selected to represent the mean vegetation height. RH100 and RH98 both result in the same correlation. In other studies, both RH100 and RH98 have been used as stand in for the upper vegetation height. Here the RH100 is selected to represent the maximum height parameters.

Table 7: Pearson correlation between ALS and GEDI mean and maximum height

Correlation with ALS max	
	R
RH100	0.64
RH98	0.64
RH95	0.63
RH90	0.61

Correlation with ALS mean	
	R
RH75	0.68
RH50	0.70
RH25	0.62

6.2.2. Foliage Height Diversity

Furthermore, it is examined whether the GEDI FHD and ALS FHD values are comparable. If the discrepancy between the two baseline datasets is too severe, validating the GEDI-based regressions against the ALS data would not be meaningful.
The correlation coefficient R showed a result of ~ 0.53, indicating a moderate positive correlation. Therefore, the data was determined to be fit to conduct validations and comparisons, although this fact has to be taken into account when evaluating the results.

6.2.3. Aboveground Biomass Density

To compute regressions for the AGBD, the GEDI values are used as trainings and validation data. Furthermore, an attempt was made to derive an AGBD raster from the ALS data. This would have opened the possibility to conduct a more comprehensive validation of the GEDI based AGBD regressions and to compare GEDI and ALS based AGBD regressions to one another.
To calculate the AGBD from the nDSM, firstly the wood volume per ha was calculated with the IMPACT Tool. The required data encompasses the nDSM, the DTM, the 10x10 m fishnet raster and a raster containing the treetops generated from the nDSM. Also, a classification raster file is needed. Hereby the Dominant Leaf Type (DLT) from the year 2018 by Copernicus was used. The resulting raster was meant to be converted into the AGBD using following formula:

Equation 3: Volume to Biomass conversion equation (Kivari et al. 2011, 7)

$$Biomass = Volume\ x\ BCEF$$

BCEF: Biomass Conversion and Expansion Factors

As BCEF several different variations according to Weiss et al. (2000, 31ff.) were tested. Hereby the conversion factors for coniferous trees (1.54), broadleaved trees (1.50) and beech trees, that are older than 120 years (1.29), were employed.

The correlation between the three ALS based AGBD rasters and the GEDI values was examined for each GEDI plot. The correlation coefficient amounted to ~ 0.45 for each raster, indicating a moderate correlation. Since the conversion only was a multiplication of the values, the correlation between the three different AGBD rasters and the GEDI values stayed the same. To enable a better review of the data the Root Mean Square Error (RMSE) for each raster was calculated (see Table 8). The results show that the biggest deviation between the ALS based, and GEDI based values, exists for the AGBD raster calculated with the BCEF for coniferous trees (404.06 Mg/ha), followed by the AGBD raster for broadleaved trees (389.73 Mg/ha) and finally the AGBD raster calculated for old beech trees (315.54 Mg/ha). All three results show a significant discrepancy of the ALS AGBD values from the GEDI AGBD values. Combined with the moderate R values, the idea to use ALS based AGBD values was dropped. The deviations were too significant to provide a meaningful comparison or validation with the GEDI data.

Table 8: R, RMSE and RMSPE values between ALS based AGBD and GEDI based AGBD values.

R, RMSE and RMSPE values between ALS based AGBD and GEDI based AGBD			
	R	RMSE (Mg/ha)	Deviation (%)
AGBD_conif	0.45	404.06	234
AGBD_broad	0.45	389.73	226
AGBD_beech	0.45	315.54	186

6.3. Correlation

The individual band correlations of different LiDAR data (ALS and GEDI) with S1 (Temporal Statistics and Texture Bands) and S2 (Temporal Statistics for the Multispectral Bands and the Indices) were studied. The R value (Bravais-Pearson correlation coefficient), as well as the R^2 coefficient of determination were calculated (see chapter 3.4) with the programming language R. When analysing the results, the negative and positive R values were viewed separately.
On the one hand, different data bases (see ALS and GEDI), and on the other hand different sampling forms in which the data was available (see fishnet grid and GEDI plots) were used. For the vegetation parameters ALS mean, ALS max and ALS FHD, the correlation between the vegetation parameters and the sentinel data within the fishnet grid (508193 cells) and the GEDI plots (1156 plots) was considered. This step was made to be able to examine how the form of the available data can affect the results. For the GEDI data RH50, RH100, FHD and AGBD only the GEDI plots were utilized to calculate the correlation. Due to covering a larger area, the GEDI plots always overlap with several cells of the fishnet grid (see Figure 9 in chapter 6.1.2.). Since the upscaling of data is usually more error-prone than the downscaling of data, the values are not converted to a single fishnet cell.

However, the different size and position of the GEDI plots compared to the fishnet grid also raises the question to what extent the ALS data should be extracted and translated into this data form. This problem also affects the Sentinel data, because their pixels are congruent with the fishnet grid. Therefore, they can be used directly to calculate the correlation with the ALS parameters within the fishnet grid. But when using the GEDI plots the Sentinel and ALS values need to be converted to fit the new data frame. Three different methods were tested to extract the mean values from the raster (see Figure 12):

- **A.** Zonal statistics: Only the pixels, whose centroid is within the plot area (Zonal Statistics tool in ArcGIS Pro, see A.)
- **B.** Weighted mean: All pixels applying a weighted mean (see B.)
- **C.** Center of footprint: Only one pixel per plot, which is fully covered by the plot (see C.).

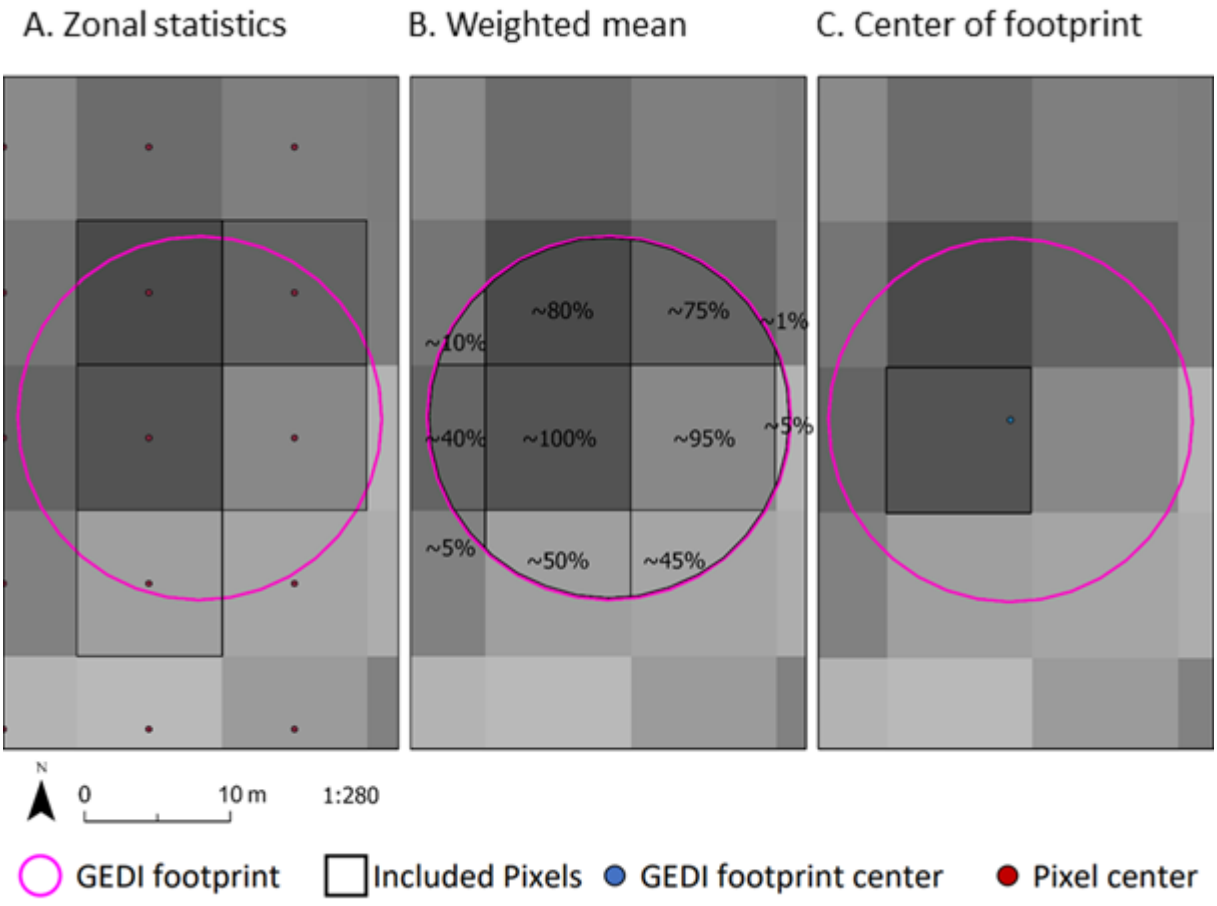

Figure 12: Different methods for the extraction of Sentinel values to GEDI plots

At the end of this work process, each Sentinel variable should have a R and R^2 value for the vegetation parameters ALS mean, max and ALS FHD based on the fishnet grid and the GEDI

plots, and for the GEDI vegetation parameters RH50, RH100, FHD and AGBD based on the GEDI plots. The results for R and R^2 are included in the calculation of the regressions in the next step.

6.4. Regression

The machine learning regression technique using the RF approach is used to create wall-to-wall vegetation parameters. This ensemble learning method grows a user-defined number of regression trees and averages their predictions (Rishmawi et al. 2021, 7). They show limited prediction power but seem to be more resistant to overfitting (García-Gutiérrez et al. 2015, 30). The regressions were calculated for the GEDI vegetation parameters AGBD, FHD, RH50 and RH100 and the ALS mean, ALS max and ALS FHD, utilizing different training samples, Sentinel variable combinations and validation data. Figure 13 depicts the workflow. Each step is explained in the following chapters.

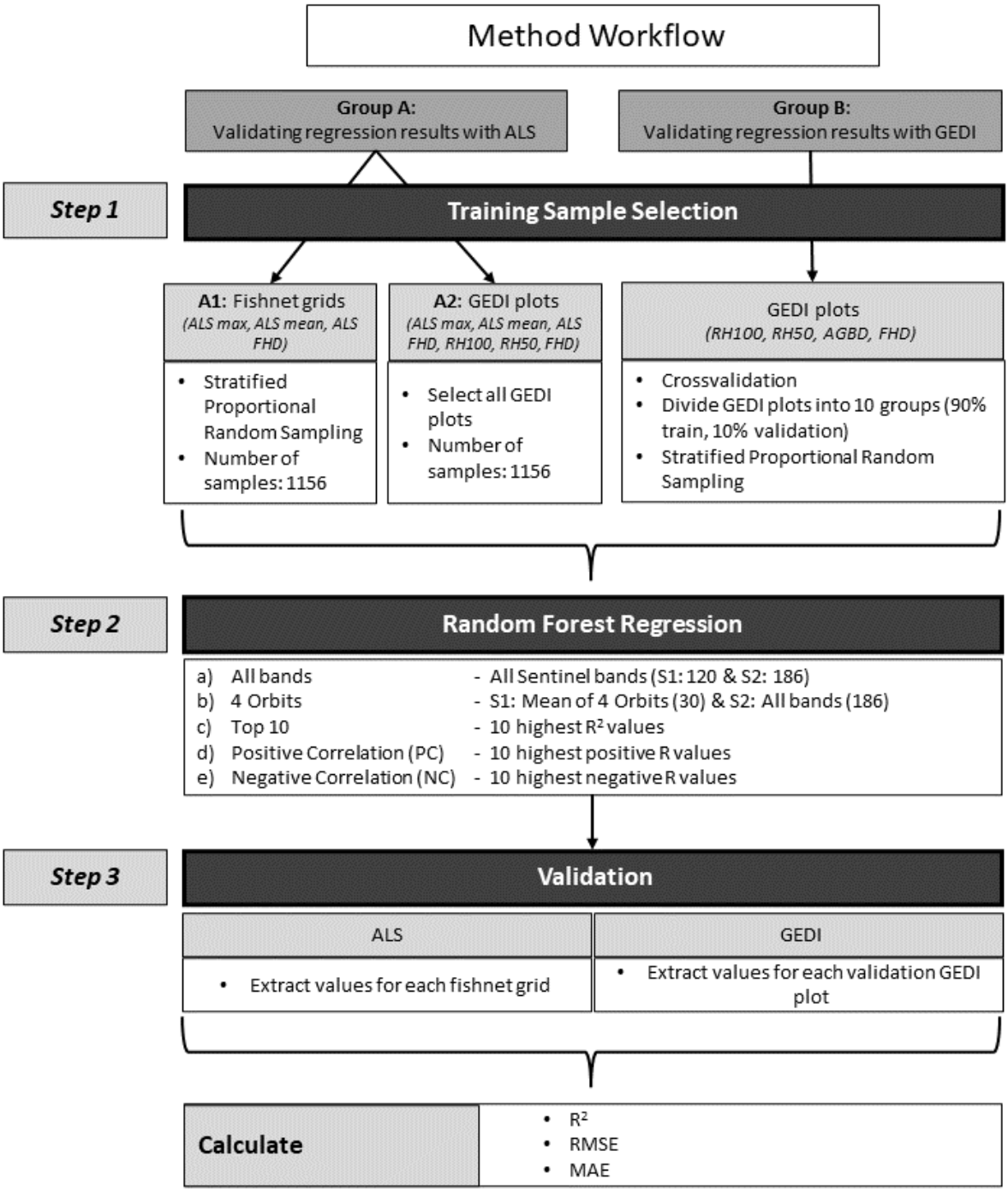

Figure 13: Workflow of calculating regression rasters based on different training data.

6.4.1. Step 1: Training Sample Selection

Different training datasets are generated depending on the data with which the calculated regressions are ultimately validated. A distinction can be made between two groups. In Group A, the results are validated with the available ALS data, in Group B with the respective GEDI data (see Figure 13).

Within Group A, two different strategies are used to select the training samples. For strategy A1, the samples are picked for the parameters ALS max, ALS mean and ALS FHD based on the fishnet grid. To ensure a representative distribution of the values, a proportional random sampling method is used. Here, each parameter is divided into representative value groups. Within each group, every individual value is assigned a random number ranging from 1-1000. All values that have been assigned the number 1 are selected and combined into a shapefile. Ultimately, each of the three training datasets should contain 1156 samples. This number was selected to ensure comparability with GEDI, since the number of GEDI samples is limited to 1156 due to the availability of the data. Strategy A2 uses all GEDI plots (1156) that are available for training and provides training datasets for ALS max, ALS mean, ALS FHD, RH50, RH100, GEDI FHD and AGBD. The ALS values are collected by calculating the mean value for each GEDI plot.

For Group B the regressions based on the GEDI data for AGBD, FHD, RH50 and RH100 are validated with the GEDI data itself through a cross-validation (see Figure 14). Here the training and validation sample sets were also created by using the proportional random stratified sampling method. The vegetation parameters were divided into representative value groups and within each group a random number between 1 and 10 was assigned. The GEDI plots were then merged into 10 shapefiles according to their number. They function later on as the validation data. The training data also consist of 10 shapefiles. They are created by merging 9 of the previously constructed shapefiles. If the validation is done with the validation dataset 1, the trainings dataset consists of set 2 to 10 (see Figure 14). The number of training plots always amounts to 1041 or 1040, and the number of validation plots amounts accordingly to 115 or 116.

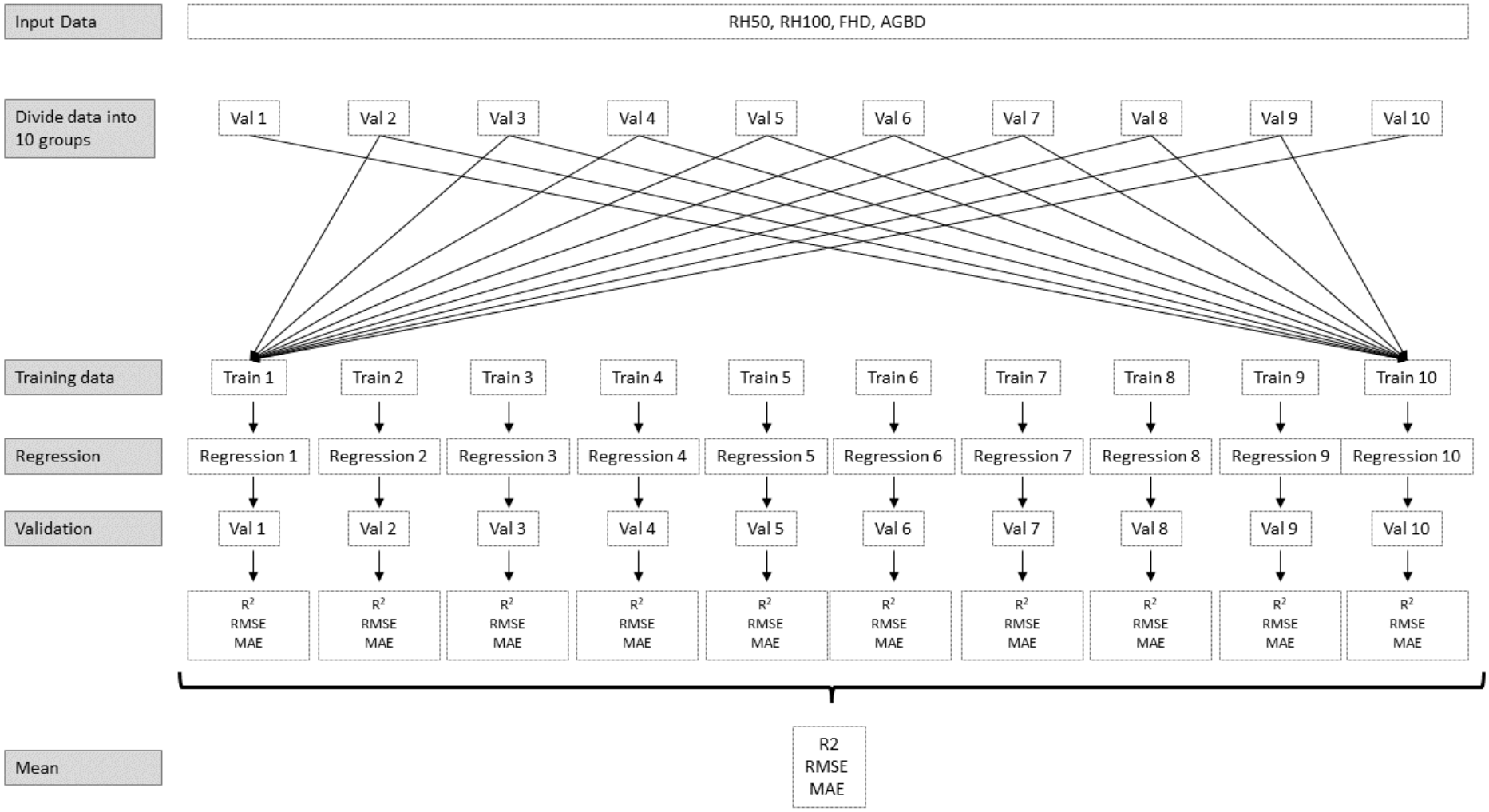

Figure 14: Cross-validation of GEDI based regressions with GEDI data

The following figures (see Figure 15, Figure 16, Figure 17 and Figure 18) display the different value distributions of the initial ALS and GEDI data and the training datasets for Group A. The training datasets for Group B were not depicted, since they do not provide much information.
The initial data values for GEDI AGBD range from 28.44 to 569.29 Mg/ha (see Figure 15). Predominantly represented is the value group 100 to 250 Mg/ha. Accordingly, this distribution is then reproduced in the ten datasets for the cross-validation. Same can be said for the other three parameters. The value distribution for the initial RH50, RH100 and GEDI FHD data can be seen in Figure 16, Figure 17and Figure 18. For strategy A2 the whole GEDI dataset for each parameter (except AGBD) is utilized as training dataset.
The mean vegetation height based on ALS mean for the whole study area ranges from 0 m to 46 m. However, most of the values are concentrated in the lower to middle height range below 25 m. The value group 0-5 m is the most prominent one with 25%. The training data based on the fishnet grids reflects this value distribution very well. The training data based on the GEDI plots differs from the value distribution of the study area in both the ALS mean and the RH50 data. They both cover a smaller value range, and the most prominent height group is 10-15 m (see Figure 16).
The maximum vegetation height for the entire study area includes 0 m up to 50 m. Most of the height values range from 20 m to 35 m. The training dataset based on the fishnet grids captures this height distribution. The training datasets based on the GEDI plots also present a similar distribution with most of the height values ranging between 20 m to 35 m. However, vegetation height values below 15 m are less represented for these two datasets compared to the whole study area. The height group 0 m to 5 m is not represented at all within the RH100 dataset, even though it accounts for 8% of the height values for the entire study area (see Figure 17).
The FHD values for the study area range from 0 to 4. The value group 2.5 to 3.0 is overly represented with 44%. The training data based on the fishnet grids covers every value group within the study area, although the exact value distribution is not reproduced completely. The training dataset, which uses ALS FHD data and the GEDI plots as samples, reflects the value distribution of the study area better. However, this training dataset also showcases shifts in the value distribution. The training dataset based on the GEDI data and the GEDI plots presents a completely different value distribution. Most of the samples have values between 3.0 and 3.5. Furthermore, this training dataset does not have any values < 1.0 (see Figure 18).
When analysing the regression results later on the different value distributions of the training datasets have to be considered.

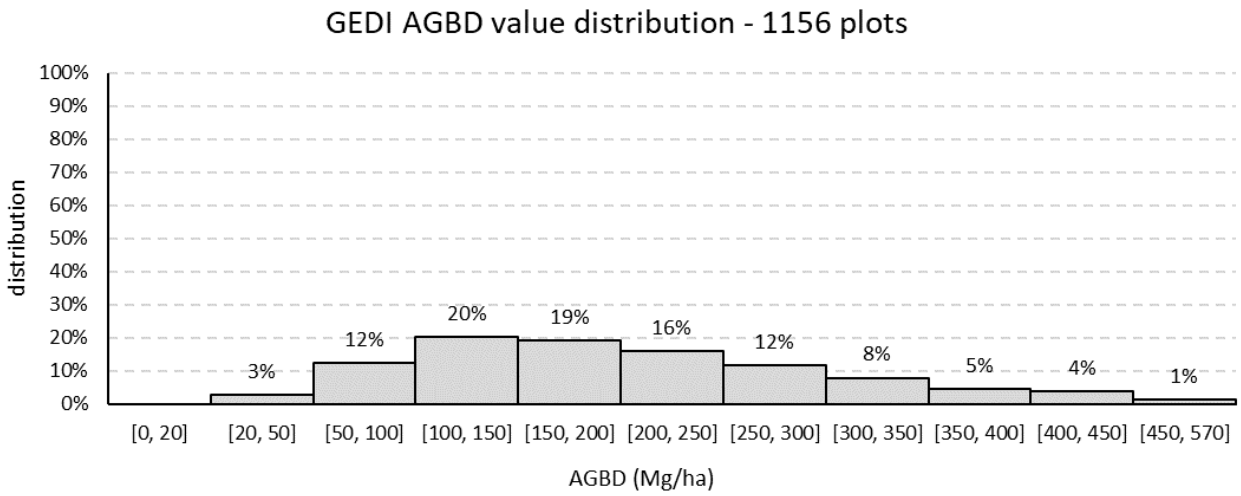

Figure 15: The value distribution of AGBD for all GEDI plots

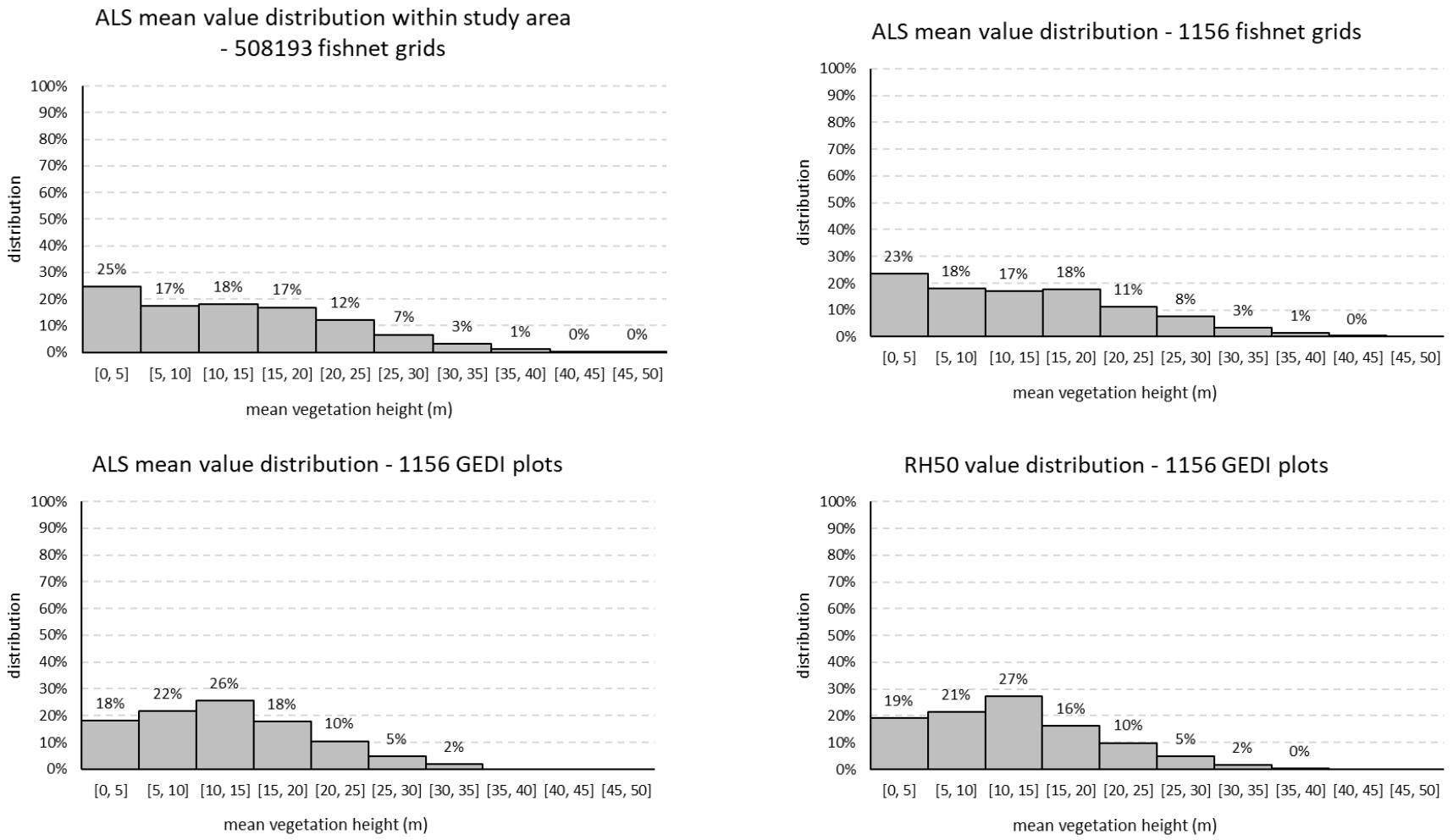

Figure 16: The value distribution of the training data and initial data for the mean vegetation height. ALS mean values for the whole study area (upper left); ALS mean training samples based on the fishnet grids (upper right); ALS mean training samples based on the GEDI plots (lower left) and for the GEDI RH50 training samples based on the GEDI plots (lower right).

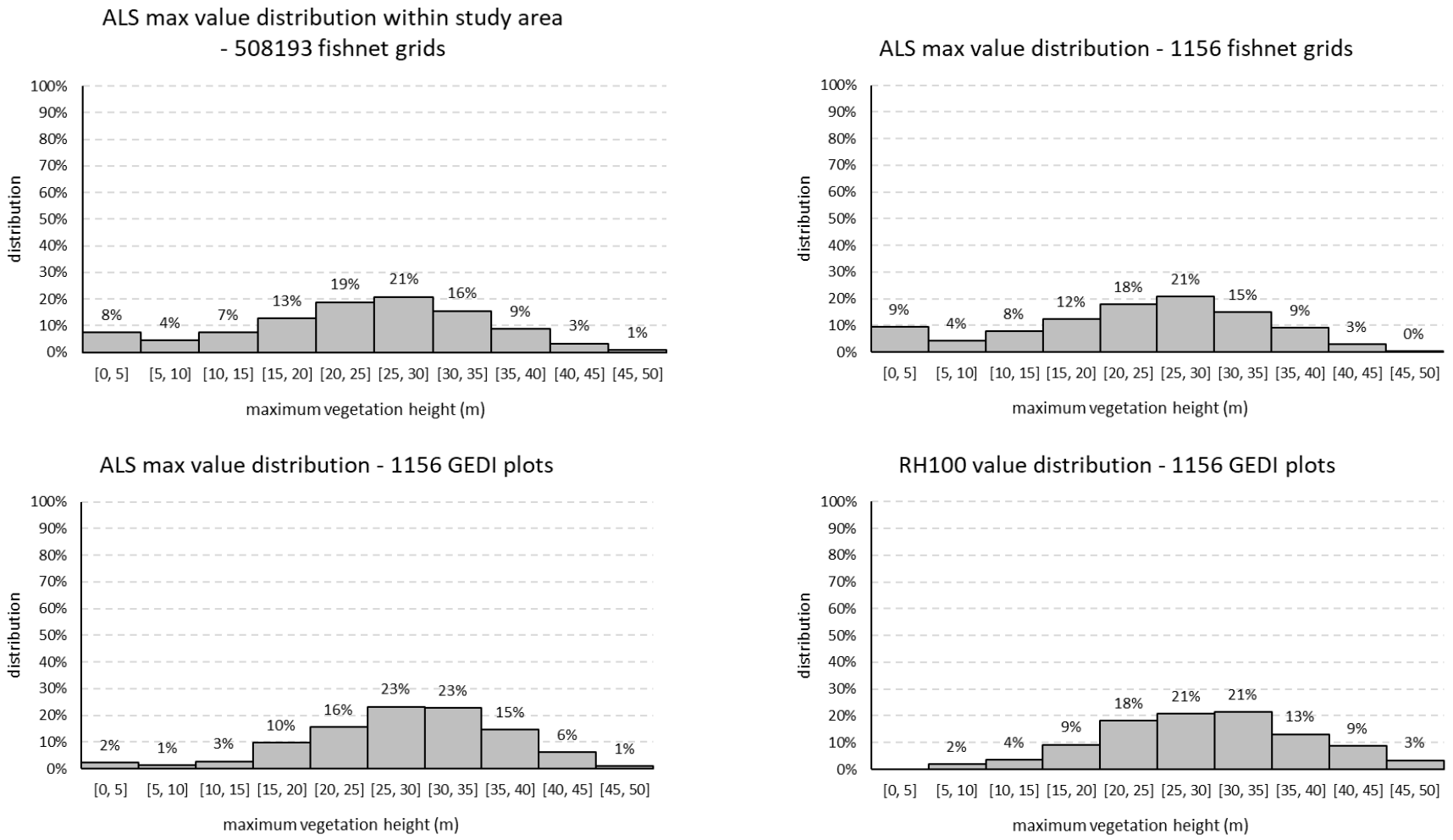

Figure 17: The value distribution of the training data and initial data for the maximum vegetation height. ALS max values for the whole study area (upper left); ALS max training samples based on the fishnet grids (upper right); ALS max training samples based on the GEDI plots (lower left) and for the GEDI RH100 training samples based on the GEDI plots (lower right).

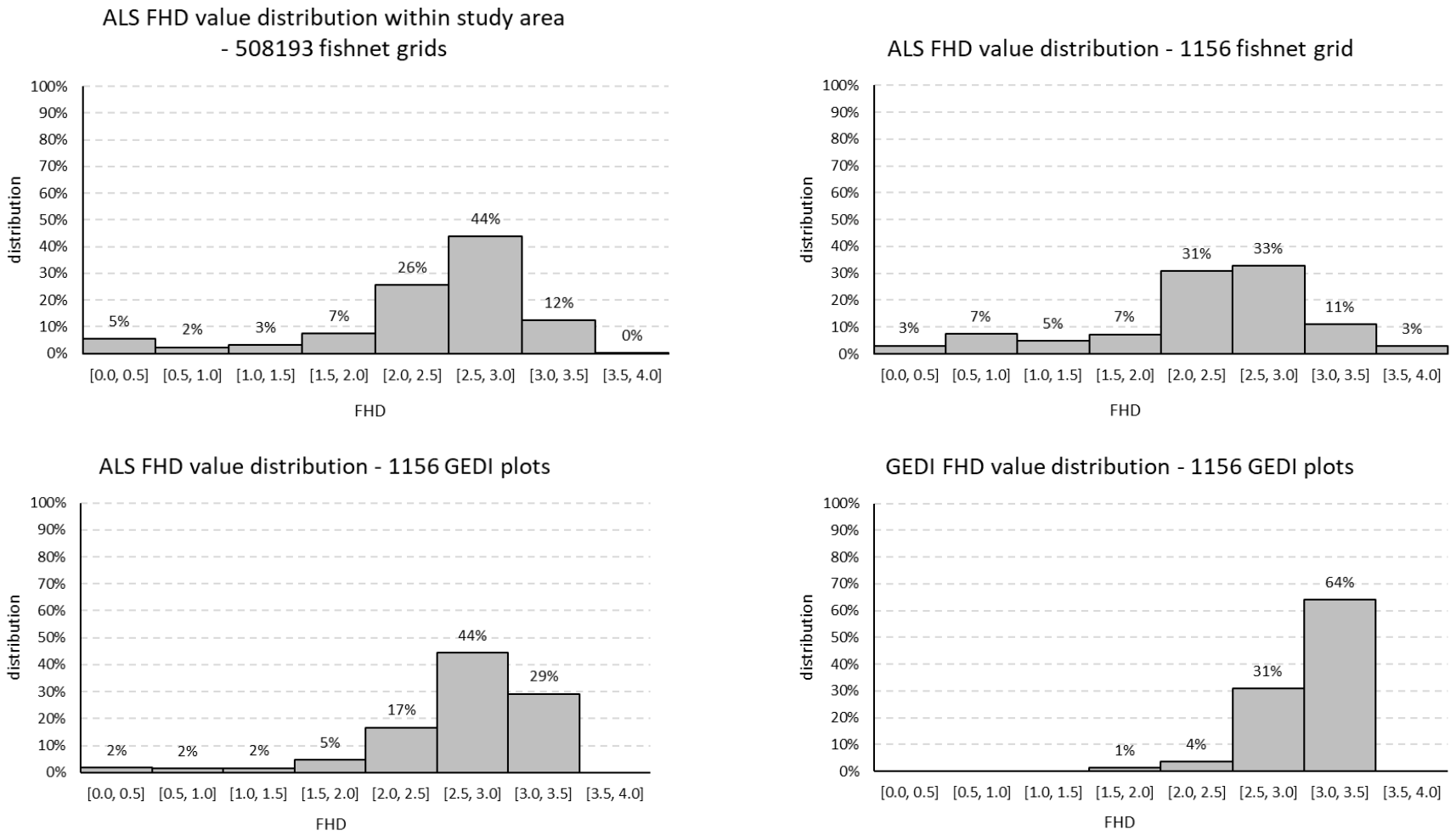

Figure 18: The value distribution of the training data and initial data for the FHD. ALS FHD values for the whole study area (upper left); ALS FHD training samples based on the fishnet grids (upper right); ALS FHD training samples based on the GEDI plots (lower left) and for the GEDI FHD training samples based on the GEDI plots (lower right).

6.4.2. Step 2: Random Forest Regression – Settings and Variations

The RF regressions were calculated with the IMPACT Tool, a software package developed by the Joanneum Research Graz. The following settings are used to calculate the regression in three steps. First, the values of the S1 and S2 images are extracted via the training samples. In this case the GEDI plots or the randomly selected fishnet grids for the ALS data. The class name for the values, that are then connected with the Sentinel data must be specified, for example RH50 or AGBD. In the next step the classifier, in this case the regressor, is trained with a repetition of 1000. The documents which are generated in this step contain information about the used features (bands). In the final step the regression rasters are calculated based on the used features. Due to the fact, that they are based on Sentinel images with a resolution of 10x10m per pixel, the resulting regressions also possess a resolution of 10x10m per pixel. The RF regressions are calculated for the GEDI vegetation parameters AGBD, FHD, RH50 and RH100 using the GEDI plots. The results are validated with the GEDI values through a cross-validation or the ALS data. Furthermore, RF regressions for the ALS mean, ALS max and ALS FHD are generated, using the GEDI plots or fishnet grid cells selected through a proportional stratified random sampling process as training data.

Five different input combinations of the Sentinel-1 and -2 raster files were tested (see Figure 13).

a) *All bands*: All available variables are used as input data, consisting of 120 S1 variables encompassing different orbits, polarisations, and texture features and 186 S2 spectral and VIs variables. In total 306 variables are utilized to calculate the regressions.
b) *4 Orbits*: Using all 186 S2 features. Furthermore, the averaged temporal statistics and GLCM bands for the two S1 polarisations are used. In total 216 variables are utilized to calculate the regressions.
c) *Top 10*: For each vegetation parameter the ten Sentinel variables with the highest coefficients of determination R^2 are utilized to calculate the regression.
d) *Positive Correlation (PC)*: For each vegetation parameter the ten variables with the highest positive Bravais-Pearson correlation coefficients R are utilized to calculate the regression.
e) *Negative Correlation (NC)*: For each vegetation parameter the ten variables with the highest negative Bravais-Pearson correlation coefficients R are utilized to calculate the regression.

The *all bands* variation is used to examine the influence of all available variables on the quality of the regression results. Since S1 images of four orbits are available, it was investigated whether calculating averaged temporal statistics and texture values for each polarisation based on the four orbits has an influence on the goodness of our results. Resulting in the variation *4 Orbits*. Also, the variations *Top 10*, *PC* and *NC* only employed ten Sentinel bands with the highest R^2 values and the highest positive and negative R values. This option was tested, because the IMPACT Tool often equipped bands with a high importance, that were not similar to the ones with high correlation results calculated in chapter 6.3. The (random) number ten was chosen as selecting criteria, because the correlation values for the different vegetation parameters differentiated significantly from each other, making it challenging to find a meaningful threshold based on the R^2 or R values. Furthermore, the combinations *PC* and *NC* were also tested, even though the R^2 is based on R and the distribution of the values is therefore the same. However, it is not possible to distinguish between a positive and negative correlation when analysing the R^2 values. It is investigated if it affects the quality of the regression results, whether they have been calculated with input variables, that only correlate positively or negatively with the relevant vegetation parameter.

6.4.3. Step 3: Validation

To evaluate the quality of a regression model, an error in its predictions has to be calculated. Commonly used error metrics are the RMSE and the Mean Absolute Error (MAE), which were both used here.

The RMSE is the standard deviation of the residuals (prediction errors), which are a measure of how far from the regression line data points are. It is calculated by obtaining the "total square error" as the sum of the individual squared errors (see Equation 4). The total square error is then divided by the number of used variables (n), which yields the mean-square error (MSE). The final step is to take the RMSE as the square root of the MSE (Willmott & Mastuura 2005, 80).

Equation 4: Root mean square error equation (Barnston 1992, 700)

$$RMSE_{f_0} = [\sum_{i=1}^{N} (z_{fi} - z_{oi})^2 / N]^{1/2}$$

- Z_f forecast
- Z_o observed valus
- n = sample size.
- $(z_{fi} – Z_{oi})^2$ = differences, squared

The MAE is the average of all absolute error values (see Equation 5).

Equation 5: Mean absolut error equation (Glen)

$$MAE = \frac{1}{n}\sum_{i=1}^{n}|x_i - x|$$

- x_i is the measurement,
- x is the true value.
- n = the number of errors,
- $|x_i - x|$ = the absolute errors.

Both RMSE and the MAE have the advantage to be dimensioned, therefore they "express[es] [the] average model-prediction error in the units of the variable of interest. [Furthermore,] these measures also have been used to represent the average difference (rather than the average error) when no set of estimates is known to be the most reliable" (Willmott & Mastuura 2005, 79). While some studies present the RMSE as a standard metric for model errors, others avoid the RMSE and only present the MAE. Even though both statistical metrics have been used for years to measure model performance, there is still no consensus on the most appropriate metric for model errors. The RMSE varies with the variability of the error magnitudes and is therefore more sensitive to outliers. The MAE however does not give more or less weight to different types of errors and instead the scores increase linearly with increases in error. But on the other hand, if the error distribution is expected to be Gaussian, the RMSE is more appropriate to represent the model performance than the MAE (Chai & Draxler 2014, 1247ff.). The coefficient of determination R^2 is well established in classical regression analysis as a regression error metric (Nagelkerke 1991, 691).

This work therefore uses the R^2, the RMSE and the MAE to evaluate the performance of the regression model. Depending on the training data used beforehand, different validation data is used. The regressions calculated for the ALS mean, ALS max and ALS FHD using fishnet grid cells as training samples, as well as the regressions generated for the ALS mean, ALS max and ALS FHD and the GEDI RH100, RH50 and FHD values using all GEDI plots as training samples are validated with the ALS mean, ALS max and the ALS FHD raster. The 10x10 fishnet created beforehand minus the higher subalpine area and the change areas, is used to accurately extract the regression and the validation values. With the regression values as the calculated/predicted and the validation values as the observed/measured values the RMSE, MAE and R^2 are computed.

Validating the regressions based on GEDI data (RH50, RH100, FHD, AGBD) via a cross-validation, utilizes the GEDI plots that have already been separated from the training data in

chapter 6.4.1. (see Figure 14). The separation was conducted so that there are no overlaps between training and validation data to guarantee independent validation. For each validation plot, the corresponding values are extracted from the calculated regressions. Then the error values RMSE, MAE and R^2 between the measured (validation) and predicted (regression) values are calculated. Since the GEDI data was split up into ten datasets consisting of training and validation samples to conduct a cross-validation, there are also ten error values for each vegetation parameter and each error metric. These are averaged so that only one (mean) RMSE, MAE and R^2 value is available for each parameter.

6.5. Further Analysis

To get a more differentiated view on the quality of both the initial ALS and GEDI data and the calculated regression results, it makes sense to also consult other, completely independent data sources.

6.5.1. Comparing AGBD Regression Results with existing Forest Inventory Data

Since it was not possible to calculate corresponding AGBD values based on the ALS data, the AGBD regressions can only be calculated and validated using the GEDI data. Thus, the comparison between airborne and spaceborne LiDAR data is missing for this vegetation parameter. To be able to ensure a comparison of the GEDI AGBD results with an external data source, the forest inventory data from the stations 700 and 2900 of the LTER initiative (EAA 2022) are utilized. Both stations are located outside the study area where the original GEDI data is available. Thus, only a comparison with the AGBD regression results can be made, as they are calculated using the Sentinel data, which also covers the two stations. AGBD values from the forest inventory at these two stations were compared to the respective regression values (see Figure 19) and the deviation between calculated AGBD and the measured AGBD can be determined.

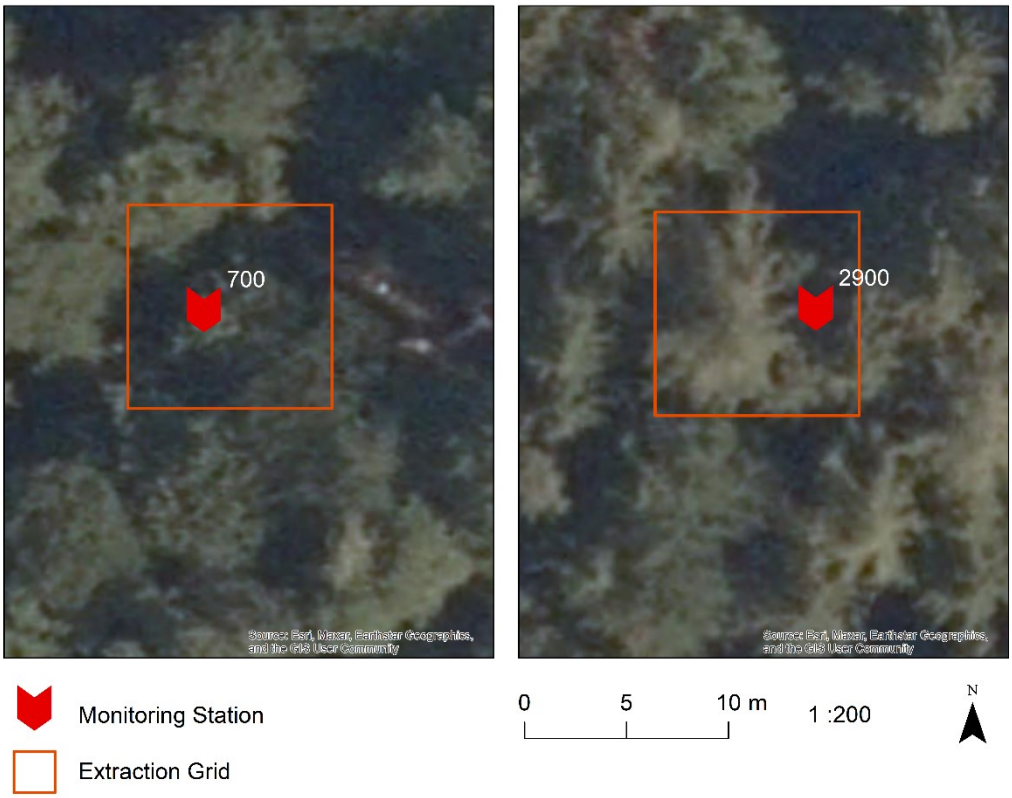

Figure 19: Pixel extent of the AGBD regression that are congruent with the two forest inventory stations.

6.5.2. Analysing the Influence of Study Area Characteristics

The influence of the study area characteristics on the error distribution of the regression results was also investigated. The three characteristics TCD, DLT and slope gradient were examined. Each characteristic is divided into different classes. The TCD is sorted into the four classes 0-25%; 25%-50%; 50-75% and 75-100%. The DLT is classified as no forest, broadleaved trees and coniferous trees. The slope gradient is also divided into four classes 0-20°; 20-40°; 40-60° and 60-80°. For each class of the study area characteristics the RMSE of the four vegetation parameters is calculated separately. The RMSEs are then compared between the different classes, and it is analyzed if there is an emerging trend.

A similar method was used by Adam et al. (2020) when analysing the influence of environmental parameters on the accuracy of GEDI canopy height estimates.

6.5.3. Visual Analysis of the Field Plots

By visually analysing and interpreting the collected field data, it is possible to juxtapose the original and the predicted data values (GEDI & ALS) for all four vegetation parameters with the actual conditions on site.

It is analyzed what different types of tree species are found on respective plots and which forest type results from it. Furthermore, the number of tree layers and the expression of the vertical structure are estimated. Due to time constraints, no precise height measurements of individual trees could be made on the respective plots. However, it was possible to provide a rough canopy height estimate by means of visual interpretation.

7. Results

7.1. Correlation

The three different extraction methods were tested for the parameters ALS mean, ALS max, RH50 and RH100 (see Figure 12). The R²s between the parameters and the Sentinel variables were calculated and compared. In Table 9 the minimum and maximum R² results for each method are listed. They achieve similar results for each parameter with very little variation. Method A (Zonal statistics) has a better R² maximum value for parameter ALS mean compared to both method B. and method C. and a higher R² maximum value for parameter ALS max and RH100 compared to method C. Therefore, this method is used for all the following results.

Table 9: Assessment of the extraction methods according to their R² minimum and maximum values

	A. Zonal statistics		B. Weighted mean		C. Center of footprint	
	R^2 - minimum	R^2 - maximum	R^2 - minimum	R^2 - maximum	R^2 - minimum	R^2 - maximum
ALS mean	0.00	0.45	0.00	0.39	0.00	0.43
RH50	0.00	0.20	0.00	0.20	0.00	0.20
ALS max	0.00	0.20	0.00	0.21	0.00	0.19
RH100	0.00	0.11	0.00	0.11	0.00	0.10

7.1.1. Correlation between ALS mean, ALS max or ALS FHD and Sentinel Bands based on Fishnet Grids

First of all, the coefficients of determination R^2 between the mean (ALS mean) and maximum (ALS max) vegetation height and the Sentinel variables for the whole research area were calculated for the spatial resolution 10x10 m per pixel. The ten highest R^2 results for ALS mean covered a value range of 0.33 to 0.38 and for ALS max a value range of 0.22 up to 0.26. It was furthermore investigated, if the tree cover density or the type of forest stand (broad leaved or coniferous) has an impact on the correlation. For ALS mean, as well as ALS max the results showed, that excluding areas with lower tree cover density or dividing the area up into the different forest types always led to a decrease of the R^2 results (see Table 29 and Table 30). The importance of the spatial resolution was also examined by calculating for ALS mean as well as ALS max the R^2 values for the resolution 10x10, 30x30 and 100x100 m per pixel (see Table 29, Table 30 and Table 31). ALS mean experiences a lot more improvement if the spatial resolution is downscaled (best results: 0.38 (10x10) – 0.44 (30x30) – 0.55 (100x100)), while ALS max experiences a deterioration of its results (best results: 0.26 (10x10) – 0.20 (30x30)

– 0.19 (100x100)). It can be said, that a larger spatial resolution leads to a higher disparity between correlation results for ALS mean and max.

Due to the first regression results showing a high susceptibility to errors in areas with mountain pine, the higher subalpine zone was excluded from the research area. The R^2 values were again calculated for ALS mean, ALS max as well as ALS FHD, but this time only for fishnet grids (10x10) outside of the high subalpine zone (see Figure 8). The ten best R^2 values for ALS mean ranged from 0.33 to 0.38 and ALS max ranged from 0.22 to 0.25 and hardly differ from the results calculated using the whole area (see Table 10 and Table 11). The results for ALS FHD range from 0.16 to 0.27 (see Table 12).

Overall, indices based on S2 mostly reap the highest correlation. Hereby the mean band of the NDVI6 has the highest results for almost every correlation between ALS mean and Sentinel. The exception is the correlation between ALS mean and Sentinel, both with a spatial resolution of 30x30. Here the median band of NLVI achieves the highest result. For ALS max the median band of NLVI most often has the highest correlation, but the best R^2 results are also achieved with the mean band of the NDVI6. ALS FHD has the strongest correlations with the S2 multispectral bands vegetation red edge (B5), green (B3), shortwave infrared (B12), red (B4) and shortwave infrared-cirrus (B11), in particular the median and mean band of the vegetation red edge band. All S1 bands on the other hand performed very poor (≤ 0.03) (see Table 32 and Table 33). One can also observe that the mean band of the temporal statistics bands most commonly achieve the highest results, followed by the median bands.

Furthermore, the correlation coefficient R was calculated for the ALS mean, ALS max and ALS FHD with the resolution 10x10 and excluding the high subalpine zone. R enables one to differentiate between a positive and negative correlation. The positive correlation for ALS mean covered a value range of 0.57 to 0.61 indicating a moderate to strong correlation and for ALS max a value range of 0.47 to 0.50 indicating a moderate correlation, while the negative correlation values for ALS mean ranged from -0.42 to -0.57 (moderate) and for ALS max from -0.32 to -0.46 (weak to moderate) (see Table 10 and Table 11). The ten highest positive correlation values for ALS FHD cover a value range of 0.28 to 0.38, showcasing a weak correlation between the ALS based FHD values and the Sentinel data. The ten best negative correlation values for ALS FHD start at -0.40 and reach up to -0.52, indicating a moderate correlation (see Table 12).

Indices that had a high positive correlation for ALS max and ALS mean, as well as ALS FHD were NDVI6, NDVI7, NLVI and NDVI8a. Furthermore, the mean and median band of NDWI had a high negative correlation with both ALS max and ALS mean. The red bands (B4) and the first vegetation red edge band (B5) had high negative correlation values with ALS mean, ALS max and ALS FHD.

Also, one can observe that the bands with the ten highest R^2 results for ALS mean are the same bands with the ten highest positive correlations. A similar situation can be observed for ALS FHD. Hereby the ten bands with the highest R^2 results are the same bands with the ten best negative correlation values.

Table 10: The ten highest R^2, the ten highest positive and highest negative R values between ALS mean and individual Sentinel variables for the study area without the higher subalpine zone (fishnet 10x10). The Sentinel variables achieving the ten highest R^2 and positive R values are the same.

ALS mean								
Parameter	Temporal Statistics Band	R^2	Parameter	Temporal Statistics Band	R (positive)	Parameter	Temporal Statistics Band	R (negative)
NDVI6	mean	0.38	NDVI6	mean	0.61	NDWI	mean	-0.57
NDVI6	med	0.37	NDVI6	med	0.61	NDWI	med	-0.55
EVI	mean	0.37	EVI	mean	0.61	NDII7	max	-0.52
EVI	med	0.36	EVI	med	0.60	B4	mean	-0.50
NLVI	med	0.34	NLVI	med	0.58	NDII7	mean	-0.50
NDVI7	mean	0.33	NDVI7	mean	0.57	NDII7	med	-0.48
NDVI8a	mean	0.33	NDVI8a	mean	0.57	B4	med	-0.48
NDVI	mean	0.33	NDVI	mean	0.57	NDII5	max	-0.47
SAVI	mean	0.33	SAVI	mean	0.57	B5	med	-0.44
MSAVI	mean	0.33	MSAVI	mean	0.57	NDWI	max	-0.44

Table 11: The ten highest R^2, the ten highest positive and highest negative R values between ALS max and individual Sentinel variables for the study area without the higher subalpine zone (fishnet 10x10).

ALS max								
Parameter	Temporal Statistics Band	R^2	Parameter	Temporal Statistics Band	R (positive)	Parameter	Temporal Statistics Band	R (negative)
NDVI6	mean	0.25	NDVI6	mean	0.50	B4	mean	-0.50
NLVI	med	0.25	NLVI	med	0.50	B5	med	-0.48
B4	mean	0.25	NDVI6	med	0.50	B4	med	-0.47
NDVI6	med	0.25	NDVI8a	mean	0.48	B5	mean	-0.46
NDVI8a	mean	0.23	NDVI7	mean	0.48	B3	mean	-0.46
NDVI7	mean	0.23	EVI	mean	0.47	B3	med	-0.46
B5	med	0.23	NDVI8a	med	0.47	NDWI	mean	-0.46
B4	med	0.22	NDVI	mean	0.47	NDWI	med	-0.45
EVI	mean	0.22	NDVI7	med	0.47	B2	mean	-0.42
NDVI8a	med	0.22	SAVI	mean	0.47	B2	med	-0.40

Table 12: The ten highest R^2, the ten highest positive and highest negative R values between ALS FHD and individual Sentinel variables for the study area without the higher subalpine zone (fishnet 10x10). The Sentinel variables achieving the ten highest R^2 and negative R values are the same.

ALS FHD								
Parameter	Temporal Statistics Band	R^2	Parameter	Temporal Statistics Band	R (positive)	Parameter	Temporal Statistics Band	R (negative)
B5	med	0.27	TCW	min	0.38	B5	med	-0.52
B5	mean	0.26	TCW	med	0.36	B5	mean	-0.51
B3	mean	0.22	TCW	mean	0.36	B3	mean	-0.47
B3	med	0.22	NLVI	med	0.33	B3	med	-0.47
B12	med	0.17	NDVI6	med	0.30	B12	med	-0.42
B4	mean	0.17	NDVI6	mean	0.29	B4	mean	-0.41
B12	mean	0.17	NLVI	mean	0.29	B12	mean	-0.41
B11	med	0.17	NDVI8a	mean	0.29	B11	med	-0.41
B4	med	0.16	NDVI7	mean	0.29	B4	med	-0.40
B12	max	0.16	NDVI8a	med	0.28	B12	max	-0.40

7.1.2. Correlation between ALS mean, ALS max, ALS FHD, RH50, RH100, AGBD or FHD and Sentinel Bands based on GEDI Plots

The GEDI plots were utilized to extract the mean value for each individual Sentinel variable and for ALS mean, ALS max and ALS FHD. The R^2 and R between the vegetation parameters based on GEDI (RH50, RH100, FHD, AGBD) or ALS (ALS mean, ALS max, ALS FHD) and the individual Sentinel variables were computed.

For the GEDI based parameters (see Table 13), RH50 achieved the highest R^2 values with a value range for the ten highest R^2 results between 0.14 and 0.16. FHD and AGBD are covering a similar range of values, with 0.06 to 0.11 for FHD and 0.08 to 0.11 for AGBD. RH100 showcased the poorest results, covering a value range of 0.05 to 0.08. The R^2 results for the ALS based parameters performed a lot better compared to the GEDI based parameters. ALS FHD covered a value range of 0.11 up to 0.19, ALS max ranged from 0.13 to 0.20 and ALS mean achieved the highest R^2 results (0.34 to 0.41), which were even higher, than the R^2 values calculated for ALS mean based on the fishnet grids.

Generally, individual variable correlation is very low for vegetation parameters based on GEDI and also the ALS max and ALS FHD. This suggests that including multiple bands for useable results is inevitable.

Most frequently the median band of the NLVI appears to be among the 10 highest R^2 results, except for ALS FHD. For RH50, AGBD and ALS mean the median band of the NLVI obtains the highest R^2 values. Furthermore, the results for the maximum vegetation height (RH100 and ALS max) and the FHD, both GEDI and ALS, appear to achieve the highest R^2 values for the mean and median bands of the single S2 bands blue (B2) and red (B4), but especially for

green (B3) and vegetation red edge (B5). Again, calculating the R^2 with S1 variables results in very low values (≤ 0.03) for all parameters (see chapter Appendix B Table 34).

When evaluating the positive and negative R values naturally the parameter with the highest positive and negative correlations is ALS mean. Showing moderate to strong positive correlations (0.58 to 0.64) and moderate negative correlations (-0.51 to -0.57), with similar bands as the correlations between ALS mean and Sentinel using the fishnet grids. ALS max, as well as ALS FHD show weak positive correlations (ALS max: 0.34 to 0.38/ALS FHD: 0.28 to 0.31) and weak to moderate negative correlations (ALS max: -0.35 to -0.45/ALS FHD: -0.33 to -0.44). Furthermore, the R values for ALS mean, ALS max and ALS FHD based on the fishnet grids and the ones for ALS mean, ALS max and ALS FHD based on the GEDI plots are compared. This reveals, that the positive correlation for ALS max using the fishnet grid (0.47 to 0.50) achieves higher values than the one using the GEDI plots (0.34 to 0.38). The negative correlation for ALS max using the fishnet grid (-0.40 to -0.50), is also better, than the one using the GEDI plots (-0.35 to -0.45). The positive correlation values for ALS FHD roughly cover the same value range (grid: 0.28 to 0.38/plots: 0.28 to 0.31), while the negative correlation values clearly show, that ALS FHD using the fishnet grid achieves better results (grid: -0.40 to -0.52/plots: -0.33 to -0.44). For the ALS mean based on the fishnet grid as well as the GEDI plots the negative (grid: -0.44 to -0.57/plots: -0.51 to -0.57) as well as the positive (grid: 0.57 to 0.61/plots: 0.58 to 0.64) correlation results cover a similar value range (see Table 10, Table 11, Table 12 and Table 13).

The vegetation parameter based on the GEDI data with the highest R values is RH50, showcasing a weak to moderate positive correlations (0.37 to 0.41) and weak negative correlations (-0.32 to -0.38). RH100 achieves weak results for the positive (0.22 to 0.27), as well as the negative (-0.22 to -0.28) correlation. So do AGBD and FHD. But it can be noted, that FHD has slightly better results for the negative (-0.25 to -0.33), than the positive (0.22 to 0.27) correlation. A similar observation can be made for AGBD, only here the positive correlation (0.29 to 0.33) achieves better results than the negative correlation (-0.26 to -0.28) (see Table 13).

The median band for the NLVI has the highest positive correlation values for all parameters except for the ALS FHD, which obtains its highest positive R value for the median band of MSAVI2. RH100, ALS max, FHD and ALS FHD show the best negative correlations for the median and mean bands of the single S2 bands green (B3), first vegetation red edge (B5) and red (B4). Furthermore, the ten highest R^2 results for ALS mean and GEDI AGBD are congruent to their ten highest positive correlation results. For the parameter ALS FHD the ten highest R^2 results are the same as the ten best negative correlation values.

Table 13: The ten highest R^2 values between GEDI (RH50, RH100, FHD, AGBD) or ALS (AL mean, ALS max, FHD) based parameters and individual Sentinel variables for the research area without the high subalpine zone (fishnet 10x10). The ten highest positive and negative Pearson correlation values between GEDI (RH50, RH100, AGBD, FHD) or ALS (ALS mean, ALS max, ALS FHD) based parameters and individual Sentinel bands for the research area without the high subalpine zone (fishnet 10x10).

GEDI RH50								
Parameter	Temporal Statistics Band	R^2	Parameter	Temporal Statistics Band	R (positive)	Parameter	Temporal Statistics Band	R (negative)
NLVI	med	0.16	NLVI	med	0.41	NDII7	min	-0.38
EVI	mean	0.16	EVI	mean	0.40	NDII5	min	-0.36
NDVI6	mean	0.16	NDVI6	mean	0.40	NDWI	mean	-0.36
EVI	med	0.16	EVI	med	0.40	NDWI	med	-0.35
NDVI6	min	0.15	NDVI6	min	0.39	PSRI	min	-0.35
EVIRE1	med	0.15	EVIRE1	med	0.39	NDII7	mean	-0.35
NDVI6	med	0.15	NDVI6	med	0.39	NDII7	med	-0.33
MSI	min	0.15	MSI	min	0.39	NDII5	mean	-0.32
NDII7	max	0.14	SAVI	mean	0.37	B4	mean	-0.32
SAVI	mean	0.14	MSAVI	mean	0.37	MSI	sd	-0.32

ALS mean								
Parameter	Temporal Statistics Band	R^2	Parameter	Temporal Statistics Band	R (positive)	Parameter	Temporal Statistics Band	R (negative)
NLVI	med	0.41	NLVI	med	0.64	NDWI	mean	-0.57
NDVI6	mean	0.37	NDVI6	mean	0.61	NDWI	med	-0.56
NDVI6	med	0.36	NDVI6	med	0.60	B4	mean	-0.56
EVI	mean	0.36	EVI	mean	0.60	NDII7	max	-0.55
EVI	med	0.36	EVI	med	0.60	B4	med	-0.55
NDVI7	mean	0.35	NDVI7	mean	0.59	B3	med	-0.54
NDVI8a	mean	0.35	NDVI8a	mean	0.59	B5	med	-0.54
NDVI	mean	0.34	NDVI	mean	0.58	NDII7	mean	-0.53
SAVI	mean	0.34	SAVI	mean	0.58	NDII7	med	-0.52
MSAVI	mean	0.34	MSAVI	mean	0.58	B3	mean	-0.51

GEDI RH100								
Parameter	Temporal Statistics Band	R^2	Parameter	Temporal Statistics Band	R (positive)	Parameter	Temporal Statistics Band	R (negative)
B5	med	0.08	NLVI	med	0.27	B5	med	-0.28
NLVI	med	0.07	NLVI	mean	0.26	B5	mean	-0.27
B5	mean	0.07	NDVI7	mean	0.23	B3	med	-0.27
B3	med	0.07	NDVI6	mean	0.23	B3	mean	-0.26
B3	mean	0.07	NDVI8a	mean	0.23	B4	mean	-0.26
B4	mean	0.07	NDVI6	min	0.23	PSRI	min	-0.24
NLVI	mean	0.07	NDVI6	med	0.22	B4	med	-0.24
PSRI	min	0.06	EVIRE1	mean	0.22	B2	mean	-0.23
B4	med	0.06	NDVI7	med	0.22	B4	max	-0.23
NDVI7	mean	0.05	EVIRE1	med	0.22	B2	med	-0.22

ALS max								
Parameter	Temporal Statistics Band	R^2	Parameter	Temporal Statistics Band	R (positive)	Parameter	Temporal Statistics Band	R (negative)
B3	med	0.20	NLVI	med	0.38	B3	med	-0.45
B5	med	0.20	NDVI7	med	0.36	B5	med	-0.45
B3	mean	0.19	NDVI8a	med	0.36	B3	mean	-0.44
B5	mean	0.18	NDVI8a	mean	0.36	B5	mean	-0.43
B4	mean	0.18	NDVI7	mean	0.35	B4	mean	-0.42
B4	med	0.18	MSAVI2	mean	0.35	B4	med	-0.42
B2	med	0.16	MSAVI2	med	0.35	B2	med	-0.40
B2	mean	0.16	NDVI	med	0.34	B2	mean	-0.40
NLVI	med	0.14	MSAVI	med	0.34	B2	min	-0.36
B2	min	0.13	SAVI	med	0.34	**B12**	med	-0.35

GEDI FHD								
Parameter	Temporal Statistics Band	R^2	Parameter	Temporal Statistics Band	R (positive)	Parameter	Temporal Statistics Band	R (negative)
B5	med	0.11	NLVI	med	0.27	B5	med	-0.33
B5	mean	0.11	TCW	min	0.26	B5	mean	-0.33
B3	mean	0.09	NLVI	mean	0.24	B3	mean	-0.30
B3	med	0.09	NDVI6	min	0.24	B3	med	-0.30
B4	mean	0.08	NDVI7	min	0.23	B4	mean	-0.28
NLVI	med	0.07	NDVI6	mean	0.22	B12	max	-0.26
TCW	min	0.07	NDVI7	mean	0.22	B12	mean	-0.25
B12	max	0.07	NDVI8a	mean	0.22	B5	min	-0.25
B12	mean	0.06	NDVI8a	min	0.22	B4	med	-0.25
B5	min	0.06	NDVI6	med	0.22	B5	max	-0.25

ALS FHD								
Parameter	Temporal Statistics Band	R^2	Parameter	Temporal Statistics Band	R (positive)	Parameter	Temporal Statistics Band	R (negative)
B3	med	0.19	MSAVI2	med	0.31	B3	med	-0.44
B3	mean	0.18	MSAVI2	mean	0.31	B3	mean	-0.42
B2	med	0.17	NDVI8a	med	0.30	B2	med	-0.41
B5	med	0.17	NDVI7	med	0.30	B5	med	-0.41
B2	mean	0.16	NDVI	med	0.29	B2	mean	-0.40
B4	med	0.16	SAVI	med	0.29	B4	med	-0.39
B5	mean	0.15	MSAVI	med	0.29	B5	mean	-0.39
B4	mean	0.15	NDVI8a	mean	0.28	B4	mean	-0.38
TCB	med	0.11	NDVI7	mean	0.28	TCB	med	-0.33
B12	med	0.11	GNDVI	med	0.28	B12	med	-0.33

GEDI AGBD								
Parameter	Temporal Statistics Band	R^2	Parameter	Temporal Statistics Band	R (positive)	Parameter	Temporal Statistics Band	R (negative)
NLVI	med	0.11	NLVI	med	0.33	B4	mean	-0.28
NDVI6	min	0.10	NDVI6	min	0.31	PSRI	min	-0.28
NDVI6	mean	0.09	NDVI6	mean	0.31	NDWI	mean	-0.27
EVI	mean	0.09	EVI	mean	0.30	PSRI	max	-0.27
EVIRE1	med	0.09	EVIRE1	med	0.30	NDII7	max	-0.27
NDVI6	med	0.09	NDVI6	med	0.30	NDWI	med	-0.27
NDVI7	mean	0.09	NDVI7	mean	0.30	B5	med	-0.27
NDVI8a	mean	0.09	NDVI8a	mean	0.29	B4	max	-0.26
EVI	med	0.09	EVI	med	0.29	B4	med	-0.26
NDVI	mean	0.08	NDVI	mean	0.29	B3	med	-0.26

Following up, the ten highest R^2 and R (positive and negative) results for each parameter are used for the modelling of the regressions (variable combinations: *Top 10, PC, NC*). Except for ALS mean and max based on the fishnet grid and ALS mean and GEDI AGBD based on the GEDI plots, that share the same results between the R^2 and positive R values. And ALS FHD, where the ten highest R^2 results are the same as the ten best negative correlation values. Here only the R^2 results are employed for the calculation of the regression. So only the variable combination *Top 10* is tested.

S1 correlations continuously performed very poorly for all parameters, no matter if based on the fishnet grid or the GEDI plots. Nonetheless the S1 bands were also employed for the RF regression, due to the fact, that the RF classifier automatically selects the most important features in the regression process.

7.1.3. Comparing Correlation Results and Used Features

The previous chapter investigated which Sentinel variables and vegetation parameters have a particularly strong correlation. This chapter examines if the correlation is crucial for the calculation of the regressions.

When computing the regressions with RF in the IMPACT Tool, a .pkl file and a .txt file are generated in the intermediate step Train a Classifier. Within the text file the features selected for further calculations are listed, as well as the feature importance. The feature importance describes the relative degree of usefulness of a specific variable for a current model and prediction (Liaw & Wiener 2002, 18).

The method *Top 10* only utilizes the ten variables with the highest R^2 values to compute the regressions. Therewith the feature importance of the input variables for the method *Top 10* is examined for each vegetation parameter and compared to the R^2 results.
Furthermore, when using all Sentinel variables for the method *all bands* to calculate the regression, only a handful of bands are selected as input variables and endowed with a certain feature importance by the IMPACT Tool. To investigate, if these variables are consistent with the bands with the strongest correlations, the used features and the feature importance for *all bands* and *Top 10* are compared. This shows how significant a high correlation between individual bands and the respective vegetation parameters is when the RF algorithm is free to choose.
Also, the used features and the feature importance for the cross-validation are examined, when using the method *all bands*. It is analyzed how often features are used when the model is run through ten times with different training datasets. An average feature importance is calculated based on the individual importance values of the different training runs.

7.1.3.1. Mean Vegetation Height

For the mean vegetation height, the used features and the feature importance for the three variations; ALS mean data within the fishnet grids, ALS mean data within the GEDI plots and RH50 data within the GEDI plots were analysed (see Figure 20).
First of all, the feature importance of the method *Top 10* is compared to the R^2 results (see Table 10 and Table 13). ALS mean (fishnet) achieves the highest feature importance 40% for the median band of NLVI which has a R^2 of 0.34. The second highest feature importance has the mean band of NDVI6 with 32%. This band has the highest correlation with $R^2 = 0.38$. The remaining bands reach a feature importance of 1-9% and cover R^2 values of 0.33 to 0.37. For ALS mean (plots) it is noticeable, that although all 10 bands for the method *Top 10* were entered into the algorithm, only six were selected. Particularly the mean band of NDVI6 has a significant feature importance with 71%. Also, it reaches the second highest correlation with $R^2 = 0.37$. The median band of NLVI has the highest R^2 value with 0.40, but only reaches a feature importance of 18%. For the parameter RH50 the mean band of NDVI6 again has the highest feature importance with 54% and the third highest R^2 value with 0.16. The other bands all have a feature importance between 3-9%. All three variations (ALS fishnet, ALS plot, GEDI) use the mean bands of EVI and NDVI6 and the median bands of EVI, NDVI6 and NLVI. Furthermore, the mean bands of NDVI8a and SAVI are used twice. However, the remaining bands only occur individually for each variation. The highest feature importance for all three variations is achieved for the mean band of NDVI6 or the median band of NLVI.

Further, the used features and feature importance for the method *all bands* are analysed and compared to the method *Top 10*. For the variation ALS mean (fishnet) ten features are used. The mean band of NDVI6 has the highest feature importance with 27%, followed by the median band of NLVI with 20% and the mean red band (B4) with 12%. The other variables only record a feature importance of 2-8%. ALS mean (plots) only employs eight features and the feature importance is distributed amongst the mean band of NDVI6 (27%) and the median (26%) and mean (23%) red band (B4). The remaining variables have a feature importance between 3-6%. For RH50 eleven features are used. It is noticeable, that five texture bands are utilized even though they all only achieve a feature importance between 4- 5%. The most significant feature importance again is achieved for the mean band of NDVI6 with 46%. The minimum band of PSRI has the second highest feature importance with 10%. For the method *all bands* the mean red band (B4) and the mean band of NDVI6 are used in all three variations. The median green (B3), red (B4) and first vegetation red edge (B5) bands and the minimum band for PSIR are used for two variations. All other bands were only used for one of the variations.

Comparing the variable combinations *Top 10* and *all bands* it can be ascertained that the mean band of NDVI6 is used by all three variations (ALS fishnet, ALS plot, GEDI) for both variable combinations and has the highest feature importance values. The median bands of NDVI6 and NLVI are also utilized by the two variable combinations for the variation ALS mean (fishnet). Otherwise, there is no feature overlap between the two variable combinations.

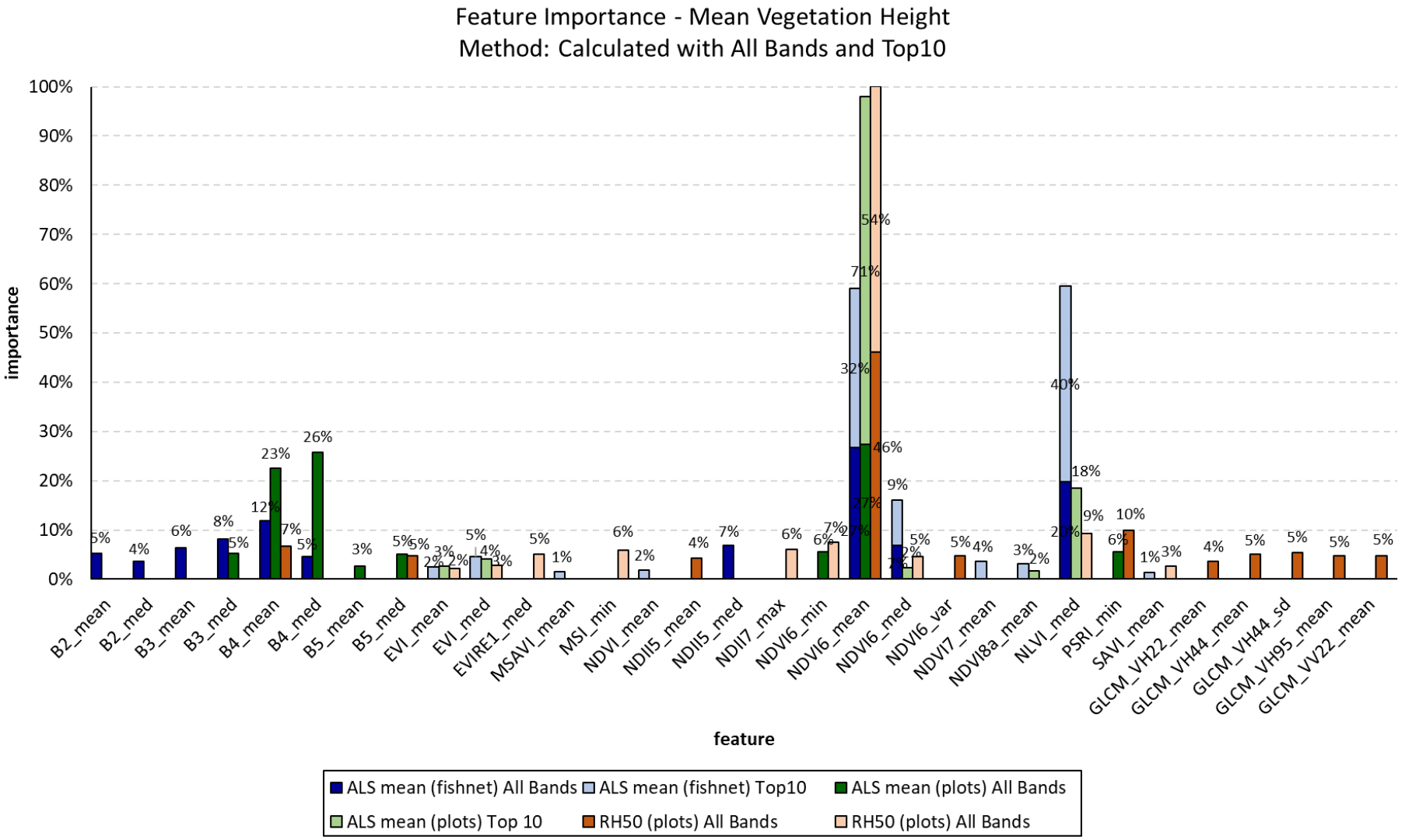

Figure 20: Comparing the used features and the feature importance for the mean vegetation height between the methods all bands and Top 10 and the three variations ALS mean (fishnet), ALS mean (plots) and GEDI RH50 (plots).

Furthermore, the used features and feature importance for the cross-validation are analysed. Hereby, the results for RH50 using the method *all bands* are looked at (see Figure 21). RH50 uses the mean band for NDVI6, the minimum band for PSRI and the standard deviation band of the GLCM for VH44 for all ten regressions achieving an averaged feature importance of 35%, 11% and 9% respectively. For nine out of ten regressions the mean band of the GLCM for VH44 and VV22, the median band for the first vegetation red edge band (B5) and the median band for NDVI6 came into use, reaching importance values of respectively 6%, 6%, 7% and 11%. In total 23 different bands were employed for the calculation of the ten RH50 regressions.

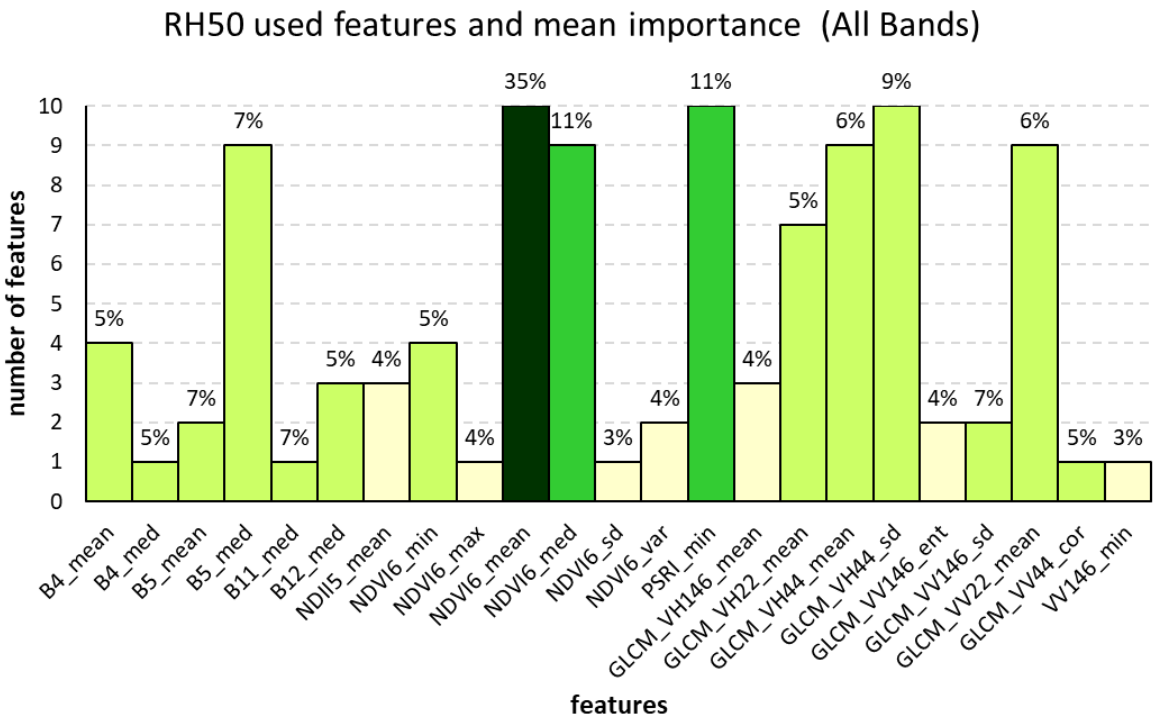

Figure 21: Frequency of used features and averaged feature importance when calculating the RH50 regressions via cross-validation employing all bands.

7.1.3.2. Maximum Vegetation Height

For the maximum vegetation height, the used features and the feature importance for the three variations; ALS max data within the fishnet grids, ALS max data within the GEDI plots and RH100 data within the GEDI plots are analysed (see Figure 22). The feature importance of the variable combination *Top 10* in relation to their respective R^2 (see Table 11 and Table 13) values is investigated.

ALS max (fishnet) has its highest feature importance 54% for the median first vegetation red edge band (B5) with a R^2 value of 0.23. Followed by the mean red band (B4) with a feature importance of 13% and a R^2 of 0.25. All other bands cover a feature importance of only 3-5%. ALS max (plots) achieves a feature importance of 50% and a R^2 value of 0.18 for the mean

first vegetation red edge band (B5). Furthermore, the median first vegetation red edge band (B5) has a feature importance of 17% and a R^2 of 0.25. The remaining bands have a feature importance between 2-7%. For RH100 the feature importance is not as heavily concentrated on a single band as for ALS max but distributed over several bands. The median first vegetation red edge band (B5) has the strongest feature importance with 19% and at the same time the highest R^2 value with 0.08. Followed by the minimum band for PSRI with a feature importance of 16% (R^2 = 0.06). Then comes the mean red band (B4) with a feature importance of 14% (R^2 = 0.079). Both the median band for NLVI (R^2 = 0.07) and the mean band for NDVI7 (R^2 = 0.05) achieve a feature importance of 10%. The remaining bands are distributed across a feature importance of 4-9 %.

Overall, all three variants use the mean and median red band (B4), the median first vegetation red edge band (B5) and the median band of NLVI. The highest feature importance is recorded for the mean and median first vegetation red edge band (B5).

Analysing the used features and feature importance for the method *all bands* it can be found that ALS max (fishnet) has the highest feature importance for the median green band (B3) with 30%, followed by the mean green band (B3) with 23%. Furthermore, the median first vegetation red edge band (B5) and the standard deviation band of the GLCM for VH44 both have a feature importance of 10%. The remaining bands achieve a feature importance of 4-6%. In total nine features are employed. ALS max (plots) registers its highest feature importance at 36% for the mean first vegetation red edge band (B5). The median first vegetation red edge band (B5) achieves a feature importance of 12%, while the other bands are located between 2-6%. In total sixteen features are used. For RH100 as many as twenty features are entertained. The one with the highest importance being the standard deviation band of GLCM for VH44 with 19%, followed by the median first vegetation red edge band (B5) with 11%. All other bands spread over a spectrum of 2-8%. For the method *all bands*, all three variations use the bands median first vegetation red edge (B5), the standard deviation band of GLCM for the orbits VH22 and VH44 and the minimum and median band of NDVI6. For each of the three variations, the variables recording the highest feature importance differentiate from each other.

Overall, only the median first vegetation red edge band (B5) is used with all three variations (ALS fishnet, ALS plots, GEDI) for the variable combinations *Top 10* as well as *all bands*. This variable also records high feature importance values for all three variations in both methods. Other used features that overlap between *Top 10* and *all bands* are the mean blue band (B2), the mean and median green band (B3), red band (B4) and NDVI6 and the minimum PSRI.

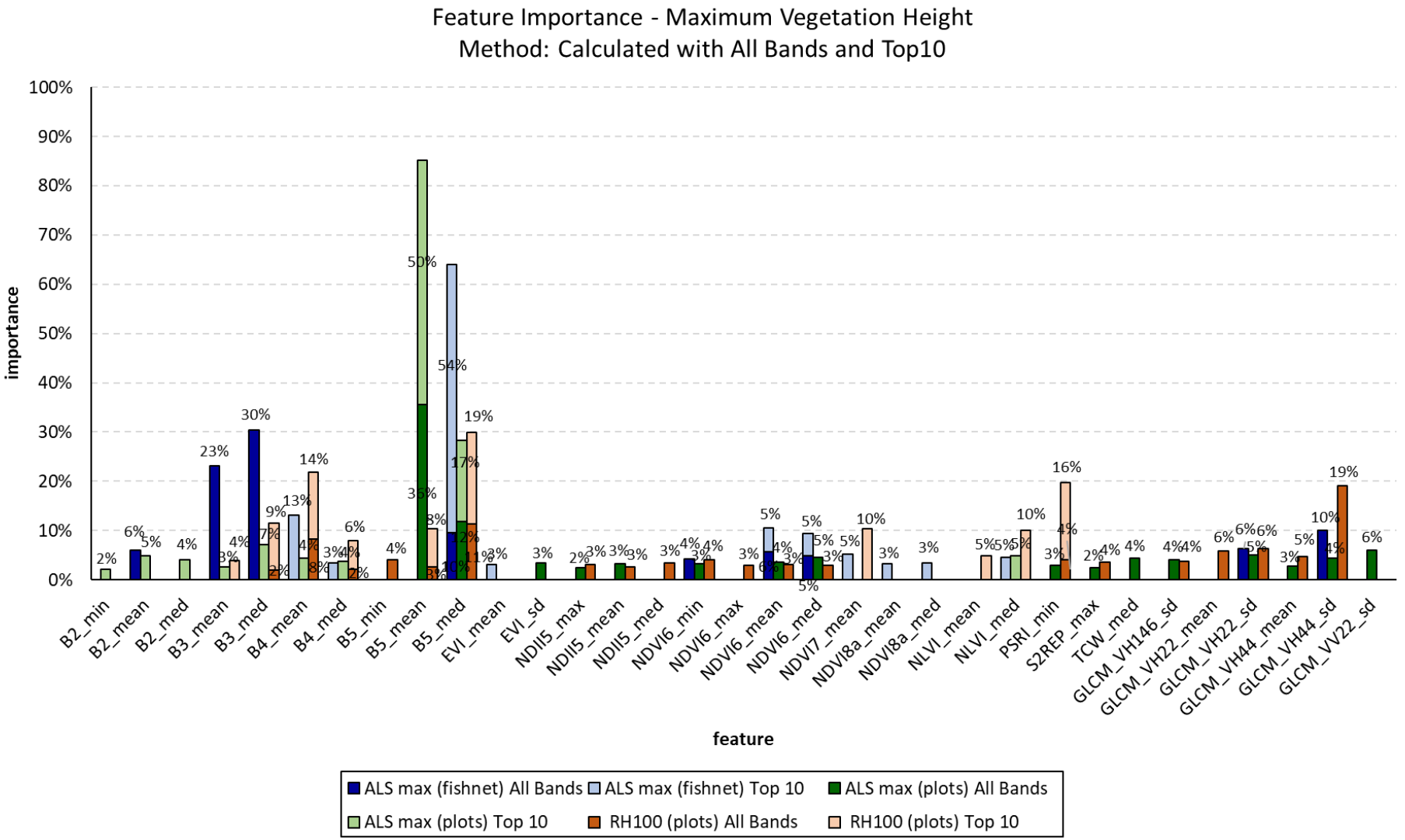

Figure 22: Comparing the used features and the feature importance for the maximum vegetation height between the methods all bands and Top 10 and the three variations ALS max (fishnet), ALS max (plots) and GEDI RH100 (plots).

The used features and feature importance for the cross-validation are also investigated (see Figure 23). Like the feature importance analysed before, the median first vegetation red edge band (B5) plays an important role. It is used for all ten regressions and has an average feature importance of 11%, which is relatively high compared to the other importance values. But the highest feature importance with 18% is given to the standard deviation band of the GLCM for the VH44. Other bands that are also used for each individual run of the RF model are the standard deviation band of the GLCM for the VH146 and the VH22 and the mean band of the GLCM for the VH22 and the VH44. Furthermore, the mean red band (B4), the minimum and mean band of the NDVI6 and the minimum band of PSRI are used for all ten regressions. Nine out of ten times the minimum first vegetation red edge band (B5) and the median band for NDII5 and NDVI6 are used. All these bands have roughly an averaged feature importance of around 5%. All in all, one can count 28 used features for the ten regressions.

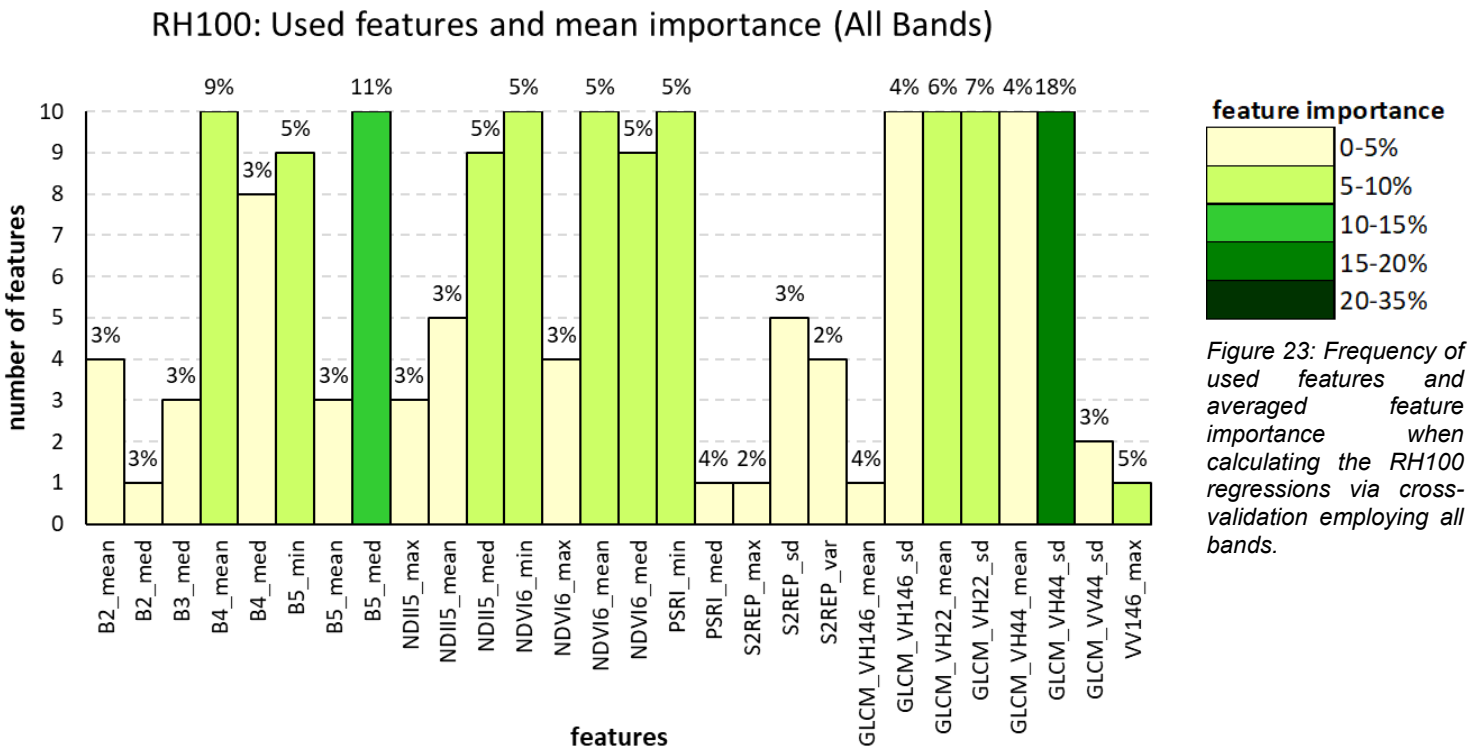

Figure 23: Frequency of used features and averaged feature importance when calculating the RH100 regressions via cross-validation employing all bands.

7.1.3.3. Foliage Height Diversity

For the FHD, the used features and the feature importance for the three variations; ALS FHD data within the fishnet grid, ALS FHD data within the GEDI plots and GEDI FHD data within the GEDI plots are analysed (see Figure 24). The feature importance of the variable combination *Top 10* in relation to their respective R^2 values (see Table 12 and Table 13) is investigated.

For the ALS FHD (fishnet) the median first vegetation red edge band (B5) has both the highest R^2 value (0.27) and the highest feature importance (35%). The median green band (B3) achieves the second highest feature importance with 24% (R^2 = 0.22). Both the mean green band (R^2 = 0.22) and the mean first vegetation red edge band (R^2 = 026) have a feature importance of 10%. The remaining bands cover a feature importance of 3-5% and R^2 values of 0.16-0.17. The two bands with the highest feature importance for the ALS FHD (plots) are the median and mean first vegetation red edge band (B5) with 31% and 30%, and R^2 values of 0.26 and 0.22. The median band of TCB, the SWIR band (B12) and the green band (B3) record a feature importance of 10%, 9% and 8% and a R^2 of 0.11, 0.11 and 0.19. The other bands are distributed between 2-3% and cover R^2 values between 0.15-0.18. Similar to RH100, the feature importance for GEDI FHD is not so heavily concentrated on a single band but is distributed over several variables. The minimum first vegetation red edge band (B5) has the highest feature importance with 23%, even though having the lowest correlation of the selected variables with R^2 = 0.06. Other bands achieving a relatively high feature importance are the median green band (B3) with 17% and a R^2 of 0.09, the mean red band (B4) with 17% and a R^2 of 0.08 and the median band of the NLVI achieving an importance of 11% and a R^2 of 0.07. The remaining bands cover a value range of 3-9% and R^2 of 0.06-0.11.

For all three variations (ALS fishnet, ALS plots, GEDI) different temporal statistics bands (minimum, mean, median) of the first vegetation red edge band (B5) achieve the highest feature importance. Also, the mean and median green band (B3) and the mean red band (B4) are used by all three variations, and some obtain a significant feature importance.

Further, the used features and feature importance for the method *all bands* are analysed and compared to the method *Top 10* (see Figure 24). For ALS FHD (fishnet) the variable with the highest feature importance is the median first vegetation red edge band (B5) with 33%. The median green band (B3) has a significant feature importance at 25%, followed by the mean green band (B3) with 10%. In total seven features are used. Most of them are temporal statistics bands of the green and the vegetation red edge band. Other bands that are utilized are the maximum band of TCB (7%) and the standard deviation band of the GLCM for VH146 (9%). The ALS FHD (plots) has two bands that are attributed with a significant feature importance. The mean and median first vegetation red edge band (B5) with 23% and 22%. The remaining bands cover a feature importance of 2-7%. In total sixteen features are employed. The feature importance of the fourteen features used for GEDI FHD is distributed quite diversly. The highest feature importance can be ascribed to the minimum first vegetation red edge band (B5) with 14%. Followed by the standard deviation of the GLCM for the VH44 and the median green band (B3) both with 11% and the mean red band (B4) with 10%. The remaining bands cover an importance spectrum of 3-7%. The mean and median first vegetation red edge bands (B5), as well as the standard deviation band of the GLCM for VH44

is utilized for all three variations (ALS fishnet, ALS plot, GEDI). Again, the highest feature importance is recorded for temporal statistics bands (minimum, mean, median) of the first vegetation red edge band (B5), but high feature importance values have also been obtained for temporal statistics bands (mean, median) of the green band (B3).

When comparing the used features between the variable combinations *all bands* and *Top 10*, it can be determined, that only the mean and median first vegetation red edge band (B5) is used for all three variations in both methods. The median green band (B3) is also utilized twice for the method *Top 10* and the method *all bands*. Otherwise, there are hardly any overlaps between used features. Considering the feature importance both *all bands* as well as *Top 10* record their highest feature importance values for different temporal statistics bands of the green band (B3) and the first vegetation red edge band (B5).

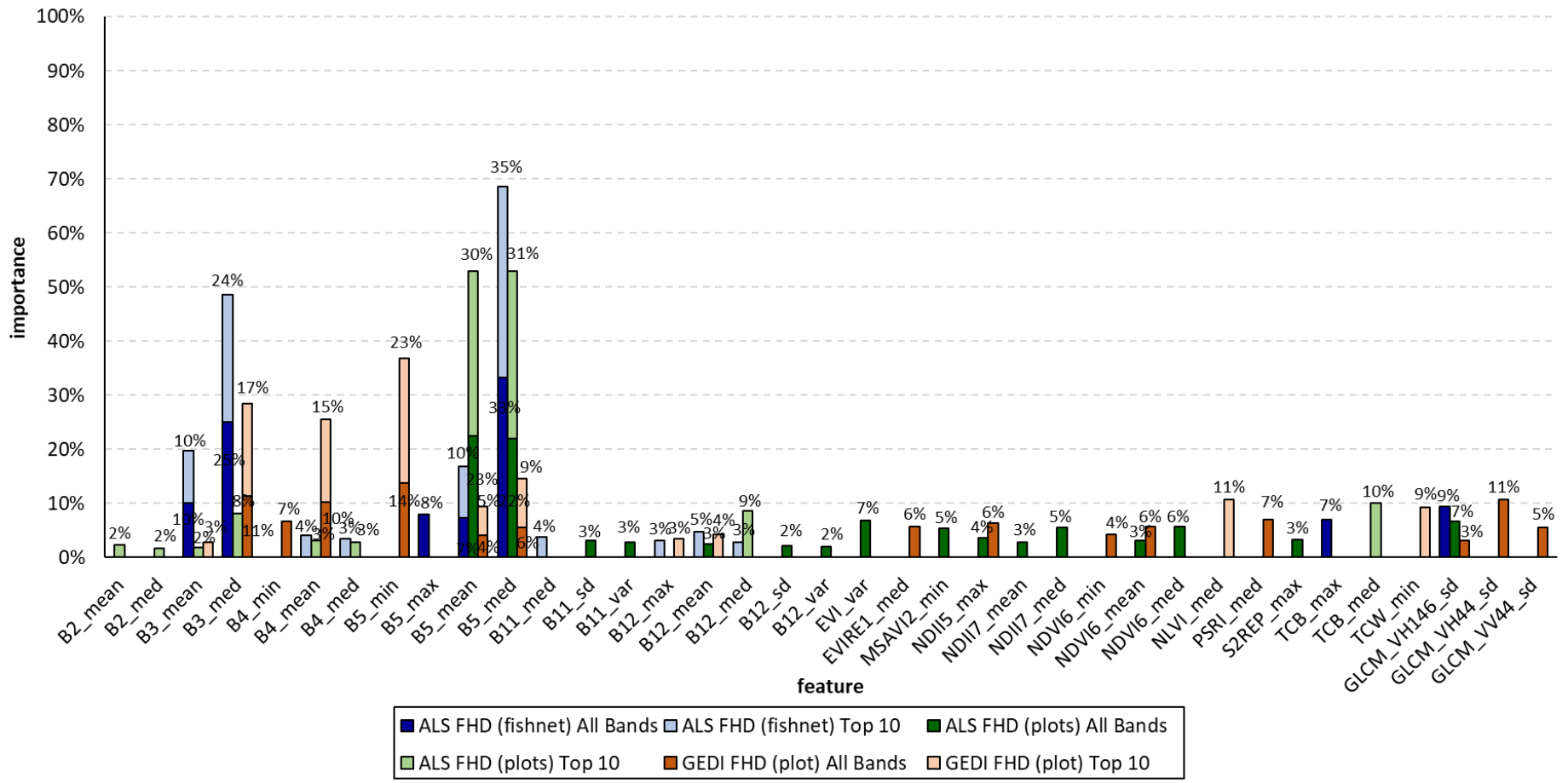

Figure 24: Comparing the used features and the feature importance for the FHD between the methods all bands and Top 10 and the three variations ALS FHD (fishnet), ALS FHD (plots) and GEDI FHD (plots).

For the ten FHD regressions calculated for the cross-validation, 47 bands were used in total (see Figure 25). However, only two bands were utilized for all ten regressions, the standard deviation of the GLCM for the VH44 and the minimum first vegetation red edge band (B5), both having an averaged feature importance of 9%. The mean red band (B4) has the highest averaged feature importance with 12% but is only used four out of ten times.

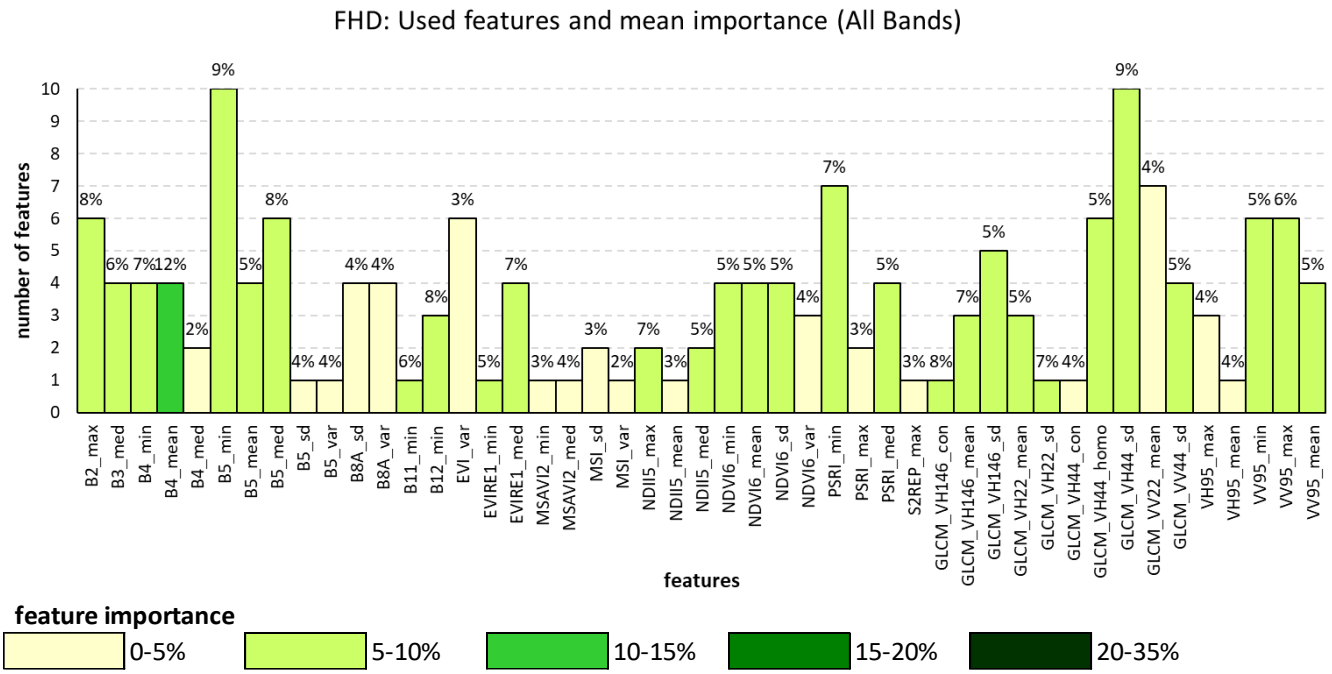

Figure 25: Frequency of used features and averaged feature importance when calculating the FHD regressions via cross-validation employing all bands.

7.1.3.4. Aboveground Biomass Density

For AGBD, only regressions trained and validated with the GEDI data through a cross-validation were modelled. Hereby for each one of the ten regressions, there is a .txt file available containing information regarding the used features and the feature importance. To be able to compare the correlation results (see Table 13) with the feature importance of the method *Top 10*, the regression with the best accuracy (lowest RMSE) was selected. This was the 10th regression presenting a RMSE of 89.85 Mg/ha (see Table 38). For the comparison between *Top 10* and *all bands* also the 10th regression for *all bands* was selected (RMSE = 84.40 Mg/ha).

The highest correlation is presented for the median band of NLVI (R^2 = 0.11) and the minimum (R^2 = 0.10) and mean (R^2 = 0.09) band of NDVI6. In terms of the feature importance these

three bands are also assigned the highest values. However, the value distribution is slightly different. The mean band of the NDVI6 is attributed with the highest feature importance of 37%, followed by the median band of the NLVI with 16% and the minimum band of the NDVI6 with 14%. The remaining bands cover a feature importance between 3-9%, even though they have almost the same R^2 values as the NLVI and the NDVI6. Calculating the AGBD regression using the training set 10 with the variable combination *all bands*, the RF model selects 11 variables. Here, the greatest feature importance with 18% is also assigned to the mean band of NDVI6. Other variables with a noticeable feature importance are the standard deviation band of GLCM for the VH44 with 16%, the mean red band (B4) with 14% and the minimum band of the PSRI with 12%. The rest of the variables have a feature importance of 4-8% (see Figure 26).

Comparing the two, it can be determined, that only three temporal statistics bands (minimum, mean, median) of the NDVI6 are utilized by *Top 10* as well as *all bands*. Furthermore, both register their highest feature importance for the mean band of NDVI6.

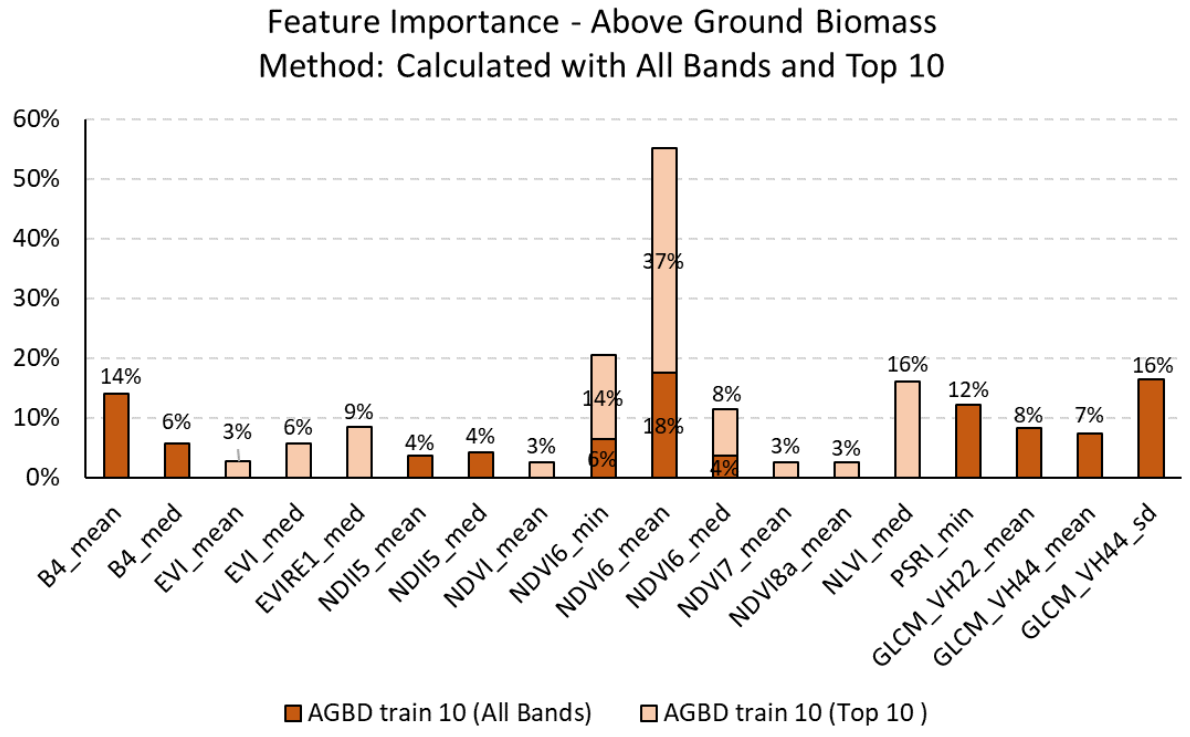

Figure 26: Comparing the used features and the feature importance for the AGBDs between the methods all bands and Top 10.

For the ten AGBD regressions calculated for the cross-validation, 30 variables were used in total (see Figure 27). AGBD records the highest averaged feature importance of 16% for both

the mean band of NDVI6 and the standard deviation of GLCM for VH44. The first variable is employed for all ten regressions the second one for nine regressions. Other bands that are used ten out of ten times are the mean red band (B4) with 11%, the minimum PSRI (8%) and the minimum (6%) band of the NDVI6. Nine out of ten times the maximum PSRI (4%) and the mean band of the GLCM for VH44 (8%) and eight out of ten times the mean band of the GLCM for VH22 (7%) and the mean NDII5 (5%) are used. Most of the other bands are listed for less than half of the regressions as used feature and only possess an averaged feature importance between 3-7%.

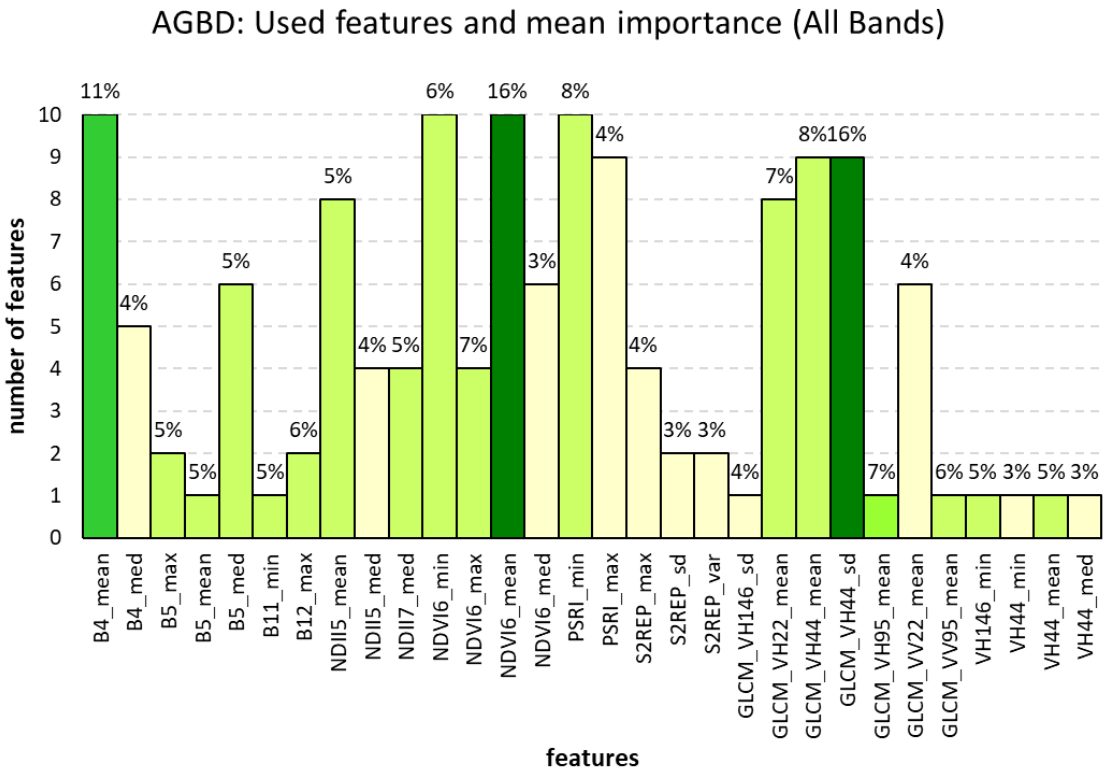

Figure 27: Frequency of used features and averaged feature importance when calculating the AGBD regressions via cross-validation employing all bands.

7.2. Random Forest Regression

Different variable combinations were employed to calculate the regressions (see Figure 13), and depending on the validation data, different training datasets were used.

It was possible to derive the maximum and mean vegetation height and the FHD from the ALS data and use them both for training the regressions and for validating the results. On the one hand, all available GEDI plots were utilized as training samples to calculate regressions for the ALS mean, ALS max, ALS FHD, GEDI RH50, GEDI RH100 and GEDI FHD. On the other hand, training samples based on the fishnet grid were used to calculate regressions for ALS

mean, ALS max and ALS FHD. All the modelled regressions were then validated with the initial ALS datasets for the mean and maximum vegetation height and the FHD values by calculating error values (R^2, RMSE, MAE).

Furthermore, GEDI data was not only used for training, but also validating the regressions. To validate the regressions based on GEDI parameters (RH50, RH100, FHD, AGBD) with GEDI data, a cross-validation with ten training and matching validation datasets was instrumentalized. For each of the datasets a regression is modelled and the error values (R^2, RMSE, MAE) are calculated. Later, the average of all ten error values for R^2, RMSE and MAE for each parameter was calculated. Also, an averaged raster based on all ten regressions for each parameter was computed.

7.2.1. Mean Vegetation Height

Firstly, the regression results using the ALS values as validation data are described (see Table 14). The mean vegetation height based on the ALS data and using cells of the fishnet grid as trainings samples has R^2 values between 0.41 and 0.46; RMSE values between 6.78 m and 7.09 m and MAE values between 5.30 m and 5.63 m. Hereby the best accuracy (the highest R^2 value and the lowest RMSE and MAE value) was achieved for the method *all bands* and *4 Orbits* both resulting in $R^2 = 0.46$, RMSE = 6.78 m and MAE = 5.30 m. For further analysis the regression modelled with the variable combination *all bands* is picked. Regressions, that were based on the ALS data and employing the GEDI plots as training samples, achieve R^2 values on a scale of 0.40 to 0.46; the RMSE values reach from 6.91 m to 7.21 m and the MAE results are located between 5.39 m and 5.73 m. The regression with the best results was the one only using the ten variables with the “best” negative R correlation (*NC*) resulting in $R^2 = 0.46$, RMSE = 6.91 m and MAE = 5.39 m. The regressions, that were calculated using the GEDI RH50 as training data and the ALS mean values as validation data, achieve R^2 values between 0.36 and 0.39, RMSE values between 7.50 m and 7.68 m and MAE values between 6.05 m and 6.20 m. Hereby there was not one standalone variable combination that could be identified as resulting in the best accuracy. There were several variable combinations that either produced better R^2 or RMSE/MAE values. The regression with the highest R^2 value (0.39) was the one using the variable combination *NC*. The model utilizing the *all bands* method resulted in the lowest error values; RMSE = 7.50 m and MAE = 6.05 m. For further analysis the regression calculated with the variable combination *all bands* is chosen. One can observe that the regressions using ALS mean as training data and the fishnet grid cells as training samples show slightly better results overall, than the regressions using ALS mean as training data and the GEDI plots as training samples, due to higher R^2 and lower RMSE and MAE values. In general, however, the statement can be made, that all regressions, that use the ALS mean

values as base (training data) have overall better results, than the regressions calculated based on the GEDI RH50 data.

In Figure 28 the best results for each parameter are portrayed, as well as the reference data and the deviation of the regressions from the reference data. The deviation is calculated by subtracting the reference raster from the regression raster. A positive value indicates an overestimation of the regression, a negative value an underestimation of the regression. The reference data for ALS mean covers a height range of 0 m – 46 m. The ALS mean regression (fishnet) stretches over a height range of 0.06 m – 30.60 m, while the ALS mean regression (plots) achieves height values of 1.21 m – 22.12 m and the RH50 regression (plots) height values of 2.72 m – 22.63 m. ALS mean (fishnet) predicts the low vegetation heights very well but underestimates the higher vegetation heights. Both ALS mean (plots) and RH50 overestimates low vegetation heights and underestimated high vegetation heights. The original height distribution is recognizable in all regressions, but it is noticeable that especially RH50 greatly overestimates the vegetation height in some clearings. In Figure 29 the percentual deviation of the best regression results from the reference data for all three variations is depicted. For the ALS mean regression (fishnet) 74% of the calculated values showcase a deviation of more than +/- 2 m. Results that have a deviation of more than +/- 4 m amount to 54% and only 14% of the results deviate more than +/- 10 m from the reference data. The ALS mean regression (plots) has a deviation of more than +/- 2 m for 76% of its results. For deviations of more than +/- 4 m and +/-10 m it has the same aberrations as ALS mean regression (fishnet). The RH50 regression deviates more than +/- 2 m for 81 % of its values. Deviations of more than +/- 4 m amount to 62 % and deviations of more than +/- 10 m to 16 These results show, that while average heights might be accurate, the local accuracy is often low.

Table 14: Validating the regression results for the mean vegetation height Group A. The R^2, RMSE and MAE are calculated for all five variable combinations using the regression results based on the ALS mean (fishnet), the ALS mean (plots) and the RH50 as predicted values and the original ALS mean values as observed values.

Validation of mean vegetation height with the ALS mean raster						
Data source	Training samples	Validation data	Method	R^2	RMSE (m)	MAE (m)
ALS mean	Fishnet grid cells (fishnet)	ALS mean raster	All bands	0.46	6.78	5.30
			4 Orbits	0.46	6.78	5.30
			Top 10	0.41	7.09	5.63
			PC	-	-	-
			NC	0.45	6.86	5.37
	All GEDI plots (plots)		All bands	0.45	6.96	5.44
			4 Orbits	0.45	6.96	5.44
			Top 10	0.40	7.21	5.73
			PC	-	-	-
			NC	0.46	6.91	5.39
GEDI RH50	All GEDI plots (plots)		All bands	0.38	7.50	6.05
			4 Orbits	0.36	7.59	6.13
			Top 10	0.36	7.66	6.18
			PC	0.36	7.68	6.20
			NC	0.39	7.53	6.08

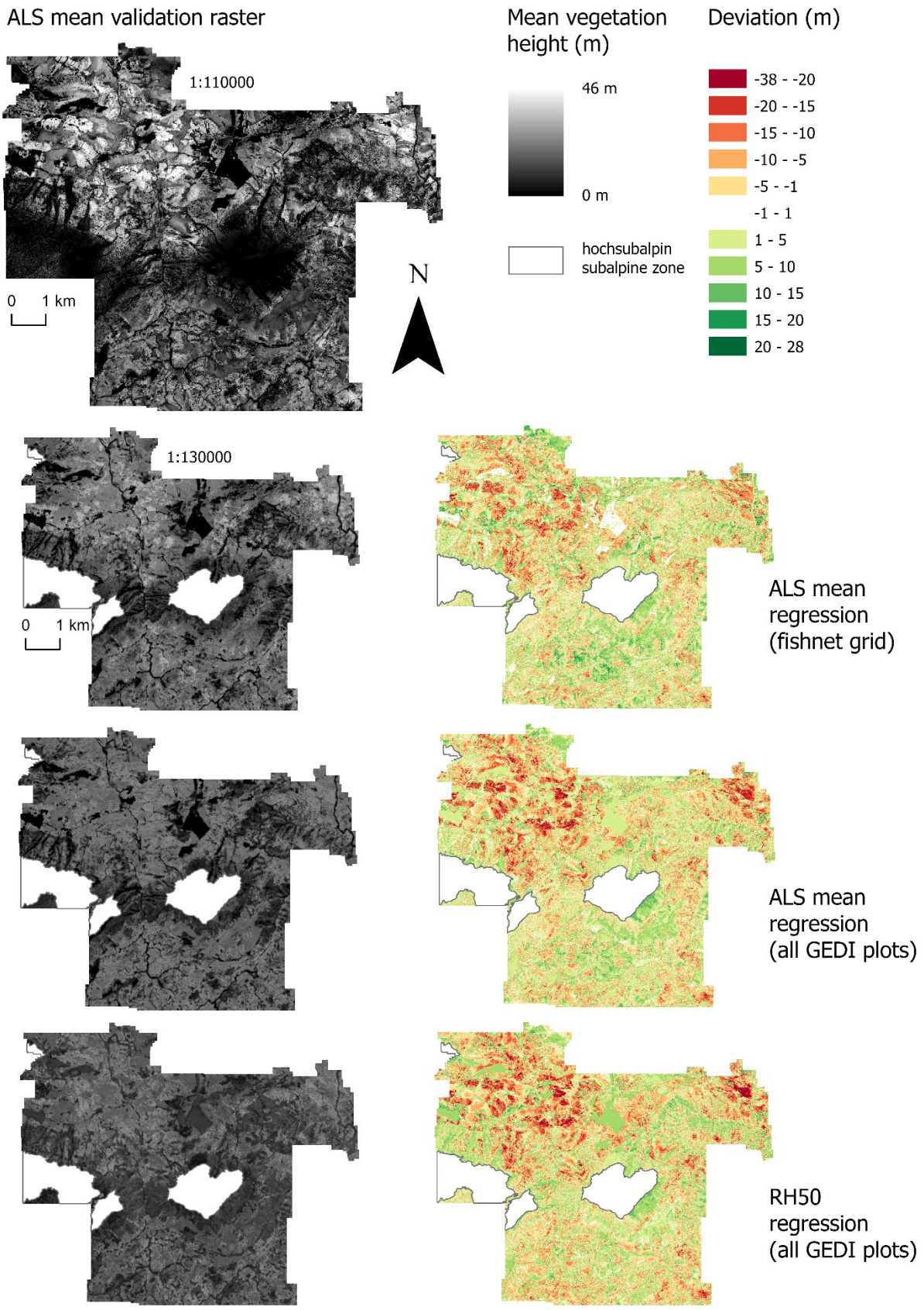

Figure 28: The best regression results for each mean vegetation height parameter using the ALS values as validation data. The regression for ALS mean using fishnet grid cells as training samples is based on the method all bands. The ALS mean regression using all GEDI plots as training samples is based on the method NC. The RH50 regression using all GEDI plots as training samples is based on the method all bands.

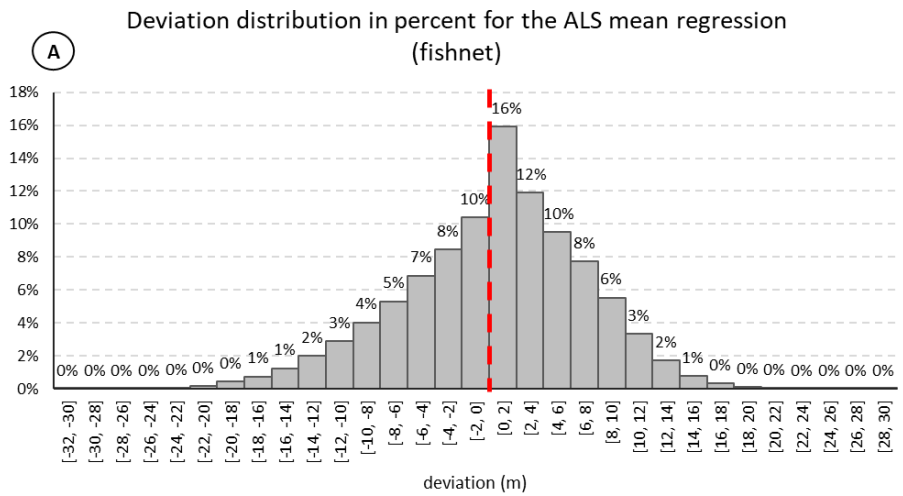

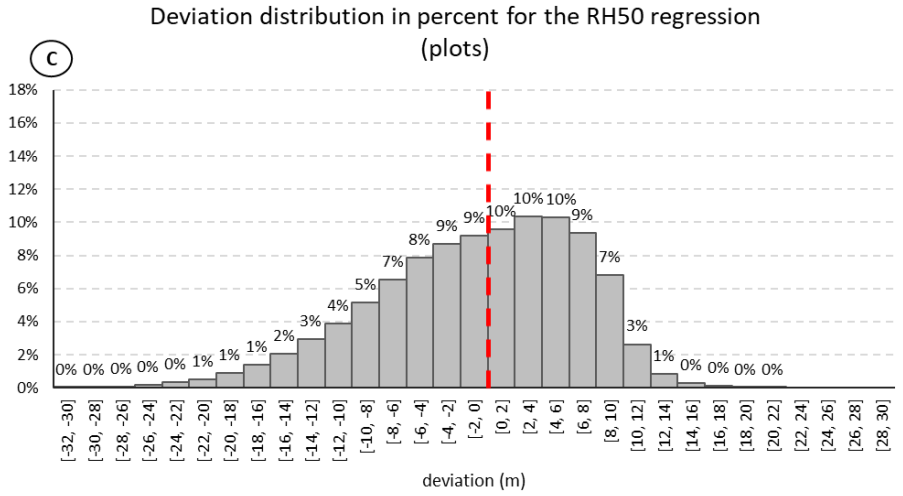

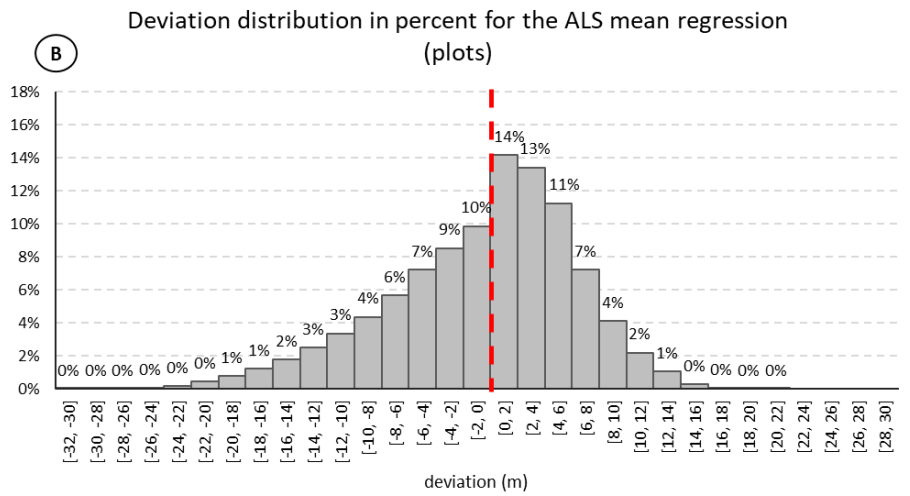

Figure 29: Deviation distribution in percent for the mean vegetation height regressions. The histograms depict the deviation of the regression results from the ALS mean validation raster. Negative values on the x-axis are interpreted as an underestimation of the regression; positive values on the x-axis are interpreted as an overestimation of the regression. A) Deviation distribution of the ALS mean regression using fishnet grid cells as training samples and the method all bands; B) deviation distribution of the ALS mean regression using the GEDI plots as training samples and the method NC; C) deviation distribution of the RH50 regression using the method all bands. The data labels are rounded values.

The RH50 regressions, that were validated with the original RH50 values through a cross-validation, show averaged R^2 values between 0.26 and 0.31; averaged RMSE values between 6.36 m and 6.59 and averaged MAE values between 5.05 m and 5.20 m (see Table 15). It can be observed, that the R^2 values are lower, compared to the R^2 values calculated for the validation of RH50 with ASL mean. On the other hand, the RMSE and MAE values show a smaller deviation than the RMSE and MAE values, that were calculated using the ALS mean as training and validation data. The highest R^2 and smallest RMSE and MAE values could be achieved by using the method *all bands* (R^2 = 0.31, RMSE = 6.36 m, MAE = 5.05 m). Analysing the percentual deviation distribution for this regression result, the mean regression has a deviation of more than +/- 2 m for 72% of its predicted values. Furthermore, it has a deviation of more than +/- 4 m for 47% and a deviation of more than +/-10 for only 8% of its calculated values (see Figure 30).

Table 15: Validating the regression results for the mean vegetation height Group B. The mean R^2, RMSE and MAE are calculated based on all ten cross-validations of the RH50 regressions for all five variable combinations.

Validation of RH50 regression with GEDI RH50 data					
Regression	**All bands**	**4 Orbits**	**Top 10**	**PC**	**NC**
R^2	0.31	0.30	0.26	0.26	0.27
RMSE (m)	6.36	6.42	6.57	6.59	6.56
MAE (m)	5.05	5.11	5.20	5.20	5.17

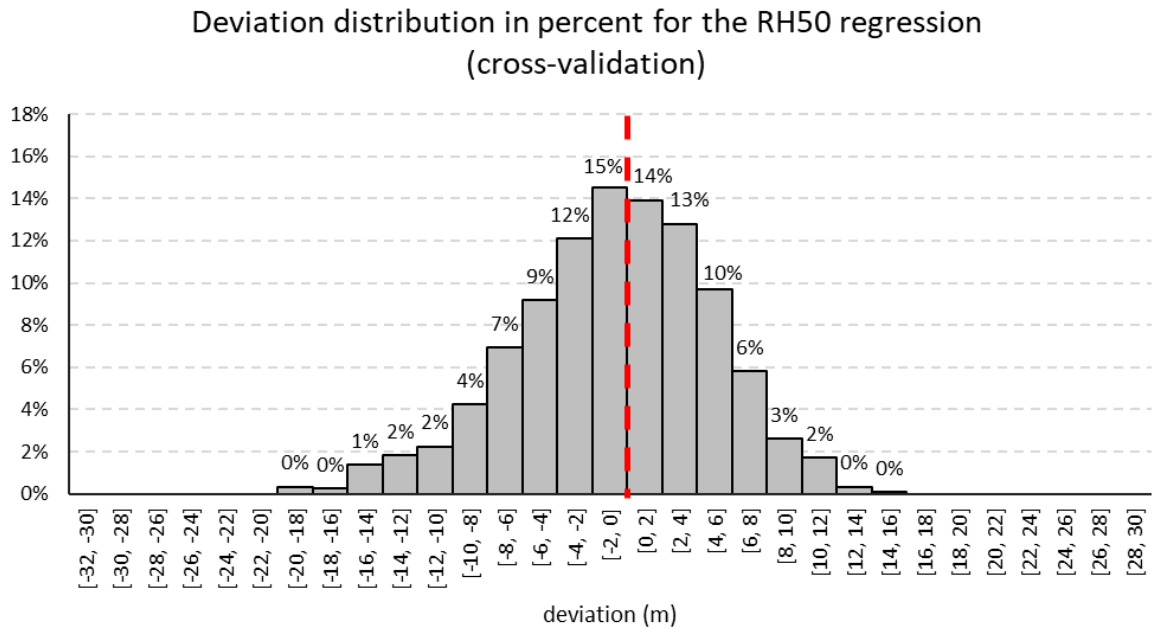

Figure 30: Deviation distribution in percent for the mean RH50 regression (all bands) validated with the GEDI data via cross-validation.

7.2.2. Maximum Vegetation Height

In Table 16 the regression results using the ALS values as validation data are described. The regressions calculated for the maximum vegetation height, using the ALS max values as trainings data and fishnet grid cells as training samples, have R^2 values between 0.26 and 0.45. The RMSE values range from 7.76 m to 9.01 m and the MAE values from 6.10 m to 7.24 m. Hereby the best regression is obtained by using the method *all bands* (R^2 = 0.45, RMSE = 7.76 m, MAE = 6.10 m). The maximum vegetation height regressions utilizing the ALS max values as training data and the GEDI plots as training samples, achieve R^2 values between 0.20 and 0.40; RMSE values between 9.38 m and 10.47 m and MAE values between 7.37 m and 8.16 m. The best R^2 and RMSE values were calculated for the method *4 Orbits* (R^2 = 0.39, RMSE = 9.38 m) and the best MAE values was achieved for the method *all bands* (MAE = 7.37 m). For further analysis the regression calculated with the variable combination *4 Orbits* is chosen. The regressions calculated by using GEDI RH100 values as training data and GEDI plots as training samples, but employing the ALS max values as validation data, have R^2 values between 0.21 and 0.35, RMSE values between 10.53 m and 11.11 m and MAE values between 8.23 m and 8.72 m. The best result is achieved with the variable combination *4 Orbits* (R^2 = 0.33, RMSE = 10.53 m, MAE = 8.22 m). Again, the regressions utilizing the ALS values as training as well as validation data have a higher accuracy, than the regressions utilizing the GEDI RH100 values for training and the ALS values for validation.

In Figure 31 the best regressions for each parameter are depicted, the reference data and the deviation of the regressions from the reference data. The reference data for ALS max covers a height range of 0 m – 50 m. The ALS max regression (fishnet) covers a height range of 0.31 m – 36.24 m; the ALS max regression based on all GEDI plots stretches from 9.85 m to 36.88 m and the RH100 regression reaches from 17.74 m to 38.93 m. ALS max (fishnet) predicts the low values very well but underestimates the high vegetation heights. ALS max (plots) overestimates the low values and underestimates the high values. RH100 severely overestimates the low heights. It also underestimates the higher vegetation heights, even though it predicts higher values than both ALS max regressions. In Figure 32 it is noticeable that the ALS max regression (plots) as well as the RH100 regression tend to overestimate, rather than underestimate its predicted values. One can see that the ALS max regression (fishnet) has a deviation of more than +/- 2 m for 79 % of its values. Furthermore, 60 % of its values deviate more than +/- 4 m from the reference data and 21 % deviate more than +/- 10 m. For the ALS max regression (plots) 83 % of its values have a deviation of more than +/- 2 m. Also, 66 % showcase a deviation of more than +/- 4 m and 28 % of more than +/- 10 m. The RH100 regression has a deviation of more than +/- 2 m for 84 % of its values. Predicted

regression values with a deviation of more than +/- 4 m amount to 69 % and with a deviation of +/- 10 m total 32 %.

Table 16: Validating the regression results for the maximum vegetation height Group A. The R², RMSE and MAE are calculated for all five variable combinations using the regression results based on the ALS max (fishnet), the ALS max (plots) and the RH100 as predicted values and the original ALS max values as observed values.

Validation of max vegetation height with the ALS max raster						
Data source	Training samples	Validation data	Method	R^2	RMSE (m)	MAE (m)
ALS max	Fishnet grid cells (fishnet)	ALS max raster	All bands	0.45	7.76	6.10
			4 Orbits	0.42	8.01	6.31
			Top 10	0.37	8.27	6.59
			PC	-	-	-
			NC	0.26	9.01	7.24
	All GEDI plots (plots)		All bands	0.39	9.43	7.37
			4 Orbits	0.40	9.39	7.39
			Top 10	0.34	9.68	7.69
			PC	0.20	10.47	8.16
			NC	0.38	9.51	7.48
GEDI RH100	All GEDI plots (plots)		All bands	0.33	10.56	8.23
			4 Orbits	0.35	10.53	8.23
			Top 10	0.27	10.83	8.57
			PC	0.21	11.11	8.72
			NC	0.28	10.81	8.53

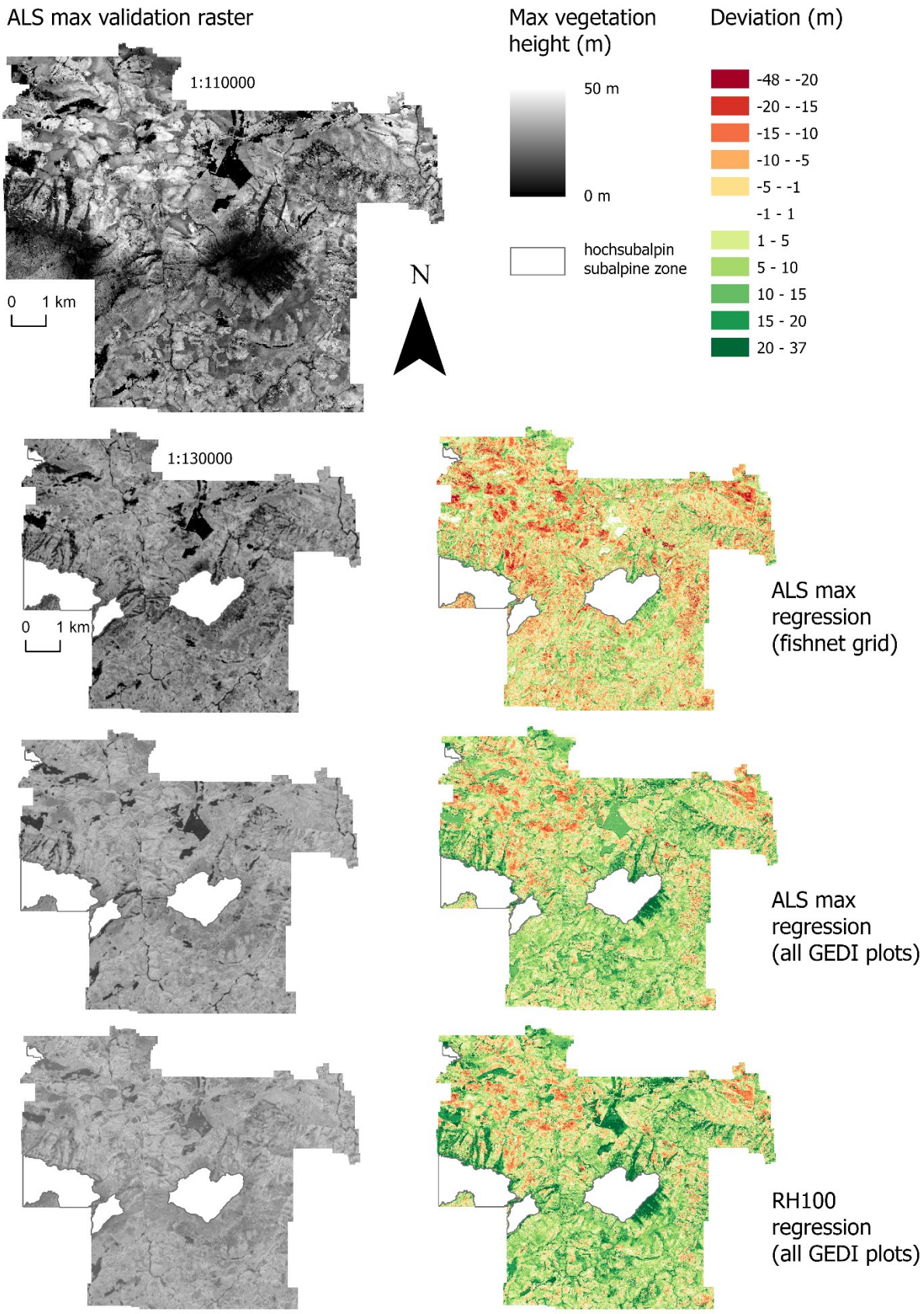

Figure 31: The best regression results for each maximum vegetation height parameter using the ALS values as validation data. The regression for ALS max using fishnet grid cells as training samples is based on the method all bands. The ALS max regression using all GEDI plots as trainings samples is based on the method 4 Orbits. The RH100 regression using all GEDI plots as trainings samples is based on the method 4 Orbits.

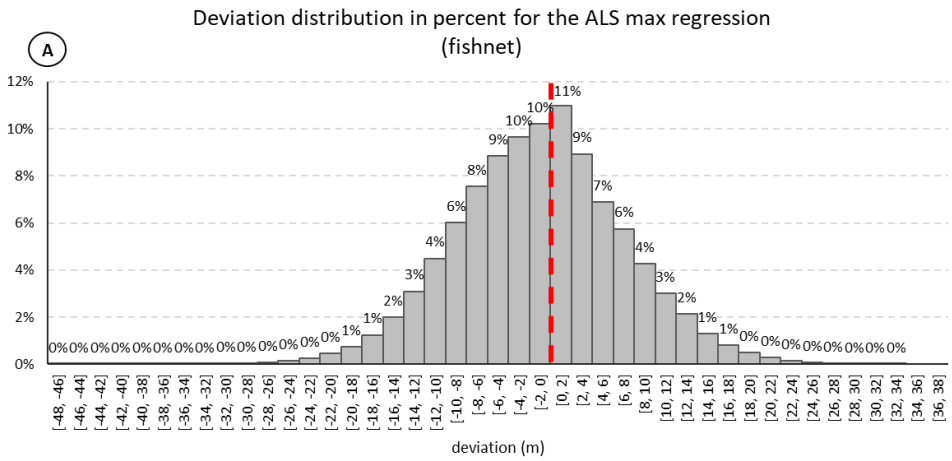

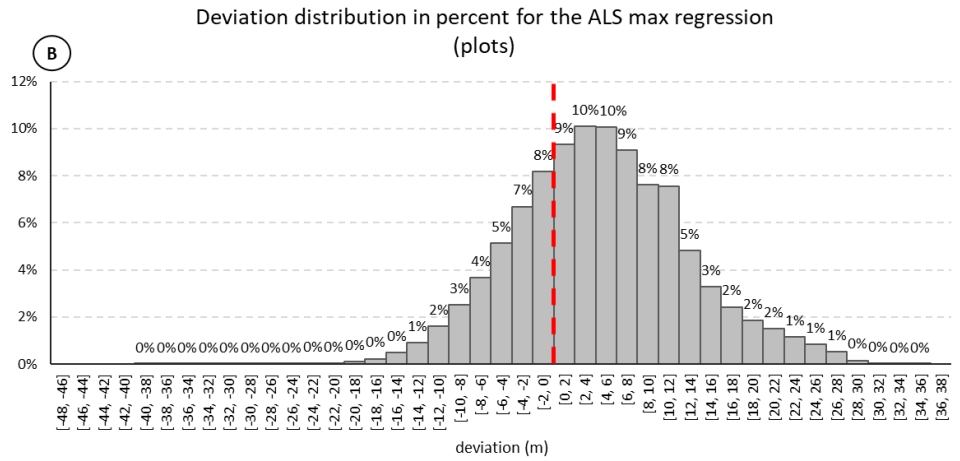

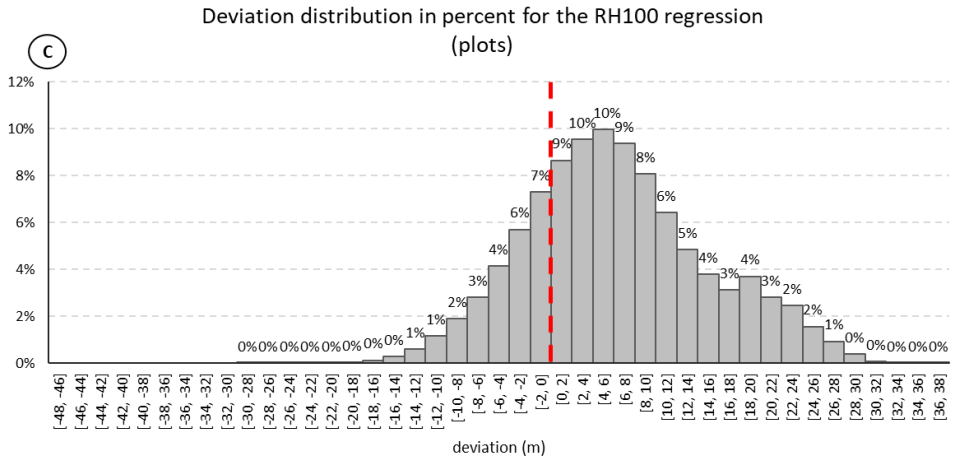

Figure 32: Deviation distribution in percent for the maximum vegetation height regressions. The histograms depict the deviation of the regression results from the ALS max validation raster. Negative values on the x-axis are interpreted as an underestimation of the regression; positive values on the x-axis are interpreted as an overestimation of the regression. A) Deviation distribution of the ALS max regression using fishnet grid cells as training samples and the method all bands; B) deviation distribution of the ALS max regression using the GEDI plots as training samples and the method 4 Orbits; C) deviation distribution of the RH100 regression using the method 4 Orbits.

Utilizing solely the GEDI RH100 values for training and validation of the regressions one achieves R^2 values between 0.12 and 0.27; RMSE values ranging from 7.51 m to 8.17 m and MAE values between 6.06 m and 6.61 m (Table 17). The best result hereby is calculated for the method *all bands* (R^2 = 0.27, RMSE = 7.51, MAE = 6.06). The deviation distribution of the mean regression for *all bands* presents a deviation of more than +/- 2 m for 79% of all predicted values. A deviation of more than +/- 4 m can be noted for 56% of the results and a deviation of more than +/ 10 m for 14% of the predicted values (see Figure 33). Compared to the results before in Table 16, the R^2 values are lower, but the RMSE and MAE values are slightly better, than the RMSE and MAE values for the regressions validated with the ALS data. Indicating that when training and validating the regressions just based on the GEDI data, the average deviation between the predicted maximum vegetation height and the actual maximum vegetation height is lower. On the other side, the predictor variables in the model do not adequately explain the variations of the maximum vegetation height.

Table 17: Validating the regression results for the maximum vegetation height Group B. The mean R^2, RMSE and MAE are calculated based on all ten cross-validations of the RH100 regressions for all five variable combinations.

Validation of RH100 regression with GEDI RH100 data					
Regression	**All bands**	**4 Orbits**	**Top 10**	**PC**	**NC**
R^2	0.27	0.23	0.18	0.12	0.15
RMSE (m)	7.51	7.75	7.98	8.17	8.15
MAE (m)	6.06	6.22	6.47	6.55	6.61

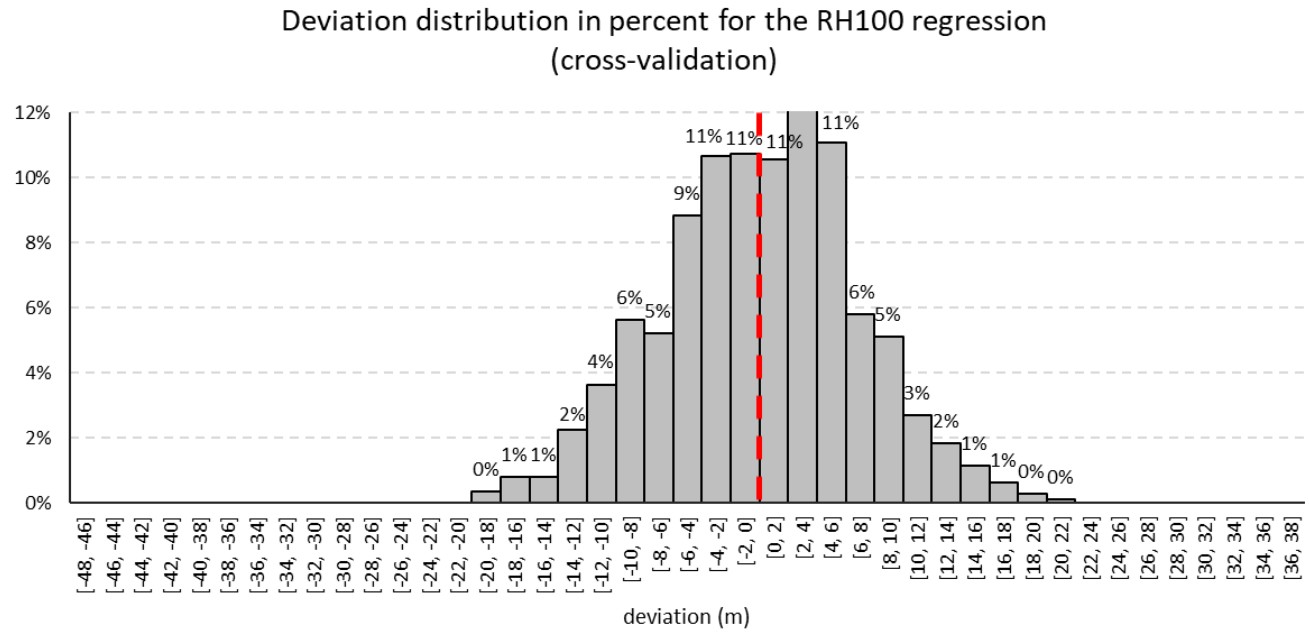

Figure 33: Deviation distribution in percent for the RH100 regression (all bands) validated with the GEDI data via cross-validation.

7.2.3. Foliage Height Diversity

Table 18 shows the regression results using the ALS values as validation data for FHD. The ALS FHD regressions employing the fishnet grid cells as training samples achieve R^2 values ranging from 0.22 – 0.35, RMSE values from 0.62 – 0.69 and MAE values from 0.46 - 0.51. The variation using the ten bands with the highest correlation (*Top 10*) produces the best results (R2 = 0.35, RMSE = 0.62, MAE = 0.46). If calculating the regressions for the ALS FHD values using the GEDI plots as training samples, the R^2 values range from 0.10 to 0.40, RMSE values from 0.65 to 0.77 and MAE values from 0.43 to 0.49. The best regression is modelled by utilizing the variable combination *all bands* (R^2 = 0.40, RMSE = 0.65, MAE = 0.43). The GEDI FHD regressions validated with the ALS FHD values have R^2 values between 0.22 and 0.31 and RMSE values between 0.93 and 0.95. The MAE values show regardless of the variable combination very low variability, and all move around the value 0.67. The best result is achieved, using the method *all bands* (R^2 = 0.31, RMSE = 0.93, MAE = 0.67). Hereby it can also be observed that the regressions, that are trained and validated with the ALS FHD values, show higher accuracy, than the regressions, that were trained with the GEDI FHD values and validated with the ALS FHD values. This was to be expected. Generating training and validation samples from the same dataset usually show smaller deviations than generating training and validation samples from two different datasets. When validating the first two models only the deviation between the actual and the predicted values must be considered. In the case of utilizing GEDI data for training and ALS data for validation there is already a deviation between the two original datasets that then adds on to the deviation between the actual and predicted value.

In Figure 34 the best regressions for each variation (ALS fishnet, ALS GEDI, GEDI) are depicted, as well as the reference data and the deviation of the regressions from the reference data. The reference data covers a value range of 0.00 to 3.80. The regression calculated based on the ALS FHD values and employing the fishnet grid cells as training samples predicts values reaching from 0.27 to 3.11. The regression calculated for the ALS FHD values employing the GEDI plots as training samples ranges from 1.11 to 3.08. The regression based on the RH100 values reaches from 2.39 to 3.23. The ALS FHD regression (fishnet) slightly overestimates low values and underestimates high values. The ALS FHD regression based on the GEDI plots overestimates the low values a lot more, as well as underestimates the high values. The GEDI FHD regression overestimates the low values significantly. However, it predicts the high values slightly better than both ALS FHD regressions. In Figure 35 the deviation distribution of the regression results from the reference data is depicted in percent. It is noticeable, that the GEDI FHD overestimates almost all of its predictions, while the ALS

FHD (fishnet) regression underestimates most of its values. Furthermore, 69 % of the deviations for the ALS FHD (fishnet) regression are more than +/- 0.2. Also, 43 % of the values deviate more than +/- 0.4 and only 9 % more than +/- 1.0. The ALS FHD regression (plots) has an aberration of more than +/- 0.2 for 62 % of its predictions, an aberration of more than +/- 0.4 for 36 % and an aberration of more than +/- 1.0 for 11 % of its values. The GEDI FHD regression showcases a deviation of more than +/- 0.2 for 79 % of its values. Deviations of more than +/- 0.4 amount to 58 % in total and deviations of more than +/- 1.0 to 19 %.

Table 18: Validating the regression results for the FHD Group A. The R^2, RMSE and MAE are calculated for all five variable combinations using the regression results based on the ALS FHD (fishnet), the ALS FHD (plots) and the GEDI FHD as predicted values and the original ALS FHD values as observed values.

Validation of FHD regression with the ALS FHD raster						
Data source	Training samples	Validation data	Method	R^2	RMSE	MAE
ALS FHD	Fishnet grid cells (fishnet)	ALS FHD raster	All bands	0.32	0.64	0.47
			4 Orbits	0.34	0.63	0.46
			Top 10	0.35	0.62	0.46
			PC	0.22	0.69	0.51
			NC	-	-	-
	All GEDI plots (plots)		All bands	0.40	0.65	0.43
			4 Orbits	0.31	0.68	0.45
			Top 10	0.40	0.66	0.44
			PC	0.10	0.77	0.49
			NC	-	-	-
GEDI FHD	All GEDI plots (plots)		All bands	0.31	0.93	0.67
			4 Orbits	0.29	0.94	0.67
			Top 10	0.28	0.94	0.67
			PC	0.22	0.95	0.67
			NC	0.27	0.95	0.67

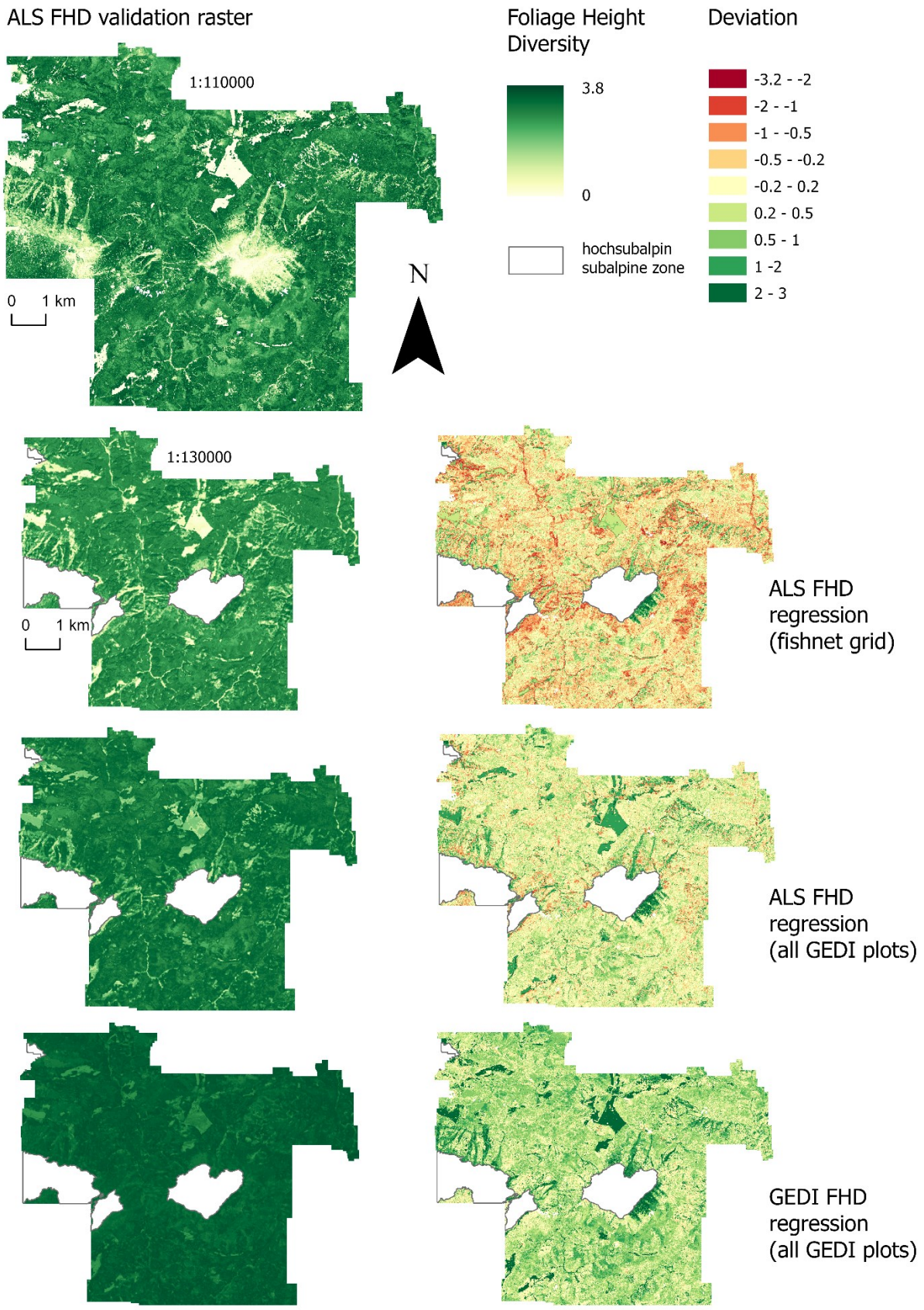

Figure 34: The best regression results for each FHD parameter using the ALS values as validation data. The regression for ALS FHD using fishnet grid cells as training samples is based on the method Top 10. The ALS FHD regression using all GEDI as trainings samples is based on the method all bands. The GEDI FHD regression using all GEDI plots as trainings samples is based on the method all bands.

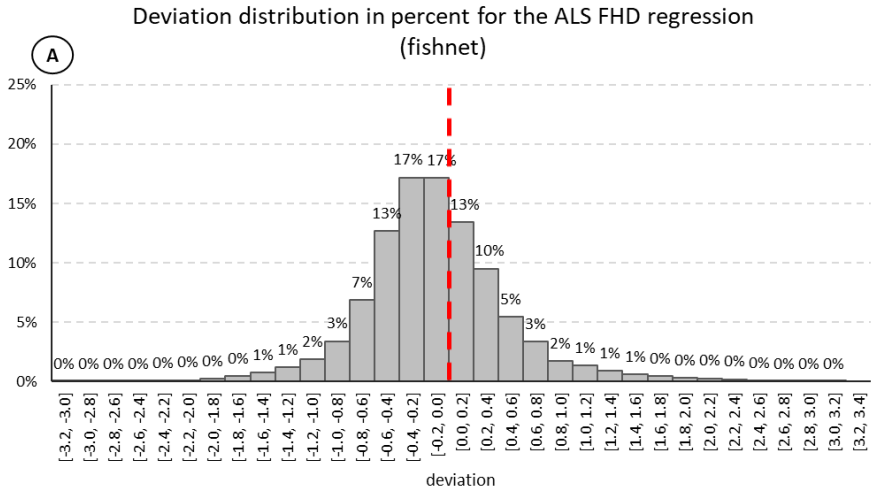

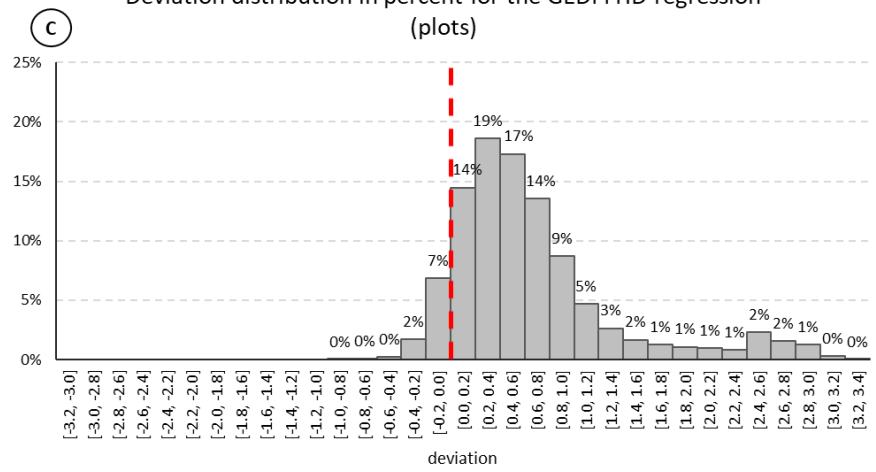

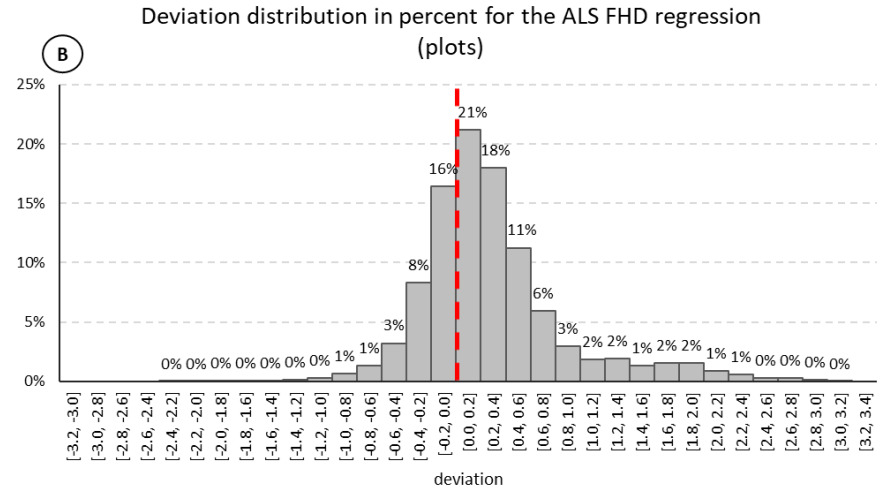

Figure 35: Deviation distribution in percent for the Foliage Height Diversity regressions. The histograms depict the deviation of the regression results from the ALS FHD validation raster. Negative values on the x-axis are interpreted as an underestimation of the regression; positive values on the x-axis are interpreted as an overestimation of the regression. A) Deviation distribution of the ALS FHD regression using fishnet grid cells as training samples and the method Top 10; B) deviation distribution of the ALS FHD regression using the GEDI plots as training samples and the method all bands; C) deviation distribution of the GEDI FHD regression using the method all bands.

If the regressions are trained and validated with the GEDI FHD values, R^2 values are between 0.10 and 0.17, RMSE values between 0.36 and 0.37 and MAE values between 0.31 and 0.32 are calculated (see Table 19). There is hardly any variation between the results of the different variable combinations. But the most effective combinations appear to be *all bands* (R^2 = 0.17, RMSE = 0.36, MAE = 0.31) and *4 Orbits* (R2 = 0.16, RMSE = 0.36, MAE = 0.31). The deviation distribution for the mean regression for *all bands* shows, that 64% of the calculated values have a deviation of more than +/- 0.2. About 20% have a deviation of more than +/- 0.4 and only 0.17 % have a deviation of more than +/- 1 (see Figure 36). Compared to the regressions, that were validated by the ALS data, the R^2 values are quite low. However, the RMSE and MAE are lower, which indicates less deviation of the regression model results from the validation data.

Table 19: Validating the regression results for the FHD Group B. The mean R², RMSE and MAE are calculated based on all ten cross-validations of the GEDI FHD regressions for all five variable combinations.

Validation of GEDI FHD regression with GEDI FHD data					
Regression	**All bands**	**4 Orbits**	**Top 10**	**PC**	**NC**
R^2	0.17	0.16	0.14	0.10	0.13
RMSE	0.36	0.36	0.37	0.37	0.37
MAE	0.31	0.31	0.31	0.32	0.31

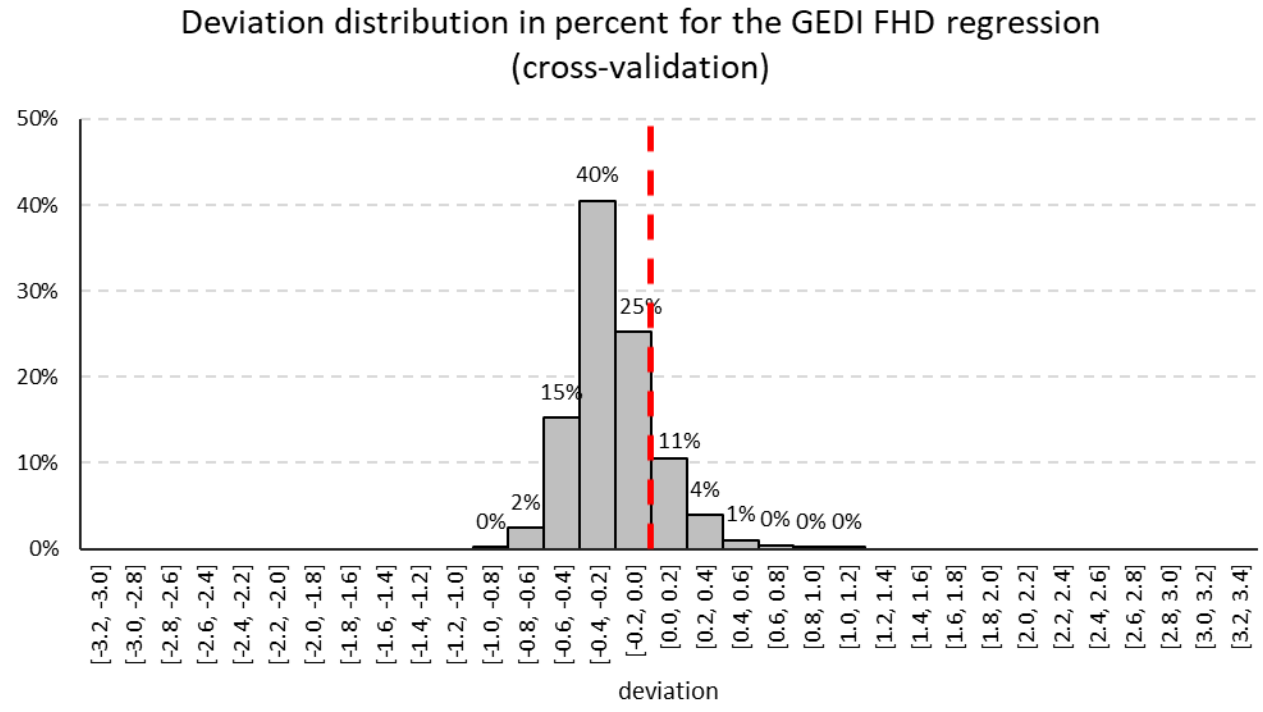

Figure 36: Deviation distribution in percent for the FHD regression (all bands) validated with the GEDI data via cross-validation.

7.2.4. Aboveground Biomass Density

For the vegetation parameter AGBD the regressions were only trained and validated, based on the GEDI data. The results for the R^2 extend over a value range of 0.16 to 0.27, the RMSE values are located between 88.11 Mg/ha and 94.57 Mg/ha and the MAE values are between 68.51 Mg/ha and 73.59 Mg/ha (see Table 20). The best result hereby is obtained, using the variation *all bands* (R^2 = 0.27, RMSE = 88.11 Mg/ha, MAE = 68.51 Mg/ha). Figure 37 depicts the averaged regression for all ten regressions calculated based on the method *all bands*. When comparing the AGBD regression with the maximum vegetation height reference data (ALS max validation data) one can see, that high AGBD values overlap with high vegetation maximum heights. The regression therefore manages to roughly reproduce the horizontal forest structure across the study area.

Table 20: Validating the regression results for the AGBD Group B. The mean R², RMSE and MAE are calculated based on all ten cross-validations of the GEDI AGBD regressions for all five variable combinations.

Validation of GEDI AGBD regression with GEDI AGBD data					
Regression	All bands	4 Orbits	Top 10	PC	NC
R^2	0.27	0.24	0.16	-	0.22
RMSE (Mg/ha)	88.11	90.02	94.57	-	91.48
MAE (Mg/ha)	68.51	69.75	73.59	-	70.68

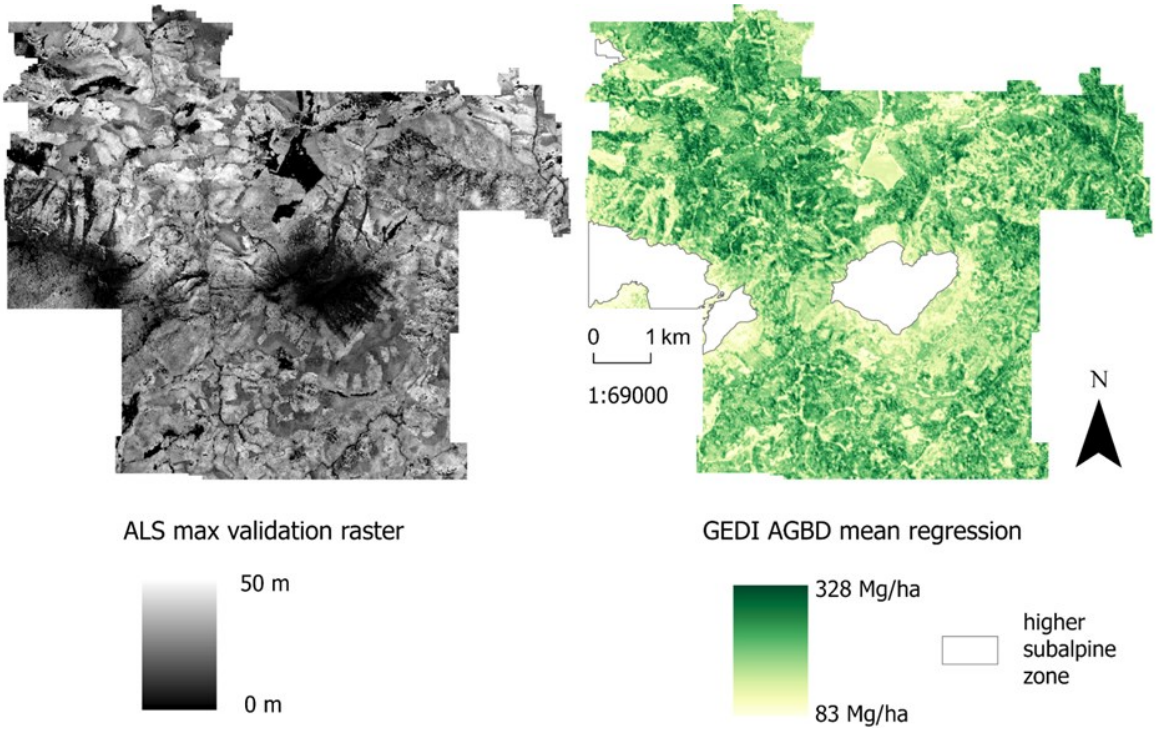

Figure 37: Mean aboveground biomass density regression using the method all bands.

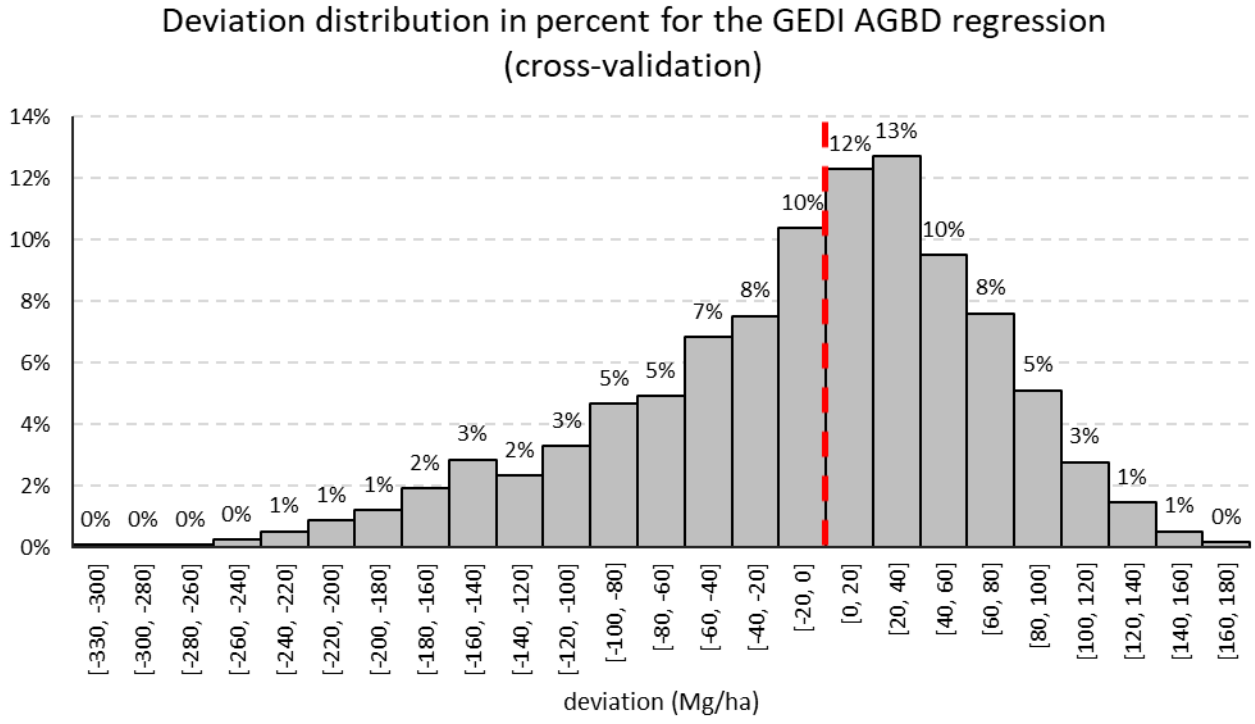

Figure 38: Deviation distribution in percent for the mean AGBD regression using the cross-validation.

7.2.5. Regression Results Summary

The results in Table 21 show, that for most parameters the best results were achieved, when using *all bands*. For both the ALS max and the RH100 regression using the GEDI plots as training samples and the ALS max values as validation data the best results were computed with the combination *4 Orbits*. Another exception is the regression calculated with the ALS mean values as training and validation data and using the GEDI plots as training samples. Hereby the model utilizing the variable combination *NC* resulted in the regression with the highest accuracy. Also, the regression calculated with the ALS FHD values as training and validation data and the fishnet grid cells as training samples obtains its best result when working with the variable combination *Top 10*.

Table 21: Variable combinations achieving the best regression results per parameter and variation.

Validation data	Training data	Method with the best results	R^2	RMSE	MAE
ALS mean	ALS mean (fishnet)	All bands	0.46	6.78 m	5.30 m
	ALS mean (plots)	NC	0.46	6.91 m	5.39 m
	RH50 (plots)	All bands	0.38	7.50 m	6.05 m
RH50	RH50	All bands	0.31	6.36 m	5.05 m
ALS max	ALS max (fishnet)	All bands	0.45	7.76 m	6.10 m
	ALS max (plots)	4 Orbits	0.40	9.39 m	7.39 m
	RH100 (plots)	4 Orbits	0.35	10.53 m	8.23 m
RH100	RH100	All bands	0.27	7.51 m	6.06 m
ALS FHD	ALS FHD (fishnet)	Top 10	0.35	0.62	0.46
	ALS FHD (plots)	All bands	0.40	0.65	0.43
	GEDI FHD (plots)	All bands	0.31	0.93	0.67
GEDI FHD	GEDI FHD	All bands	0.17	0.36	0.31
GEDI AGBD	GEDI AGBD	All bands	0.27	88.11 Mg/ha	68.51 Mg/ha

7.3. Further Analysis

7.3.1. Comparing Regression Results to Field Inventory Data

To determine the deviation of the calculated AGBD values from the measured AGBD values, the AGBD value of the forest inventory is subtracted from the AGBD value of the regression. This is done for all five methods except the variable combination *PC*. It is omitted because the ten bands for *PC* are the same as those for *Top 10* and therefore produce an identical regression raster. If a positive result for the calculated deviation is received, the AGBD is overestimated by the regression. A negative result indicates an underestimation.

At both stations, the AGBD regressions significantly underestimated the AGBD from the forest inventory data, especially at station 2900 (see Table 22 and Table 23). At station 700 the deviations range from ~94 Mg/ha to ~28 Mg/ha and at station 2900 from ~242 Mg/ha to ~177 Mg/ha. For station 700, the smallest deviation with 10% was achieved for the *NC* method. For station 2900, the lowest deviation with 43% could be determined for the *Top 10* method.

Table 22: Comparison of the AGBD mean regression values with the field inventory data (station 700).

Deviation GEDI AGBD regression values from forest inventory data (station 700)					
Regression	All bands	4 Orbits	Top 10	PC	NC
Reference value (Mg/ha)	287.74				
AGBD regression (Mg/ha)	228.08	194.07	252.43	-	259.73
Deviation (Mg/ha)	59.66	93.67	35.31	-	28.01
Deviation (%)	21 %	33 %	12 %	-	10 %

Table 23: Comparison of the AGBD mean regression values with the field inventory data (station 2900).

Deviation GEDI AGBD regression values from forest inventory data (station 2900)					
Regression	All bands	4 Orbits	Top 10	PC	NC
Reference value (Mg/ha)	414.23				
AGBD regression (Mg/ha)	172.65	206.15	237.66	-	211.52
Deviation (Mg/ha)	241.58	208.08	176.57	-	202.71
Deviation (%)	58 %	50 %	43 %	-	49 %

7.3.2. Analysing the Influence of Study Area Characteristics

The results used for this analysis again only focus on the regressions with the highest accuracy for each vegetation parameter (see Table 21). For each class of the study area characteristics a RMSE is calculated.

When analysing the TCD it can be observed that the RMSE values of the mean vegetation height continuously increase with an increasing TCD for most variations. Only the regression, which was calculated using the RH50 values as training data and the ALS mean values as validation data, has a higher RMSE value for the first class (*0-25 %)* than for the second class (*25-50%*). In contrast, for the maximum vegetation height as well as the FHD, the highest RMSE value mostly corresponds to the lowest TCD class and then decreases continuously. The RMSE for AGBD also increases with growing TCD values but decreases again for the TCD class with the highest values (see Figure 39).

For the mean vegetation height, the RMSE values for the *no forest* and *coniferous trees* classes are lower than for the *broadleaved trees* class, with *no forest* mostly showcasing the lowest RMSE values and *broadleaved trees* the highest RMSE values. The same can be observed for the AGBD regression results. For the maximum vegetation height and the FHD

the RMSE values for the *no forest* class are higher than the other RMSE values and the RMSE values for the *broadleaved trees* class usually are the lowest. Hardly any variations can be observed for the maximum height regression trained and validated with the ALS data using the fishnet grids as samples, the regression using the RH100 GEDI data as training and validation data and the FHD regression using the FHD GEDI data as training and validation data (see Figure 40).

The slope inclination is also divided into four classes (see Figure 41). The mean vegetation height regressions validated with ALS consistently have their highest error values within the second class (*20°-40°*) and the lowest error values within the fourth class (*60°-80°*). The RMSE value for the mean vegetation height regression, which is trained and validated with GEDI RH50 values, shows hardly any variations for the different slope classes. The maximum vegetation height regressions ALS max (plots) and RH100, both validated with ALS data, and the RH100 mean regression validated with GEDI data, present higher RMSE values within the first class (*0°-20°*). The RMSE values then decrease within the second class (*20°-40°*) and then continuously increase with increasing slope inclination. The RMSE values for the ALS max (fishnet) regression increase continuously with increasing slope gradient. For all FHD regressions it can be observed that the RMSE values increase with increasing slope inclination, the only outliers being the RMSE values within the first class (*0°-20°*) which are always higher than the RMSE values within the second class (*20°-40°*). For the parameter AGBD it can be clearly observed that the RMSE values increase with increasing slope inclination.

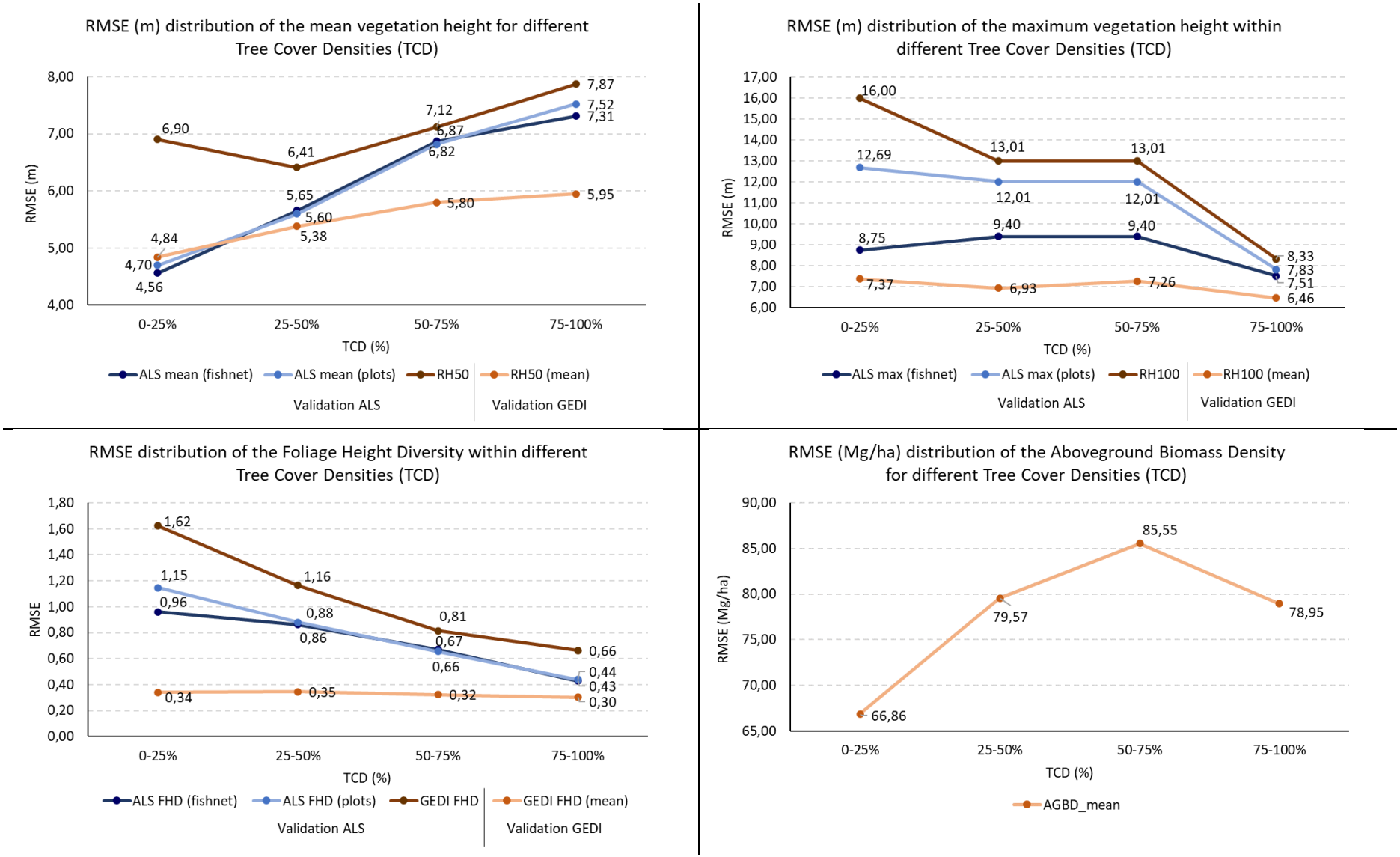

Figure 39: RMSE distribution of the four vegetation parameters within different Tree Cover Densities (TCD). Upper left: Mean vegetation height. Upper right: Maximum vegetation height. Lower left: FHD. Lower right: AGBD.

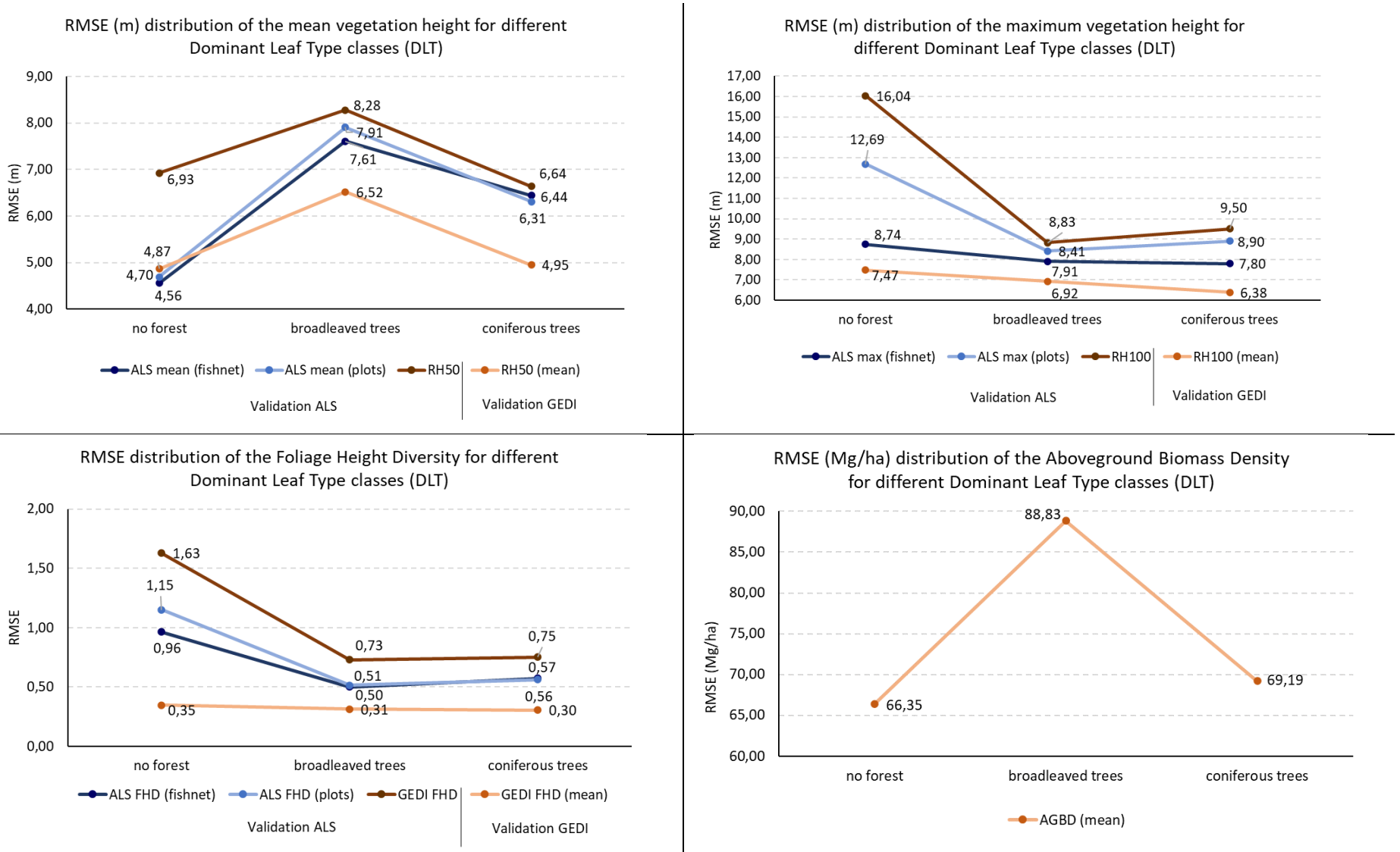

Figure 40: RMSE distribution of the four vegetation parameters for different Dominant Leaf Type classes (DLT). Upper left: Mean vegetation height. Upper right: Maximum vegetation height. Lower left: FHD. Lower right: AGBD.

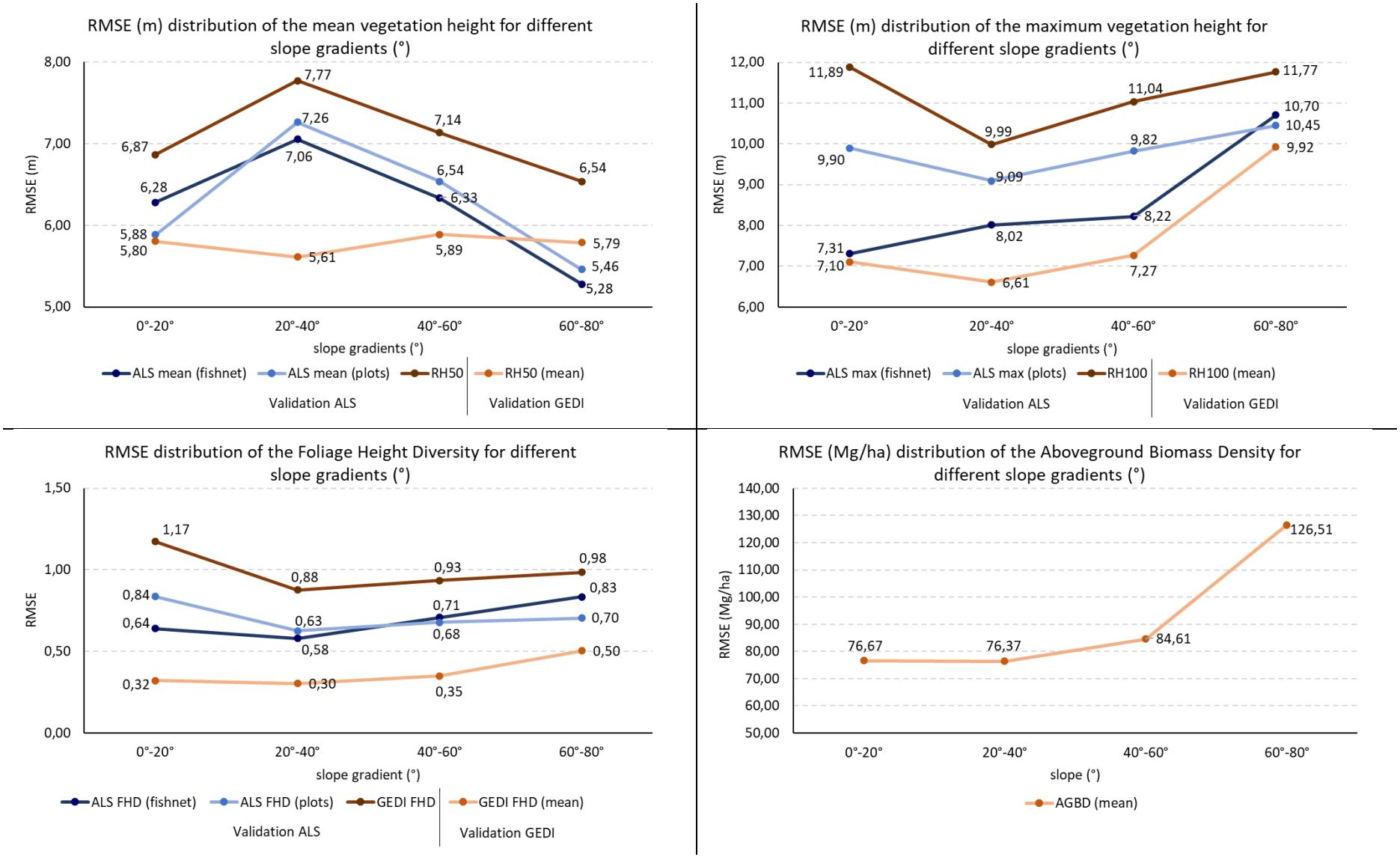

Figure 41: RMSE distribution of the four vegetation parameters for different slope gradients (°). Upper left: Mean vegetation height. Upper right: Maximum vegetation height. Lower left: FHD. Lower right: AGBD.

7.3.3. Quantitative and qualitative Analysis of the Regression Results based on four exemplary Plots

To support the analysis of the regression results with field data, four of the visited plots were selected. Each one of them represent a distinctive forest type (see Figure 42): Old growth beech forest (plot 6349), mixed forest (plot 1960), monoculture spruce forest (plot 1559) and young beech forest (plot 1951).

Firstly, the conditions on site were analysed. Further, the available GEDI data for each plot was compared with the respective values of the regression results, calculated based on the GEDI data. For each plot the averaged regression value was calculated through Zonal Statistics. It was analysed how far the predicted values deviated from the measured values. A negative value thus means that the regression underestimated the original value, a positive value overestimated it. Only regressions calculated with the variable combination *all bands* were employed, considering this method resulted in the lowest error values for each vegetation parameter as explained in the chapter 7.2.

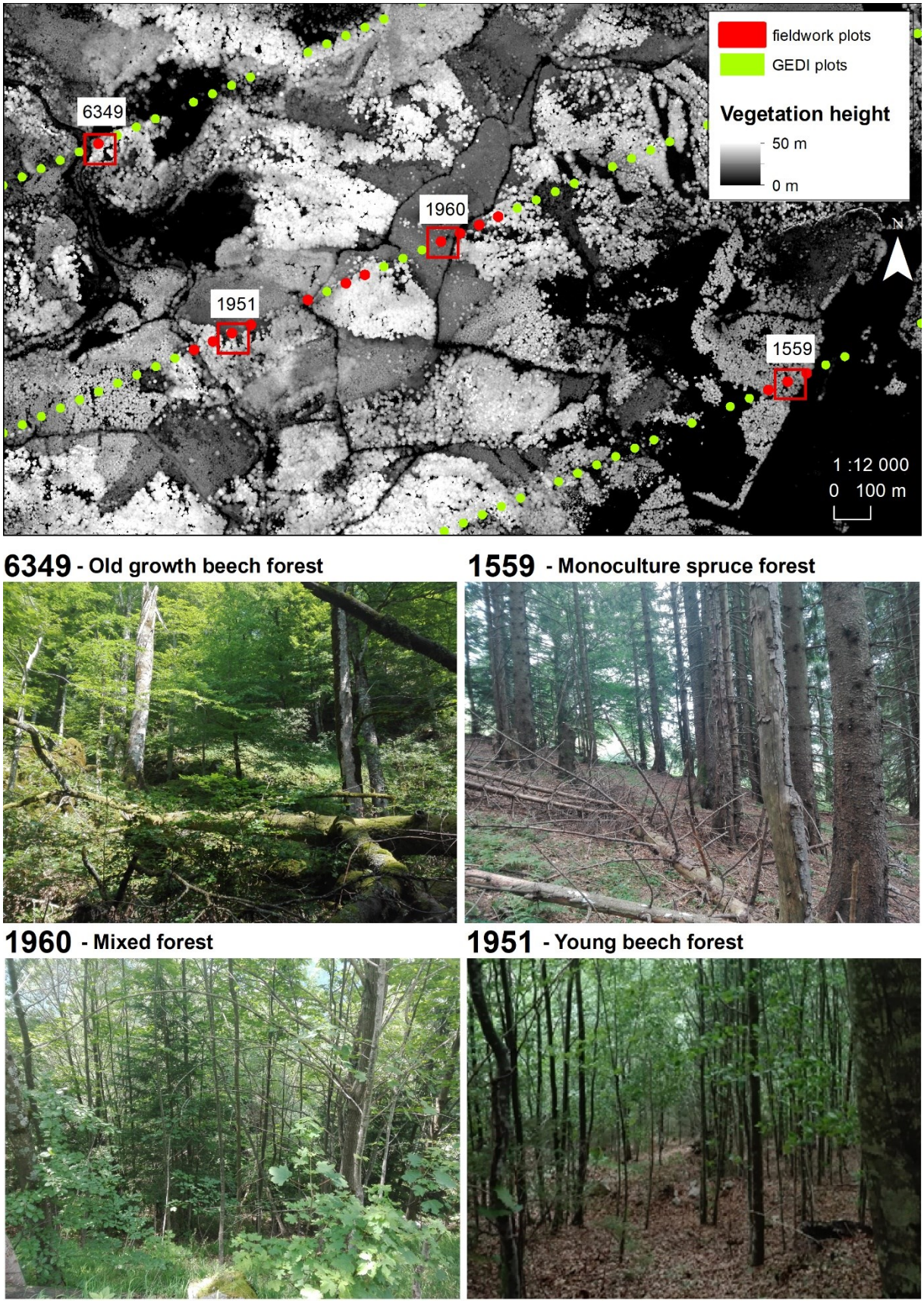

Figure 42: Field plots representing different forest types.

7.3.3.1. Plot 6349 - Old Growth Beech Forest

Plot 6349 is a prime example of an old growth forest. The study site is dominated by old beech trees and lying and standing deadwood. The clearing is naturally rejuvenated by young beech (see Figure 42). The number of layers is classified as two and the vertical structure of the forest could be described as medium. The plot itself is located at an altitude of 686 m a.s.l. and has a slope of 30°. The maximum canopy height according to ALS is 37.08 m and 46 m according to GEDI. The average height for ALS is 25.00 m and 11.08 m for GEDI. The ALS FHD value is 2.64 and the GEDI FHD value is 2.97. The GEDI AGBD is specified as 288.92 Mg/ha (see Table 28).

The averaged regression value for RH100 is 36.30 m (see Table 24). This is an underestimation of the GEDI value by 9.70 m or 21%. The RH50 average is 14.57 m. It overestimates the actual GEDI value by 3.49 m or 31%. The FHD value is 2.86 and underestimates GEDI by 0.11 or 4%. The predicted ABGD is 245.87 Mg/ha. The initial GEDI value is underestimated by 43.05 Mg/ha or 15%. Comparing the regression results with the nDSM in Figure 43, it can be seen, that the horizontal forest structure is roughly depicted by all four vegetation parameters. A road and river are running through the map from the upper left-hand corner down to the middle, dividing the forest. Furthermore, a clearing (in this case a pasture) is also clearly visible in the top right corner of the map. The forest structure itself can be interpreted as highly structured and heterogeneous based on the nDSM. There are mostly tall trees, especially in the right field of the map, interspersed with clearings. The image presented by the nDSM would be consistent with the old growth forest conditions found on site. In particular, the pasture in the upper right edge of the map is clearly visible in the regressions AGBD, FHD and RH100. In the regression for RH50, this pasture is not as prominent, but the river and road are more visible.

Table 24: Deviation of the regression results from the original GEDI data for plot 6349.

6349	GEDI	Regression			Method
		Mean	Mean Deviation	Percent	
AGBD (Mg/ha)	288.92	245.87	-43.05	-15%	All bands
FHD	2.97	2.86	-0.11	-4%	All bands
RH50 (m)	11.08	14.57	3.49	31%	All bands
RH100 (m)	46.00	36.30	-9.70	-21%	All bands

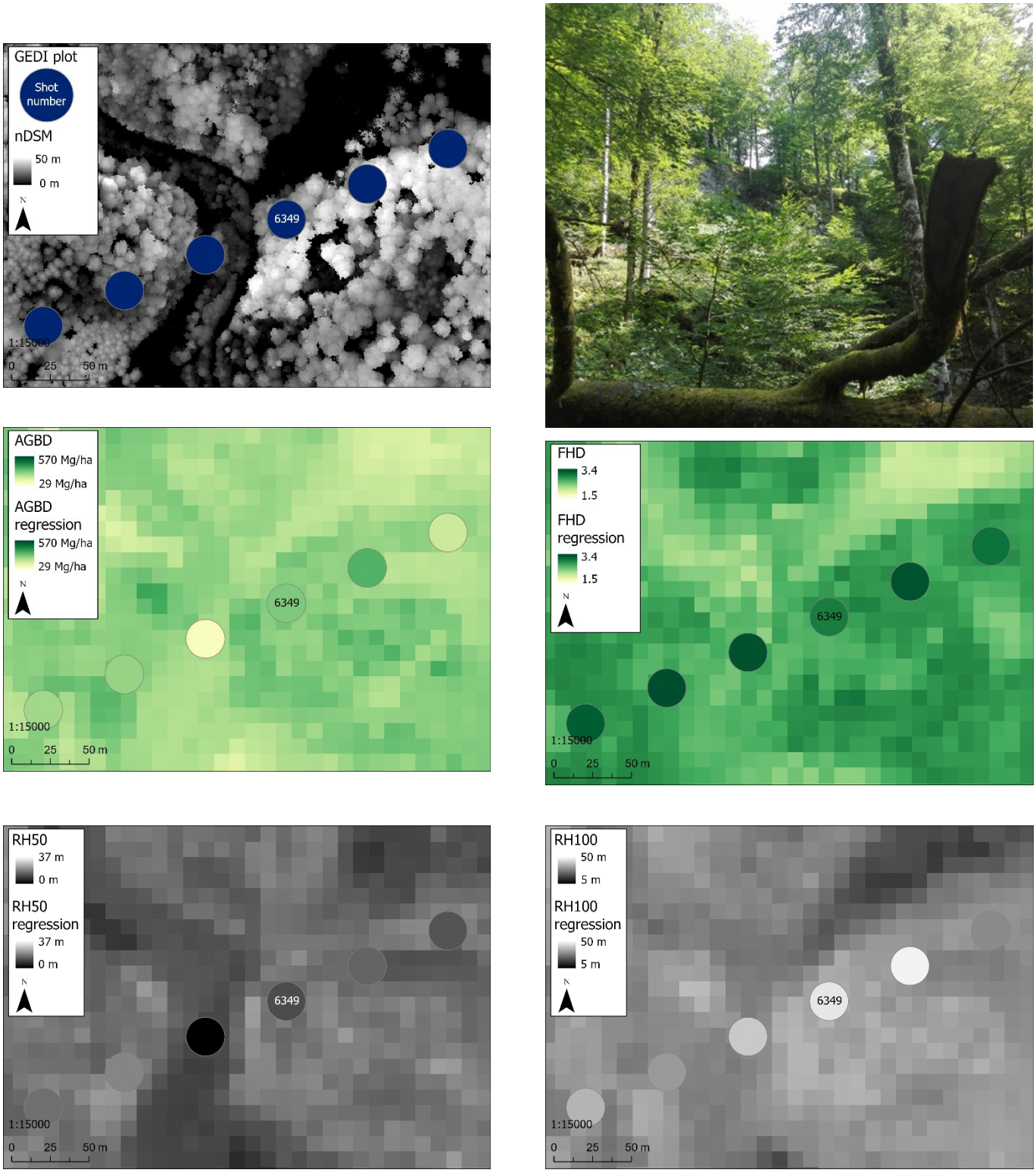

Figure 43: Plot 6349. Top: normalized Digital Surface Model; Upper Left: Above Ground Biomass Density; Upper Right: Foliage Height Diversity; Lower Left: RH50 (mean vegetation height); Lower Right: RH100 (maximum vegetation height). The GEDI plots depict the original GEDI values the raster depicts the regression values.

7.3.3.2. Plot 1960 - Mixed Forest

Due to its steep slope gradient of 35° located at 1010 m a.s.l., the conditions of Plot 1960 were only examined by looking down from the official path. The plots vegetation is defined as mixed forest, consisting of maple, spruce, and ash (see Figure 42). The plot is estimated to be two-layered and of high vertical structure. The maximum height according to ALS is 21.05 m, according to GEDI 12.13 m. The mean vegetation height stands at 14.89 m according to ALS and 1.08 m according to GEDI RH50. The ALS FHD is 2.04 and the GEDI FHD is 2.30. The GEDI AGBD value is 45.53 Mg/ha (see Table 28).

Furthermore, the regression values are compared to the initial GEDI values (see Table 25). The predicted average value for RH100 amounts to 27.58 m. Compared to GEDI, this is a deviation of 15.45 m and therefore an overestimation of 127%. With a deviation of 8.65 m or 801 % the predicted RH50 average value (9.73 m) also overestimates the initial GEDI value immensely. The FHD value is 2.80 and has a deviation of 0.50 from the GEDI, overestimating it by 22%. The regression for AGBD shows an averaged result of 153.55 Mg/ha. The original GEDI value is overestimated by 108.02 Mg/ha or 237%. Analysing the visual depiction of the regression results with the forest structure given by the nDSM, one can differentiate between the young, low-growth forest stock on the maps left hand side and the older, high-growth forest stock on the maps right hand side (see Figure 44). The vegetation parameters RH50, RH100 and AGBD all present lower values on the left-hand side and higher values on the right-hand side. It is noticeable that this differentiation is not recognizable for the FHD regression.

The calculated “overestimation” is probably in reality not an overestimation at all considering the height difference between GEDI and ALS, which is probably caused by the steep terrain. Previous assessments (Adam et al. 2020, 1) have shown that GEDI does not return reliable results in steep terrain. Comparing the maximum height of ALS (21.05 m) to the regression (27.58 m), the overestimation is much less.

Table 25: Deviation of the regression results from the original GEDI data for plot 1960.

1960	GEDI	Regression			Method
		Mean	Mean Deviation	Percent	
AGBD (Mg/ha)	45.53	153.55	108.02	237%	all bands
FHD	2.30	2.80	0.50	22%	all bands
RH50 (m)	1.08	9.73	8.65	801%	all bands
RH100 (m)	12.13	27.58	15.45	127%	all bands

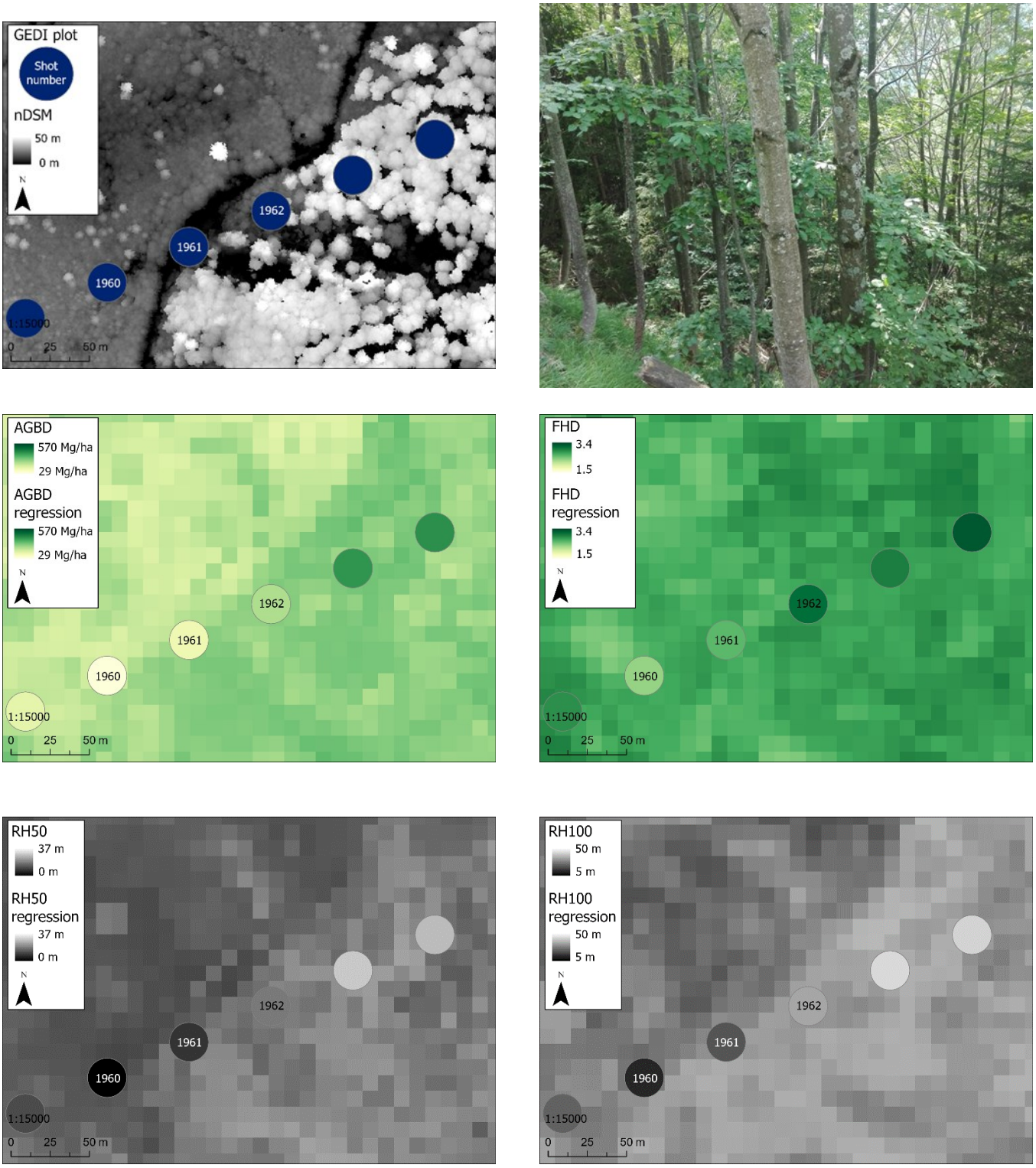

Figure 44: Plot 1960. Top: normalized Digital Surface Model; Upper Left: Above Ground Biomass Density; Upper Right: Foliage Height Diversity; Lower Left: RH50 (mean vegetation height); Lower Right: RH100 (maximum vegetation height). The GEDI plots depict the original GEDI values the raster depicts the regression values.

7.3.3.3. Plot 1559 - Monoculture Spruce Forest

Plot 1559 is located at an altitude of 1238 m a.s.l., has a slope gradient of 18° and presents as a typical example of a forest monoculture. The forest consists solely of densely growing, same age spruce trees with big tree diameters (see Figure 42). It can be estimated that the trees reach a height of 30 m. The crown base height is about halfway up the trees at approximately 15 m height above ground. Further, abundant lying and standing deadwood is present. The number of layers is estimated to be 1, the vertical structure can be classified as lightly structured. The top vegetation height measured by ALS is 29.36 m and by GEDI RH100 34.04 m. The mean vegetation height is 18.07 m according to ALS and 17.04 m according to GEDI. The FHD value calculated based on the ALS data presents a value of 2.80. GEDI provides a FHD value of 3.30. The GEDI AGBD value is 253.80 Mg/ha (see Table 28).
Table 26 presents the regression results. The average RH100 is 30.67 m, resulting in a deviation of -3.37 m to the original GEDI value. The original GEDI value is thus underestimated by 10%. The calculated RH50 value is 11.53 m and underestimates the actual GEDI value by 5.51 m or 32%. The predicted FHD value is 2.89 and underestimates the baseline value by 0.41 or 13%. The average AGBD value is 201.53 Mg/ha. Thus, it underestimates the original GEDI value by 52.26 Mg/ha or 21%. If one compares the nDSM with the regression results (see Figure 45), the forest area stands out clearly from the surrounding alpine meadows for all four parameters. It is noticeable that in the AGBD regression forest and meadow can be clearly distinguished. However, the AGBD values for the forest are too low. Also, the FHD is certainly too high for a simple one-layered stand. However, the deadwood could influence the FHD value. Further, the comparison of ALS and GEDI heights indicate, that the GEDI values are not very accurate in this difficult terrain.

Table 26: Deviation of the regression results from the original GEDI data for plot 1559.

1559	GEDI	Regression			Method
		Mean	Mean Deviation	Percent	
AGBD (Mg/ha)	253.80	201.53	-52.26	-21%	all bands
FHD	3.3	2.89	-0.41	-13%	all bands
RH50 (m)	17.04	11.53	-5.51	-32%	all bands
RH100 (m)	34.04	30.67	-3.37	-10%	all bands

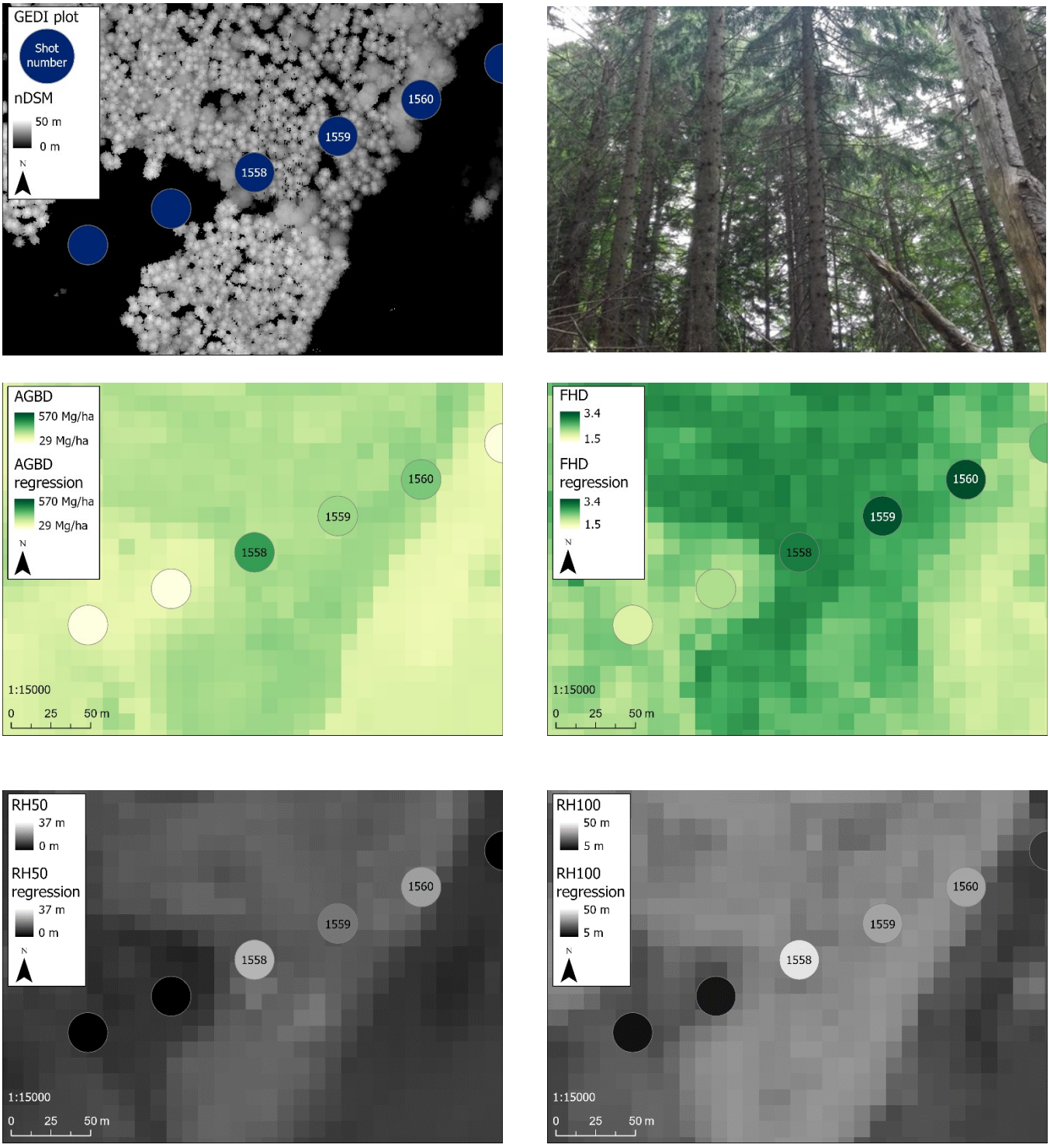

Figure 45: Plot 1559. Top: normalized Digital Surface Model; Upper Left: Above Ground Biomass Density; Upper Right: Foliage Height Diversity; Lower Left: RH50 (mean vegetation height); Lower Right: RH100 (maximum vegetation height). The GEDI plots depict the original GEDI values the raster depicts the regression values.

7.3.3.4. Plot 1951 - Young Beech Forest

Plot 1951 is located at an altitude of 762 m and has a relatively steep slope with 33°. It is characterized by beech forest that mostly consists of young trees (see Figure 42). Two or three older beech trees are present, as well as a few young spruce trees. Basically, the plot shows a high level of structuring, but no distinct layers. The number of layers is estimated to be multi-layered. The vertical structure is estimated to be highly structured. The top vegetation height for ALS is 38.15 m and for GEDI 25.7 m. According to ALS, the mean vegetation height amounts to 19.75 m and according to GEDI it is 10.15 m. The ALS FHD value is 2.55 and the GEDI FHD value is 2.92. For AGBD GEDI presents a value of 145.55 Mg/ha (see Table 28). Table 27 compares the GEDI data with the regression values. For RH100 the average value 30.98 m is calculated. This overestimates the GEDI value by 5.28 m or 21%. The predicted average value for RH50 is 13.02 m. The result deviates from the GEDI baseline value by 2.82 m and thus overestimates it by 28%. The average value of 2.83 is predicted for FHD, underestimating the initial GEDI value by 0.09 or 3%. For AGBD the average value 203.98 Mg/ha is calculated. The predicted value overestimates the original GEDI value by 58.43 Mg/ha or 40%. Visually comparing the regression results for the four parameters with the nDSM shows that the forest structure is very roughly depicted (see Figure 46). For all four parameters, fine differences between forest areas with high and low vegetation can be noticed. The low RH50, RH100 and AGBD values assigned to the upper right corner of the map fit the low vegetation height depicted by the nDSM. The FHD regression only predicts low values for forest areas with very low vegetation heights. The older beech forest in the lower half of the map has higher RH50, RH100, AGBD and FHD values. The small clearings within the tall stand are also recognizable trough lower RH50, RH100, AGBD and FHD values.

Table 27: Deviation of the regression results from the original GEDI data for plot 1951.

1951	GEDI	Regression			Method
		Mean	Mean Deviation	Percent	
AGBD (Mg/ha)	145.56	203.98	58.43	40%	all bands
FHD	2.92	2.83	-0.09	-3%	all bands
RH50 (m)	10.15	13.02	2.87	28%	all bands
RH100 (m)	25.70	30.98	5.28	21%	all bands

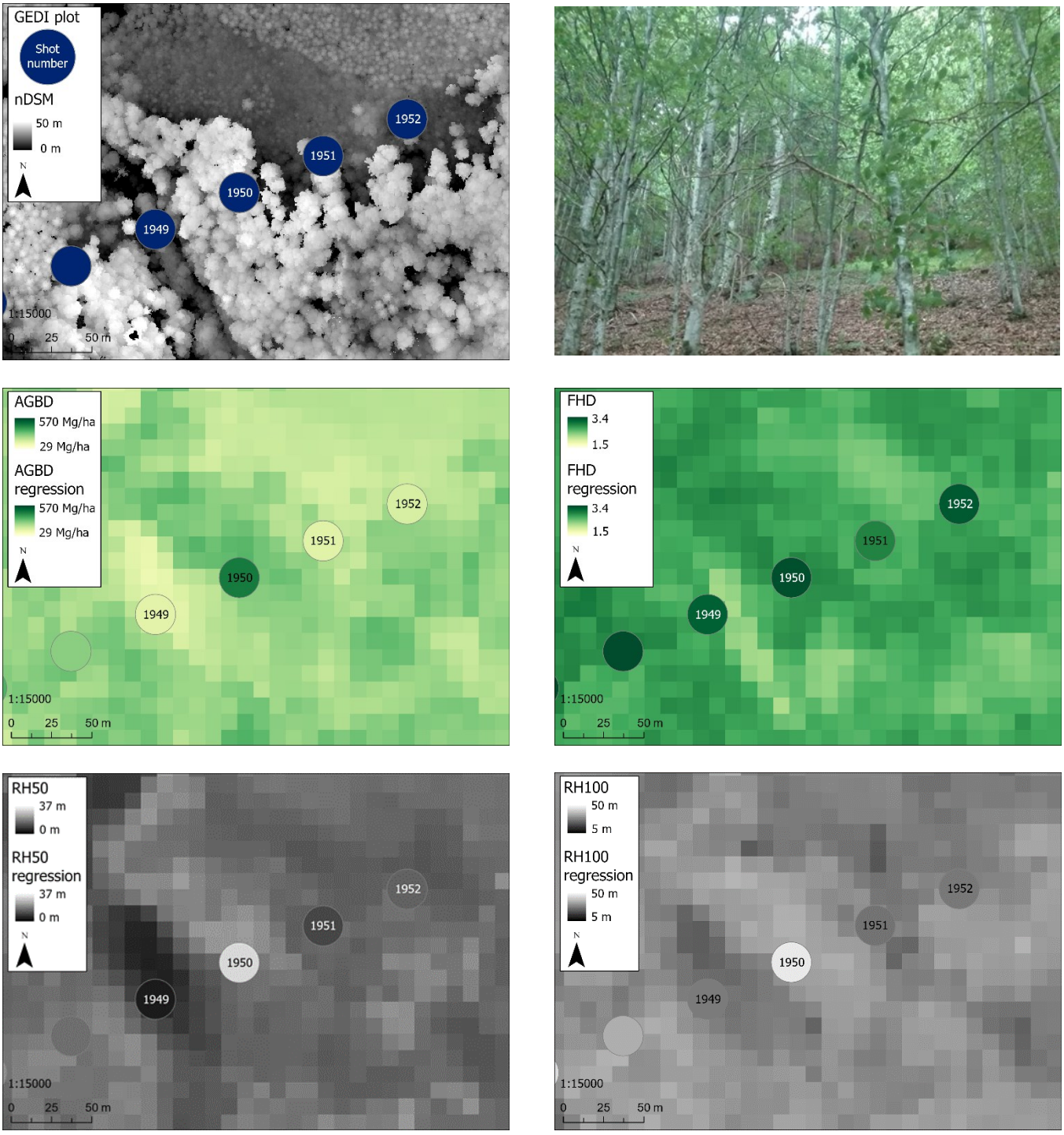

Figure 46: Plot 1951. Top: normalized Digital Surface Model; Upper Left: Above Ground Biomass Density; Upper Right: Foliage Height Diversity; Lower Left: RH50 (mean vegetation height); Lower Right: RH100 (maximum vegetation height). The GEDI plots depict the original GEDI values the raster depicts the regression values.

8. Discussion

8.1. Vegetation Height

The mean vegetation height shows a moderate to strong positive correlation with vegetation indices that are calculated using the vegetation red edge bands (NDVI6, NDVI7, NLVI) and the NIR (EVI, NDVI, NDVI8a, SAVI). Among them the mean band of the NDVI6 for the ALS mean (fishnet) and the median band of the NLVI for the ALS mean (plots) and RH100 (plots) achieve the strongest correlation values; R^2/R = 0.38/0.61, R^2/R = 0.41/0.64 and R^2/R = 0.16/0.41 respectively. Also, the mean band of the NDVI6 as well as the median band of the NLVI appear to be among the most contributing variables for the mean vegetation height, reaching a feature importance of up to 71% and 40% respectively. Compared to the mean vegetation height the correlation values between the maximum vegetation height and the Sentinel variables are lower. But like the other parameter the maximum vegetation height shows positive weak to moderate correlations with vegetation indices that are calculated using the vegetation red edge bands (NDVI6, NDVI7, NLVI) and the NIR (NDVI8a, EVI). The highest R^2 value for the maximum vegetation height (ALS fishnet) was achieved for the mean band of the NDVI6 resulting in R^2/R = 0.25/0.50. Other studies that had directly comparable examples for the correlation between the mean or maximum vegetation height and vegetation red edge based indices such as NDVI6, NDVI7 or NLVI could not be found. Most utilized more common indices such as the NDVI, EVI or SAVI (Fagua et al. 2019, Pascual et al. 2010, Liu et al. 2019). Fagua et al. (2019) for example observed the correlations between the canopy height (RH98) and the NDVI and EVI, with the best results being R = 0.56 and R = 0.66 respectively. Our results showed a slightly weaker correlation between the mean band of the NDVI and the maximum vegetation height (ALS max (fishnet): R = 0.47, ALS max (plots): R = 0.34, RH100 (plots): R = 0.22) as well as the mean vegetation height (ALS mean (fishnet): R = 0.58, ALS mean (plots): R = 0.57, RH50 (plots): R =0.37) (see Table 10, Table 11 & Table 13). The correlation values between the mean band of the EVI and the mean vegetation height were slightly stronger (ALS mean (fishnet): R = 0.61, ALS mean (plots): R = 0.60, RH50 (plots): R = 0.40), for the maximum vegetation height slightly weaker (ALS max (fishnet): R = 0.47, ALS max (plots): R = 0.30, RH100 (plots): R = 0.21) (see Table 10, Table 11, Table 13 & Table 34). Another study that also observed the correlation between the mean vegetation height and the NDVI was Pascual et al. (2010), their strongest correlation resulting in R = 0.73. Even though no direct comparison could be found for the correlation or feature importance of vegetation red edge based indices, most studies noted that adding vegetation red edge indices did improve their results. Li et al. (2020) discovered that the red edge NDVIs contributed the

most when estimating the forest canopy height (RH95), next to the texture variable contrast of the NDVI or the VV backscattering coefficient. Xi et al. (2022) also discovered that one of the most important variables when mapping the forest canopy height was the NDVI_B86 and the NDVI_B8a7, calculated "(B8-B6)/(B8+B6)" and "(B8a-B7)/(BA+B7)". Other vegetation red edge indices were the RENDVI a ("(B5-B4)/(B5+B4)") and the RNDVI b ("(B6-B5)/(B6+B5)") utilized by Jiang et al. (2021), achieving a feature importance of ~7% and ~6% respectively, when estimating the forest canopy height (RH98). Another variable that played an important role in predicting the mean vegetation height in our study was the mean and median band of the red band (B4), the highest feature importance amounting to 23% and 26% respectively (see Figure 20). The red band (B4) had a weak to moderate negative correlation to the mean vegetation height (ALS mean (fishnet): R = -0.57, ALS mean (plots): R= -0.56, RH50 (plots): R = -0.32) as well as the maximum vegetation height (ALS max (fishnet): R= -0.50, ALS max (plots): R = -0.42, RH100 (plots): R = -0.26) (see Table 10, Table 11 & Table 13). But when predicting the maximum vegetation height the red band (B4) only contributed little. The most important bands appeared to be the mean and median band of the green (B3) and first vegetation red edge (B5) band, achieving feature importance values of up to 30% (B3_med) or 54% (B5_med) (see Figure 22). These results agreed with the median green band (B3) and the median first vegetation red edge band (B5) recording the highest correlation results with the maximum vegetation height (ALS max (plots) & RH100 (plots)), resulting in R^2/R = 0.20/-0.45 and R^2/R = 0.08/-0.28 respectively (see Table 13). Other studies also observed that the S2 B3 and B5 played an important role in predicting the canopy height. Perez et al. (2022) discovered that the B5 is quite relevant for the mean vegetation height (R^2 = 0.21) as well as the maximum vegetation height (R^2 = 0.18). Hallik et al. (2019) also observed a negative correlation between the average vegetation height and the first vegetation red edge band (B5) and the green band (B3), R = -0.30 and R = -0.45 respectively. For Liu et al. (2019) the B3 is one of the most important variables in the RF model when mapping the canopy height achieving a feature importance of ~18%. Gao et al. (2019) also observed a strong negative correlation between the natural vegetation height and the reflectivity of green light bands, resulting in R = -0.86. The reflectivity in the green band, red band, vegetation red edge bands or NIR bands is directly related to the chlorophyll content of the vegetation. Chlorophyll shows strong absorption in the red band and reflection in the green, vegetation red edge and NIR bands. Studies have shown that with increasing tree height the chlorophyll content decreases. Rajsnerová et al. (2015) found a decrease in total chlorophyll content in the upper canopy leaves of beech trees. Räim et al. (2012) observed that needles of taller Norway spruce trees had a lower mass-based chlorophyll concentration. Furthermore, taller/older trees have a higher dry mass per area and volume than younger trees (Räim et al. 2012, 3). This would

explain the negative correlation between the S2 bands and the mean and maximum vegetation height.
Furthermore, both the mean and the maximum vegetation height have a weak to very weak correlation with all S1 backscatter and texture variables. But, when analysing the feature importance, it was apparent, that S1 variables did contribute to the prediction of the mean and maximum vegetation height. Especially the textural mean and standard deviation band of the VH polarisation.

The best regression results for the mean vegetation height as well as the maximum vegetation height (see Table 21) regarding the RMSE and MAE values were in both cases achieved by using the GEDI data as training and validation datasets. Resulting in the values RMSE = 6.36 m and MAE = 5.05 m for the mean vegetation height and RMSE = 7.51 m, and MAE = 6.06 m for the maximum vegetation height, but only achieving R^2 values of 0.31 and 0.27 respectively. The highest R^2 values were calculated for the regressions utilizing the ALS data as training and validation dataset and the fishnet grid cells as training samples. For the mean vegetation height, the $R^2 = 0.46$, and for the maximum vegetation height the $R^2 = 0.45$. Compared to other studies our regressions are a lot less accurate. Calculating the canopy height Li et al. (2020) achieved results of R = 0.78 and RMSE = 2.64 m for their DL model and a R = 0.68 and RMSE = 2.93 m for their RF model. It must be noted though that Li et al. (2020) use a far lower resolution of only 250x250 m per pixel. Although they conduct this study for a fairly large area (2773 km²) with challenging topography (elevation ranging from 585 to 1230 m) their results are better probably because extreme values are averaged over the larger pixel size. Our regression results have shown that values at the extreme upper or lower end of the value spectrum are typically underestimated or overestimated (see Figure 28 & Figure 31). Torres de Almeida et al. (2022) also assess the potential of S1 and S2 satellite data to model the canopy height. The highest accuracy was obtained when using the RF algorithm and 20 m resolution features only from the S2 data (R^2=0.58, RMSE = 4.92). Airborne LiDAR data was used for training (100 samples) the algorithm and the cross-validation (28 samples). Most of the models performed better when using S1 and S2 data with a 20 m instead of a 10 m resolution. Furthermore, the study was conducted in the Atlantic Forest of Parana, Brazil, which is mostly characterized by flat terrain. One study presenting good regression results with high resolution (10x10m per pixel) for large areas with challenging terrain is the one conducted by Lang et al. (2019). They utilized S2 data to estimate the vegetation height with a Convolutional Neural Network (CNN) for the two study areas Gabon and Switzerland. For validation LVIS LiDAR data and an already existing canopy height model are used. For Switzerland a MAE of 1.7 m and a RMSE of 3.4m was calculated, and for Gabon, the MAE was 4.3 m and the RMSE 5.6 m. Another study that is very comparable to ours is Kacic et al.

(2023) combining S1 and S2 imagery with GEDI samples to assess the wall-to-wall forest canopy height (RH95) at a 10 m resolution for the whole of Germany. Resulting in a $R^2 = 0.65$, a MAE = 4.4 m and a RMSE = 6.6 m. In our study we utilize the RH100 instead of the RH95 values as stand in for the canopy height. This could be a reason why the RMSE and MAE values for the regressions trained and validated by the GEDI data are larger compared to the results of Kacic et al. (2023). Furthermore, our R^2 values were a lot lower, the highest being $R^2 = 0.27$. An explanation for this can be Kacic et al. (2023) utilizing 10000 (train: 70%; test: 30%) GEDI samples per model compared to our 1156 GEDI samples in total.

8.2. Foliage Height Diversity

Overall, the green band (B3) and the first vegetation red edge band (B5) seem to have the highest correlation values with the FHD based on GEDI as well as ALS data. The strongest correlation values were calculated between the ALS FHD (fishnet) and the median and mean band of the first vegetation red edge band (B5) and the median and mean band of the green band (B3), resulting in $R^2/R = 0.27/-0.52$, $R^2/R = 0.26/-0.51$, $R^2/R = 0.22/-0.47$ and $R^2/R = 0.22/-0.47$ (see Table 12) respectively. When analysing the feature importance, it is noticeable that the median green band (B3) and the mean and median first vegetation red edge band (B5) are contributing the most, achieving values of up to 24%, 30% and 35% respectively (see Figure 24). Similar to the vegetation height the FHD has very weak to weak correlations with the S1 data overall. Still the method *all bands* adds GLCM standard deviation bands of the S1 VH146, VH44 and VV44 . The standard deviation band of the VH44 even achieving a feature importance of 11% for the GEDI FHD regression. No direct comparison with other studies considering the correlation between S1 and S2 data and the FHD could be made. Further analysis shows a weak to moderate correlation between the FHD and the mean vegetation height (ALS: R=0.39, GEDI: R=0.58) and a moderate to strong correlation between the FHD and the maximum vegetation height (ALS: R=0.54, GEDI: R=0.72). This can explain why the FHD shows similar correlations for the S1 and S2 data.

The FHD regression (see Table 21) with the lowest RMSE (0.36) and MAE (0.31) values was calculated using the GEDI data for training and validation. The FHD regression with the highest R^2 (0.40) value was calculated using the ALS FHD data for training and validation and the GEDI plots as samples. There are very few studies projecting FHD values to a larger area by combining them with satellite multispectral and SAR data. Lee et al. (2020) for example estimate the forest vertical structure. The data on the vertical structure is collected through a field survey and combined with multi-seasonal optical satellite imagery and topographic data. Hereby the vertical structure is presented in the form of three classes: single layer, double

layer, and triple layer. The FHD index would allow a more nuanced assessment of the vertical structure. Other researchers try to utilize FHD as an input variable to model the forest diversity for example Ren et al. (2023). The study aims to characterize forest tree species diversity by using GEDI LiDAR data and S2 imagery. The FHD index turned out to be one of the most important variables. Kacic et al. (2021) investigated the wall-to-wall mapping of the FHD. They assessed the vegetation structure characteristics for the complete Paraguayan Chaco an area of 240000 km² (or 24000000 ha) by fusing S1, S2 and GEDI data. 700000 filtered GEDI samples were used to train (90%) and validate (10%) the maps modelled not only for FHD, but also PAI, canopy height and total canopy cover. The FHD regression achieved a mean R^2 = 0.47 and a median R^2 = 0.48, the RMSE and MAE resulted in 0.3 and 0.2 respectively. The RMSE and MAE results are comparable to our values for the regressions trained and validated with GEDI. Kacic et al. (2021) possibly managed to achieve slightly better results by modelling the FHD values in a very flat and homogenous terrain that is characterised by forests with low heights and a low vertical structure and by using the spatial resolution 30x30 m. Furthermore, our R^2 value estimated for the regression trained and validated with GEDI only resulted in 0.17. This could be due to Kacic et al. (2021) utilizing a much larger dataset.

8.3. Aboveground Biomass Density

The AGBD GEDI values have their highest correlation with the median band of the NLVI (R^2 = 0.11/R=0.33), followed by the minimum (R^2=0.10/R=0.31) and mean (R^2=0.09/R=0.31) band of the NDVI6 (see Table 13). Similarly, to the vegetation heights and the FHD, the AGBD only has very low R^2 values ranging from 0.00 to 0.03 for the correlation between S1 data and AGBD (see Table 34). Debastiani et al. (2019) also had results that showed a very poor correlation between S1 backscatter values and the AGB, but still demonstrated, that the use of the GLCM texture variables led to an improvement in AGB estimates. This can also be observed for our study. Only employing the 10 variables with the best correlation (*Top 10*) to calculate the AGBD regressions results in a mean R^2 of 0.16. While utilizing the method *all bands* results in a mean R^2 of 0.27 (see Table 20). When analysing the feature importance of the used variables between the method *Top 10* and *all bands* (see Figure 26) the mean band of the NDVI6 is the feature with the highest importance in both cases, 39% and 20% respectively. The method *Top 10* attributes the second and third highest feature importance to the minimum band of the NDVI6 (16%) and the median band of the NLVI (12%). The method *all bands* shows the second highest feature importance for the GLCM standard deviation band of the VH44 (17%) (see Figure 26), indicating, that the addition of S1 texture data resulted in an improvement of the regression results. Another variable with a high feature importance

(12%) is the mean band of the red band (B4). Wang et al. (2023) yielded a similar feature importance (12.93%) for the red band when estimating the AGB for mixed broadleaved and pine forest in the northeast of China. They also had the NDVI ranked as one of the most contributing variables with a feature importance of 10.14%. Overall, the only feature the method *Top 10* and *all bands* have in common is the NDVI6, matching with the knowledge, that the NDVI has been proven to be an essential variable in estimating forest parameters (Wang et al. 2023, 9).

The deviation of the ALS derived AGBD values from the GEDI values were quite significant. Therefore, we could not compare the regressions based on space-borne with air-borne AGBD values. These circumstances prevented the analysis of the predicted AGBD data for the whole study area and limited it to the GEDI plots. It is therefore questionable how meaningful the results of the AGBD regressions are. Nevertheless, it was possible to undertake a cross-validation with the GEDI data, achieving its best results for the method *all bands* with R^2 = 0.27, RMSE = 88.11 (Mg/ha) and MAE of 68.51 (Mg/ha).

Compared to other studies the regression results of this study proved to be a lot less accurate (see Nandy et al. 2021, Liu et al. 2019, Debastiani et al. 2019). Nandy et al. (2021) were able to predict the forest AGB with R^2 = 0.68 and RMSE = 25.18 Mg/ha using a RF model consisting only of spectral variables. When incorporating forest height information into the model the results improved (R^2 = 0.83 and RMSE = 19.98 Mg/ha). Liu et al. (2019) calculated the AGB using three RF models for the forest types of coniferous forest, broadleaved forest and mixed forest. The results demonstrated, that the three AGB estimation models performed better separately than the model built by grouping them all together, resulting in R^2 = 0.42 and RMSE = 31.02 Mg/ha. The best results were achieved for the broadleaved forest model with R^2 = 0.74 and RMSE = 23.40 Mg/ha, followed by the coniferous forest model with R^2 = 0.74 and RMSE = 24.21 Mg/ha and the mixed forest model with R^2 = 0.69 and RMSE = 24.14 Mg/ha. In addition to the spectral vegetation indices derived from S2, Liu et al. (2019) included biophysical variables (LAI, fraction of vegetation cover etc.), topographic variables (aspect, slope etc.) and the forest stand mean height derived from S1 into the models to estimate the AGB. Debastiani et al. (2019) estimated the AGB for tropical forests using three variable combinations (treatments) and 12 machine learning algorithms. The first treatment utilized the backscatter of the S1 VV and VH polarisation. The second treatment added S1 textural metrics, and the third treatment added S2 bands and derived vegetation indices. The results for most of the 12 algorithms improved, when more variables were added. For each of the three treatments the Robust Regression model (58.03 – 57.76 – 47.66 Mg/ha) achieved the best and the Random Tree model (83.65 – 85.37 – 71.00 Mg/ha) the worst results. The results of the RF model (63.89 – 62.40 – 50.30 Mg/ha) are in the middle field, compared to the other results.

It is noticeable that the other studies, despite using significantly less training and validation data for larger areas, still achieve better results. Even though the AGBD results are presented at the same high spatial resolution (10x10 m) as our results (Nandy et al. 2021; Liu et al. 2019). Only Debastiani et al. (2019) use a lower spatial resolution of 100x100 m. Our study uses a cross-validation with a training dataset of 1041/1040 plots and a validation dataset of 115/116 plots to calculate the AGBD for an area of 5600 ha. In comparison Nandy et al. (2021) estimate the AGB for an area of 145600 ha using 100 plots for training and 30 plots for validation. While Liu et al. (2019) use 28 plots for broadleaf, 33 plots for coniferous and 18 plots for mixed forest validation for an area of 3901700 ha. Debastiani et al. (2019) also only use 286 plots in total for training and validation. This discrepancy can eventually be connected to the more challenging nature of our study area, that encompasses a height range of ~1260 m and a median slope gradient of 32°. The other studies are conducted in completely flat terrain (Debastiani et al. 2019, 111), undulating (Nandy et al. 2021, 2) or hilly terrain (Liu et al. 2019, 3). Also, Debastiani et al. (2019) utilize airborne LiDAR data to calculate the AGB values, while Nandy et al. (2021) as well as Liu et al. (2019) employ field data to calculate the AGB. Both data sources would deliver very accurate information. Especially the collected field data would not be affected by error values within the original dataset, due to a high slope inclination. Furthermore, it must be noted that a lower RMSE value does not necessarily indicate a better result. Debastiani et al. (2019) demonstrated in their study that the random tree model resulted in the lowest RMSE values but represented the variability of the AGB values best.

Analysing the AGBD regression visually, it can be seen from Figure 37 that the AGBD value distribution corresponds to the vegetation height. It can be observed that low AGBD values prevail in areas that are known to be alpine pastures, whereas higher AGBD values predominate in areas with higher vegetation heights. This statement is supported by the correlation coefficient R calculated between the AGBD regression (*all bands* mean) and the mean and maximum vegetation height based on the original ALS data and the GEDI regressions. The correlation between AGBD and ALS mean and max, results in R = 0.57 and R = 0.55 respectively, showing a moderate correlation. While calculating the correlation between AGBD and the RH50 and RH100 regression results in R = 0.89 between AGBD and the mean height, and R = 0.88 between AGBD and the maximum height, showing a very strong correlation.

In order not to rely solely on the cross-validation, a comparison between the mean AGBD regression (*all bands*) and global biomass maps is also used. Since the free access to biomass maps is limited, the reference data utilized has a significantly larger resolution or an earlier recording date. The Global Forest Biomass Map (GEOCARBON) from Wageningen University (Avitabile et al., 2016) is compared to our results. Its most recent status is 2016, it has a

resolution of 1.11x1.11 km per pixel and indicates the biomass in the unit Mg/ha. Furthermore, a biomass map from the CEDA archive is employed (Santoro et al. 2023). It has been recorded in 2020, has a resolution of 100x100 m per pixel and uses the unit Mg/ha. The GEOCARBON map shows a value range of 97.01 - 234.74 Mg/ha and has a mean value of 181.49 Mg/ha and a median value of 185.10 Mg/ha for the study area. The CEDA map has a value range of 0.00 - 468.00 Mg/ha, a mean value of 287.75 Mg/ha and a median value of 313.00 Mg/ha within the study area. Our mean AGBD regression covers a value range of 82.55 - 327.71 Mg/ha and has a mean value of 194.18 Mg/ha and a median value of 196.02 Mg/ha. The predicted AGBD values are therefore within a realistic range for the study area. But the different value distributions within the two reference datasets makes it difficult to conduct a clear assessment regarding the quality of our AGBD map.
Additionally, a comparison was made with field data collected at the monitoring stations in the Zöbelboden. This, however, was limited to an extremely small areal and only the values of one pixel are compared with the measured data per station. Although this enables an interesting comparison, it can by no means be used to determine the quality of the regression. Also, since the surveys are located outside the study area, no comparison can be made with the measured GEDI or ALS data, only with the regression results. It is still noticeable that the station (700) (see Table 22) located within mixed/beech forest achieves a higher accuracy than the station (2900) (see Table 23) located within the coniferous forest. The influence of the forest type on the regression results was further investigated in chapter 7.3.2. and chapter 8.6.

8.4. Correlation Summary

When analysing the correlation results for the different vegetation parameters the following observations could be made:

1) The strongest correlations were recorded for S2 bands and VIs.
2) All vegetation parameters had weak or very weak correlations with S1 backscatter and texture variables.

The variables with the highest positive and negative correlation values often overlap between the different vegetation parameters, especially between the mean vegetation height and the AGBD and the maximum vegetation height and the FHD. The highest R^2 results for the mean vegetation height and the AGBD were quite similar. The mean vegetation height and the AGBD both had their strongest R^2 results for the median band of the NLVI (AGBD: R^2/R=

0.11/0.33; ALS mean (plots): R^2/R = 0.41/0.64). Other variables that frequently achieved high correlations were the EVI and particularly the NDVI6. The mean and maximum vegetation height also showed strong correlations with similar VIs when utilizing the fishnet grid for the value extraction. Both had their highest R^2 value for the mean band of the NDVI6 (Mean: R^2/R = 0.38/0.61; Max: R^2/R = 0.25/0.50). When utilizing the GEDI plots the highest correlation values achieved for the maximum vegetation height differed significantly from those of the mean vegetation height. Like the FHD the maximum vegetation height showed a noticeable correlation to S2 multispectral bands such as B3, B4 and B5. The variables with the highest correlation generally also showcased the highest feature importance when calculating the models. For the maximum vegetation height and the FHD the B3, B4 and B5 contributed the most and for the AGBD and the mean vegetation height the B4 and NDVI6 were most important. The NLVI was also quite significant for the mean vegetation height. As previously discussed in chapter 8.1, the significance of B3, B4 and B5 for the vegetation parameters can be explained by the spectral properties of chlorophyll. Furthermore, it is noticeable that VIs utilizing red edge bands (NDVI6, NLVI) have significant correlations with the vegetation parameters and play an important role in predicting them. The red edge region is defined as the spectral region between the wavelengths 680 and 750 nm where there is a sharp change in the vegetation reflectance (Xie et al. 2018, 2). Chrysafis et al. (2017) compared S2 and Landsat 8 data in the mapping of growing stock volume in a Mediterranean forest. They found that using the S2 RE1 band instead of the NIR band improved the accuracy of the results, but only marginally. Astola et al. (2019) also compared the performance of S2 and Landsat 8 data for forest variable prediction in the boreal forest of Southern Finland for the mean tree height. They found that the first vegetation red edge band (B5) was the best predictor, followed by the second vegetation red edge band (B6). Generally, the S2 data outperformed the Landsat 8 data and models utilizing the S2 variables without the red edge bands performed 1.6% worse on average than models using all S2 image bands. Further studies also demonstrated the S2 vegetation red edge bands and VIs with red edge bands improved the accuracy of vegetation parameter predictions (Perez et al. 2022, Li et al. 2020, Chen et al. 2021). Furthermore, it can be observed that the mean and the median temporal statistics bands have the highest correlation and feature importance values for all vegetation parameters. Indicating that these are the most significant temporal statistic aggregations to summarize the reflectance of the Sentinel data within the given time periods.

For all vegetation parameters the S1 backscatter, and texture variables show only a weak to overwhelmingly very weak correlation. A reason for this can be the very complex topography of our study area. It is known that geometric distortion is an inherent error of SAR images because of side-looking geometry and topographic relief. Mountainous terrain is known to

cause foreshortening, layover, and shadows (Chen et al. 2018, 1). Still, when analysing the used features and feature importance of models employing the band compositions *all bands* and *4 Orbits*, S1 derived variables are also employed. Especially the mean and standard deviation texture bands of the cross-polarisation VH, which sometimes reached quite high feature importance values, such as 16 % (see Figure 27) or even 19 % (see Figure 22). Models utilizing the band combinations *all bands* or *4 Orbits* generally perform better (see Table 21), indicating that adding the texture variables can improve the results. Other studies made similar observations, such as Chen et al. (2021) when combining field samples, GEDI, S1 and S2 imagery to estimate the forest stand volume. Within their study the correlation coefficient R only showed a weak to very weak correlation between the stand volume and S1 backscatter and texture variables. Nevertheless, the texture characteristics of the SAR imagery turned out to be very beneficial for the volume estimation. However, they discovered that the overall influence of SAR backscatter was marginal. They also concluded that the texture features from VV were more relevant than those from VH, contrary to our study. Debastiani et al. (2019) also employed S1 data with VV and VH polarisation to estimate the AGB. The results show that S1 backscatter values were poorly correlated with the AGB, but the use of the GLCM texture led to an improvement in AGB estimates by most algorithms. Overall, the addition of texture and optical data provided a noticeable improvement (3%) over models with SAR backscatter only. Another option would be to use SAR data with longer wavelengths (e.g. L and P) instead. They can penetrate the forest canopy and capture the backscatter from branches and trunks making them more sensitive towards the vertical forest structure. Compared to them the short wavelength C-band backscatter that is provided by S1 only has limited ability to capture the vertical structural information of forests (Sothe et al. 2022, 14). Other studies have utilized them and achieved promising results regarding their estimation power. When combining LiDAR data with S1 and S2 data to estimate the AGB, Guerra-Hernandez et al. (2022) concluded, that the S1 SAR C-band polarisation had only a limited effect on the RF model accuracy showing a feature importance of < 6.5%. The ALOS2/PALSAR2 L-band data, which they included in the study, had a much higher importance for predicting the AGB. Three of the top 5 predictors were L-band derived backscatter information. Sothe et al. (2022) also compared SAR C-band to L-band data when estimating the canopy height and the AGB, coming to the same conclusion. They also discovered in their study that the cross polarized data (VH) from both SAR sensors were more important than co-polarized data (VV), similar to our study. The cross polarized data indicates the volumetric scattering from vegetation related to tree leaves and branches, while co-polarized is mainly indicative of double bounce scattering associated with tree trunks, buildings or inundated vegetation.

Moreover, quite often the VH polarisation of the ascending orbit 44 is attributed with the highest feature importance compared to other GLCM features. Futhermore, it is used most often, followed by the descending orbit 22.

8.5. Regression Summary

Examining and comparing our results with other studies showed that the accuracy of our regressions was mostly smaller for all four vegetation parameters (mean and maximum vegetation height, FHD, AGBD). Explanations for this can be:

1) High spatial resolution of the modelled regressions.
2) Complex terrain of the study area.
3) Complex vegetation structure.

Other studies often used lower spatial resolutions compared to the 10 m resolution of our results. Torres de Almeida et al. (2022), Potapov et al. (2021), Debastiani et al. (2019) or Sothe et al. (2022) for example modelled vegetation parameters with the spatial resolutions 20 m, 30 m, 100 m or 250 m respectively. A high spatial resolution offers the advantage of capturing more details, while low spatial resolutions often produce biases due to the large pixel size. Less common surface features are often underestimated, causing a negative bias, and more common components can be overestimated, causing a positive bias (Haack & Rafter 2010, 71). But a high spatial resolution image will not always lead to a better interpretation. Coarse resolution images sieve out unnecessary details and offer a certain level of generalization, when interpreting the image for a large area (Mahavir 2000, 127). When predicting for example the vegetation height for a resolution of 250 m, within these ~6 ha of forest a wide range of canopy height can be included, due to a difference in tree age and disturbance histories that are all aggregated into one pixel (Sothe et al. 2022, 14). Extreme outliers are therefore erased from the dataset and more “averaged” values are presented.
Other studies also utilize the spatial resolution 10 m, for example Nandy et al. (2021), Kacic et al. (2021) or Liu et al. (2019). But their study areas were situated in flat or undulating terrain and did not have the same topographic complexity as our study area. There the slope inclination ranged from 0° to 89° with a median gradient of 32°. On sloped and forested terrain, LiDAR returns from both vegetation and ground can occur at the same height and therefore might not be distinguishable in the return waveform, especially since the ground returns are spread out over different heights. The error is therefore already present in the original dataset that is used for training and validation (Adam et al. 2020, 20). An exemplary area with difficult characteristics causing this kind of problem can be the GEDI plot 1960 (see Figure 44)

Also, our study area possesses a very diverse vegetation structure ranging from homogeneous spruce monoculture to old-growth beech forest with natural rejuvenation (see Figure 42). Nandy et al. (2021, 6) themselves noted that their good results could be explained by the relatively homogeneous conditions of forest canopy complemented by few topographic variations. It can be noted that the value range of different vegetation parameters for other studies was limited compared to our study, indicating more homogeneous vegetation structures. For example, our datasets for the maximum vegetation height ranged from 0.00 m to 50.00 m for the airborne data and 5.39 m to 49.97 m for the GEDI data, covering a value scale of 50.00 m and 44.58 m respectively. Even the mean vegetation height covered a broad value range; 0.00 m to 45.75 m for the airborne and 0.00 m to 36.60 m for the spaceborne data. In comparison Nandy et al. (2021) field-measured tree height only ranging from 14.20 m to 32.40 m, with a mean of 25.53 m and a value range of 18.20 m. Kacic et al. (2021) also conducted their study in an area with flat terrain (Paraguayan Chaco). Furthermore, the modelled canopy height only ranges from 1.80 m to 17.60 m, with a mean value of roughly 5.30 m and a value range of 15.8 m. Multilayered structures are not that prevalent within that forest ecosystem, which would cause the most limitations for GEDI derived canopy height estimates. Overall, the vegetation is rather low and rather sparse (mean total canopy cover: 19.5 %). For Liu et al. (2019) the canopy height ranged from 9.00 m to 36.00 m with the mean height being 19.00 m and the value range 27.00 m. Similar conditions could be observed for the AGBD. Our initial GEDI dataset included 28.44 Mg/ha as minimum and 569.29 Mg/ha as maximum values, covering a value range of 540.85 Mg/ha in total. For Liu et al. (2019) the AGB ranged from 12.64 Mg/ha to 285.43 Mg/ha covering a value range equalling 272.79 Mg/ha. The AGB of Debastiani et al. (2019) ranged between 139 Mg/ha to 516 Mg/ha, with a value range of 377 Mg/ha.

Commonalities between areas with high deviations were also investigated. This was only done for regressions that were validated with the ALS data, so the whole study area could be examined. Areas with high deviations for the mean and maximum vegetation height and the FHD were analysed. The best regression results for the variations ALS (fishnet), ALS (plots) and GEDI (plots) were combined. It was observed that the mean and maximum vegetation height were overestimated for areas with low vegetation in clearings and at the forest edge (see Figure 47) and underestimated for areas with high vegetation (see Figure 48). Similar observations were made by Sothe et al. (2022). Maps for GEDI as well as ICESat-2 tended to overestimate smaller trees (< 5m) and underestimate taller trees (> 20m). Reasons given for that was the 10-year gap between the recording date of the ALS data and the spaceborne data. During this period forest growth and disturbance can occur. Also, the ALS data did not cover the tallest forests within the research area and the ALS data used the RH95, while the spaceborne LiDAR utilized the RH98 for estimating the canopy height (Sothe et al. 2022, 13).

For our study the airborne and spaceborne data was only recorded 1 to 2 years apart from each other. This could explain the underestimation of the higher vegetation to some extent. Furthermore, large-footprint LiDAR is more prone to errors in tree height estimation for low stature forests. Young stands often show dense understory, especially coniferous trees possessing many little intersecting branches below the crown attenuating the laser return from the terrain (Hilbert & Schmullius 2012, 2227f.). When comparing the original ALS and GEDI data there is an already existing difference, which then influences the modelled outcome. But this would only explain, why models utilizing GEDI data overestimated the vegetation height in certain areas, Models using the ALS data also over- and underestimated the original input data. Another reason for the overestimation of the vegetation height in clearings and at the forest edge can be due to the spatial resolution of 10 m. A pixel overlapping with the forest edge can include the canopy of high trees even though the trees are not situated within the pixel itself. Also, the overestimation of low vegetation heights and the underestimation of high vegetation heights can be due to the value distribution of the initial ALS and GEDI data. High mean (> 25 m) and maximum (> 35 m) vegetation heights are not overly represented within the datasets and therefore the training samples (see Figure 16 & Figure 17). Low maximum vegetation heights (< 5 m) are also only sparsely present within the initial ALS dataset and not at all represented within the GEDI dataset (see Figure 17). The averaged FHD regressions overestimated the original ALS FHD values for low vegetation and clearings, but also areas with high vegetations (see Figure 47). Furthermore, very few areas could be identified, where the averaged FHD underestimated the original values (see Figure 48). Comparing the initial ALS FHD values to the initial GEDI FHD values (see Figure 18), the ALS dataset ranges from 0.00 to 3.80, while the GEDI dataset only encompasses FHD values ranging from 1.49 to 3.39, explaining why especially the GEDI based regression is more prone to overestimation.

Further investigations considering the influence of the study area characteristics on the regression results were made in chapter 8.6.

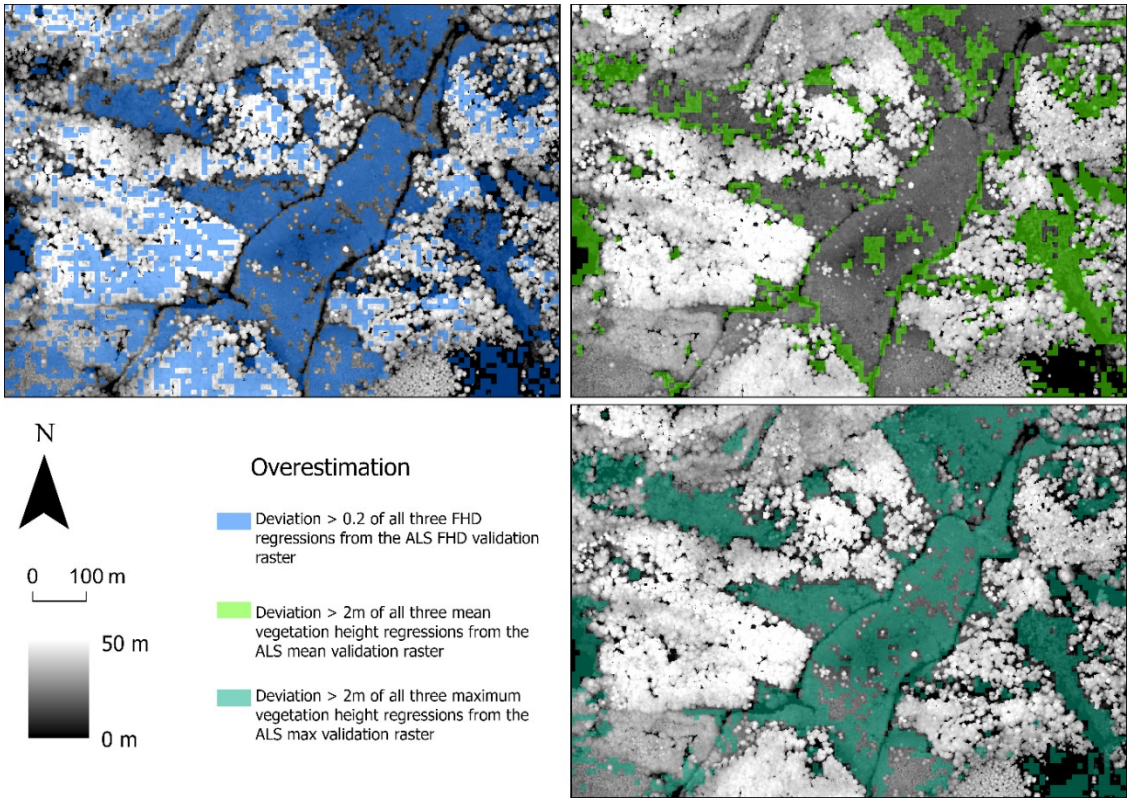

Figure 47: Overestimation of the regressions. Exemplary areas where all three variations (ALS fishnet, ALS plot, GEDI value) for the parameters mean vegetation height, maximum vegetation height and FHD overestimate the ALS validation values.

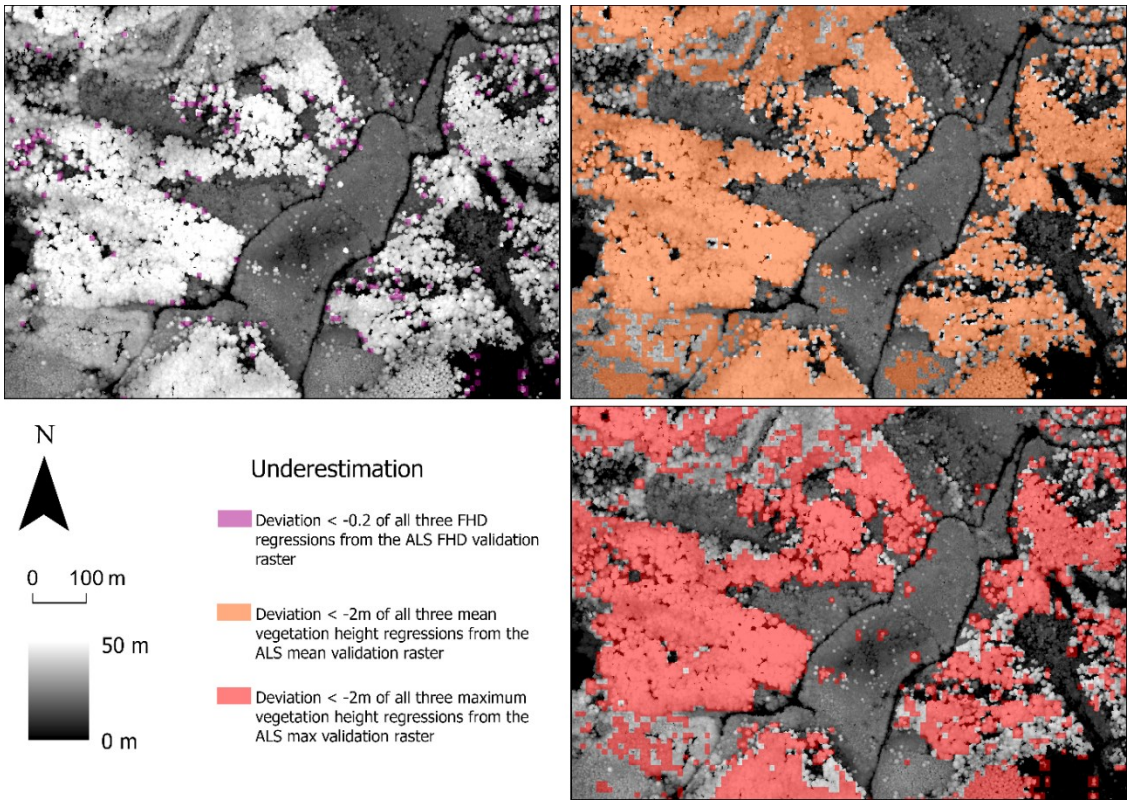

Figure 48: Underestimation of the regressions. Exemplary areas where all three variations (ALS fishnet, ALS plot, GEDI value) for the parameters mean vegetation height, maximum vegetation height and FHD underestimate the ALS validation values.

8.6. Influence of Study Area Characteristics

It can be observed that most of the RMSE values for the different variations (ALS fishnet, ALS plots, GEDI plots, GEDI cross-validation) of the vegetation parameters are distributed in a similar way among the classes of the study area characteristics as can be seen in Figure 39, Figure 40 and Figure 41. Indicating, that the study area characteristics could be having an influence on the accuracy of the regression results.

Overall, it can be analysed that the regressions trained and validated with GEDI data have less variations of the RMSE values among different TCD, DLT and slope classes. This can be due to the smaller number of GEDI plots compared to the fishnet grid cells which cover the whole study area. Due to this some of the TCD, DLT or slope classes can be underrepresented or overrepresented within the GEDI plots. For example, this can be observed especially for GEDI plots covering areas with slope inclinations > 60°. Only 3 plots of the entire dataset are present within this class.

Furthermore, it is noticeable that the RMSE distribution of the vegetation parameters maximum vegetation height and FHD react quite similar for each study area characteristic, while the RMSE distribution of the mean vegetation height is mostly contrary to both. The RMSE distribution of the AGBD is like the mean vegetation height considering the forest type and similar to the maximum vegetation height and FHD considering the slope gradient. Three study area characteristics were investigated:

1) The canopy cover (TCD)
2) The forest type (DLT)
3) And the slope inclination.

It can be observed that a high TCD corresponds to a decreasing accuracy for the mean vegetation height and partly the AGBD (see Figure 39). With increasing canopy cover the number of laser impulses that can penetrate the canopy and reach the ground decreases (Adam et al. 2020, 18). Adam et al. (2020) as well as Wang et al. (2019) discovered that this has mainly a negative influence on the accuracy of the DTM. But one could consider, that with decreased penetration of the canopy cover the layers below the top vegetation layer are not registered, therefore possibly leading to an underestimation of the mean vegetation height and the AGBD. Falkowski et al. (2008) discovered that high canopy cover conditions lead to a decreased accuracy of detecting individual trees. On the other hand, a low TCD records a decreasing accuracy for the maximum vegetation height and the FHD (see Figure 39). A significantly lower accuracy of the CHM (RH100) in areas with a canopy cover smaller than 25% was also observed in Adam et al. (2020) study. They suggested that this can be due to

the location of the GEDI plots in sloped areas. It can happen that the return signals from the canopy top might not exceed the waveform recording start threshold. The waveform recording is therefore triggered by lower canopy layers or ground return signals and the height difference between the waveform signal start and the ground elevation is underestimated. When Adam et al. (2020) removed plots in steep areas the accuracy of the CHM in areas with low canopy cover improved (Adam et al. 2020, 21). This differentiation was not conducted for this study, it can therefore not be said if it applies to our results.

Considering the forest type the mean vegetation height as well as the AGBD show a lower accuracy for the *broadleaved trees* class compared to the *coniferous trees* class and the *no forest* class (see Figure 40). Many studies have observed a higher accuracy of LiDAR CHM in coniferous forest than in deciduous or mixed forest (Adam et al. 2020; Wasser et al. 2013). This is because deciduous forests tend to have a more closed structure with less gaps for the laser impulse to detect the ground through (Adam et al. 2020, 20). Within our study area most of the trees within the *broadleaved trees* class are beech trees, while most of the trees within the *coniferous trees* class are spruce trees. Their growth properties vary from each other. The crown diameter of spruce increases continually with age. If additional space is provided through the removal of surrounding trees, they can only react slowly and to a limited degree. Throughout the trees lifespan the relation between crown size, needle biomass and timber volume stays relatively inflexible. On the contrary, beech trees can react with a pronounced increase in crown size, depending on the availability of light. It then may take some time for the relationship between timber and crown volume to adjust. They are known to form closed canopies, even with low tree density. This is referred to as sculpted crown. Therefore, these parameters are not as strongly related for beech trees as they are for spruce trees (Heurich & Thoma 2008, 657f.). The reduced relation between timber volume, crown volume and leaf biomass combined with the impermeable canopy cover, could explain the reduced accuracy of the AGBD estimation for the *broadleaved trees* class. For the maximum vegetation height as well as the FHD the accuracy for the *broadleaved* and *coniferous trees* classes is quite similar. A significant decrease in accuracy can be observed for the class *no forest*. Especially for the regressions utilizing the GEDI plots as training samples and validating the regressions with the ALS data (see Figure 40). This steep decline could be due to the size and form of the GEDI plots. If the footprint captures the backscatter of a meadow with one single tree, the maximum vegetation height is the maximum height of this tree. This would also apply to maximum vegetation height aggregated into one fishnet grid. But contrary to the GEDI plot the fishnet grid overlaps precisely with one Sentinel pixel. Therefore, the multispectral and textural characteristics are more representative for the conditions recorded in this sample. While the GEDI plot aggregates the values of several Sentinel pixels. The maximum vegetation height and FHD value are then set in a wrong relation to the multispectral and textural conditions

leading to a distortion when calculating the regressions. Furthermore, it has to be noted for both parameters based on the GEDI dataset, but especially the FHD, that lower values are not represented (see Figure 17 & Figure 18).

According to literature the steeper the slope the more the accuracy of the estimated vegetation height decreases (Adam et al. 2020; Hilbert & Schmullius 2012; Harding & Carabajal 2005; Yang et al. 2011). Contrary to this, it is noticeable for our study that a low slope gradient does not necessarily correlate with a low RMSE value (see Figure 41). It is possible that other study area characteristics have a larger influence on the RMSE distribution than the slope inclination or that the combination of different study area characteristics can increase or decrease the deviation of the regression results.

Analysing the RMSE distribution of the mean vegetation height according to different study area characteristics could support this hypothesis. The mean vegetation height has its highest RMSE values for the second slope class *20°-40°*. Otherwise, the RMSE decreases again with increasing slope inclination (see Figure 41). This can be observed for the regressions validated with the ALS data. The regression validated with the GEDI data shows little variation at all. Furthermore, for the mean vegetation height higher RMSE values correlate in general with higher TCD values (see Figure 39). The fourth TCD class *75%-100%* is particularly prominent (64 %) within the second slope class *20°-40° (see* Figure 49), both having the highest RMSE values for most of the regression results (TCD: 5.95 m – 7.87 m/slope: 5.61 m -7.77 m). While the first TCD class *0%-25%* is the dominant class (49%) within the fourth slope class *60°-80°* (see Figure 49), both showcasing the lowest RMSE values for most of the regression results (TCD: 4.56 m-6.90 m/slope: 5.28 m-6.54 m). But it must be noted that the TCD class *75%-100%* is also the dominant class (60%) within the slope inclination *0°-20°*, which has significantly lower RMSE values (5.80 m-6.87 m) than the second slope class *20°-40°*. Regarding the forest type, the mean vegetation height has its highest RMSE values for the *broadleaved forest* class (6.52 m-8.28 m) and its lowest RMSE values mostly for the *no forest* class (4.59 m-6.93 m). The *coniferous forest* class (4.95 m-6.64 m) also has significantly lower error values (see Figure 40). Within the slope inclination *20°-40°* the *broadleaved forest* class dominates most of the area with 54%, while the *no forest* class has its lowest share with only 12%. On the other hand, within the slope inclination *60°-80°* the *broadleaved forest* only amounts to 10% of the area while the *no forest* and *coniferous forest* class dominate with 47 % and 43 % respectively (see Figure 50). In this case areas with low slope gradients are dominated by the *broadleaved forest* class and a high TCD, all presenting high RMSE values for the mean vegetation height. Furthermore, areas with high slope gradients are dominated by the *no forest* class, the *coniferous forest* class and low TCD values, all three presenting low RMSE values for the mean vegetation height. Usually, an increasing slope correlates with an increasing error value. According to this analysis one can assume that for the error

distribution of the mean vegetation height regression the TCD and the forest type are more influential than the slope gradient. Hilbert & Schmullius (2012) found that patchy or less dense forests can lead to waveforms with discrete canopy and ground return despite the steep surface topography, because the laser pulse is more likely to reach the real terrain if there is a gap in the canopy cover. Furthermore, it must be noted that the slope inclination *0°-20°* has lower error values than the slope inclination *20°-40°*. Even though the slope inclination *0°-20°* has a very similar TCD value distribution and a higher presence of the *broadleaved forest* class (36%) than the *no forest* class (21%) (see Figure 49 & Figure 50). It is therefore more likely that the combination of different study area characteristics can either increase or decrease the deviation of predicted regression values from the reference data.

The maximum vegetation height has the expected RMSE distribution of increasing RMSE values with increasing slope gradient except for the slope inclination 0°-20°, which also presents increasing RMSE values (see Figure 41). Analysing the other study area characteristics one can observe that increasing TCD values correlate with decreasing RMSE values, with the fourth TCD class *75%-100%* presenting the lowest RMSE values (see Figure 39). Furthermore, the *broadleaved* class and the *coniferous* class correspond to low RMSE values, while significantly higher RMSE values are in part presented for the *no forest* class (see Figure 40). The TCD class *75%-100%* as well as the *broadleaved* and *coniferous* class dominate within the areas that have a slope inclination of 0°-20°. The high RMSE values for relatively low slope gradients can therefore not be explained through the influence of other study area characteristics. The same can be said for the RMSE distribution of the FHD regression. Here it can also be observed that in part the slope inclination 0°-20° presents the highest RMSE values. The FHD regression also corresponds to increasing TCD values with decreasing RMSE values (see Figure 39) and has lower RMSE values for the *broadleaved* and *coniferous* class than for the no forest class (see Figure 40) same as the maximum vegetation height.

8.7. Influence of the utilized Data (ALS vs. GEDI)

When analysing the regression results within the context of the utilized data several observations can be made:

a) With few exceptions the variable combination *all bands* always results in the most accurate regressions.
b) For Group A (validating with ALS data) the regressions trained with ALS data and fishnet grid cell samples always achieve the best accuracy compared to the regressions utilizing the GEDI plots

c) Group B (validating with GEDI data) mostly has lower RMSE and MAE values than all Group A results.
d) Group A has higher R^2 values than all group B results.

Point a): In most cases the variable combination achieving the regressions with the highest accuracy was *all bands*. There were four exceptions (see Table 21). The maximum vegetation height regressions utilizing ALS (R^2 = 0.40, RMSE = 9.39 m, MAE = 7.39 m) and GEDI (R^2 = 0.35, RMSE = 10.53 m, MAE = 8.23 m) data within the GEDI plots for training and validating the results with the ALS data both achieved the highest accuracy for the variable combination *4 Orbits*. Compared to the variable combination *all bands* with the second best accuracy the improvement was not that significant (ALS max (plots): R^2 = 0.39, RMSE = 9.43 m, MAE = 7.37 m; GEDI RH100 (plots): R^2 = 0.33, RMSE = 10.56 m, MAE = 8.23 m). Comparing the used features and their importance between the models using *all bands* or *4 Orbits* shows that mostly the same multispectral bands and vegetation indices were utilized. When using the combination *4 Orbits* the importance of these variables was slightly higher. A significant difference was noticeable for the use of texture and S1 backscatter features. None of these features were used for the regression based on the ALS data using the *4 Orbits* combination. The GEDI regression did use the mean and standard deviation GLCM bands for the averaged VH polarisation, but the feature importance was a lot smaller compared to the variable combination *all bands*. Indicating that averaging the four different S1 orbits into one dataset lessens their importance, when calculating the vegetation parameters. The combination *NC* resulted in the highest accuracy for the mean vegetation height regression when training and validating the model with ALS data and utilizing the GEDI plots as samples (R^2 = 0.46, RMSE = 6.91 m, MAE = 5.39 m). The second best accuracy again was achieved for the variable combination *all bands* (R^2 = 0.45, RMSE = 6.96 m, MAE = 5.44 m). Some of the used features for *all bands* and *NC* were the same such as the green (B3), the red (B4) and the first vegetation red edge (B5) band. For both the red band (B4) was among the most important features. The utilized vegetation indices differentiated from each other. *All bands* employed the NDVI6, while *NC* employed the NDII7, the PSRI and the NDWI. The combination *Top 10* achieved the highest accuracy for the FHD regressions when utilizing the ALS FHD values for training and validation and the fishnet grid cells as samples (R^2 = 0.35, RMSE = 0.62, MAE = 0.46) compared to the variable combination *4 Orbits* (R^2 = 0.34, RMSE = 0.63, MAE =0.46) or *all bands* (R^2 =0.32; RMSE = 0.64; MAE = 0.47). Comparing the used features and their importance between these three combinations it can be observed that all utilize the green (B3) and the first vegetation red edge (B5) band with roughly the same importance. Furthermore, *Top 10* adds the SWIR (B11/B12) and the red (B4) band and does not utilize vegetation indices or texture variables.

For the observations b), c) and d) the following three reasons were identified:

1) Validation data from the same or a different source
2) Amount of training and validation data
3) Shape of the training samples (pixels vs. GEDI plots)

With regards to 1), models employing ALS data for training and validation achieve better result compared to models utilizing GEDI data for training and ALS data for validation. Extracting the training data from the same dataset that is also used to validate the results, can influence the model into predicting values that are closer to the validation data. One has to consider that the RH50 values for the study area have a correlation of R = 0.70 with the ALS mean, RH100 has a correlation with ALS max of R = 0.64 and FHD only has a correlation of R = 0.53 with ALS FHD. These discrepancies are of course picked up by the model, continued and ultimately reflected in the results. It can be seen when implementing the cross-validation with the GEDI values that the results for the models using the GEDI data improve. Also, it must be considered that the acquisition date for the ALS data was the year 2018, while the GEDI data was recorded in the years 2019 and 2020. Even though this is not a huge time span, still some noticeable vegetation growth can take place. For example, depending on their age spruce, a dominant tree in our study area, can grow up to 50 cm in height when they are young and 20-25 cm per year when they are older than 50 years (Hilbert & Schmullius 2012, 2230). Furthermore, GEDI (second release Version 2) has a mean systematic geolocation error of 10.3 m (Beck et al. 2021, 17). In a scattered tree ecosystem, a horizontal offset of this size can result in several meters of height errors, affecting model calibration and validation at the GEDI footprint level.

Considering 2), the amount of data available for both ALS and GEDI can also influence the regression outcomes. When validating the regressions with the GEDI values the amount of available data is limited to the plots. This could have the side effect that extreme outliers in the regression results are left out by chance. Analysing the cross-validation GEDI models it is noticeable that they achieve lower RMSE and MAE values in most cases even compared to the models trained and validated with ALS data utilizing fishnet grid cells as samples. Their R^2 values on the other hand were always lower than the R^2 values calculated for the models validated with the ALS data. Indicating that the predicted values of models trained and validated with the GEDI data show less deviation from the observed values in the dataset but are not good at explaining the variations of the prediction model (Shastry et al. 2017, 100). Furthermore, when selecting the training samples the ALS dataset offers a much larger value pool than the GEDI plots (508193 vs 1156). Even though the number of training samples is kept at 1156 to ensure comparability, the ALS fishnet grid samples are more representative of the ALS values for the whole study area. Comparing the value distribution of the training

samples with the value distribution of the ALS data for the entire study area, it can be noted that the training datasets based on the fishnet grid cells mostly present a similar or almost the same value distribution. This is the case for ALS mean and ALS max, where the deviations for the value groups between the training data and the total area are mostly only 1% or less (see Figure 16 & Figure 17). When ALS mean and max training samples are used within the form of GEDI plots their value distribution corresponds more closely to the value distribution of the GEDI data. Certain height groups are thus more strongly represented in one training dataset than the other. A similar outcome can be observed for the FHD values (see Figure 18). While the ALS FHD values for the fishnet grid as well as the plot training samples are both representative for the FHD value distribution within the study area. The FHD value distribution for the GEDI plots is mainly concentrated in higher value classes and does not represent smaller values at all. Explaining why the FHD regressions based on the GEDI values are prone to overestimation (see Figure 34).

3), the fishnet grid cells are congruent with the pixels of the S1 and S2 images utilized as variables. When using the GEDI plots as training samples one first has to extract and average the values of the ALS data and the S1 and S2 variables for each plot to train the model, which then again produces a regression presented as a 10x10 m per pixel raster. It can be that information is lost during this process and the same can be said for the regressions based on the GEDI data. Translating data contained within a round footprint 25 m in diameter into a raster consisting of square pixels sized 10x10 m could lead to a slight distortion of the results. Packalen et al. (2023) investigated the influence of circular or square plots when predicting the AGB. Their findings showed that when a model fitted to circular plots is used to predict for square plots the RMSE is slightly underestimated. Given reasons for this were that the variance of the response variable and the number of edge trees is greater on the square plots. Our results match with the observations of this study.

9. Conclusion

Based on the experiments and analysis performed, the research questions can be answered:

(1) Which S1 and S2 variables are best suited to estimate the vegetation parameters mean and maximum vegetation height, FHD and AGBD in combination with LiDAR data in an alpine forest?

S2 bands and VIs based on the S2 bands had the strongest correlations with the vegetation parameters. Especially the NDVI6 and the NLVI with the mean vegetation height and the AGBD. Both are calculated with vegetation red edge bands, that are quite influential in estimating the vegetation structure and characteristics, as discovered in other studies. The maximum vegetation height and the FHD had strong correlations with the first vegetation red edge band (B5) and the green band (B3). Compared to the other parameters the mean vegetation height had the strongest correlations with the Sentinel variables. Also, vegetation parameters derived from GEDI data had weaker correlations than vegetation parameters based on ALS data in general. It is difficult to determine if this has an impact on the regression results. In this case the selection of the training and validation data is likely more influential. Most of the variables with strong correlations were also attributed with a high feature importance when modelling the vegetation parameters. The AGBD as well as the mean vegetation height had a high feature importance for the NDVI6 and the red band (B4). Modelling the mean vegetation height also showed a high feature importance for the NLVI. The maximum vegetation height and the FHD had a high feature importance for the green band (B3), and the first vegetation red edge band (B5). Also, the red band (B4) contributed noticeably to the prediction of the FHD. Furthermore, the mean and median temporal statistics bands of the spectral bands and the VIs generally have the strongest correlation values and the highest feature importance. Indicating that this is the best way to aggregate the reflectance values of the Sentinel data for the chosen time period.

The S1 backscatter, and texture variables did not have strong correlations with any of the parameters. Still, they were often used by the RF model as features and sometimes achieved a high feature importance especially the mean and standard deviation texture bands of the VH polarisation. Both the variable combination *all bands* and *4 Orbits* did include texture variables and overwhelmingly achieved better regression results in contrast to the variable combinations *Top 10*, *NC* and *PC*. It can be concluded that adding the texture variables did improve the results of the RF model, which would be in accordance with other studies. When comparing the used features of the band combinations *all bands* to *4 Orbits*, *all bands*

employed more texture variables than *4 Orbits*, indicating, that combining the images of all four orbits into one dataset did not improve the quality of the data. Even though the S1 variables only had weak to very weak correlations to the vegetation parameters, they still played a role in predicting the outcome and even improving it. Still the feature importance was only marginal, seldomly reaching over 10%. Another option would be to utilize L-band data, as other studies did, noticing a significant improvement in their predicted values compared to utilizing C-band data.

(2) When utilizing LiDAR data in combination with S1 and S2 data for the assessment of wall-to-wall vegetation parameters, what qualitative differences can be detected between spaceborne and airborne LiDAR data?

Both the regressions relying on the ALS data as well as the GEDI data for training and validation always achieved their highest accuracies when employing the variable combination *all bands*. The regressions with the best accuracy for the mean vegetation height were modelled for the ALS data utilizing the fishnet grid cells as samples resulting in R^2 = 0.46, RMSE = 6.78 m and MAE = 5.30 m and for the GEDI data (cross-validation) resulting in R^2 = 0.31, RMSE = 6.36 m and MAE = 5.05 m. The maximum vegetation height also achieved the highest accuracies for the ALS data utilizing fishnet samples showcasing the following results R^2 = 0.45, RMSE = 7.76 m and MAE = 6.10 m and for the GEDI data (cross-validation) with R^2 = 0.27, RMSE = 7.51 m and MAE = 6.06 m. The FHD predicted its best regressions for the model utilizing the ALS data and the GEDI plots as samples resulting in R^2 = 0.40, RMSE = 0.65 and MAE = 0.43 and for the GEDI data (cross-validation) resulting in R^2=0.17, RMSE = 0.36 and MAE = 0.31. For the AGBD it was only possible to model the regressions based on the GEDI data (cross-validation). The best results being R^2 = 0.27, RMSE = 88.11 Mg/ha and MAE = 68.51 Mg/ha.When comparing the GEDI regressions (cross-validation) with the ALS regressions (fishnet/plot) the calculated RMSE and MAE values are quite similar, with the GEDI regressions mostly achieving the lower values. But when analysing the R^2 values for the GEDI regressions (cross-validation), they are significantly lower than the R^2 values of all the regressions employing the ALS dataset for validation. This can be due to the limited GEDI data available for validation. The complete GEDI dataset only includes 1156 plots compared to the 508193 individual values for the ALS dataset. Furthermore, the circular form of the GEDI sample plots compared to the square samples of the ALS data has an influence on the results. This is one explanation why the regressions calculated with the ALS data utilizing GEDI plots as samples mostly achieved a lower accuracy than the regressions calculated with ALS data and fishnet grid cells as samples. Also, the plot samples had other spatial locations than the fishnet samples, resulting in different value distributions within the training datasets. The

regressions with the lowest accuracy were utilizing GEDI values as training data and ALS values as validation data. This is mainly due to the already existing deviation between the original datasets. The regressions based on GEDI had much narrower value ranges than the ones predicted with ALS data in general, often over- or underestimating the original values. Nevertheless, they managed to reproduce the horizontal patterns of the vegetation parameters across our study area. Compared to other studies our results achieved lower accuracies. Reasons for this can be the small-scale complex topography of the study area terrain, the highly structured and diverse vegetation and the small spatial resolutions of our regressions. Generally, the ALS data was better suited to reproduce the variability of the vegetation parameters across our study area. However, the GEDI data provided viable results. Considering the advantages of GEDI data, such as a much broader temporal and spatial availability, as well as lower costs, it is an adequate alternative to ALS data. Able to deliver meaningful results, when modelling vegetation parameters even in areas with challenging conditions (highly structured forest, steep slopes). It can be especially helpful for providing data in remote areas or for detecting temporal changes within a forest.

Also, our study has shown that the study area characteristics such as the forest type, the canopy cover and the slope inclination have a potential influence on the results. For example, dividing the study area into different forest type classes and calculating the regressions separately for each class could provide more accurate information. This can be the subject of further research.

V. Bibliography

Adam, M., Urbazaev, M., Dubois, C., & Schmullius, C. (2020). Accuracy assessment of GEDI terrain elevation and canopy height estimates in European temperate forests: Influence of environmental and acquisition parameters. *Remote Sensing*, *12*(23), 3948.

Arnold, M., Powell, B., Shanley, P., & Sunderland, T. C. (2011). Forests, biodiversity and food security. The international forestry review, 13(3), 259-264.

Astola, H., Häme, T., Sirro, L., Molinier, M., & Kilpi, J. (2019). Comparison of Sentinel-2 and Landsat 8 imagery for forest variable prediction in boreal region. *Remote Sensing of Environment*, *223*, 257-273.

Atzberger, C.; Zeug, G.; Defourny, P.; Aragão, L.; Hammarström, L.; Immitzer, M (2020). Monitoring of Forests through Remote Sensing. URL: https://ec.europa.eu/environment/forests/pdf/report_monitoring_forests_through_remote_sensing.pdf. (Accessed on the 10.06.2022)

Avitabile V, Herold M, Heuvelink G, Lewis SL, Phillips OL, Asner GP et al. (2016). An integrated pan-tropical biomass maps using multiple reference datasets. *Global Change Biology,* 22: 1406–1420. doi:10.1111/gcb.13139.

Bahrenberg, G., Giese, E., Mevenkamp, N., & Nipper, J. (2010). Statistische Methoden in der Geographie. *Jahrbücher des Nassauischen Vereins für Naturkunde*, *131*, 133-134.

Barnston, A. G. (1992). Correspondence among the correlation, RMSE, and Heidke forecast verification measures; refinement of the Heidke score. *Weather and Forecasting*, *7*(4), 699-709.

Beck, J., Wirt, B., Armston, J., Hofton, M., Luthcke, S., & Tang, H. (2021). Global ecosystem dynamics investigation (GEDI) level 02 user guide. *Document version*, *2*.

Bergen, K. M., Goetz, S. J., Dubayah, R. O., Henebry, G. M., Hunsaker, C. T., Imhoff, M. L., Nelson, R. F., Parker, G., G. & Radeloff, V. C. (2009). Remote sensing of vegetation 3-D structure for biodiversity and habitat: Review and implications for lidar and radar spaceborne missions. Journal of Geophysical Research: Biogeosciences, 114(G2).

BFW – Bundesforschungszentrum für Wald (2022). Österreichische Waldinventur. Waldinformationen aus erster Hand umfassend. Kompetent. Aktuell. URL: https://www.waldinventur.at/#/. (Accessed on the 04.03.2023)

Bourbigot, M., Johnsen, H., Piantanida, R., Hajduch, G., Poullaouec, J., & Hajduch, G. (2016). Sentinel-1 product definition. *ESA Unclassified–For Official Use, availabe at:* https://sentinels.copernicus.eu/documents/247904/1877131/Sentinel-1-Product-Definition (Accessed on the 09.08.2022).

Boyd, D. S., & Danson, F. M. (2005). Satellite remote sensing of forest resources: three decades of research development. Progress in Physical Geography, 29(1), 1-26.

Breiman, L. (1996). Bagging predictors. *Machine learning*, *24*, 123-140.

Breiman, L. (2001). Random forests. *Machine learning*, *45*, 5-32.

Chai, T., & Draxler, R. R. (2014). Root mean square error (RMSE) or mean absolute error (MAE)? Arguments against avoiding RMSE in the literature. *Geoscientific model development*, *7*(3), 1247-1250.

Chan, Y. K., & Koo, V. (2008). An introduction to synthetic aperture radar (SAR). Progress In Electromagnetics Research B, 2, 27-60.

Chen, L., Ren, C., Zhang, B., Wang, Z., Liu, M., Man, W., & Liu, J. (2021). Improved estimation of forest stand volume by the integration of GEDI LiDAR data and multi-sensor imagery in the Changbai Mountains Mixed forests Ecoregion (CMMFE), northeast China. International Journal of Applied Earth Observation and Geoinformation, 100, 102326.

Chen, Q., Baldocchi, D., Gong, P., & Kelly, M. (2006). Isolating individual trees in a savanna woodland using small footprint lidar data. Photogrammetric Engineering & Remote Sensing, 72(8), 923-932.

Chen, X., Sun, Q., & Hu, J. (2018). Generation of complete SAR geometric distortion maps based on DEM and neighbor gradient algorithm. *Applied Sciences*, *8*(11), 2206.

Chrysafis, I., Mallinis, G., Siachalou, S., & Patias, P. (2017). Assessing the relationships between growing stock volume and Sentinel-2 imagery in a Mediterranean forest ecosystem. *Remote Sensing Letters*, *8*(6), 508-517.

Debastiani, A. B., Sanquetta, C. R., Dalla Corte, A. P., Pinto, N. S., & Rex, F. E. (2019). Evaluating SAR-optical sensor fusion for aboveground biomass estimation in a Brazilian tropical forest. Annals of Forest Research, 62(2), 109-122.

Di Tommaso, S., Wang, S., & Lobell, D. B. (2021). Combining GEDI and Sentinel-2 for wall-to-wall mapping of tall and short crops. *Environmental Research Letters*, *16*(12), 125002.

Drusch, M., Del Bello, U., Carlier, S., Colin, O., Fernandez, V., Gascon, F., Hoersch, B., Isola, C., Laberinti, P., Martimort, P., Meygret, A., Spoto, F., Sy, O., Marchese, F., & Bargellini, P. (2012). Sentinel-2: ESA's optical high-resolution mission for GMES operational services. Remote sensing of Environment, 120, 25-36.

Dubayah, R. O., & Drake, J. B. (2000). Lidar remote sensing for forestry. Journal of forestry, 98(6), 44-46.

Dubayah, R.; Hofton, M.; Blair, J.; Armston, J.; Tang, H. & Luthcke, S. (2021a). GEDI L2A Elevation and Height Metrics Data Global Footprint Level V002. URL: https://doi.org/10.5067/GEDI/GEDI02_A.002. (Accessed on the 09.08.2022).

Dubayah, R., Tang, H., Armston, J., Luthcke, S., Hofton, M., Blair, J. (2021b). GEDI L2B Canopy Cover and Vertical Profile Metrics Data Global Footprint Level V002 [Data set]. NASA EOSDIS Land Processes DAAC. Accessed 2022-08-09 from https://doi.org/10.5067/GEDI/GEDI02_B.002

Dubayah, R.O., Armston, J., Kellner, J.R., Duncanson, L., Healey, S.P., Patterson, P.L., Hancock, S., Tang, H., Bruening, J., Hofton, M.A., Blair, J.B., & Luthcke, S.B. (2022). GEDI L4A Footprint Level Aboveground Biomass Density, Version 2.1. ORNL DAAC, Oak Ridge, Tennessee, USA. https://doi.org/10.3334/ORNLDAAC/2056

Dudley, N., & Stolton, S. (2003). Running pure: the importance of forest protected areas to drinking water. World Bank/WWF Alliance for Forest Conservation and Sustainable Use.

EAA – Environment Agency Austria (2022). LTER Zöbelboden - Austria. URL: https://deims.org/8eda49e9-1f4e-4f3e-b58e-e0bb25dc32a6. (Accessed on the 01.03.2023)

EEA – European Environment Agency (2020a): Dominant Leaf Type 2018 (raster 10 m), Europe, 3-yearly, Sep. 2020. URL: https://sdi.eea.europa.eu/catalogue/copernicus/api/records/7b28d3c1-b363-4579-9141-bdd09d073fd8?language=all. (Accessed on the 10.10.2023).

EEA – European Environment Agency (2020b): Tree Cover Density 2018 (raster 10 m), Europe, 3-yearly, Sep. 2020. URL: https://sdi.eea.europa.eu/catalogue/copernicus/api/records/486f77da-d605-423e-93a9-680760ab6791?language=all. (Accessed on the 10.10.2023).

ESAa – European Space Agency: Sentinel-1 operations. URL: https://www.esa.int/Enabling_Support/Operations/Sentinel-1_operations. (Accessed on the 05.05.2022)

ESAb – European Space Agency: Orbit. URL: https://sentinels.copernicus.eu/web/sentinel/missions/sentinel-1/satellite-description/orbit. (Accessed on the 09.08.2022)

ESAc – European Space Agency: Sentinel-2. URL: https://www.esa.int/Applications/Observing_the_Earth/Copernicus/Sentinel-2. (Accessed on the 06.05.2022)

ESAd – European Space Agency: MultiSpectral Instrument (MSI) Overview. URL: https://sentinel.esa.int/web/sentinel/technical-guides/sentinel-2-msi/msi-instrument. (Accessed on the 25.07.2022).

Egelseer J. (2021). Welterbe-Vermittlung im Nationalpark Kalkalpen. URL. https://www.interreg-central.eu/Content.Node/WH-Communication-Education-Concept-for-Kalkalpen-Nationalpar.pdf. (Accessed on the 14.05.2022)

Emerson, R. W. (2015). Causation and Pearson's correlation coefficient. *Journal of visual impairment & blindness*, *109*(3), 242-244.

Eskelson, B. N., Barrett, T. M., & Temesgen, H. (2009). Imputing mean annual change to estimate current forest attributes. *Silva Fennica*, *43*(4).

Evans, J. D. (1996). *Straightforward statistics for the behavioral sciences*. Thomson Brooks/Cole Publishing Co.

Eysn, L., Hollaus, M., Schadauer, K., & Pfeifer, N. (2012). Forest delineation based on airborne LIDAR data. Remote Sensing, 4(3), 762-783.

Fagua, J. C., Jantz, P., Rodriguez-Buritica, S., Duncanson, L., & Goetz, S. J. (2019). Integrating LiDAR, multispectral and SAR data to estimate and map canopy height in tropical forests. *Remote Sensing*, *11*(22), 2697.

Falkowski, M. J., Smith, A. M., Gessler, P. E., Hudak, A. T., Vierling, L. A., & Evans, J. S. (2008). The influence of conifer forest canopy cover on the accuracy of two individual tree measurement algorithms using lidar data. *Canadian Journal of Remote Sensing*, *34*(sup2), S338-S350.

FAO – Food and Agriculture Organization of the United Nations (2020). Global Forest Resources Assessment 2020: Main report. Rome.

FAO – Food and Agriculture Organization of the United Nations (2022). The State of the World's Forests 2022. Forest pathways for green recovery and building inclusive, resilient and sustainable economies. Rome, FAO. https://doi.org/10.4060/cb9360en

Fouladinejad, F., Matkan, A., Hajeb, M., & Brakhasi, F. (2019). HISTORY AND APPLICATIONS OF SPACE-BORNE LIDARS. *International Archives of the Photogrammetry, Remote Sensing & Spatial Information Sciences*.

Franklin, S. E. (2001). *Remote sensing for sustainable forest management*. CRC press.

Frantz, D., Haß, E., Uhl, A., Stoffels, J., & Hill, J. (2018). Improvement of the Fmask algorithm for Sentinel-2 images: Separating clouds from bright surfaces based on parallax effects. *Remote sensing of environment*, *215*, 471-481.

Friedlingstein, P., O'Sullivan, M., Jones, M. W., Andrew, R. M., Gregor, L., Hauck, J., ... & Zheng, B. (2022). Global carbon budget 2022. *Earth System Science Data*, *14*(11), 4811-4900.

Galvão, T. L., Novell-Leruth, G., Kuznetsova, A., Tedim, J., & Gomes, J. R. (2020). Elucidating structure–property relationships in aluminum alloy corrosion inhibitors by machine learning. *The Journal of Physical Chemistry C*, *124*(10), 5624-5635

Gao, K., & Liu, X. (2019, April). Hyperspectral characteristics of vegetation height in Urumqi Nanshan meadow steppe in different months. In *IOP Conference Series: Materials Science and Engineering* (Vol. 490, No. 7, p. 072004). IOP Publishing.

Gašparović, M., & Dobrinić, D. (2020). Comparative assessment of machine learning methods for urban vegetation mapping using multitemporal sentinel-1 imagery. *Remote Sensing*, *12*(12), 1952.

GEDI – Global Ecosystem Dynamics Investigation (2022a). Calibration/Validation. URL: https://gedi.umd.edu/science/calibration-validation/. (Accessed on the 05.07.2022).

GEDI – Global Ecosystem Dynamics Investigation (2022b). Timeline. URL: https://gedi.umd.edu/mission/timeline/. (Accessed on the 29.09.2023).

GEDI – Global Ecosystem Dynamics Investigation (2022c). Specifications. URL: https://gedi.umd.edu/instrument/specifications/. (Accessed on the 05.07.2022).

GEDI – Global Ecosystem Dynamics Investigation (2022d). Calibration/Validation. URL: https://gedi.umd.edu/science/calibration-validation/. (Accessed on the 10.06.2022).

Goetz, S., & Dubayah, R. (2011). Advances in remote sensing technology and implications for measuring and monitoring forest carbon stocks and change. Carbon Management, 2(3), 231-244.

García-Gutiérrez, J., Martínez-Álvarez, F., Troncoso, A., & Riquelme, J. C. (2015). A comparison of machine learning regression techniques for LiDAR-derived estimation of forest variables. Neurocomputing, 167, 24-31.

Guerra-Hernández, J., Narine, L., Pascual, A., Gonzalez-Ferreiro, E., Botequim, B., Malambo, L., Neuschwander, A., Popescu, S. & Godinho, S. (2022). Aboveground biomass mapping by integrating ICESat-2, SENTINEL-1, SENTINEL-2, ALOS2/PALSAR2, and topographic information in Mediterranean forests. *GIScience & Remote Sensing*, *59*(1), 1509-1533

Haack, B., & Rafter, A. (2010). Regression estimation techniques with remote sensing: a review and case study. *Geocarto International*, *25*(1), 71-82.

Hallik, L., Kuusk, A., Lang, M., & Kuusk, J. (2019). Reflectance properties of hemiboreal mixed forest canopies with focus on red edge and near infrared spectral regions. *Remote Sensing*, *11*(14), 1717.

Haralick, R. M., Shanmugam, K., & Dinstein, I. H. (1973). Textural features for image classification. IEEE Transactions on systems, man, and cybernetics, (6), 610-621.

Harding, D. J., & Carabajal, C. C. (2005). ICESat waveform measurements of within-footprint topographic relief and vegetation vertical structure. *Geophysical research letters*, *32*(21).

Harris, N. L., Gibbs, D. A., Baccini, A., Birdsey, R. A., De Bruin, S., Farina, M., Fatoyinbo, L., Hansen, M., Herold, M., Houghton, R., Potapov, P., Suarez, D., Roman-Cuesta, R., Saatchi, S., Slay, C., Turubanova, S. & Tyukavina, A. (2021). Global maps of twenty-first century forest carbon fluxes. *Nature Climate Change*, *11*(3), 234-240.

Hashimoto, H., Imanishi, J., Hagiwara, A., Morimoto, Y., & Kitada, K. (2004, October). Estimating forest structure indices for evaluation of forest bird habitats by an airborne laser-scanner. In *Proceedings of the ISPRS working group VIII/2 laser-scanners for forest and landscape assessment* (pp. 254-257). Freiburg Germany.

Hauk, E., Niese, G., Schadauer, K. (2016). Instruktion für die Feldarbeit der Österreichischen Waldinventur 2016 + (04/2020). URL: https://www.waldinventur.at/2016_Dienstanweisung_%C3%96WI_Fassung2020.pdf. (Accessed on the 03.02.2023).

Heurich, M., & Thoma, F. (2008). Estimation of forestry stand parameters using laser scanning data in temperate, structurally rich natural European beech (Fagus sylvatica) and Norway spruce (Picea abies) forests. *Forestry*, *81*(5), 645-661.

Hicks, C., Woroniecki, S., Fancourt, M., Bieri, M., Garcia Robles, H., Trumper, K., & Mant, R. (2014). The relationship between biodiversity, carbon storage and the provision of other ecosystem services: Critical Review for the Forestry Component of the International Climate Fund. Cambridge: United Nations Environment Programme.

Hilbert, C., & Schmullius, C. (2012). Influence of surface topography on ICESat/GLAS forest height estimation and waveform shape. *Remote Sensing*, *4*(8), 2210-2235.

Hirschmugl, M., Lippl, F., & Sobe, C. (2023). Assessing the Vertical Structure of Forests Using Airborne and Spaceborne LiDAR Data in the Austrian Alps. *Remote Sensing*, *15*(3), 664.

Hudak, A. T., Lefsky, M. A., Cohen, W. B., & Berterretche, M. (2002). Integration of lidar and Landsat ETM+ data for estimating and mapping forest canopy height. *Remote sensing of Environment*, *82*(2-3), 397-416.

Hudak, A. T., Crookston, N. L., Evans, J. S., Hall, D. E., & Falkowski, M. J. (2008). Nearest neighbor imputation of species-level, plot-scale forest structure attributes from LiDAR data. *Remote Sensing of Environment*, *112*(5), 2232-2245.

Huete, A. R. (2012). Vegetation indices, remote sensing and forest monitoring. Geography Compass, 6(9), 513-532.

Huete, A. R., Miura, T., Yoshioka, H., Ratana, P., & Broich, M. (2014). Indices of vegetation activity. *Biophysical applications of satellite remote sensing*, 1-41.

Hurtt, G., Zhao, M., Sahajpal, R., Armstrong, A., Birdsey, R., Campbell, E., Dolan, K., Dubayah, R., Fisk, J.P., Planagan, S., Huang, C., Huang, W., Johnson, K., Lamb, R., Ma, L., Marks, R., O'Leary, D., O'Neil-Dunne, J., Swatantran, A. & Tang, H. (2019). Beyond MRV: high-resolution forest carbon modeling for climate mitigation planning over Maryland, USA. Environmental Research Letters, 14(4), 045013.

IVA – Industrieverband Agrar (2016). Baum des Jahres 2017: Die Fichte. URL: https://www.iva.de/iva-magazin/haus-garten/baum-des-jahres-2017-die-fichte. (Accessed on the 28.01.2022).

Jiang, F., Zhao, F., Ma, K., Li, D., & Sun, H. (2021). Mapping the forest canopy height in Northern China by synergizing ICESat-2 with Sentinel-2 using a stacking algorithm. *Remote Sensing*, *13*(8), 1535.

Jovanović, I., Dragišić, A., Ostojić, D., & Krsteski, B. (2019). Beech forests as world heritage in aspect to the next extension of the ancient and primeval beech forests of the Carpathians and other regions of Europe world heritage site. Zaštita prirode, 69(1-2), 15-32.

Kacic, P., Hirner, A., & Da Ponte, E. (2021). Fusing Sentinel-1 and-2 to model GEDI-derived vegetation structure characteristics in GEE for the Paraguayan Chaco. *Remote Sensing*, *13*(24), 5105.

Kacic, P., Thonfeld, F., Gessner, U., & Kuenzer, C. (2023). Forest structure characterization in Germany: novel products and analysis based on GEDI, sentinel-1 and sentinel-2 data. *Remote Sensing*, *15*(8), 1969.

Kilian, W., Müller, F., & Starlinger, F. (1994). Die forstlichen Wuchsgebiete Österreichs. *FBVA-berichte*, *82*, 55-57.

Khan, M. Y., Qayoom, A., Nizami, M. S., Siddiqui, M. S., Wasi, S., & Raazi, S. M. K. U. R. (2021). Automated prediction of Good Dictionary EXamples (GDEX): a comprehensive experiment with distant supervision, machine learning, and word embedding-based deep learning techniques. *Complexity*, *2021*, 1-18.

Kivari, A., Xu, W., & Otukol, S. (2011). Volume to biomass conversion for British Columbia forests. *Victoria, BC: Forest Analysis and Inventory Branch, Ministry of Forests and Range. https://www2. gov. bc. ca/assets/gov/farming-natural-resources-and-industry/forestry/stewardship/forest-analysis-inventory/growth-yield/volume_to_biomass_conversion_report_edit_mp_jan_31_*.

Lang, N., Schindler, K., & Wegner, J. D. (2019). Country-wide high-resolution vegetation height mapping with Sentinel-2. Remote Sensing of Environment, 233, 111347.

Latifi, H., Nothdurft, A., & Koch, B. (2010). Non-parametric prediction and mapping of standing timber volume and biomass in a temperate forest: application of multiple optical/LiDAR-derived predictors. *Forestry*, *83*(4), 395-407.

Leckie, D. G. (1990). Advances in remote sensing technologies for forest surveys and management. *Canadian Journal of Forest Research*, *20*(4), 464-483.

Lee, Y. S., Lee, S., & Jung, H. S. (2020). Mapping forest vertical structure in Gong-ju, Korea using Sentinel-2 satellite images and artificial neural networks. *Applied Sciences*, *10*(5), 1666.

Lefsky, M. A., Cohen, W. B., Parker, G. G., & Harding, D. J. (2002). Lidar remote sensing for ecosystem studies: Lidar, an emerging remote sensing technology that directly measures the three-dimensional distribution of plant canopies, can accurately estimate vegetation structural attributes and should be of particular interest to forest, landscape, and global ecologists. *BioScience*, *52*(1), 19-30.

Lewis, P., & Hancock, S. (2007). LiDAR for vegetation applications. *UCL, Gower St, London, UK*.

Li, A., Dhakal, S., Glenn, N. F., Spaete, L. P., Shinneman, D. J., Pilliod, D. S., Arkle, R. S. & McIlroy, S. K. (2017). Lidar aboveground vegetation biomass estimates in shrublands: Prediction, uncertainties and application to coarser scales. *Remote Sensing*, *9*(9), 903.

Li, W., Niu, Z., Shang, R., Qin, Y., Wang, L., & Chen, H. (2020). High-resolution mapping of forest canopy height using machine learning by coupling ICESat-2 LiDAR with Sentinel-1, Sentinel-2 and Landsat-8 data. International Journal of Applied Earth Observation and Geoinformation, 92, 102163.

Liaw, A., & Wiener, M. (2002). Classification and regression by randomForest. *R news*, *2*(3), 18-22.

Lim, K., Treitz, P., Wulder, M., St-Onge, B., & Flood, M. (2003). LiDAR remote sensing of forest structure. Progress in physical geography, 27(1), 88-106.

Lindenmayer, D. B., Franklin, J. F., & Fischer, J. (2006). General management principles and a checklist of strategies to guide forest biodiversity conservation. Biological conservation, 131(3), 433-445.

Liu, M., Cao, C., Dang, Y., & Ni, X. (2019). Mapping forest canopy height in mountainous areas using ZiYuan-3 stereo images and Landsat data. *Forests*, *10*(2), 105.

MacArthur, R. H., & MacArthur, J. W. (1961). On bird species diversity. *Ecology*, *42*(3), 594-598.

Mahavir, D. (2000). High (spatial) resolution vs. Low resolution images: a planner's view point. International archives of photogrammetry and Remote Sensing, 33(7).

Misra, S., Li, H., & He, J. (2019). *Machine learning for subsurface characterization*. Gulf Professional Publishing.

Morin, D., Planells, M., Guyon, D., Villard, L., Mermoz, S., Bouvet, A., Thevenon, H., Dejoux, J., Toan, T. & Dedieu, G. (2019). Estimation and mapping of forest structure parameters from open access satellite images: Development of a generic method with a study case on coniferous plantation. Remote Sensing, 11(11), 1275.

Nagelkerke, N. J. (1991). A note on a general definition of the coefficient of determination. *Biometrika*, *78*(3), 691-692

Nandy, S., Srinet, R., & Padalia, H. (2021). Mapping forest height and aboveground biomass by integrating ICESat-2, Sentinel-1 and Sentinel-2 data using Random Forest algorithm in northwest Himalayan foothills of India. Geophysical Research Letters, 48(14), e2021GL093799.

NASA – National Aeronautics and Space Administration (2003). Geoscience Laser Altimeter System. The Next Generation Space Lidar. URL: https://attic.gsfc.nasa.gov/glas/. (Accessed on the 21.11.2022).

NASA – National Aeronautics and Space Administration (2021). LVIS. Land, Vegetation, and Ice Sensor. URL: https://lvis.gsfc.nasa.gov/Home/index.html. (Accessed on the 21.11.2022).

Nationalpark O. ö. Kalkalpen GmbH (2011a). Nationalpark Kalkalpen. URL: https://www.kalkalpen.at/de/Nationalpark_Kalkalpen. (Stand: 12.05.2022).

Nationalpark O. ö. Kalkalpen GmbH (2011b). Nationalpark Kalkalpen – Geschichte. URL: https://www.kalkalpen.at/de/Nationalpark_Kalkalpen/Geschichte. (Accessed on the 12.05.2022).

Nationalpark O. ö. Kalkalpen GmbH (2011c). Nationalpark Kalkalpen – Biodiversität. URL: https://www.kalkalpen.at/system/web/zusatzseite.aspx?page=12&letter=ALLE&detailonr=221686404&menuonr=222369936. (Accessed on the 12.05.2022).

Nationalpark O. ö. Kalkalpen GmbH (2011d). Nationalpark Kalkalpen – Lebensräume: URL: https://www.kalkalpen.at/de/LEBENSRAeUME. (Accessed on the 12.05.2022)

Nationalpark O. ö. Kalkalpen GmbH. (2016). Natürliche Buchenwälder des Nationalpark Kalkalpen, Schutz und Erbe alter Wälder – Band 16, Schriftenreihe Nationalpark Kalkalpen; 164 S.

Nationalpark O. ö. Kalkalpen GmbH (2020). Kurzfassung Managementplan Nationalpark Kalkalpen 2021 – 2030; 64 S

Nationalpark O. ö. Kalkalpen GmbH (2022). Nationalpark Kalkalpen – UNESCO Weltnaturerbe Buchenwälder. URL: https://www.kalkalpen.at/de/UNESCO_Weltnaturerbe_Buchenwaelder. (Accessed on the 12.05.2022).

NovAtel Inc. (2016). SPAN IMU-FSAS. URL: https://hexagondownloads.blob.core.windows.net/public/Novatel/assets/Documents/Papers/FSAS/FSAS.pdf. (Accessed on the 23.01.2023).

Packalen, P., Strunk, J., Maltamo, M., & Myllymäki, M. (2023). Circular or square plots in ALS-based forest inventories—does it matter?. Forestry, 96(1), 49-61.

Pascual, C., Garcia-Abril, A., Cohen, W. B., & Martin-Fernandez, S. (2010). Relationship between LiDAR-derived forest canopy height and Landsat images. *International Journal of Remote Sensing*, *31*(5), 1261-1280.

Pathak, B., & Barooah, D. (2013). Texture analysis based on the gray-level co-occurrence matrix considering possible orientations. International Journal of Advanced Research in Electrical, Electronics and Instrumentation Engineering, 2(9), 4206-4212.

Pereira-Pires, J. E., Mora, A., Aubard, V., Silva, J., & Fonseca, J. M. (2021). Assessment of Sentinel-2 Spectral Features to Estimate Forest Height with the New GEDI Data. In Doctoral Conference on Computing, Electrical and Industrial Systems (pp. 123-131). Springer, Cham.

Pekel, E. (2020). Estimation of soil moisture using decision tree regression. *Theoretical and Applied Climatology*, *139*(3-4), 1111-1119.

Perez, G. G., Bourscheidt, V., Lopes, L. E., Takata, J. T., Ferreira, P. A., & Boscolo, D. (2022). Use of Sentinel 2 imagery to estimate vegetation height in fragments of Atlantic Forest. *Ecological Informatics*, *69*, 101680.

Pflugmacher, D., Rabe, A., Peters, M., & Hostert, P. (2019). Mapping pan-European land cover using Landsat spectral-temporal metrics and the European LUCAS survey. *Remote sensing of environment*, *221*, 583-595.

Potapov, P., Li, X., Hernandez-Serna, A., Tyukavina, A., Hansen, M. C., Kommareddy, A., Pickens, A., Turubanova, S., Tang, H., Edibaldo Silva, C., Armston, J., Dubayah, R., Blair, J.B. & Hofton, M. (2021). Mapping global forest canopy height through integration of GEDI and Landsat data. *Remote Sensing of Environment*, *253*, 112165.

Popescu, S. C., Zhao, K., Neuenschwander, A., & Lin, C. (2011). Satellite lidar vs. small footprint airborne lidar: Comparing the accuracy of aboveground biomass estimates and forest structure metrics at footprint level. Remote Sensing of Environment, 115(11), 2786-2797.

Räim, O., Kaurilind, E., Hallik, L., & Merilo, E. (2012). Why does needle photosynthesis decline with tree height in Norway spruce?. *Plant Biology*, *14*(2), 306-314.

Rajsnerová, P., Klem, K., Holub, P., Novotná, K., Večeřová, K., Kozáčiková, M., Rivas-Ubach, A., Sardans, J., Marek, M., Peñuelas, J. & Urban, O. (2015). Morphological, biochemical and physiological traits of upper and lower canopy leaves of European beech tend to converge with increasing altitude. *Tree Physiology*, *35*(1), 47-60.

Ren, C., Jiang, H., Xi, Y., Liu, P., & Li, H. (2023). Quantifying temperate forest diversity by integrating GEDI LiDAR and multi-temporal sentinel-2 imagery. *Remote Sensing*, *15*(2), 375.

Rishmawi, K., Huang, C., & Zhan, X. (2021). Monitoring key forest structure attributes across the conterminous united states by integrating GEDI LiDAR measurements and VIIRS data. Remote Sensing, 13(3), 442.

Rösch, M., Sonnenschein, R., Buchelt, S., & Ullmann, T. (2022). Comparing PlanetScope and Sentinel-2 Imagery for Mapping Mountain Pines in the Sarntal Alps, Italy. Remote Sensing, 14(13), 3190.

Roy, D. P., Ju, J., Kline, K., Scaramuzza, P. L., Kovalskyy, V., Hansen, M., Loveland, T. R., Vermote, E. & Zhang, C. (2010). Web-enabled Landsat Data (WELD): Landsat ETM+ composited mosaics of the conterminous United States. Remote Sensing of Environment, 114(1), 35-49.

Santoro, M.; Cartus, O. (2023): ESA Biomass Climate Change Initiative (Biomass_cci): Global datasets of forest above-ground biomass for the years 2010, 2017, 2018, 2019 and 2020, v4. NERC EDS Centre for Environmental Data Analysis, *21 April 2023*. doi:10.5285/af60720c1e404a9e9d2c145d2b2ead4e. https://dx.doi.org/10.5285/af60720c1e404a9e9d2c145d2b2ead4e

Saunders, L. J., Russell, R. A., & Crabb, D. P. (2012). The coefficient of determination: what determines a useful R2 statistic? *Investigative ophthalmology & visual science*, *53*(11), 6830-6832.

Shastry, A., Sanjay, H. A., & Bhanusree, E. (2017). Prediction of crop yield using regression techniques. *International Journal of Soft Computing*, *12*(2), 96-102.

Shugart, H. H., Saatchi, S., & Hall, F. G. (2010). Importance of structure and its measurement in quantifying function of forest ecosystems. Journal of Geophysical Research: Biogeosciences, 115(G2).

Silva, C. A., Saatchi, S., Garcia, M., Labriere, N., Klauberg, C., Ferraz, A., Ferraz, A., Meyer, V., Jeffery, K. J., Abernethy, K., White, L., Zhao, K., Lewis, S. L. & Hudak, A. T. (2018). Comparison of small-and large-footprint lidar characterization of tropical forest aboveground structure and biomass: a case study from Central Gabon. *IEEE Journal of Selected Topics in Applied Earth Observations and Remote Sensing*, *11*(10), 3512-3526.

Skidmore, A. K., Coops, N. C., Neinavaz, E., Ali, A., Schaepman, M. E., Paganini, M., Kissling, W.D., Vihervaara, P., Darvishzadeh, R., Feilhauer, H., Fernandez, M., Fernández, N., Gorelick, N., Geizendorffer, I., Heiden, U., Heurich, M., Hobern, D., Holzwarth, S., Muller-Karger, F., Van De Kerchove, R. Lausch, A., Leitau, P., Lock, M. Mücher, C., O'Conner, B.,

Rocchini, D., Turner, W., Kees Vis, J., Wang, T., Wegmann, M. & Wingate, V. (2021). Priority list of biodiversity metrics to observe from space. Nature ecology & evolution, 5(7), 896-906.

Sothe, C., Gonsamo, A., Lourenço, R. B., Kurz, W. A., & Snider, J. (2022). Spatially continuous mapping of forest canopy height in Canada by combining GEDI and ICESat-2 with PALSAR and Sentinel. *Remote Sensing*, *14*(20), 5158.

Stojanova, D., Panov, P., Gjorgjioski, V., Kobler, A., & Džeroski, S. (2010). Estimating vegetation height and canopy cover from remotely sensed data with machine learning. *Ecological Informatics*, *5*(4), 256-266.

Torres de Almeida, C., Gerente, J., Rodrigo dos Prazeres Campos, J., Caruso Gomes Junior, F., Providelo, L. A., Marchiori, G., & Chen, X. (2022). Canopy Height Mapping by Sentinel 1 and 2 Satellite Images, Airborne LiDAR Data, and Machine Learning. *Remote Sensing*, *14*(16), 4112.

UNESCO – United Nations Educational, Scientific and Cultural Organization (Hrsg.): The contribution of the Kalkalpen National Park to the World Natural Heritage. URL: https://www.weltnaturerbe-buchenwaelder.at/national-park-kalkalpen/. (Stand: 12.05.2022).

Van Leeuwen, M., & Nieuwenhuis, M. (2010). Retrieval of forest structural parameters using LiDAR remote sensing. *European Journal of Forest Research*, *129*, 749-770.

Vauhkonen, J., Korpela, I., Maltamo, M., & Tokola, T. (2010). Imputation of single-tree attributes using airborne laser scanning-based height, intensity, and alpha shape metrics. *Remote Sensing of Environment*, *114*(6), 1263-1276.

Verhelst, K., Gou, Y., Herold, M., & Reiche, J. (2021). Improving forest baseline maps in tropical wetlands using gedi-based forest height information and sentinel-1. *Forests*, *12*(10), 1374.

Wang, C., Zhu, X., Nie, S., Xi, X., Li, D., Zheng, W., & Chen, S. (2019). Ground elevation accuracy verification of ICESat-2 data: A case study in Alaska, USA. *Optics express*, *27*(26), 38168-38179.

Wang, C., Elmore, A. J., Numata, I., Cochrane, M. A., Shaogang, L., Huang, J., Zhao, Y. & Li, Y. (2022). Factors affecting relative height and ground elevation estimations of GEDI among forest types across the conterminous USA. GIScience & Remote Sensing, 59(1), 975-999.

Wang, Y., Peng, Y., Hu, X., & Zhang, P. (2023). Fine-Resolution Forest Height Estimation by Integrating ICESat-2 and Landsat 8 OLI Data with a Spatial Downscaling Method for Aboveground Biomass Quantification. *Forests*, *14*(7), 1414.

Wasser, L., Day, R., Chasmer, L., & Taylor, A. (2013). Influence of vegetation structure on lidar-derived canopy height and fractional cover in forested riparian buffers during leaf-off and leaf-on conditions. *PLoS One*, *8*(1), e54776.

Weiss, P., Schieler, K., Schadauer, K., & Englisch, M. (2000). *Die Kohlenstoffbilanz des österreichischen Waldes und Betrachtungen zum Kyoto-Protokoll* (Vol. 106). Wien: Umweltbundesamt.

Willmott, C. J., & Matsuura, K. (2005). Advantages of the mean absolute error (MAE) over the root mean square error (RMSE) in assessing average model performance. Climate research, 30(1), 79-82.

Xie, Q., Dash, J., Huang, W., Peng, D., Qin, Q., Mortimer, H., Casa, R., Pignatti, S., Laneve, G., Pascucci, S., Dong, Y. & Ye, H. (2018). Vegetation indices combining the red and red-edge spectral information for leaf area index retrieval. *IEEE Journal of selected topics in applied earth observations and remote sensing*, *11*(5), 1482-1493.

Xi, Z., Xu, H., Xing, Y., Gong, W., Chen, G., & Yang, S. (2022). Forest canopy height mapping by synergizing ICESat-2, Sentinel-1, Sentinel-2 and topographic information based on machine learning methods. *Remote Sensing*, *14*(2), 364.

Yang, W., Ni-Meister, W., & Lee, S. (2011). Assessment of the impacts of surface topography, off-nadir pointing and vegetation structure on vegetation lidar waveforms using an extended geometric optical and radiative transfer model. *Remote Sensing of Environment*, *115*(11), 2810-2822.

Zald, H. S., Wulder, M. A., White, J. C., Hilker, T., Hermosilla, T., Hobart, G. W., & Coops, N. C. (2016). Integrating Landsat pixel composites and change metrics with lidar plots to

predictively map forest structure and aboveground biomass in Saskatchewan, Canada. *Remote Sensing of Environment*, *176*, 188-201.

Zhu, Z., & Woodcock, C. E. (2012). Object-based cloud and cloud shadow detection in Landsat imagery. *Remote sensing of environment*, *118*, 83-94.

Zwerenz, K. (2015). Statistik, Einführung in die computergestützte Datenanalyse, 6.

VI. Appendix

A. Additional Data

Table 28: Exemplary field plots.

Shot number	Attributes		Image captured on the
1568	Vegetation characteristics	Coniferous forest; dead wood; regrowing trees	
	Altimeter / slope	670 m a.s.l. / 29°	
	Maximum height	34.41 m (GEDI) / 33.55 m (ALS)	
	Mean height	20.04 m (GEDI) / 22.75 m (ALS)	
	FHD	3.31 (GEDI) / 2.82 (ALS)	
	AGBD	299.99 Mg/ha (GEDI)	
6510	Vegetation characteristics	Clearing; natural regeneration; hazelnut trees	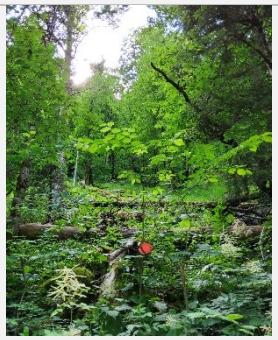
	Altimeter / slope	674 m a.s.l. / 41°	
	Maximum height	47.61 m (GEDI) / 39.29 m (ALS)	
	Mean height	24.65 m (GEDI) / 23.06 m (ALS)	
	FHD	3.32 (GEDI) / 2.98 (ALS)	
	AGBD	421.88 Mg/ha (GEDI)	
6511	Vegetation characteristics	Edge of the forest by the creek; scrub	
	Altimeter / slope	643 m a.s.l. / 17°	
	Maximum height	31.79 m (GEDI) / 29.49 m (ALS)	
	Mean height	6.36 m (GEDI) / 8.99 m (ALS)	
	FHD	3.22 (GEDI) / 2.61 (ALS)	
	AGBD	171.60 Mg/ha (GEDI)	
6349	Vegetation characteristics	Old growth forest; standing and fallen dead trees; natural regeneration beech	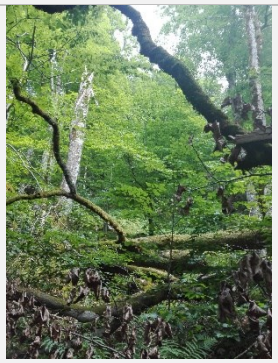
	Altimeter / slope	686 m a.s.l. / 30°	
	Maximum height	46 m (GEDI) / 37.08 m (ALS)	
	Mean height	11.08 m (GEDI) / 25.00 m (AlS)	
	FHD	2.97 (GEDI) / 2.64 (ALS)	
	AGBD	288.92 Mg/ha (GEDI)	

1949	Vegetation characteristics	Street; brook; mixed forest	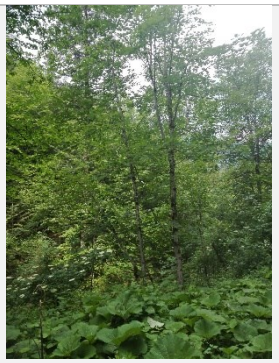
	Altimeter / slope	686 m a.s.l. /21°	
	Maximum height	26.88 m (GEDI) / 30.61 m (ALS)	
	Mean height	4.04 m (GEDI) / 8.51 m (ALS)	
	FHD	3.19 (GEDI) / 2.65 (ALS)	
	AGBD	141.69 Mg/ha (GEDI)	
1950	Vegetation characteristics	Beech pure stock; natural regeneration	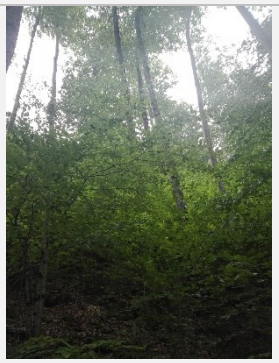
	Altimeter / slope	727 m a.s.l. / 35°	
	Maximum height	46.22 m (GEDI) / 45.76 m (ALS)	
	Mean height	31.17 m (GEDI) / 27.43 m (ALS)	
	FHD	3.21 (GEDI) / 2.76 (ALS)	
	AGBD	456.31 Mg/ha (GEDI)	
1951	Vegetation characteristics	80% beech; spruce in undergrowth; highly structured; no distinct layers	
	Altimeter / slope	762 m a.s.l. /33°	
	Maximum height	25.7 m (GEDI) / 38.15 m (ALS)	
	Mean height	10.15 m (GEDI) / 19.75 m (ALS)	
	FHD	2.92 (GEDI) / 2.55 (ALS)	
	AGBD	145.55 Mg/ha (GEDI)	
1952	Vegetation characteristics	Beech and spruce; no distinct layer; no young growth; high stem count	
	Altimeter / slope	796 m a.s.l. / 42°	
	Maximum height	26.62 m (GEDI) / 25.96 m (ALS)	
	Mean height	14.01 m (GEDI) / 12.95 m (ALS)	
	FHD	2.95 (GEDI) / 2.19 (ALS)	
	AGBD	169.09 Mg/ha (GEDI)	
1953	Vegetation characteristics	Beech, spruce and sycamore	
	Altimeter / slope	884 m a.s.l. / 35°	
	Maximum height	33.49 m (GEDI) / 39.1 m (ALS)	
	Mean height	15.99 m (GEDI) /10.55 m (ALS)	
	FHD	3.12 (GEDI) / 2.50 (ALS)	
	AGBD	211.09 Mg/ha (GEDI)	

1955	Vegetation characteristics	1. Layer beech 2. Layer spruce	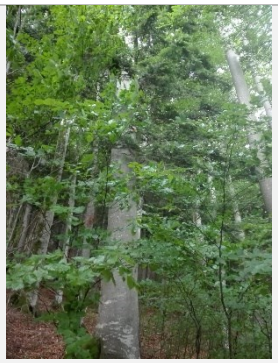
	Altimeter / slope	936 m a.s.l. / 38°	
	Maximum height	44.61 m (GEDI) / 39.13 m (ALS)	
	Mean height	13.37 m (GEDI) / 29.14 m (ALS)	
	FHD	2.93 (GEDI) / 2.78 (ALS)	
	AGBD	234.08 Mg/ha (GEDI)	
1956	Vegetation characteristics	Beech and fir	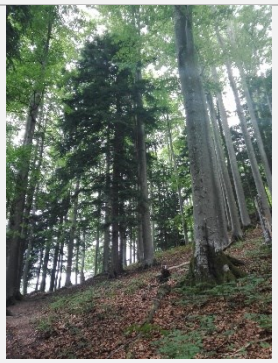
	Altimeter / slope	959 m a.s.l. / 24°	
	Maximum height	39.52 m (GEDI) / 40.24 m (ALS)	
	Mean height	26.82 m (GEDI) / 34.52 m (ALS)	
	FHD	3.31 (GEDI) / 2.03 (ALS)	
	AGBD	358.10 Mg/ha (GEDI)	
1960	Vegetation characteristics	Sycamore, fir and ash-tree (Wrong GEDI plot?)	
	Altimeter / slope	1010 m a.s.l. / 35°	
	Maximum height	12.13 m (GEDI) / 21.05 m (ALS)	
	Mean height	1.08 m (GEDI) / 14.89 m (ALS)	
	FHD	2.30 (GEDI) / 2.04 (ALS)	
	AGBD	45.53 Mg/ha (GEDI)	
1961	Vegetation characteristics	One big beech tree; beech and spruce in second layer	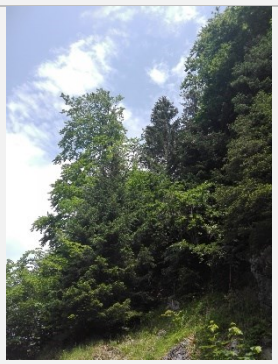
	Altimeter / slope	1037 m a.s.l. / 34°	
	Maximum height	20.19 m (GEDI) / 32.48 m (ALS)	
	Mean height	7.49 m (GEDI) / 10.06 m (ALS)	
	FHD	2.56 (GEDI) / 2.87 (ALS)	
	AGBD	110.92 Mg/ha (GEDI)	
1962	Vegetation characteristics	Beech and spruce	
	Altimeter / slope	1040 m a.s.l. / 39°	
	Maximum height	34.54 m (GEDI) / 41.44 m (ALS)	
	Mean height	17.49 m (GEDI) / 15.76 m (ALS)	
	FHD	3.09 (GEDI) / 2.66 (ALS)	
	AGBD	226.95 Mg/ha (GEDI)	

1558	Vegetation characteristics	Monoculture spruce; lying deadwood	
	Altimeter / slope	1224 m a.s.l. / 21°	
	Maximum height	45.63 m (GEDI) / 30.84 m (ALS)	
	Mean height	25.92 m (GEDI) / 18.46 m (ALS)	
	FHD	2.98 (GEDI) / 2.73 (ALS)	
	AGBD	392.32 Mg/ha (GEDI)	
1559	Vegetation characteristics	Monoculture spruce; lying deadwood	
	Altimeter / slope	1238 m a.s.l. / 18°	
	Maximum height	34.04 m (GEDI) / 29.36 m (ALS)	
	Mean height	17.04 m (GEDI) / 18.07 m (ALS)	
	FHD	3.30 (GEDI) / 2.80 (ALS)	
	AGBD	253.80 Mg/ha (GEDI)	
1560	Vegetation characteristics	Edge of the forest; beech; spruce	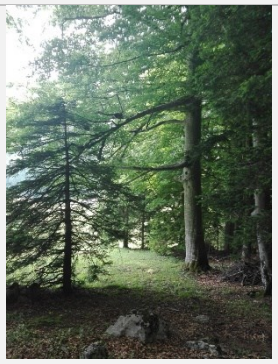
	Altimeter / slope	1249 m a.s.l. / 19°	
	Maximum height	34.45 m (GEDI) / 27.52 m (ALS)	
	Mean height	22.92 m (GEDI) / 18.73 m (ALS)	
	FHD	3.34 (GEDI) / 2.46 (ALS)	
	AGBD	294.37 Mg/ha (GEDI)	

B. Correlation

Table 29: The ten highest R^2 values between individual Sentinel variables and the mean vegetation height (ALS mean) both with the spatial resolution 10x10 m per pixel. Different corelations are ALS mean (total area). ALS mean 75 (only grids with a tree cover density (TCD) > 75%). ALS mean broadleaved forest (only grids that are located in broadleaved forest and have a TCD >75%) and ALS mean coniferous forest (only grids that are locate in coniferous forest and have a TCD > 75%).

ALS mean (10x10)		
Parameter	Temporal Statistics Band	R^2
NDVI6	mean	0.38
EVI	mean	0.37
NDVI6	med	0.36
EVI	med	0.36
NLVI	med	0.34
NDVI7	mean	0.33
NDVI8a	mean	0.33
SAVI	mean	0.33
MSAVI	mean	0.33
NDVI	mean	0.33

ALS mean 75 (10x10)		
Parameter	Temporal Statistics Band	R^2
NDVI6	mean	0.18
NDVI7	mean	0.17
NDVI8a	mean	0.17
NDVI	mean	0.17
SAVI	mean	0.17
MSAVI	mean	0.17
NDVI6	med	0.17
EVI	mean	0.17
EVI	med	0.17
NDVI7	med	0.16

ALS mean broadleaved forest (10x10)		
Parameter	Temporal Statistics Band	R^2
NDVI7	mean	0.11
NDVI6	mean	0.11
NDVI8a	mean	0.11
EVI	med	0.10
NDVI7	med	0.10
EVI	mean	0.10
NDVI	mean	0.10
SAVI	mean	0.10
MSAVI	mean	0.10
NDVI8a	med	0.10

ALS mean coniferous forest (10x10)		
Parameter	Temporal Statistics Band	R^2
NDVI6	mean	0.18
NDVI7	mean	0.17
NDVI8a	mean	0.17
NDVI	mean	0.16
SAVI	mean	0.16
MSAVI	mean	0.16
NDVI6	med	0.16
NDVI6	min	0.16
MSAVI2	mean	0.15
EVI	mean	0.15

Table 30: The ten highest R^2 values between individual Sentinel variables and the maximum vegetation height (ALS max) both with the spatial resolution 10x10 m per pixel. Different correlations are ALS max (total area). ALS max 75 (only grids with a tree cover density (TCD) > 75%). ALS max broadleaved forest (only grids that are located in broadleaved forest and have a TCD >75%) and ALS max coniferous forest (only grids that are locate in coniferous forest and have a TCD > 75%).

ALS max (10x10)		
Parameter	Temporal Statistics Band	R^2
NDVI6	mean	0.26
NDVI6	med	0.25
NLVI	med	0.25
NDVI8a	mean	0.24
NDVI7	mean	0.24
EVI	mean	0.22
NDVI	mean	0.22
SAVI	mean	0.22
MSAVI	mean	0.22
NDVI6	min	0.22

ALS max 75 (10x10)		
Parameter	Temporal Statistics Band	R^2
NLVI	med	0.06
NDVI6	mean	0.06
NDVI8a	mean	0.06
NDVI7	mean	0.06
NDVI6	min	0.05
NDVI8a	med	0.05
NDVI7	med	0.05
NDVI6	med	0.05
NDVI6	max	0.05
NLVI	mean	0.05

ALS max broadleaved forest (10x10)		
Parameter	Temporal Statistics Band	R^2
NLVI	med	0.04
NLVI	mean	0.03
NDII5	med	0.03
NDII5	mean	0.03
NDVI6	min	0.02
NDVI6	mean	0.02
NDVI8a	mean	0.02
NDVI7	mean	0.02
TCB	med	0.02
NDVI8a	max	0.02

ALS max coniferous forest (10x10)		
Parameter	Temporal Statistics Band	R^2
NLVI	med	0.08
NDVI8a	mean	0.07
NDVI6	mean	0.07
NDVI7	mean	0.07
NLVI	mean	0.06
NDVI6	min	0.06
NDVI6	max	0.06
NDVI8a	med	0.06
NDVI7	med	0.05
NDVI6	med	0.05

Table 31: The ten highest R^2 values between ALS mean or ALS max and individual Sentinel variables for the 30x30 m and 100x100 m fishnet.

ALS mean (30x30)		
Parameter	Temporal Statistics Band	R^2
NLVI	med	0.44
EVI	mean	0.42
EVI	med	0.41
MSAVI	mean	0.40
MSAVI	med	0.38
NDVI	mean	0.38
NDWI	mean	0.36
GNDVI	mean	0.36
MSAVI2	mean	0.36
NDVI	med	0.35

ALS max (30x30)		
Parameter	Temporal Statistics Band	R^2
NLVI	med	0.20
NLVI	mean	0.18
MSAVI	mean	0.17
MSAVI	mean	0.16
EVI	mean	0.15
MSAVI	med	0.15
NDVI	mean	0.15
EVI	med	0.14
MSAVI2	med	0.14
MSAVI	max	0.14

ALS mean (100x100)		
Parameter	Temporal Statistics Band	R^2
NDVI6	mean	0.55
NLVI	med	0.53
NDVI6	med	0.53
EVI	mean	0.52
EVI	med	0.51
NDVI8a	mean	0.49
NDVI7	mean	0.49
NDVI6	min	0.49
NDVI	mean	0.48
MSAVI	mean	0.48

ALS max (100x100)		
Parameter	Temporal Statistics Band	R^2
NDVI6	min	0.19
PSRI	mean	0.18
NDVI6	max	0.18
NLVI	mean	0.17
PSRI	min	0.17
NDVI6	mean	0.17
NDVI7	max	0.16
NDVI8a	max	0.16
NLVI	med	0.15
NDVI8a	mean	0.15

Table 32: R² values calculated with the ALS mean or ALS max and all Sentinel variables utilizing the fishnet grid cell sizes 10x10 m, 30x30 m and 100x100 m including the higher subalpine zone. Correlations calculated for the spatial resolution 10x10 m also include the R² values between ALS mean or ALS max and all Sentinel variables only within areas with a Tree Cover Density >75%, only within areas covered by broadleaved forest and only within areas covered by coniferous forest.

Parameter	ALS mean (10x10)				Parameter	ALS max (10x10)				Parameter	ALS mean (30x30)	ALS max (30x30)	Parameter	ALS mean (100x100)	ALS max (100x100)
	R^2 (total)	R^2 (>75%)	R^2 (broadleaved)	R^2 (coniferous)		R^2 (total)	R^2 (>75%)	R^2 (broadleaved)	R^2 (coniferous)		R^2	R^2		R^2	R^2
B2_max	0.07	0.06	0.01	0.06	B2_max	0.08	0.01	0.00	0.00	B2_max	0.11	0.08	B2_max	0.16	0.08
B2_mean	0.16	0.12	0.08	0.11	B2_mean	0.13	0.02	0.00	0.00	B2_mean	0.20	0.12	B2_mean	0.26	0.05
B2_med	0.16	0.10	0.05	0.10	B2_med	0.12	0.01	0.00	0.00	B2_med	0.19	0.10	B2_med	0.23	0.03
B2_min	0.09	0.07	0.03	0.07	B2_min	0.10	0.01	0.00	0.00	B2_min	0.11	0.10	B2_min	0.14	0.05
B2_sd	0.06	0.06	0.01	0.05	B2_sd	0.06	0.01	0.00	0.00	B2_sd	0.09	0.06	B2_sd	0.14	0.08
B2_var	0.02	0.01	0.00	0.00	B2_var	0.03	0.02	0.00	0.00	B2_var	0.05	0.05	B2_var	0.12	0.12
B3_max	0.08	0.08	0.01	0.06	B3_max	0.10	0.01	0.00	0.01	B3_max	0.13	0.10	B3_max	0.17	0.08
B3_mean	0.18	0.11	0.07	0.10	B3_mean	0.14	0.03	0.00	0.00	B3_mean	0.22	0.15	B3_mean	0.26	0.06
B3_med	0.19	0.12	0.04	0.11	B3_med	0.17	0.02	0.00	0.00	B3_med	0.23	0.14	B3_med	0.27	0.04
B3_min	0.06	0.02	0.00	0.02	B3_min	0.09	0.01	0.00	0.00	B3_min	0.07	0.10	B3_min	0.07	0.05
B3_sd	0.05	0.06	0.00	0.05	B3_sd	0.06	0.01	0.00	0.00	B3_sd	0.08	0.04	B3_sd	0.12	0.04
B3_var	0.02	0.02	0.00	0.02	B3_var	0.03	0.01	0.00	0.00	B3_var	0.05	0.05	B3_var	0.12	0.09
B4_max	0.16	0.13	0.05	0.11	B4_max	0.13	0.01	0.00	0.00	B4_max	0.22	0.14	B4_max	0.28	0.13
B4_mean	0.25	0.11	0.04	0.08	B4_mean	0.19	0.01	0.00	0.00	B4_mean	0.31	0.18	B4_mean	0.39	0.12
B4_med	0.23	0.10	0.07	0.07	B4_med	0.17	0.03	0.00	0.00	B4_med	0.29	0.16	B4_med	0.36	0.09
B4_min	0.11	0.10	0.04	0.09	B4_min	0.12	0.01	0.00	0.00	B4_min	0.14	0.12	B4_min	0.17	0.10
B4_sd	0.13	0.08	0.06	0.06	B4_sd	0.11	0.01	0.00	0.00	B4_sd	0.18	0.09	B4_sd	0.24	0.09
B4_var	0.04	0.04	0.00	0.01	B4_var	0.04	0.02	0.00	0.00	B4_var	0.08	0.06	B4_var	0.17	0.11
B5_max	0.11	0.09	0.01	0.04	B5_max	0.13	0.01	0.00	0.00	B5_max	0.14	0.12	B5_max	0.17	0.08
B5_mean	0.16	0.06	0.01	0.03	B5_mean	0.17	0.04	0.00	0.00	B5_mean	0.21	0.16	B5_mean	0.22	0.06
B5_med	0.19	0.09	0.06	0.09	B5_med	0.18	0.01	0.00	0.01	B5_med	0.24	0.16	B5_med	0.26	0.05
B5_min	0.03	0.03	0.00	0.02	B5_min	0.07	0.02	0.00	0.00	B5_min	0.04	0.08	B5_min	0.04	0.05
B5_sd	0.05	0.05	0.04	0.05	B5_sd	0.05	0.03	0.00	0.00	B5_sd	0.07	0.03	B5_sd	0.09	0.02
B5_var	0.04	0.03	0.00	0.01	B5_var	0.05	0.03	0.00	0.00	B5_var	0.06	0.05	B5_var	0.11	0.05
B6_max	0.04	0.03	0.01	0.04	B6_max	0.00	0.00	0.00	0.00	B6_max	0.06	0.00	B6_max	0.12	0.04
B6_mean	0.02	0.02	0.00	0.02	B6_mean	0.00	0.00	0.00	0.00	B6_mean	0.03	0.00	B6_mean	0.08	0.02
B6_med	0.02	0.01	0.00	0.00	B6_med	0.00	0.00	0.00	0.00	B6_med	0.03	0.00	B6_med	0.07	0.03
B6_min	0.01	0.01	0.00	0.00	B6_min	0.00	0.00	0.00	0.00	B6_min	0.02	0.01	B6_min	0.04	0.00
B6_sd	0.00	0.00	0.00	0.00	B6_sd	0.00	0.00	0.00	0.00	B6_sd	0.01	0.02	B6_sd	0.02	0.09
B6_var	0.00	0.00	0.00	0.00	B6_var	0.00	0.00	0.00	0.00	B6_var	0.00	0.01	B6_var	0.01	0.05
B7_max	0.07	0.05	0.01	0.03	B7_max	0.01	0.01	0.00	0.00	B7_max	0.10	0.01	B7_max	0.17	0.07
B7_mean	0.05	0.04	0.01	0.06	B7_mean	0.00	0.00	0.00	0.00	B7_mean	0.08	0.00	B7_mean	0.14	0.04
B7_med	0.05	0.02	0.02	0.03	B7_med	0.00	0.00	0.00	0.00	B7_med	0.07	0.01	B7_med	0.14	0.05
B7_min	0.03	0.00	0.00	0.00	B7_min	0.00	0.00	0.00	0.00	B7_min	0.04	0.00	B7_min	0.07	0.00
B7_sd	0.00	0.00	0.00	0.00	B7_sd	0.00	0.00	0.00	0.00	B7_sd	0.01	0.03	B7_sd	0.03	0.11
B7_var	0.00	0.00	0.00	0.00	B7_var	0.00	0.00	0.00	0.00	B7_var	0.00	0.01	B7_var	0.01	0.06
B8_max	0.05	0.03	0.00	0.02	B8_max	0.00	0.00	0.00	0.00	B8_max	0.08	0.01	B8_max	0.16	0.06
B8_mean	0.04	0.02	0.00	0.02	B8_mean	0.00	0.00	0.00	0.00	B8_mean	0.06	0.00	B8_mean	0.12	0.03
B8_med	0.03	0.01	0.00	0.01	B8_med	0.00	0.00	0.00	0.00	B8_med	0.05	0.00	B8_med	0.12	0.04
B8_min	0.02	0.01	0.00	0.00	B8_min	0.00	0.00	0.00	0.00	B8_min	0.04	0.00	B8_min	0.06	0.00
B8_sd	0.00	0.00	0.00	0.00	B8_sd	0.00	0.00	0.00	0.00	B8_sd	0.00	0.03	B8_sd	0.03	0.12
B8_var	0.00	0.00	0.00	0.00	B8_var	0.00	0.00	0.00	0.00	B8_var	0.00	0.01	B8_var	0.01	0.08

B8a_max	0.07	0.03	0.00	0.03	B8a_max	0.01	0.01	0.00	0.00	B8a_max	0.09	0.01	B8a_max	0.16	0.07
B8a_mean	0.05	0.01	0.00	0.01	B8a_mean	0.00	0.00	0.00	0.00	B8a_mean	0.07	0.00	B8a_mean	0.12	0.03
B8a_med	0.04	0.02	0.00	0.03	B8a_med	0.00	0.00	0.00	0.00	B8a_med	0.06	0.00	B8a_med	0.12	0.04
B8a_min	0.03	0.01	0.00	0.01	B8a_min	0.00	0.00	0.00	0.00	B8a_min	0.04	0.00	B8a_min	0.07	0.00
B8a_sd	0.00	0.00	0.00	0.00	B8a_sd	0.00	0.00	0.00	0.00	B8a_sd	0.00	0.02	B8a_sd	0.02	0.10
B8a_var	0.00	0.00	0.00	0.00	B8a_var	0.00	0.00	0.00	0.00	B8a_var	0.00	0.01	B8a_var	0.01	0.06
B11_max	0.05	0.04	0.01	0.02	B11_max	0.06	0.03	0.00	0.00	B11_max	0.06	0.02	B11_max	0.04	0.00
B11_mean	0.04	0.04	0.02	0.03	B11_mean	0.06	0.03	0.00	0.00	B11_mean	0.04	0.03	B11_mean	0.03	0.00
B11_med	0.05	0.05	0.04	0.04	B11_med	0.06	0.00	0.00	0.00	B11_med	0.05	0.04	B11_med	0.04	0.00
B11_min	0.00	0.00	0.00	0.00	B11_min	0.01	0.01	0.00	0.00	B11_min	0.00	0.02	B11_min	0.00	0.01
B11_sd	0.06	0.05	0.02	0.05	B11_sd	0.03	0.01	0.00	0.00	B11_sd	0.07	0.00	B11_sd	0.06	0.01
B11_var	0.06	0.04	0.01	0.04	B11_var	0.04	0.03	0.00	0.00	B11_var	0.07	0.00	B11_var	0.07	0.01
B12_max	0.14	0.10	0.07	0.09	B12_max	0.13	0.01	0.00	0.00	B12_max	0.17	0.08	B12_max	0.18	0.02
B12_mean	0.13	0.10	0.05	0.10	B12_mean	0.13	0.01	0.00	0.00	B12_mean	0.16	0.09	B12_mean	0.17	0.03
B12_med	0.13	0.11	0.04	0.08	B12_med	0.12	0.01	0.00	0.00	B12_med	0.17	0.09	B12_med	0.18	0.03
B12_min	0.03	0.03	0.01	0.03	B12_min	0.05	0.03	0.00	0.00	B12_min	0.03	0.05	B12_min	0.03	0.03
B12_sd	0.13	0.11	0.03	0.07	B12_sd	0.08	0.01	0.00	0.00	B12_sd	0.16	0.03	B12_sd	0.18	0.00
B12_var	0.07	0.06	0.01	0.06	B12_var	0.07	0.01	0.00	0.00	B12_var	0.11	0.03	B12_var	0.15	0.00
EVI_max	0.19	0.06	0.04	0.05	EVI_max	0.13	0.02	0.01	0.03	EVI_max	0.22	0.12	EVI_max	0.31	0.15
EVI_mean	0.37	0.17	0.10	0.15	EVI_mean	0.22	0.04	0.01	0.04	EVI_mean	0.42	0.15	EVI_mean	0.52	0.15
EVI_med	0.36	0.17	0.10	0.14	EVI_med	0.22	0.04	0.01	0.04	EVI_med	0.41	0.14	EVI_med	0.51	0.13
EVI_min	0.26	0.08	0.02	0.08	EVI_min	0.15	0.01	0.00	0.02	EVI_min	0.30	0.10	EVI_min	0.37	0.11
EVI_sd	0.02	0.02	0.00	0.02	EVI_sd	0.01	0.00	0.00	0.00	EVI_sd	0.02	0.00	EVI_sd	0.02	0.00
EVI_var	0.12	0.07	0.01	0.08	EVI_var	0.09	0.02	0.00	0.03	EVI_var	0.14	0.05	EVI_var	0.20	0.05
GNDVI_max	0.15	0.04	0.03	0.03	GNDVI_max	0.12	0.02	0.01	0.02	GNDVI_max	0.17	0.10	GNDVI_max	0.25	0.11
GNDVI_mean	0.32	0.15	0.07	0.13	GNDVI_mean	0.21	0.03	0.00	0.04	GNDVI_mean	0.36	0.14	GNDVI_mean	0.47	0.11
GNDVI_med	0.31	0.14	0.07	0.11	GNDVI_med	0.20	0.03	0.00	0.03	GNDVI_med	0.35	0.12	GNDVI_med	0.45	0.09
GNDVI_min	0.20	0.06	0.01	0.06	GNDVI_min	0.13	0.01	0.00	0.01	GNDVI_min	0.23	0.09	GNDVI_min	0.33	0.11
GNDVI_sd	0.06	0.03	0.00	0.03	GNDVI_sd	0.03	0.01	0.00	0.00	GNDVI_sd	0.07	0.02	GNDVI_sd	0.12	0.04
GNDVI_var	0.05	0.03	0.00	0.04	GNDVI_var	0.04	0.01	0.00	0.01	GNDVI_var	0.06	0.02	GNDVI_var	0.13	0.05
MSAVI_max	0.20	0.08	0.05	0.06	MSAVI_max	0.15	0.03	0.01	0.03	MSAVI_max	0.26	0.14	MSAVI_max	0.34	0.15
MSAVI_mean	0.33	0.17	0.10	0.16	MSAVI_mean	0.22	0.05	0.01	0.05	MSAVI_mean	0.40	0.17	MSAVI_mean	0.48	0.14
MSAVI_med	0.30	0.16	0.09	0.13	MSAVI_med	0.21	0.04	0.01	0.04	MSAVI_med	0.38	0.15	MSAVI_med	0.46	0.12
MSAVI_min	0.25	0.08	0.02	0.09	MSAVI_min	0.17	0.02	0.00	0.03	MSAVI_min	0.32	0.13	MSAVI_min	0.38	0.14
MSAVI_sd	0.15	0.06	0.01	0.08	MSAVI_sd	0.10	0.02	0.00	0.02	MSAVI_sd	0.19	0.07	MSAVI_sd	0.23	0.08
MSAVI_var	0.10	0.05	0.01	0.08	MSAVI_var	0.08	0.02	0.00	0.03	MSAVI_var	0.15	0.07	MSAVI_var	0.20	0.09
MSAVI2_max	0.18	0.08	0.05	0.06	MSAVI2_max	0.14	0.03	0.01	0.03	MSAVI2_max	0.24	0.14	MSAVI2_max	0.32	0.14
MSAVI2_mea	0.29	0.16	0.08	0.15	MSAVI2_mea	0.21	0.04	0.01	0.05	MSAVI2_mea	0.36	0.16	MSAVI2_mea	0.45	0.13
MSAVI2_med	0.27	0.15	0.09	0.13	MSAVI2_med	0.19	0.04	0.01	0.04	MSAVI2_med	0.34	0.14	MSAVI2_med	0.42	0.11
MSAVI2_min	0.15	0.03	0.01	0.06	MSAVI2_min	0.11	0.01	0.00	0.02	MSAVI2_min	0.20	0.09	MSAVI2_min	0.25	0.10
MSAVI2_sd	0.09	0.02	0.00	0.05	MSAVI2_sd	0.07	0.01	0.00	0.02	MSAVI2_sd	0.12	0.06	MSAVI2_sd	0.16	0.07
MSAVI2_var	0.06	0.02	0.00	0.05	MSAVI2_var	0.06	0.01	0.00	0.02	MSAVI2_var	0.10	0.06	MSAVI2_var	0.17	0.09
MSI_max	0.10	0.02	0.00	0.01	MSI_max	0.05	0.00	0.00	0.00	MSI_max	0.16	0.05	MSI_max	0.21	0.04
MSI_mean	0.21	0.05	0.02	0.05	MSI_mean	0.09	0.00	0.01	0.00	MSI_mean	0.31	0.07	MSI_mean	0.37	0.06
MSI_med	0.19	0.04	0.01	0.04	MSI_med	0.08	0.00	0.01	0.00	MSI_med	0.29	0.07	MSI_med	0.36	0.06
MSI_min	0.24	0.06	0.02	0.06	MSI_min	0.10	0.00	0.01	0.00	MSI_min	0.35	0.06	MSI_min	0.41	0.05
MSI_sd	0.17	0.05	0.02	0.06	MSI_sd	0.06	0.00	0.01	0.00	MSI_sd	0.25	0.03	MSI_sd	0.31	0.02
MSI_var	0.11	0.05	0.02	0.05	MSI_var	0.05	0.00	0.00	0.00	MSI_var	0.18	0.02	MSI_var	0.24	0.01
NDII5_max	0.22	0.05	0.01	0.06	NDII5_max	0.09	0.00	0.02	0.00	NDII5_max	0.00	0.00	NDII5_max	0.38	0.04
NDII5_mean	0.19	0.03	0.00	0.05	NDII5_mean	0.07	0.01	0.03	0.00	NDII5_mean	0.00	0.00	NDII5_mean	0.33	0.05

NDII5_med	0.18	0.03	0.00	0.04	NDII5_med	0.07	0.01	0.03	0.00	NDII5_med	0.00	0.00	NDII5_med	0.33	0.05
NDII5_min	0.09	0.01	0.00	0.02	NDII5_min	0.03	0.01	0.02	0.00	NDII5_min	0.00	0.00	NDII5_min	0.17	0.03
NDII5_sd	0.11	0.04	0.01	0.03	NDII5_sd	0.05	0.00	0.00	0.00	NDII5_sd	0.00	0.00	NDII5_sd	0.19	0.01
NDII5_var	0.07	0.03	0.01	0.02	NDII5_var	0.04	0.00	0.00	0.00	NDII5_var	0.00	0.00	NDII5_var	0.14	0.00
NDII7_max	0.27	0.08	0.03	0.08	NDII7_max	0.14	0.00	0.00	0.00	NDII7_max	0.00	0.00	NDII7_max	0.43	0.08
NDII7_mean	0.25	0.07	0.02	0.09	NDII7_mean	0.13	0.00	0.01	0.00	NDII7_mean	0.00	0.00	NDII7_mean	0.40	0.08
NDII7_med	0.24	0.06	0.02	0.08	NDII7_med	0.12	0.00	0.01	0.00	NDII7_med	0.00	0.00	NDII7_med	0.39	0.08
NDII7_min	0.16	0.03	0.00	0.05	NDII7_min	0.08	0.00	0.01	0.00	NDII7_min	0.00	0.00	NDII7_min	0.28	0.07
NDII7_sd	0.18	0.08	0.04	0.06	NDII7_sd	0.10	0.01	0.00	0.00	NDII7_sd	0.00	0.00	NDII7_sd	0.30	0.03
NDII7_var	0.11	0.05	0.03	0.04	NDII7_var	0.06	0.01	0.00	0.00	NDII7_var	0.00	0.00	NDII7_var	0.22	0.02
NDVI_max	0.20	0.08	0.05	0.06	NDVI_max	0.15	0.03	0.01	0.03	NDVI_max	0.23	0.12	NDVI_max	0.34	0.15
NDVI_mean	0.33	0.17	0.10	0.16	NDVI_mean	0.22	0.05	0.01	0.05	NDVI_mean	0.38	0.15	NDVI_mean	0.48	0.14
NDVI_med	0.30	0.16	0.09	0.13	NDVI_med	0.21	0.04	0.01	0.04	NDVI_med	0.35	0.14	NDVI_med	0.46	0.12
NDVI_min	0.25	0.08	0.02	0.09	NDVI_min	0.17	0.02	0.00	0.03	NDVI_min	0.29	0.12	NDVI_min	0.38	0.14
NDVI_sd	0.15	0.06	0.01	0.08	NDVI_sd	0.10	0.02	0.00	0.02	NDVI_sd	0.16	0.05	NDVI_sd	0.23	0.08
NDVI_var	0.10	0.05	0.01	0.08	NDVI_var	0.08	0.02	0.00	0.03	NDVI_var	0.11	0.05	NDVI_var	0.20	0.09
NDVI6_max	0.27	0.13	0.08	0.11	NDVI6_max	0.19	0.05	0.02	0.06	NDVI6_max	0.00	0.00	NDVI6_max	0.41	0.18
NDVI6_mean	0.38	0.18	0.11	0.18	NDVI6_mean	0.26	0.06	0.02	0.07	NDVI6_mean	0.00	0.00	NDVI6_mean	0.55	0.17
NDVI6_med	0.37	0.17	0.10	0.16	NDVI6_med	0.25	0.05	0.02	0.05	NDVI6_med	0.00	0.00	NDVI6_med	0.53	0.14
NDVI6_min	0.32	0.14	0.06	0.16	NDVI6_min	0.22	0.05	0.02	0.06	NDVI6_min	0.00	0.00	NDVI6_min	0.49	0.19
NDVI6_sd	0.06	0.04	0.01	0.07	NDVI6_sd	0.05	0.02	0.01	0.02	NDVI6_sd	0.00	0.00	NDVI6_sd	0.12	0.05
NDVI6_var	0.06	0.04	0.01	0.07	NDVI6_var	0.05	0.02	0.01	0.03	NDVI6_var	0.00	0.00	NDVI6_var	0.12	0.05
NDVI7_max	0.19	0.08	0.06	0.07	NDVI7_max	0.15	0.04	0.02	0.04	NDVI7_max	0.00	0.00	NDVI7_max	0.34	0.16
NDVI7_mean	0.33	0.17	0.11	0.17	NDVI7_mean	0.24	0.06	0.02	0.07	NDVI7_mean	0.00	0.00	NDVI7_mean	0.49	0.15
NDVI7_med	0.31	0.16	0.10	0.14	NDVI7_med	0.22	0.05	0.02	0.05	NDVI7_med	0.00	0.00	NDVI7_med	0.46	0.13
NDVI7_min	0.26	0.08	0.02	0.10	NDVI7_min	0.19	0.03	0.00	0.04	NDVI7_min	0.00	0.00	NDVI7_min	0.40	0.15
NDVI7_sd	0.16	0.06	0.01	0.08	NDVI7_sd	0.11	0.02	0.00	0.03	NDVI7_sd	0.00	0.00	NDVI7_sd	0.25	0.08
NDVI7_var	0.10	0.05	0.01	0.08	NDVI7_var	0.08	0.02	0.00	0.04	NDVI7_var	0.00	0.00	NDVI7_var	0.22	0.09
NDVI8a_max	0.19	0.08	0.05	0.06	NDVI8a_max	0.15	0.04	0.02	0.04	NDVI8a_max	0.00	0.00	NDVI8a_max	0.33	0.16
NDVI8a_mea	0.33	0.17	0.10	0.17	NDVI8a_mea	0.24	0.06	0.02	0.07	NDVI8a_mea	0.00	0.00	NDVI8a_mea	0.49	0.15
NDVI8a_med	0.31	0.16	0.10	0.14	NDVI8a_med	0.22	0.05	0.02	0.05	NDVI8a_med	0.00	0.00	NDVI8a_med	0.46	0.13
NDVI8a_min	0.25	0.08	0.02	0.10	NDVI8a_min	0.18	0.03	0.00	0.04	NDVI8a_min	0.00	0.00	NDVI8a_min	0.39	0.15
NDVI8a_sd	0.15	0.06	0.01	0.08	NDVI8a_sd	0.11	0.02	0.00	0.03	NDVI8a_sd	0.00	0.00	NDVI8a_sd	0.25	0.08
NDVI8a_var	0.09	0.05	0.01	0.08	NDVI8a_var	0.08	0.03	0.00	0.04	NDVI8a_var	0.00	0.00	NDVI8a_var	0.22	0.10
NDWI_max	0.20	0.06	0.01	0.06	NDWI_max	0.13	0.01	0.00	0.01	NDWI_max	0.23	0.09	NDWI_max	0.33	0.11
NDWI_mean	0.32	0.15	0.07	0.13	NDWI_mean	0.21	0.03	0.00	0.04	NDWI_mean	0.36	0.14	NDWI_mean	0.47	0.11
NDWI_med	0.31	0.14	0.07	0.11	NDWI_med	0.20	0.03	0.00	0.03	NDWI_med	0.35	0.12	NDWI_med	0.45	0.09
NDWI_min	0.15	0.04	0.03	0.03	NDWI_min	0.12	0.02	0.01	0.02	NDWI_min	0.17	0.10	NDWI_min	0.25	0.11
NDWI_sd	0.06	0.03	0.00	0.03	NDWI_sd	0.03	0.01	0.00	0.00	NDWI_sd	0.07	0.02	NDWI_sd	0.12	0.04
NDWI_var	0.05	0.03	0.00	0.04	NDWI_var	0.04	0.01	0.00	0.01	NDWI_var	0.06	0.02	NDWI_var	0.13	0.05
NLVI_max	0.01	0.00	0.00	0.00	NLVI_max	0.01	0.01	0.01	0.02	NLVI_max	0.01	0.03	NLVI_max	0.01	0.06
NLVI_mean	0.23	0.06	0.06	0.06	NLVI_mean	0.18	0.05	0.03	0.06	NLVI_mean	0.30	0.18	NLVI_mean	0.38	0.17
NLVI_med	0.34	0.12	0.09	0.12	NLVI_med	0.25	0.06	0.04	0.08	NLVI_med	0.44	0.20	NLVI_med	0.53	0.15
NLVI_min	0.23	0.05	0.02	0.07	NLVI_min	0.15	0.01	0.00	0.02	NLVI_min	0.27	0.10	NLVI_min	0.30	0.08
NLVI_sd	0.00	0.00	0.00	0.00	NLVI_sd	0.00	0.00	0.00	0.01	NLVI_sd	0.00	0.01	NLVI_sd	0.00	0.03
NLVI_var	0.00	0.00	0.00	0.00	NLVI_var	0.00	0.00	0.00	0.00	NLVI_var	0.00	0.00	NLVI_var	0.00	0.02
PSRI_max	0.17	0.05	0.01	0.07	PSRI_max	0.11	0.01	0.00	0.01	PSRI_max	0.00	0.00	PSRI_max	0.33	0.10
PSRI_mean	0.14	0.03	0.01	0.08	PSRI_mean	0.11	0.02	0.01	0.04	PSRI_mean	0.01	0.00	PSRI_mean	0.25	0.18
PSRI_med	0.08	0.01	0.00	0.05	PSRI_med	0.08	0.01	0.00	0.02	PSRI_med	0.01	0.00	PSRI_med	0.17	0.15
PSRI_min	0.06	0.04	0.03	0.04	PSRI_min	0.06	0.03	0.01	0.04	PSRI_min	0.00	0.00	PSRI_min	0.13	0.17

PSRI_sd	0.08	0.01	0.00	0.03	PSRI_sd	0.04	0.00	0.00	0.00	PSRI_sd	0.00	0.00	PSRI_sd	0.17	0.01
PSRI_var	0.06	0.02	0.00	0.03	PSRI_var	0.04	0.00	0.00	0.00	PSRI_var	0.00	0.00	PSRI_var	0.15	0.01
S2REP_max	0.00	0.00	0.00	0.00	S2REP_max	0.00	0.00	0.00	0.00	S2REP_max	0.00	0.00	S2REP_max	0.04	0.01
S2REP_mean	0.01	0.01	0.01	0.00	S2REP_mean	0.00	0.00	0.00	0.00	S2REP_mean	0.00	0.00	S2REP_mean	0.30	0.07
S2REP_med	0.07	0.04	0.01	0.03	S2REP_med	0.02	0.00	0.00	0.00	S2REP_med	0.00	0.00	S2REP_med	0.40	0.09
S2REP_min	0.00	0.00	0.00	0.00	S2REP_min	0.00	0.00	0.00	0.00	S2REP_min	0.00	0.00	S2REP_min	0.09	0.03
S2REP_sd	0.00	0.00	0.00	0.00	S2REP_sd	0.00	0.00	0.00	0.00	S2REP_sd	0.00	0.00	S2REP_sd	0.08	0.03
S2REP_var	0.00	0.00	0.00	0.00	S2REP_var	0.00	0.00	0.00	0.00	S2REP_var	0.00	0.00	S2REP_var	0.03	0.03
SAVI_max	0.20	0.08	0.05	0.06	SAVI_max	0.15	0.03	0.01	0.03	SAVI_max	0.00	0.00	SAVI_max	0.34	0.15
SAVI_mean	0.33	0.17	0.10	0.16	SAVI_mean	0.22	0.05	0.01	0.05	SAVI_mean	0.00	0.00	SAVI_mean	0.48	0.14
SAVI_med	0.30	0.16	0.09	0.13	SAVI_med	0.21	0.04	0.01	0.04	SAVI_med	0.00	0.00	SAVI_med	0.46	0.12
SAVI_min	0.25	0.08	0.02	0.09	SAVI_min	0.17	0.02	0.00	0.03	SAVI_min	0.00	0.00	SAVI_min	0.38	0.14
SAVI_sd	0.15	0.06	0.01	0.08	SAVI_sd	0.10	0.02	0.00	0.02	SAVI_sd	0.00	0.00	SAVI_sd	0.23	0.08
SAVI_var	0.10	0.05	0.01	0.08	SAVI_var	0.08	0.02	0.00	0.03	SAVI_var	0.00	0.00	SAVI_var	0.20	0.09
TCB_max	0.01	0.02	0.00	0.01	TCB_max	0.04	0.00	0.01	0.01	TCB_max	0.00	0.00	TCB_max	0.00	0.00
TCB_mean	0.01	0.03	0.00	0.02	TCB_mean	0.04	0.00	0.02	0.03	TCB_mean	0.00	0.00	TCB_mean	0.00	0.00
TCB_med	0.01	0.02	0.00	0.02	TCB_med	0.05	0.00	0.02	0.03	TCB_med	0.00	0.00	TCB_med	0.00	0.00
TCB_min	0.00	0.02	0.00	0.01	TCB_min	0.01	0.00	0.01	0.03	TCB_min	0.00	0.00	TCB_min	0.01	0.01
TCB_sd	0.03	0.00	0.00	0.01	TCB_sd	0.02	0.00	0.00	0.00	TCB_sd	0.00	0.00	TCB_sd	0.02	0.02
TCB_var	0.03	0.00	0.00	0.01	TCB_var	0.03	0.00	0.00	0.00	TCB_var	0.00	0.00	TCB_var	0.04	0.00
TCW_max	0.00	0.02	0.00	0.00	TCW_max	0.01	0.01	0.00	0.00	TCW_max	0.00	0.00	TCW_max	0.00	0.00
TCW_mean	0.09	0.00	0.00	0.04	TCW_mean	0.08	0.01	0.01	0.00	TCW_mean	0.00	0.00	TCW_mean	0.11	0.01
TCW_med	0.09	0.00	0.00	0.04	TCW_med	0.08	0.01	0.01	0.00	TCW_med	0.00	0.00	TCW_med	0.13	0.02
TCW_min	0.14	0.00	0.01	0.04	TCW_min	0.11	0.00	0.00	0.00	TCW_min	0.00	0.00	TCW_min	0.19	0.02
TCW_sd	0.14	0.03	0.02	0.05	TCW_sd	0.09	0.00	0.00	0.00	TCW_sd	0.00	0.00	TCW_sd	0.24	0.02
TCW_var	0.08	0.03	0.02	0.04	TCW_var	0.07	0.00	0.00	0.00	TCW_var	0.00	0.00	TCW_var	0.21	0.03
VH146_max	0.00	0.00	0.00	0.00	VH146_max	0.00	0.00	0.00	0.00	VH146_max	0.00	0.00	VH146_max	0.00	0.01
VH146_mean	0.00	0.00	0.00	0.00	VH146_mean	0.00	0.00	0.00	0.00	VH146_mean	0.00	0.00	VH146_mean	0.00	0.01
VH146_med	0.00	0.00	0.00	0.00	VH146_med	0.00	0.00	0.00	0.00	VH146_med	0.00	0.00	VH146_med	0.00	0.01
VH146_min	0.00	0.00	0.00	0.00	VH146_min	0.00	0.00	0.00	0.00	VH146_min	0.00	0.00	VH146_min	0.00	0.01
VH146_sd	0.00	0.00	0.00	0.00	VH146_sd	0.00	0.00	0.00	0.00	VH146_sd	0.00	0.00	VH146_sd	0.00	0.01
VH146_var	0.00	0.00	0.00	0.00	VH146_var	0.00	0.00	0.00	0.00	VH146_var	0.00	0.00	VH146_var	0.00	0.00
VH22_max	0.00	0.00	0.00	0.00	VH22_max	0.00	0.00	0.00	0.00	VH22_max	0.00	0.00	VH22_max	0.00	0.01
VH22_mean	0.00	0.00	0.00	0.00	VH22_mean	0.00	0.00	0.00	0.00	VH22_mean	0.00	0.00	VH22_mean	0.00	0.01
VH22_med	0.00	0.00	0.00	0.00	VH22_med	0.00	0.00	0.00	0.00	VH22_med	0.00	0.00	VH22_med	0.00	0.01
VH22_min	0.00	0.00	0.00	0.00	VH22_min	0.00	0.00	0.00	0.00	VH22_min	0.00	0.00	VH22_min	0.01	0.01
VH22_sd	0.00	0.00	0.00	0.00	VH22_sd	0.00	0.00	0.00	0.00	VH22_sd	0.00	0.00	VH22_sd	0.00	0.02
VH22_var	0.00	0.00	0.00	0.00	VH22_var	0.00	0.00	0.00	0.00	VH22_var	0.00	0.00	VH22_var	0.00	0.01
VH44_max	0.00	0.00	0.00	0.00	VH44_max	0.00	0.00	0.00	0.00	VH44_max	0.00	0.00	VH44_max	0.01	0.02
VH44_mean	0.00	0.00	0.00	0.00	VH44_mean	0.00	0.00	0.00	0.00	VH44_mean	0.00	0.00	VH44_mean	0.01	0.02
VH44_med	0.00	0.00	0.00	0.00	VH44_med	0.00	0.00	0.00	0.00	VH44_med	0.00	0.00	VH44_med	0.01	0.02
VH44_min	0.00	0.00	0.00	0.00	VH44_min	0.00	0.00	0.00	0.00	VH44_min	0.00	0.00	VH44_min	0.01	0.02
VH44_sd	0.00	0.00	0.00	0.00	VH44_sd	0.00	0.00	0.00	0.00	VH44_sd	0.00	0.00	VH44_sd	0.00	0.01
VH44_var	0.00	0.00	0.00	0.00	VH44_var	0.00	0.00	0.00	0.00	VH44_var	0.00	0.00	VH44_var	0.00	0.01
VH95_max	0.00	0.00	0.00	0.00	VH95_max	0.00	0.00	0.00	0.00	VH95_max	0.00	0.00	VH95_max	0.00	0.00
VH95_mean	0.00	0.00	0.00	0.00	VH95_mean	0.00	0.00	0.00	0.00	VH95_mean	0.00	0.00	VH95_mean	0.00	0.00
VH95_med	0.00	0.00	0.00	0.00	VH95_med	0.00	0.00	0.00	0.00	VH95_med	0.00	0.00	VH95_med	0.00	0.00
VH95_min	0.00	0.00	0.00	0.00	VH95_min	0.00	0.00	0.00	0.00	VH95_min	0.00	0.00	VH95_min	0.00	0.00
VH95_sd_sd	0.00	0.00	0.00	0.00	VH95_sd_sd	0.00	0.00	0.00	0.00	VH95_sd_sd	0.00	0.00	VH95_sd_sd	0.00	0.00
VH95_var	0.00	0.00	0.00	0.00	VH95_var	0.00	0.00	0.00	0.00	VH95_var	0.00	0.00	VH95_var	0.00	0.00

VV146_max	0.00	0.00	0.00	0.00	VV146_max	0.00	0.00	0.00	0.00	VV146_max	0.00	0.00	VV146_max	0.00	0.01
VV146_mean	0.00	0.00	0.00	0.00	VV146_mean	0.00	0.00	0.00	0.00	VV146_mean	0.00	0.00	VV146_mean	0.00	0.01
VV146_med	0.00	0.00	0.00	0.00	VV146_med	0.00	0.00	0.00	0.00	VV146_med	0.00	0.00	VV146_med	0.00	0.01
VV146_min	0.00	0.00	0.00	0.00	VV146_min	0.00	0.00	0.00	0.00	VV146_min	0.00	0.00	VV146_min	0.01	0.02
VV146_sd	0.00	0.00	0.00	0.00	VV146_sd	0.00	0.00	0.00	0.00	VV146_sd	0.00	0.00	VV146_sd	0.00	0.01
VV146_var	0.00	0.00	0.00	0.00	VV146_var	0.00	0.00	0.00	0.00	VV146_var	0.00	0.00	VV146_var	0.00	0.00
VV22_max	0.00	0.00	0.00	0.00	VV22_max	0.00	0.00	0.00	0.00	VV22_max	0.00	0.01	VV22_max	0.00	0.02
VV22_mean	0.00	0.00	0.00	0.00	VV22_mean	0.00	0.00	0.00	0.00	VV22_mean	0.00	0.01	VV22_mean	0.01	0.02
VV22_med	0.00	0.00	0.00	0.00	VV22_med	0.00	0.00	0.00	0.00	VV22_med	0.00	0.01	VV22_med	0.01	0.02
VV22_min	0.00	0.00	0.00	0.00	VV22_min	0.00	0.00	0.00	0.00	VV22_min	0.00	0.01	VV22_min	0.01	0.02
VV22_sd	0.00	0.00	0.00	0.00	VV22_sd	0.00	0.00	0.00	0.00	VV22_sd	0.00	0.00	VV22_sd	0.00	0.02
VV22_var	0.00	0.00	0.00	0.00	VV22_var	0.00	0.00	0.00	0.00	VV22_var	0.00	0.00	VV22_var	0.00	0.01
VV44_max	0.00	0.00	0.00	0.00	VV44_max	0.00	0.00	0.00	0.00	VV44_max	0.00	0.00	VV44_max	0.01	0.02
VV44_mean	0.00	0.00	0.00	0.00	VV44_mean	0.00	0.00	0.00	0.00	VV44_mean	0.00	0.00	VV44_mean	0.01	0.02
VV44_med	0.00	0.00	0.00	0.00	VV44_med	0.00	0.00	0.00	0.00	VV44_med	0.00	0.00	VV44_med	0.01	0.02
VV44_min	0.00	0.00	0.00	0.00	VV44_min	0.00	0.00	0.00	0.00	VV44_min	0.00	0.00	VV44_min	0.01	0.02
VV44_sd	0.00	0.00	0.00	0.00	VV44_sd	0.00	0.00	0.00	0.00	VV44_sd	0.00	0.00	VV44_sd	0.00	0.02
VV44_var	0.00	0.00	0.00	0.00	VV44_var	0.00	0.00	0.00	0.00	VV44_var	0.00	0.00	VV44_var	0.00	0.00
VV95_max	0.00	0.00	0.00	0.00	VV95_max	0.00	0.00	0.00	0.00	VV95_max	0.00	0.00	VV95_max	0.00	0.00
VV95_mean	0.00	0.00	0.00	0.00	VV95_mean	0.00	0.00	0.00	0.00	VV95_mean	0.00	0.00	VV95_mean	0.00	0.00
VV95_med	0.00	0.00	0.00	0.00	VV95_med	0.00	0.00	0.00	0.00	VV95_med	0.00	0.00	VV95_med	0.00	0.00
VV95_min	0.00	0.00	0.00	0.00	VV95_min	0.00	0.00	0.00	0.00	VV95_min	0.00	0.00	VV95_min	0.00	0.00
VV95_sd	0.00	0.00	0.00	0.00	VV95_sd	0.00	0.00	0.00	0.00	VV95_sd	0.00	0.00	VV95_sd	0.00	0.00
VV95_var	0.00	0.00	0.00	0.00	VV95_var	0.00	0.00	0.00	0.00	VV95_var	0.00	0.00	VV95_var	0.00	0.00
GLCM_VH146_con	0.00	0.00	0.00	0.00	GLCM_VH146_con	0.00	0.00	0.00	0.00	GLCM_VH146_con	0.00	0.00	GLCM_VH146_con	0.00	0.00
GLCM_VH146_cor	0.00	0.00	0.00	NA	GLCM_VH146_cor	0.00	0.00	0.00	NA	GLCM_VH146_cor	NA	NA	GLCM_VH146_cor	0.00	0.01
GLCM_VH146_dis	0.00	0.00	0.00	0.00	GLCM_VH146_dis	0.00	0.00	0.00	0.00	GLCM_VH146_dis	0.00	0.00	GLCM_VH146_dis	0.00	0.01
GLCM_VH146_ent	0.00	0.00	0.00	0.00	GLCM_VH146_ent	0.00	0.00	0.00	0.00	GLCM_VH146_ent	0.00	0.00	GLCM_VH146_ent	0.00	0.00
GLCM_VH146_homo	0.00	0.00	0.00	0.00	GLCM_VH146_homo	0.00	0.00	0.00	0.00	GLCM_VH146_homo	0.00	0.00	GLCM_VH146_homo	0.00	0.01
GLCM_VH146_mean	0.00	0.00	0.00	0.00	GLCM_VH146_mean	0.00	0.00	0.00	0.00	GLCM_VH146_mean	0.00	0.00	GLCM_VH146_mean	0.00	0.00
GLCM_VH146_sec	0.00	0.00	0.00	0.00	GLCM_VH146_sec	0.00	0.00	0.00	0.00	GLCM_VH146_sec	0.00	0.00	GLCM_VH146_sec	0.00	0.00
GLCM_VH146_var	0.00	0.00	0.00	0.00	GLCM_VH146_var	0.00	0.00	0.00	0.00	GLCM_VH146_var	0.00	0.00	GLCM_VH146_var	NA	NA
GLCM_VH22_con	0.00	0.00	0.00	0.00	GLCM_VH22_con	0.00	0.00	0.00	0.00	GLCM_VH22_con	0.00	0.00	GLCM_VH22_con	0.00	0.01
GLCM_VH22_cor	0.00	0.00	0.00	NA	GLCM_VH22_cor	0.00	0.00	0.00	NA	GLCM_VH22_cor	0.00	0.00	GLCM_VH22_cor	0.00	0.00
GLCM_VH22_dis	0.00	0.00	0.00	0.00	GLCM_VH22_dis	0.00	0.00	0.00	0.00	GLCM_VH22_dis	0.00	0.00	GLCM_VH22_dis	0.00	0.02
GLCM_VH22_ent	0.00	0.00	0.00	0.00	GLCM_VH22_ent	0.00	0.00	0.00	0.01	GLCM_VH22_ent	0.00	0.00	GLCM_VH22_ent	0.00	0.02
GLCM_VH22_homo	0.00	0.00	0.00	0.00	GLCM_VH22_homo	0.00	0.00	0.00	0.00	GLCM_VH22_homo	0.00	0.00	GLCM_VH22_homo	0.00	0.02
GLCM_VH22_mean	0.00	0.00	0.00	0.00	GLCM_VH22_mean	0.00	0.00	0.00	0.00	GLCM_VH22_mean	0.00	0.00	GLCM_VH22_mean	0.00	0.01
GLCM_VH22_sec	0.00	0.00	0.00	0.00	GLCM_VH22_sec	0.00	0.00	0.00	0.01	GLCM_VH22_sec	0.00	0.00	GLCM_VH22_sec	0.00	0.02
GLCM_VH22_var	0.00	0.00	0.00	0.00	GLCM_VH22_var	0.00	0.00	0.00	0.00	GLCM_VH22_var	0.00	0.00	GLCM_VH22_var	0.00	0.01
GLCM_VH44_con	0.00	0.00	0.00	0.00	GLCM_VH44_con	0.00	0.00	0.00	0.00	GLCM_VH44_con	0.00	0.00	GLCM_VH44_con	0.00	0.00
GLCM_VH44_cor	0.00	0.00	0.00	NA	GLCM_VH44_cor	0.00	0.00	0.00	NA	GLCM_VH44_cor	NA	NA	GLCM_VH44_cor	NA	NA
GLCM_VH44_diss	0.00	0.00	0.00	0.00	GLCM_VH44_diss	0.00	0.00	0.00	0.00	GLCM_VH44_diss	0.00	0.00	GLCM_VH44_diss	0.00	0.00
GLCM_VH44_ent	0.00	0.00	0.00	0.00	GLCM_VH44_ent	0.00	0.00	0.00	0.00	GLCM_VH44_ent	0.00	0.00	GLCM_VH44_ent	0.00	0.01
GLCM_VH44_homo	0.00	0.00	0.00	0.00	GLCM_VH44_homo	0.00	0.00	0.00	0.00	GLCM_VH44_homo	0.00	0.00	GLCM_VH44_homo	0.00	0.01
GLCM_VH44_mean	0.00	0.00	0.00	0.00	GLCM_VH44_mean	0.00	0.00	0.00	0.00	GLCM_VH44_mean	0.00	0.00	GLCM_VH44_mean	0.00	0.00
GLCM_VH44_sec	0.00	0.00	0.00	0.00	GLCM_VH44_sec	0.00	0.00	0.00	0.00	GLCM_VH44_sec	0.00	0.00	GLCM_VH44_sec	0.00	0.01
GLCM_VH44_var	0.00	0.00	0.00	0.00	GLCM_VH44_var	0.00	0.00	0.00	0.00	GLCM_VH44_var	0.00	0.00	GLCM_VH44_var	0.00	0.00
GLCM_VH95_con	0.00	0.00	0.00	0.00	GLCM_VH95_con	0.00	0.00	0.00	0.00	GLCM_VH95_con	0.00	0.00	GLCM_VH95_con	0.00	0.00
GLCM_VH95_cor	0.00	0.00	0.00	NA	GLCM_VH95_cor	0.00	0.00	0.00	NA	GLCM_VH95_cor	NA	NA	GLCM_VH95_cor	0.00	0.00

GLCM_VH95_dis	0.00	0.00	0.00	0.00	GLCM_VH95_dis	0.00	0.00	0.00	0.00	GLCM_VH95_dis	0.00	0.00	GLCM_VH95_dis	0.00	0.01
GLCM_VH95_ent	0.00	0.00	0.00	0.00	GLCM_VH95_ent	0.00	0.00	0.00	0.00	GLCM_VH95_ent	0.00	0.00	GLCM_VH95_ent	0.00	0.01
GLCM_VH95_homo	0.00	0.00	0.00	0.00	GLCM_VH95_homo	0.00	0.00	0.00	0.00	GLCM_VH95_homo	0.00	0.00	GLCM_VH95_homo	0.00	0.01
GLCM_VH95_mean	0.00	0.01	0.01	0.00	GLCM_VH95_mean	0.00	0.00	0.01	0.00	GLCM_VH95_mean	0.00	0.00	GLCM_VH95_mean	0.00	0.00
GLCM_VH95_sec	0.00	0.00	0.00	0.00	GLCM_VH95_sec	0.00	0.00	0.00	0.00	GLCM_VH95_sec	0.00	0.00	GLCM_VH95_sec	0.00	0.01
GLCM_VH95_var	0.00	0.00	0.00	0.00	GLCM_VH95_var	0.00	0.00	0.00	0.00	GLCM_VH95_var	0.00	0.00	GLCM_VH95_var	0.00	0.00
GLCM_VV146_con	0.00	0.00	0.00	0.00	GLCM_VV146_con	0.00	0.00	0.00	0.00	GLCM_VV146_con	0.00	0.00	GLCM_VV146_con	0.00	0.00
GLCM_VV146_cor	0.00	0.00	0.00	NA	GLCM_VV146_cor	0.00	0.00	0.00	NA	GLCM_VV146_cor	NA	NA	GLCM_VV146_cor	0.00	0.00
GLCM_VV146_dis	0.00	0.00	0.00	0.00	GLCM_VV146_dis	0.00	0.00	0.00	0.00	GLCM_VV146_dis	0.00	0.00	GLCM_VV146_dis	0.00	0.00
GLCM_VV146_ent	0.00	0.00	0.00	0.00	GLCM_VV146_ent	0.00	0.00	0.00	0.00	GLCM_VV146_ent	0.00	0.00	GLCM_VV146_ent	0.00	0.00
GLCM_VV146_homo	0.00	0.00	0.00	0.00	GLCM_VV146_homo	0.00	0.00	0.00	0.00	GLCM_VV146_homo	0.00	0.00	GLCM_VV146_homo	0.00	0.00
GLCM_VV146_mean	0.00	0.00	0.00	0.00	GLCM_VV146_mean	0.00	0.00	0.00	0.00	GLCM_VV146_mean	0.00	0.00	GLCM_VV146_mean	0.00	0.00
GLCM_VV146_sec	0.00	0.00	0.00	0.00	GLCM_VV146_sec	0.00	0.00	0.00	0.00	GLCM_VV146_sec	0.00	0.00	GLCM_VV146_sec	0.00	0.00
GLCM_VV146_var	0.00	0.00	0.00	0.00	GLCM_VV146_var	0.00	0.00	0.00	0.00	GLCM_VV146_var	0.00	0.00	GLCM_VV146_var	NA	NA
GLCM_VV22_con	0.00	0.00	0.00	0.00	GLCM_VV22_con	0.00	0.00	0.00	0.00	GLCM_VV22_con	0.00	0.00	GLCM_VV22_con	0.00	0.00
GLCM_VV22_cor	0.00	0.00	0.00	NA	GLCM_VV22_cor	0.00	0.00	0.00	NA	GLCM_VV22_cor	NA	NA	GLCM_VV22_cor	NA	NA
GLCM_VV22_dis	0.00	0.00	0.00	0.00	GLCM_VV22_dis	0.00	0.00	0.00	0.00	GLCM_VV22_dis	0.00	0.00	GLCM_VV22_dis	0.00	0.01
GLCM_VV22_ent	0.00	0.00	0.00	0.00	GLCM_VV22_ent	0.00	0.00	0.00	0.00	GLCM_VV22_ent	0.00	0.00	GLCM_VV22_ent	0.00	0.01
GLCM_VV22_homo	0.00	0.00	0.00	0.00	GLCM_VV22_homo	0.00	0.00	0.00	0.00	GLCM_VV22_homo	0.00	0.00	GLCM_VV22_homo	0.00	0.01
GLCM_VV22_mean	0.00	0.00	0.00	0.00	GLCM_VV22_mean	0.00	0.00	0.00	0.00	GLCM_VV22_mean	0.00	0.00	GLCM_VV22_mean	0.00	0.01
GLCM_VV22_sec	0.00	0.00	0.00	0.00	GLCM_VV22_sec	0.00	0.00	0.00	0.00	GLCM_VV22_sec	0.00	0.00	GLCM_VV22_sec	0.00	0.01
GLCM_VV22_var	0.00	0.00	0.00	0.00	GLCM_VV22_var	0.00	0.00	0.00	0.00	GLCM_VV22_var	0.00	0.00	GLCM_VV22_var	0.00	0.00
GLCM_VV44_con	0.00	0.00	0.00	0.00	GLCM_VV44_con	0.00	0.00	0.00	0.00	GLCM_VV44_con	0.00	0.00	GLCM_VV44_con	0.00	0.00
GLCM_VV44_cor	0.00	0.00	0.00	NA	GLCM_VV44_cor	0.00	0.00	0.00	NA	GLCM_VV44_cor	NA	NA	GLCM_VV44_cor	NA	NA
GLCM_VV44_diss	0.00	0.00	0.00	0.00	GLCM_VV44_diss	0.00	0.00	0.00	0.00	GLCM_VV44_diss	0.00	0.00	GLCM_VV44_diss	0.00	0.01
GLCM_VV44_ent	0.00	0.00	0.00	0.00	GLCM_VV44_entr	0.00	0.00	0.00	0.00	GLCM_VV44_ent	0.00	0.00	GLCM_VV44_ent	0.00	0.01
GLCM_VV44_homo	0.00	0.00	0.00	0.00	GLCM_VV44_homo	0.00	0.00	0.00	0.00	GLCM_VV44_homo	0.00	0.00	GLCM_VV44_homo	0.00	0.01
GLCM_VV44_mean	0.00	0.00	0.00	0.00	GLCM_VV44_mean	0.00	0.00	0.00	0.00	GLCM_VV44_mean	0.00	0.00	GLCM_VV44_mean	0.00	0.00
GLCM_VV44_sec	0.00	0.00	0.00	0.00	GLCM_VV44_sec	0.00	0.00	0.00	0.00	GLCM_VV44_sec	0.00	0.00	GLCM_VV44_sec	0.00	0.01
GLCM_VV44_var	0.00	0.00	0.00	0.00	GLCM_VV44_var	0.00	0.00	0.00	0.00	GLCM_VV44_var	0.00	0.00	GLCM_VV44_var	0.00	0.00
GLCM_VV95_con	0.00	0.00	0.00	0.00	GLCM_VV95_con	0.00	0.00	0.00	0.00	GLCM_VV95_con	0.00	0.00	GLCM_VV95_con	0.00	0.00
GLCM_VV95_cor	0.00	0.00	0.00	NA	GLCM_VV95_cor	0.00	0.00	0.00	NA	GLCM_VV95_cor	NA	NA	GLCM_VV95_cor	NA	NA
GLCM_VV95_dis	0.00	0.00	0.00	0.00	GLCM_VV95_dis	0.00	0.00	0.00	0.00	GLCM_VV95_dis	0.00	0.00	GLCM_VV95_dis	0.00	0.01
GLCM_VV95_ent	0.00	0.00	0.00	0.00	GLCM_VV95_ent	0.00	0.00	0.00	0.00	GLCM_VV95_ent	0.00	0.00	GLCM_VV95_ent	0.00	0.01
GLCM_VV95_homo	0.00	0.00	0.00	0.00	GLCM_VV95_homo	0.00	0.00	0.00	0.00	GLCM_VV95_homo	0.00	0.00	GLCM_VV95_homo	0.00	0.01
GLCM_VV95_mean	0.00	0.00	0.00	0.00	GLCM_VV95_mean	0.00	0.00	0.00	0.00	GLCM_VV95_mean	0.00	0.00	GLCM_VV95_mean	0.00	0.00
GLCM_VV95_sec	0.00	0.00	0.00	0.00	GLCM_VV95_sec	0.00	0.00	0.00	0.00	GLCM_VV95_sec	0.00	0.00	GLCM_VV95_sec	0.00	0.01
GLCM_VV95_var	0.00	0.00	0.00	0.00	GLCM_VV95_var	0.00	0.00	0.00	0.00	GLCM_VV95_var	0.00	0.00	GLCM_VV95_var	0.00	0.00

Table 33: R^2 and R values calculated with ALS mean, ALS max or ALS FHD and all Sentinel variables for the fishnet grid cell size 10x10 m without the higher subalpine zone.

Parameter	ALS mean		Parameter	ALS max		Parameter	ALS FHD	
	R^2	R		R^2	R		R^2	R
B2_max	0.07	-0.27	B2_max	0.09	-0.29	B2_max	0.05	-0.23
B2_mean	0.16	-0.41	B2_mean	0.18	-0.42	B2_mean	0.16	-0.40
B2_med	0.16	-0.40	B2_med	0.16	-0.40	B2_med	0.15	-0.39
B2_min	0.09	-0.30	B2_min	0.11	-0.34	B2_min	0.12	-0.34
B2_sd	0.06	-0.24	B2_sd	0.06	-0.25	B2_sd	0.03	-0.16
B2_var	0.02	-0.14	B2_var	0.03	-0.16	B2_var	0.01	-0.11
B3_max	0.09	-0.30	B3_max	0.11	-0.33	B3_max	0.10	-0.31
B3_mean	0.18	-0.42	B3_mean	0.22	-0.46	B3_mean	0.22	-0.47
B3_med	0.19	-0.44	B3_med	0.22	-0.46	B3_med	0.22	-0.47
B3_min	0.06	-0.24	B3_min	0.09	-0.31	B3_min	0.12	-0.34
B3_sd	0.05	-0.23	B3_sd	0.06	-0.24	B3_sd	0.03	-0.17
B3_var	0.02	-0.15	B3_var	0.03	-0.18	B3_var	0.02	-0.13
B4_max	0.16	-0.40	B4_max	0.16	-0.40	B4_max	0.10	-0.31
B4_mean	0.25	-0.50	B4_mean	0.25	-0.50	B4_mean	0.17	-0.41
B4_med	0.23	-0.48	B4_med	0.22	-0.47	B4_med	0.16	-0.40
B4_min	0.11	-0.33	B4_min	0.13	-0.36	B4_min	0.11	-0.33
B4_sd	0.13	-0.35	B4_sd	0.12	-0.34	B4_sd	0.06	-0.24
B4_var	0.04	-0.19	B4_var	0.04	-0.21	B4_var	0.03	-0.16
B5_max	0.11	-0.33	B5_max	0.14	-0.38	B5_max	0.16	-0.40
B5_mean	0.17	-0.41	B5_mean	0.22	-0.46	B5_mean	0.26	-0.51
B5_med	0.20	-0.44	B5_med	0.23	-0.48	B5_med	0.27	-0.52
B5_min	0.03	-0.18	B5_min	0.07	-0.27	B5_min	0.10	-0.32
B5_sd	0.05	-0.22	B5_sd	0.05	-0.23	B5_sd	0.03	-0.18
B5_var	0.04	-0.19	B5_var	0.05	-0.21	B5_var	0.03	-0.18
B6_max	0.04	0.21	B6_max	0.00	0.04	B6_max	0.06	-0.24
B6_mean	0.02	0.15	B6_mean	0.00	-0.01	B6_mean	0.07	-0.27
B6_med	0.02	0.13	B6_med	0.00	-0.03	B6_med	0.08	-0.29
B6_min	0.01	0.12	B6_min	0.00	-0.02	B6_min	0.03	-0.17
B6_sd	0.00	0.06	B6_sd	0.00	0.04	B6_sd	0.01	-0.12
B6_var	0.00	0.01	B6_var	0.00	-0.02	B6_var	0.02	-0.15
B7_max	0.07	0.27	B7_max	0.01	0.10	B7_max	0.04	-0.20

B7_mean	0.05	0.23	B7_mean	0.00	0.06	B7_mean	0.05	-0.21
B7_med	0.05	0.22	B7_med	0.00	0.06	B7_med	0.05	-0.22
B7_min	0.03	0.18	B7_min	0.00	0.03	B7_min	0.02	-0.14
B7_sd	0.00	0.07	B7_sd	0.00	0.05	B7_sd	0.02	-0.12
B7_var	0.00	0.02	B7_var	0.00	0.00	B7_var	0.02	-0.15
B8_max	0.05	0.22	B8_max	0.00	0.05	B8_max	0.05	-0.22
B8_mean	0.04	0.19	B8_mean	0.00	0.01	B8_mean	0.05	-0.22
B8_med	0.03	0.18	B8_med	0.00	0.00	B8_med	0.05	-0.23
B8_min	0.02	0.16	B8_min	0.00	0.00	B8_min	0.02	-0.14
B8_sd	0.00	0.03	B8_sd	0.00	0.01	B8_sd	0.01	-0.12
B8_var	0.00	-0.02	B8_var	0.00	-0.05	B8_var	0.02	-0.15
B8a_max	0.07	0.26	B8**a**_max	0.01	0.10	B8**a**_max	0.04	-0.21
B8a_mean	0.05	0.22	B8**a**_mean	0.00	0.05	B8**a**_mean	0.05	-0.22
B8a_med	0.04	0.20	B8**a**_med	0.00	0.04	B8**a**_med	0.06	-0.24
B8a_min	0.03	0.17	B8**a**_min	0.00	0.02	B8**a**_min	0.02	-0.14
B8a_sd	0.00	0.05	B8**a**_sd	0.00	0.04	B8**a**_sd	0.01	-0.12
B8a_var	0.00	0.00	B8**a**_var	0.00	-0.01	B8**a**_var	0.02	-0.14
B11_max	0.05	-0.22	B11_max	0.06	-0.25	B11_max	0.15	-0.39
B11_mean	0.04	-0.19	B11_mean	0.06	-0.25	B11_mean	0.15	-0.39
B11_med	0.05	-0.22	B11_med	0.07	-0.27	B11_med	0.17	-0.41
B11_min	0.00	-0.05	B11_min	0.02	-0.13	B11_min	0.06	-0.24
B11_sd	0.06	-0.24	B11_sd	0.03	-0.17	B11_sd	0.03	-0.18
B11_var	0.06	-0.24	B11_var	0.04	-0.19	B11_var	0.04	-0.21
B12_max	0.14	-0.38	B12_max	0.14	-0.37	B12_max	0.16	-0.40
B12_mean	0.13	-0.36	B12_mean	0.14	-0.37	B12_mean	0.17	-0.41
B12_med	0.14	-0.37	B12_med	0.15	-0.38	B12_med	0.17	-0.42
B12_min	0.03	-0.17	B12_min	0.05	-0.23	B12_min	0.08	-0.27
B12_sd	0.13	-0.36	B12_sd	0.08	-0.29	B12_sd	0.06	-0.25
B12_var	0.09	-0.30	B12_var	0.07	-0.27	B12_var	0.07	-0.26
DVI_max	0.00	0.03	DVI_max	0.06	0.09	DVI_max	0.02	-0.15
DVI_mean	0.00	0.01	DVI_mean	0.07	0.10	DVI_mean	0.02	-0.14
DVI_med	0.00	-0.03	DVI_med	0.06	0.10	DVI_med	0.02	-0.14
DVI_min	0.00	-0.02	DVI_min	0.03	0.07	DVI_min	0.01	-0.09
DVI_sd	0.00	-0.02	DVI_sd	0.01	0.07	DVI_sd	0.01	-0.12
DVI_var	0.00	0.05	DVI_var	0.00	0.08	DVI_var	0.02	-0.14

EVI_max	0.19	0.44	EVI_max	0.14	0.38	EVI_max	0.04	0.21
EVI_mean	0.37	0.61	EVI_mean	0.22	0.47	EVI_mean	0.06	0.25
EVI_med	0.36	0.60	EVI_med	0.21	0.46	EVI_med	0.06	0.25
EVI_min	0.26	0.51	EVI_min	0.15	0.38	EVI_min	0.03	0.19
EVI_sd	0.02	-0.13	EVI_sd	0.00	-0.07	EVI_sd	0.00	-0.01
EVI_var	0.12	-0.34	EVI_var	0.08	-0.29	EVI_var	0.03	-0.17
EVIRE1_max	0.03	0.17	EVIRE1_max	0.04	0.15	EVIRE1_max	0.01	0.11
EVIRE1_mean	0.09	0.28	EVIRE1_mean	0.08	0.22	EVIRE1_mean	0.04	0.21
EVIRE1_med	0.09	0.28	EVIRE1_med	0.10	0.30	EVIRE1_med	0.04	0.21
EVIRE1_min	0.02	0.14	EVIRE1_min	0.14	0.38	EVIRE1_min	0.02	0.13
EVIRE1_sd	0.01	0.11	EVIRE1_sd	0.00	0.04	EVIRE1_sd	0.00	0.06
EVIRE1_var	0.00	0.05	EVIRE1_var	0.00	-0.04	EVIRE1_var	0.00	0.01
GNDVI_max	0.16	0.40	GNDVI_max	0.13	0.36	GNDVI_max	0.06	0.24
GNDVI_mean	0.32	0.57	GNDVI_mean	0.21	0.46	GNDVI_mean	0.08	0.28
GNDVI_med	0.31	0.55	GNDVI_med	0.20	0.45	GNDVI_med	0.07	0.27
GNDVI_min	0.19	0.44	GNDVI_min	0.13	0.35	GNDVI_min	0.03	0.18
GNDVI_sd	0.05	-0.23	GNDVI_sd	0.03	-0.16	GNDVI_sd	0.00	-0.03
GNDVI_var	0.05	-0.22	GNDVI_var	0.03	-0.18	GNDVI_var	0.00	-0.06
MSAVI_max	0.20	0.45	MSAVI_max	0.15	0.39	MSAVI_max	0.05	0.23
MSAVI_mean	0.33	0.57	MSAVI_mean	0.22	0.47	MSAVI_mean	0.07	0.27
MSAVI_med	0.30	0.55	MSAVI_med	0.20	0.45	MSAVI_med	0.07	0.27
MSAVI_min	0.25	0.50	MSAVI_min	0.16	0.40	MSAVI_min	0.05	0.22
MSAVI_sd	0.14	-0.38	MSAVI_sd	0.09	-0.30	MSAVI_sd	0.02	-0.15
MSAVI_var	0.10	-0.31	MSAVI_var	0.07	-0.27	MSAVI_var	0.02	-0.15
MSAVI2_max	0.19	0.43	MSAVI2_max	0.15	0.38	MSAVI2_max	0.05	0.23
MSAVI2_mea	0.29	0.54	MSAVI2_mea	0.21	0.46	MSAVI2_mean	0.08	0.28
MSAVI2_med	0.27	0.52	MSAVI2_med	0.19	0.44	MSAVI2_med	0.07	0.27
MSAVI2_min	0.15	0.38	MSAVI2_min	0.11	0.33	MSAVI2_min	0.04	0.19
MSAVI2_sd	0.09	-0.30	MSAVI2_sd	0.06	-0.25	MSAVI2_sd	0.02	-0.14
MSAVI2_var	0.06	-0.25	MSAVI2_var	0.05	-0.23	MSAVI2_var	0.02	-0.14
MSI_max	0.10	0.31	MSI_max	0.05	0.22	MSI_max	0.02	0.14
MSI_mean	0.21	0.45	MSI_mean	0.09	0.30	MSI_mean	0.03	0.18
MSI_med	0.19	0.43	MSI_med	0.08	0.29	MSI_med	0.03	0.18
MSI_min	0.24	0.49	MSI_min	0.10	0.31	MSI_min	0.04	0.19
MSI_sd	0.17	-0.41	MSI_sd	0.06	-0.25	MSI_sd	0.02	-0.15

MSI_var	0.12	-0.34	MSI_var	0.05	-0.23	MSI_var	0.02	-0.15
NDII5_max	0.22	-0.47	NDII5_max	0.09	-0.30	NDII5_max	0.03	-0.18
NDII5_mean	0.19	-0.43	NDII5_mean	0.07	-0.27	NDII5_mean	0.03	-0.16
NDII5_med	0.18	-0.42	NDII5_med	0.07	-0.26	NDII5_med	0.02	-0.15
NDII5_min	0.10	-0.31	NDII5_min	0.04	-0.19	NDII5_min	0.01	-0.11
NDII5_sd	0.11	-0.33	NDII5_sd	0.05	-0.23	NDII5_sd	0.02	-0.15
NDII5_var	0.07	-0.27	NDII5_var	0.04	-0.19	NDII5_var	0.02	-0.13
NDII7_max	0.27	-0.52	NDII7_max	0.14	-0.37	NDII7_max	0.05	-0.22
NDII7_mean	0.25	-0.50	NDII7_mean	0.13	-0.35	NDII7_mean	0.04	-0.21
NDII7_med	0.23	-0.48	NDII7_med	0.12	-0.34	NDII7_med	0.04	-0.20
NDII7_min	0.16	-0.40	NDII7_min	0.08	-0.29	NDII7_min	0.02	-0.16
NDII7_sd	0.18	-0.43	NDII7_sd	0.10	-0.32	NDII7_sd	0.04	-0.20
NDII7_var	0.11	-0.33	NDII7_var	0.07	-0.26	NDII7_var	0.03	-0.18
NDVI_max	0.20	0.45	NDVI_max	0.15	0.39	NDVI_max	0.05	0.23
NDVI_mean	0.33	0.57	NDVI_mean	0.22	0.47	NDVI_mean	0.07	0.27
NDVI_med	0.30	0.55	NDVI_med	0.20	0.45	NDVI_med	0.07	0.27
NDVI_min	0.25	0.50	NDVI_min	0.16	0.40	NDVI_min	0.05	0.22
NDVI_sd	0.14	-0.38	NDVI_sd	0.09	-0.30	NDVI_sd	0.02	-0.15
NDVI_var	0.10	-0.31	NDVI_var	0.07	-0.27	NDVI_var	0.02	-0.15
NDVI6_max	0.28	0.53	NDVI6_max	0.20	0.44	NDVI6_max	0.06	0.24
NDVI6_mean	0.38	0.61	NDVI6_mean	0.25	0.50	NDVI6_mean	0.09	0.29
NDVI6_med	0.37	0.61	NDVI6_med	0.25	0.50	NDVI6_med	0.09	0.30
NDVI6_min	0.31	0.55	NDVI6_min	0.21	0.46	NDVI6_min	0.06	0.25
NDVI6_sd	0.06	-0.24	NDVI6_sd	0.04	-0.20	NDVI6_sd	0.01	-0.08
NDVI6_var	0.06	-0.24	NDVI6_var	0.04	-0.21	NDVI6_var	0.01	-0.10
NDVI7_max	0.20	0.44	NDVI7_max	0.15	0.39	NDVI7_max	0.05	0.23
NDVI7_mean	0.33	0.57	NDVI7_mean	0.23	0.48	NDVI7_mean	0.08	0.29
NDVI7_med	0.31	0.55	NDVI7_med	0.22	0.47	NDVI7_med	0.08	0.28
NDVI7_min	0.25	0.50	NDVI7_min	0.18	0.42	NDVI7_min	0.06	0.24
NDVI7_sd	0.15	-0.39	NDVI7_sd	0.10	-0.32	NDVI7_sd	0.03	-0.17
NDVI7_var	0.10	-0.31	NDVI7_var	0.08	-0.28	NDVI7_var	0.03	-0.17
NDVI8a_max	0.19	0.44	NDVI8a_max	0.15	0.39	NDVI8a_max	0.05	0.23
NDVI8a_mea	0.33	0.57	NDVI8a_mea	0.23	0.48	NDVI8a_mean	0.08	0.29
NDVI8a_med	0.30	0.55	NDVI8a_med	0.22	0.47	NDVI8a_med	0.08	0.28
NDVI8a_min	0.24	0.49	NDVI8a_min	0.17	0.42	NDVI8a_min	0.05	0.23

NDVI8a_sd	0.15	-0.38	NDVI8a_sd	0.10	-0.31	NDVI8a_sd	0.03	-0.16
NDVI8a_var	0.09	-0.30	NDVI8a_var	0.08	-0.27	NDVI8a_var	0.03	-0.16
NDWI_max	0.19	-0.44	NDWI_max	0.13	-0.35	NDWI_max	0.03	-0.18
NDWI_mean	0.32	-0.57	NDWI_mean	0.21	-0.46	NDWI_mean	0.08	-0.28
NDWI_med	0.31	-0.55	NDWI_med	0.20	-0.45	NDWI_med	0.07	-0.27
NDWI_min	0.16	-0.40	NDWI_min	0.13	-0.36	NDWI_min	0.06	-0.24
NDWI_sd	0.05	-0.23	NDWI_sd	0.03	-0.16	NDWI_sd	0.00	-0.03
NDWI_var	0.05	-0.22	NDWI_var	0.03	-0.18	NDWI_var	0.00	-0.06
NLVI_max	0.01	0.08	NLVI_max	0.02	0.13	NLVI_max	0.01	0.09
NLVI_mean	0.23	0.48	NLVI_mean	0.19	0.43	NLVI_mean	0.08	0.29
NLVI_med	0.34	0.58	NLVI_med	0.25	0.50	NLVI_med	0.11	0.33
NLVI_min	0.22	0.47	NLVI_min	0.15	0.39	NLVI_min	0.06	0.24
NLVI_sd	0.00	-0.01	NLVI_sd	0.00	0.06	NLVI_sd	0.00	0.04
NLVI_var	0.00	-0.04	NLVI_var	0.00	0.01	NLVI_var	0.00	0.00
PSRI_max	0.16	-0.40	PSRI_max	0.10	-0.32	PSRI_max	0.03	-0.17
PSRI_mean	0.12	-0.35	PSRI_mean	0.10	-0.32	PSRI_mean	0.03	-0.16
PSRI_med	0.07	-0.26	PSRI_med	0.06	-0.25	PSRI_med	0.01	-0.12
PSRI_min	0.06	-0.24	PSRI_min	0.06	-0.24	PSRI_min	0.01	-0.12
PSRI_sd	0.08	-0.28	PSRI_sd	0.04	-0.20	PSRI_sd	0.01	-0.10
PSRI_var	0.07	-0.26	PSRI_var	0.04	-0.20	PSRI_var	0.01	-0.12
S2REP_max	0.00	-0.04	S2REP_max	0.00	-0.03	RVI_max	0.00	0.04
S2REP_mean	0.01	0.10	S2REP_mean	0.00	0.05	RVI_mean	0.01	0.12
S2REP_med	0.07	0.27	S2REP_med	0.02	0.15	RVI_med	0.01	0.08
S2REP_min	0.00	0.05	S2REP_min	0.00	0.04	RVI_min	0.02	0.12
S2REP_sd	0.00	-0.06	S2REP_sd	0.00	-0.05	RVI_sd	0.02	-0.12
S2REP_var	0.00	-0.02	S2REP_var	0.00	-0.02	RVI_var	0.01	-0.10
SAVI_max	0.20	0.45	SAVI_max	0.15	0.39	S2REP_max	0.00	-0.01
SAVI_mean	0.33	0.57	SAVI_mean	0.22	0.47	S2REP_mean	0.00	0.03
SAVI_med	0.30	0.55	SAVI_med	0.20	0.45	S2REP_med	0.01	0.09
SAVI_min	0.25	0.50	SAVI_min	0.16	0.40	S2REP_min	0.00	0.01
SAVI_sd	0.14	-0.38	SAVI_sd	0.09	-0.30	S2REP_sd	0.00	-0.02
SAVI_var	0.10	-0.31	SAVI_var	0.07	-0.27	S2REP_var	0.00	-0.01
TCB_max	0.01	-0.09	TCB_max	0.05	-0.22	SAVI_max	0.05	0.23
TCB_mean	0.01	-0.09	TCB_mean	0.05	-0.23	SAVI_mean	0.07	0.27
TCB_med	0.01	-0.11	TCB_med	0.06	-0.25	SAVI_med	0.07	0.27

TCB_min	0.00	0.00	TCB_min	0.02	-0.13	SAVI_min	0.05	0.22
TCB_sd	0.03	-0.16	TCB_sd	0.02	-0.14	SAVI_sd	0.02	-0.15
TCB_var	0.03	-0.18	TCB_var	0.03	-0.18	SAVI_var	0.02	-0.15
TCW_max	0.01	0.08	TCW_max	0.01	0.11	TBC_max	0.12	-0.35
TCW_mean	0.10	0.31	TCW_mean	0.09	0.30	TBC_mean	0.14	-0.38
TCW_med	0.10	0.32	TCW_med	0.09	0.31	TBC_med	0.15	-0.39
TCW_min	0.15	0.39	TCW_min	0.12	0.35	TBC_min	0.05	-0.22
TCW_sd	0.14	-0.38	TCW_sd	0.09	-0.30	TBC_sd	0.02	-0.16
TCW_var	0.08	-0.29	TCW_var	0.07	-0.26	TBC_var	0.03	-0.19
PSRI_max	0.16	-0.40	PSRI_max	0.10	-0.32	TCW_max	0.05	0.21
PSRI_mean	0.12	-0.35	PSRI_mean	0.10	-0.32	TCW_mean	0.13	0.36
PSRI_med	0.07	-0.26	PSRI_med	0.06	-0.25	TCW_med	0.13	0.36
PSRI_min	0.06	-0.24	PSRI_min	0.06	-0.24	TCW_min	0.14	0.38
PSRI_sd	0.08	-0.28	PSRI_sd	0.04	-0.20	TCW_sd	0.06	-0.25
PSRI_var	0.07	-0.26	PSRI_var	0.04	-0.20	TCW_var	0.06	-0.25
VH146_max	0.00	0.01	VH146_max	0.00	0.01	VH146_max	0.01	0.11
VH146_mean	0.00	0.01	VH146_mean	0.00	0.01	VH146_mean	0.02	0.12
VH146_med	0.00	0.01	VH146_med	0.00	0.01	VH146_med	0.02	0.12
VH146_min	0.00	0.02	VH146_min	0.00	0.02	VH146_min	0.02	0.13
VH146_sd	0.00	0.03	VH146_sd	0.00	0.03	VH146_sd	0.00	0.05
VH146_var	0.00	0.02	VH146_var	0.00	0.02	VH146_var	0.00	0.04
VH22_max	0.00	0.02	VH22_max	0.00	0.02	VH22_max	0.03	0.18
VH22_mean	0.00	0.02	VH22_mean	0.00	0.02	VH22_mean	0.04	0.19
VH22_med	0.00	0.02	VH22_med	0.00	0.02	VH22_med	0.04	0.19
VH22_min	0.00	0.02	VH22_min	0.00	0.02	VH22_min	0.04	0.19
VH22_sd	0.00	0.03	VH22_sd	0.00	0.03	VH22_sd	0.01	0.10
VH22_var	0.00	0.01	VH22_var	0.00	0.01	VH22_var	0.00	0.07
VH44_max	0.00	0.01	VH44_max	0.00	0.01	VH44_max	0.02	0.13
VH44_mean	0.00	0.01	VH44_mean	0.00	0.01	VH44_mean	0.02	0.15
VH44_med	0.00	0.01	VH44_med	0.00	0.01	VH44_med	0.02	0.15
VH44_min	0.00	0.01	VH44_min	0.00	0.01	VH44_min	0.03	0.16
VH44_sd	0.00	0.01	VH44_sd	0.00	0.01	VH44_sd	0.00	0.05
VH44_var	0.00	0.01	VH44_var	0.00	0.01	VH44_var	0.00	0.04
VH95_max	0.00	0.01	VH95_max	0.00	0.01	VH95_max	0.01	0.11
VH95_mean	0.00	0.00	VH95_mean	0.00	0.00	VH95_mean	0.02	0.13

VH95_med	0.00	0.00	VH95_med	0.00	0.00	VH95_med	0.02	0.13
VH95_min	0.00	0.01	VH95_min	0.00	0.01	VH95_min	0.02	0.14
VH95_sd	0.00	0.04	VH95_sd	0.00	0.04	VH95_sd	0.00	0.05
VH95_var	0.00	0.03	VH95_var	0.00	0.03	VH95_var	0.00	0.03
VV146_max	0.00	0.06	VV146_max	0.00	0.06	VV146_max	0.01	0.11
VV146_mean	0.00	0.02	VV146_mean	0.00	0.02	VV146_mean	0.01	0.12
VV146_med	0.00	0.07	VV146_med	0.00	0.07	VV146_med	0.01	0.12
VV146_min	0.00	0.01	VV146_min	0.00	0.01	VV146_min	0.02	0.12
VV146_sd	0.00	0.00	VV146_sd	0.00	0.00	VV146_sd	0.00	0.05
VV146_var	0.00	0.01	VV146_var	0.00	0.01	VV146_var	0.00	0.03
VV22_max	0.00	0.07	VV22_max	0.00	0.07	VV22_max	0.03	0.17
VV22_mean	0.00	0.01	VV22_mean	0.00	0.01	VV22_mean	0.04	0.19
VV22_med	0.00	0.01	VV22_med	0.00	0.01	VV22_med	0.04	0.19
VV22_min	0.00	0.01	VV22_min	0.00	0.01	VV22_min	0.04	0.19
VV22_sd	0.00	0.00	VV22_sd	0.00	0.00	VV22_sd	0.01	0.11
VV22_var	0.00	0.02	VV22_var	0.00	0.02	VV22_var	0.00	0.05
VV44_max	0.00	0.03	VV44_max	0.00	0.03	VV44_max	0.01	0.12
VV44_mean	0.00	0.03	VV44_mean	0.00	0.03	VV44_mean	0.02	0.14
VV44_med	0.00	0.01	VV44_med	0.00	0.01	VV44_med	0.02	0.14
VV44_min	0.00	0.02	VV44_min	0.00	0.02	VV44_min	0.02	0.15
VV44_sd	0.00	0.02	VV44_sd	0.00	0.02	VV44_sd	0.00	0.05
VV44_var	0.00	0.01	VV44_var	0.00	0.01	VV44_var	0.00	0.04
VV95_max	0.00	0.01	VV95_max	0.00	0.01	VV95_max	0.01	0.09
VV95_mean	0.00	0.00	VV95_mean	0.00	0.00	VV95_mean	0.01	0.12
VV95_med	0.00	0.00	VV95_med	0.00	0.00	VV95_med	0.01	0.12
VV95_min	0.00	0.00	VV95_min	0.00	0.00	VV95_min	0.02	0.13
VV95_sd	0.00	0.03	VV95_sd	0.00	0.03	VV95_sd	0.00	0.04
VV95_var	0.00	0.03	VV95_var	0.00	0.03	VV95_var	0.00	0.02
GLCM_VH146_con	0.00	0.00	GLCM_VH146_con	0.00	0.00	GLCM_VH146_con	0.00	0.02
GLCM_VH146_cor	0.00	-0.02	GLCM_VH146_cor	0.00	0.04	GLCM_VH146_cor	0.00	0.00
GLCM_VH146_dis	0.00	0.01	GLCM_VH146_dis	0.00	0.00	GLCM_VH146_dis	0.00	0.06
GLCM_VH146_eng	0.00	-0.01	GLCM_VH146_eng	0.00	0.02	GLCM_VH146_eng	0.02	-0.13
GLCM_VH146_ent	0.00	0.01	GLCM_VH146_ent	0.00	0.01	GLCM_VH146_ent	0.02	0.13
GLCM_VH146_homo	0.00	0.00	GLCM_VH146_homo	0.00	0.00	GLCM_VH146_homo	0.01	-0.10
GLCM_VH146_mean	0.00	0.01	GLCM_VH146_mean	0.00	0.01	GLCM_VH146_mean	0.03	0.16

GLCM_VH146_var	0.00	0.01	GLCM_VH146_var	0.00	0.00	GLCM_VH146_sd	0.00	0.06
GLCM_VH146_sec	0.00	0.01	GLCM_VH146_sec	0.00	0.00	GLCM_VH146_sec	0.02	-0.13
GLCM_VH22_con	0.00	0.00	GLCM_VH22_con	0.00	0.02	GLCM_VH22_con	0.00	0.01
GLCM_VH22_cor	0.00	-0.03	GLCM_VH22_cor	0.00	0.02	GLCM_VH22_cor	0.00	-0.02
GLCM_VH22_dis	0.00	0.00	GLCM_VH22_dis	0.00	0.03	GLCM_VH22_dis	0.00	0.05
GLCM_VH22_eng	0.00	-0.01	GLCM_VH22_eng	0.00	-0.02	GLCM_VH22_eng	0.02	-0.14
GLCM_VH22_ent	0.00	0.01	GLCM_VH22_ent	0.00	0.03	GLCM_VH22_ent	0.02	0.14
GLCM_VH22_homo	0.00	0.01	GLCM_VH22_homo	0.00	0.03	GLCM_VH22_homo	0.01	-0.11
GLCM_VH22_mean	0.00	0.01	GLCM_VH22_mean	0.00	0.02	GLCM_VH22_mean	0.05	0.22
GLCM_VH22_var	0.00	0.01	GLCM_VH22_var	0.00	0.01	GLCM_VH22_sd	0.00	0.06
GLCM_VH22_sec	0.00	0.01	GLCM_VH22_sec	0.00	0.03	GLCM_VH22_sec	0.02	-0.14
GLCM_VH44_con	0.00	0.01	GLCM_VH44_con	0.00	0.02	GLCM_VH44_con	0.00	0.04
GLCM_VH44_cor	0.00	-0.01	GLCM_VH44_cor	0.00	0.02	GLCM_VH44_cor	0.00	0.00
GLCM_VH44_dis	0.00	0.00	GLCM_VH44_diss	0.00	0.01	GLCM_VH44_dis	0.01	0.07
GLCM_VH44_eng	0.00	0.02	GLCM_VH44_eng	0.00	-0.01	GLCM_VH44_eng	0.03	-0.17
GLCM_VH44_ent	0.00	0.01	GLCM_VH44_ent	0.00	0.03	GLCM_VH44_ent	0.03	0.17
GLCM_VH44_homo	0.00	0.00	GLCM_VH44_homo	0.00	0.00	GLCM_VH44_homo	0.02	-0.12
GLCM_VH44_mean	0.00	0.00	GLCM_VH44_mean	0.00	0.02	GLCM_VH44_mean	0.04	0.21
GLCM_VH44_var	0.00	0.00	GLCM_VH44_var	0.00	0.02	GLCM_VH44_sd	0.01	0.08
GLCM_VH44_sec	0.00	0.00	GLCM_VH44_sec	0.00	0.01	GLCM_VH44_sec	0.03	-0.17
GLCM_VH95_con	0.00	0.00	GLCM_VH95_con	0.00	0.03	GLCM_VH95_con	0.00	0.00
GLCM_VH95_cor	0.00	0.00	GLCM_VH95_cor	0.00	0.01	GLCM_VH95_cor	0.00	-0.01
GLCM_VH95_dis	0.00	0.00	GLCM_VH95_dis	0.00	0.04	GLCM_VH95_dis	0.00	0.02
GLCM_VH95_eng	0.00	-0.02	GLCM_VH95_eng	0.00	-0.02	GLCM_VH95_eng	0.01	-0.11
GLCM_VH95_ent	0.00	0.00	GLCM_VH95_ent	0.00	0.03	GLCM_VH95_ent	0.01	0.11
GLCM_VH95_homo	0.00	0.00	GLCM_VH95_homo	0.00	0.04	GLCM_VH95_homo	0.01	-0.08
GLCM_VH95_mean	0.00	0.03	GLCM_VH95_mean	0.00	0.00	GLCM_VH95_mean	0.02	0.15
GLCM_VH95_var	0.00	0.02	GLCM_VH95_var	0.00	0.01	GLCM_VH95_sd	0.00	0.02
GLCM_VH95_sec	0.00	0.00	GLCM_VH95_sec	0.00	0.03	GLCM_VH95_sec	0.01	-0.11
GLCM_VV146_con	0.00	0.00	GLCM_VV146_con	0.00	0.01	GLCM_VV146_con	0.00	0.02
GLCM_VV146_cor	0.00	-0.01	GLCM_VV146_cor	0.00	0.03	GLCM_VV146_cor	0.00	-0.02
GLCM_VV146_dis	0.00	0.00	GLCM_VV146_dis	0.00	0.01	GLCM_VV146_dis	0.00	0.05
GLCM_VV146_eng	0.00	0.02	GLCM_VV146_eng	0.00	-0.01	GLCM_VV146_eng	0.01	-0.10
GLCM_VV146_ent	0.00	0.01	GLCM_VV146_ent	0.00	0.00	GLCM_VV146_ent	0.01	0.10
GLCM_VV146_homo	0.00	0.00	GLCM_VV146_homo	0.00	0.00	GLCM_VV146_homo	0.01	-0.08

GLCM_VV146_mean	0.00	0.01	GLCM_VV146_mean	0.00	0.01	GLCM_VV146_mean	0.03	0.17
GLCM_VV146_var	0.00	0.01	GLCM_VV146_var	0.00	0.00	GLCM_VV146_sd	0.00	0.05
GLCM_VV146_sec	0.00	0.01	GLCM_VV146_sec	0.00	0.01	GLCM_VV146_sec	0.01	-0.11
GLCM_VV22_con	0.00	0.00	GLCM_VV22_con	0.00	0.01	GLCM_VV22_con	0.00	0.00
GLCM_VV22_cor	0.00	-0.01	GLCM_VV22_cor	0.00	-0.01	GLCM_VV22_cor	0.00	-0.01
GLCM_VV22_dis	0.00	0.01	GLCM_VV22_dis	0.00	0.02	GLCM_VV22_dis	0.00	0.03
GLCM_VV22_eng	0.00	0.01	GLCM_VV22_eng	0.00	-0.01	GLCM_VV22_eng	0.01	-0.12
GLCM_VV22_ent	0.00	0.01	GLCM_VV22_ent	0.00	0.03	GLCM_VV22_ent	0.01	0.11
GLCM_VV22_homo	0.00	0.01	GLCM_VV22_homo	0.00	0.00	GLCM_VV22_homo	0.01	-0.08
GLCM_VV22_mean	0.00	0.00	GLCM_VV22_mean	0.00	0.02	GLCM_VV22_mean	0.06	0.24
GLCM_VV22_var	0.00	0.00	GLCM_VV22_var	0.00	0.01	GLCM_VV22_sd	0.00	0.03
GLCM_VV22_sec	0.00	0.01	GLCM_VV22_sec	0.00	0.03	GLCM_VV22_sec	0.02	-0.12
GLCM_VV44_con	0.00	0.01	GLCM_VV44_con	0.00	0.02	GLCM_VV44_con	0.00	0.02
GLCM_VV44_cor	0.00	-0.02	GLCM_VV44_cor	0.00	-0.03	GLCM_VV44_cor	0.00	-0.01
GLCM_VV44_dis	0.00	0.01	GLCM_VV44_diss	0.00	0.02	GLCM_VV44_dis	0.00	0.06
GLCM_VV44_eng	0.00	0.01	GLCM_VV44_eng	0.00	-0.02	GLCM_VV44_eng	0.02	-0.14
GLCM_VV44_ent	0.00	0.01	GLCM_VV44_ent	0.00	0.03	GLCM_VV44_ent	0.02	0.13
GLCM_VV44_homo	0.00	0.00	GLCM_VV44_homo	0.00	0.00	GLCM_VV44_homo	0.01	-0.10
GLCM_VV44_mean	0.00	0.01	GLCM_VV44_mean	0.00	0.02	GLCM_VV44_mean	0.04	0.20
GLCM_VV44_var	0.00	0.01	GLCM_VV44_var	0.00	0.02	GLCM_VV44_sd	0.00	0.06
GLCM_VV44_sec	0.00	0.01	GLCM_VV44_sec	0.00	0.02	GLCM_VV44_sec	0.02	-0.14
GLCM_VV95_con	0.00	0.00	GLCM_VV95_con	0.00	0.02	GLCM_VV95_con	0.00	0.00
GLCM_VV95_cor	0.00	0.00	GLCM_VV95_cor	0.00	0.00	GLCM_VV95_cor	0.00	-0.01
GLCM_VV95_dis	0.00	0.00	GLCM_VV95_dis	0.00	0.02	GLCM_VV95_dis	0.00	0.01
GLCM_VV95_eng	0.00	0.01	GLCM_VV95_eng	0.00	-0.01	GLCM_VV95_eng	0.01	-0.09
GLCM_VV95_ent	0.00	0.01	GLCM_VV95_ent	0.00	0.02	GLCM_VV95_ent	0.01	0.09
GLCM_VV95_homo	0.00	0.00	GLCM_VV95_homo	0.00	0.02	GLCM_VV95_homo	0.00	-0.06
GLCM_VV95_mean	0.00	0.01	GLCM_VV95_mean	0.00	0.01	GLCM_VV95_mean	0.02	0.15
GLCM_VV95_var	0.00	0.01	GLCM_VV95_var	0.00	0.01	GLCM_VV95_sd	0.00	0.02
GLCM_VV95_sec	0.00	0.01	GLCM_VV95_sec	0.00	0.02	GLCM_VV95_sec	0.01	-0.09

Table 34: R^2 and R values calculated with the GEDI vegetation parameters and the Sentinel variables. The GEDI plots are utilized to extract the values of the Sentinel variables, as well as the values of the ALS mean, ALS max and ALS FHD dataset. The correlation between the ALS values and the Sentinel variables confined to the GEDI plots is also calculated.

Parameter	GEDI		ALS		Parameter	GEDI		ALS		Parameter	GEDI		ALS		Parameter	GEDI	
	RH50		ALS mean			RH100		ALS max			FHD		ALS FHD			AGBD	
	R^2	R	R^2	R		R^2	R	R^2	R		R^2	R	R^2	R		R^2	R
B2_max	0.03	-0.17	0.07	-0.27	B2_max	0.02	-0.14	0.04	-0.20	B2_max	0.02	-0.15	0.05	-0.21	B2_max	0.02	-0.15
B2_mean	0.07	-0.26	0.23	-0.48	B2_mean	0.05	-0.23	0.16	-0.40	B2_mean	0.06	-0.24	0.16	-0.40	B2_mean	0.06	-0.24
B2_med	0.06	-0.25	0.24	-0.49	B2_med	0.05	-0.22	0.16	-0.40	B2_med	0.05	-0.23	0.17	-0.41	B2_med	0.05	-0.23
B2_min	0.04	-0.20	0.15	-0.38	B2_min	0.04	-0.20	0.13	-0.36	B2_min	0.05	-0.23	0.07	-0.26	B2_min	0.04	-0.20
B2_sd	0.02	-0.15	0.05	-0.23	B2_sd	0.01	-0.11	0.02	-0.14	B2_sd	0.01	-0.11	0.04	-0.20	B2_sd	0.02	-0.13
B2_var	0.02	-0.14	0.04	-0.20	B2_var	0.01	-0.12	0.02	-0.14	B2_var	0.02	-0.13	0.03	-0.17	B2_var	0.02	-0.13
B3_max	0.04	-0.20	0.11	-0.33	B3_max	0.04	-0.19	0.07	-0.27	B3_max	0.04	-0.21	0.07	-0.27	B3_max	0.04	-0.19
B3_mean	0.07	-0.26	0.26	-0.51	B3_mean	0.07	-0.26	0.19	-0.44	B3_mean	0.09	-0.30	0.18	-0.42	B3_mean	0.06	-0.25
B3_med	0.08	-0.28	0.29	-0.54	B3_med	0.07	-0.27	0.20	-0.45	B3_med	0.09	-0.30	0.19	-0.44	B3_med	0.07	-0.26
B3_min	0.02	-0.15	0.08	-0.29	B3_min	0.04	-0.20	0.11	-0.32	B3_min	0.06	-0.24	0.03	-0.18	B3_min	0.03	-0.16
B3_sd	0.02	-0.15	0.06	-0.24	B3_sd	0.01	-0.11	0.02	-0.15	B3_sd	0.02	-0.12	0.06	-0.25	B3_sd	0.02	-0.13
B3_var	0.02	-0.15	0.05	-0.22	B3_var	0.01	-0.12	0.02	-0.15	B3_var	0.02	-0.13	0.05	-0.21	B3_var	0.02	-0.14
B4_max	0.09	-0.30	0.19	-0.44	B4_max	0.05	-0.23	0.09	-0.30	B4_max	0.06	-0.25	0.07	-0.27	B4_max	0.07	-0.26
B4_mean	0.11	-0.32	0.32	-0.56	B4_mean	0.07	-0.26	0.18	-0.42	B4_mean	0.08	-0.28	0.15	-0.38	B4_mean	0.08	-0.28
B4_med	0.09	-0.30	0.30	-0.55	B4_med	0.06	-0.24	0.18	-0.42	B4_med	0.06	-0.25	0.16	-0.39	B4_med	0.07	-0.26
B4_min	0.05	-0.22	0.14	-0.37	B4_min	0.05	-0.22	0.12	-0.34	B4_min	0.06	-0.24	0.04	-0.21	B4_min	0.04	-0.21
B4_sd	0.08	-0.28	0.16	-0.39	B4_sd	0.03	-0.19	0.05	-0.23	B4_sd	0.04	-0.21	0.07	-0.26	B4_sd	0.05	-0.23
B4_var	0.04	-0.21	0.09	-0.30	B4_var	0.03	-0.17	0.05	-0.21	B4_var	0.03	-0.18	0.06	-0.24	B4_var	0.04	-0.19
B5_max	0.04	-0.21	0.12	-0.34	B5_max	0.04	-0.21	0.08	-0.29	B5_max	0.06	-0.25	0.08	-0.28	B5_max	0.04	-0.21
B5_mean	0.06	-0.25	0.24	-0.49	B5_mean	0.07	-0.27	0.18	-0.43	B5_mean	0.11	-0.33	0.15	-0.39	B5_mean	0.06	-0.25
B5_med	0.08	-0.28	0.29	-0.54	B5_med	0.08	-0.28	0.20	-0.45	B5_med	0.11	-0.33	0.17	-0.41	B5_med	0.07	-0.27
B5_min	0.02	-0.14	0.05	-0.23	B5_min	0.04	-0.19	0.08	-0.28	B5_min	0.06	-0.25	0.02	-0.13	B5_min	0.02	-0.15
B5_sd	0.01	-0.10	0.04	-0.19	B5_sd	0.00	-0.07	0.01	-0.09	B5_sd	0.01	-0.08	0.05	-0.23	B5_sd	0.01	-0.09
B5_var	0.01	-0.12	0.04	-0.20	B5_var	0.01	-0.08	0.01	-0.11	B5_var	0.01	-0.09	0.05	-0.23	B5_var	0.01	-0.11
B6_max	0.03	0.18	0.04	0.20	B6_max	0.00	0.00	0.00	-0.03	B6_max	0.01	-0.08	0.02	-0.13	B6_max	0.01	0.09
B6_mean	0.02	0.13	0.01	0.10	B6_mean	0.00	-0.06	0.01	-0.12	B6_mean	0.02	-0.13	0.03	-0.16	B6_mean	0.00	0.05
B6_med	0.01	0.12	0.01	0.07	B6_med	0.00	-0.07	0.02	-0.13	B6_med	0.02	-0.13	0.03	-0.19	B6_med	0.00	0.03
B6_min	0.00	0.06	0.01	0.07	B6_min	0.01	-0.08	0.01	-0.11	B6_min	0.02	-0.13	0.00	-0.05	B6_min	0.00	0.00
B6_sd	0.01	0.10	0.01	0.09	B6_sd	0.01	0.08	0.01	0.08	B6_sd	0.00	0.03	0.02	-0.13	B6_sd	0.01	0.08
B6_var	0.01	0.07	0.00	0.06	B6_var	0.00	0.06	0.00	0.05	B6_var	0.00	0.02	0.02	-0.14	B6_var	0.00	0.06
B7_max	0.04	0.21	0.06	0.24	B7_max	0.00	0.01	0.00	-0.01	B7_max	0.00	-0.06	0.01	-0.11	B7_max	0.01	0.11
B7_mean	0.03	0.18	0.03	0.18	B7_mean	0.00	-0.03	0.00	-0.07	B7_mean	0.01	-0.09	0.02	-0.13	B7_mean	0.01	0.08
B7_med	0.03	0.17	0.03	0.17	B7_med	0.00	-0.03	0.01	-0.07	B7_med	0.01	-0.09	0.02	-0.15	B7_med	0.01	0.08
B7_min	0.01	0.10	0.01	0.12	B7_min	0.00	-0.06	0.01	-0.09	B7_min	0.01	-0.11	0.00	-0.04	B7_min	0.00	0.03
B7_sd	0.01	0.09	0.01	0.09	B7_sd	0.01	0.07	0.01	0.07	B7_sd	0.00	0.03	0.01	-0.12	B7_sd	0.01	0.07
B7_var	0.01	0.07	0.01	0.07	B7_var	0.00	0.05	0.00	0.05	B7_var	0.00	0.02	0.01	-0.12	B7_var	0.00	0.06

B8_max	0.03	0.17	0.03	0.17	B8_max	0.00	-0.02	0.00	-0.05	B8_max	0.01	-0.09	0.02	-0.14	B8_max	0.01	0.07
B8_mean	0.02	0.15	0.01	0.12	B8_mean	0.00	-0.06	0.01	-0.11	B8_mean	0.01	-0.12	0.02	-0.15	B8_mean	0.00	0.05
B8_med	0.02	0.15	0.01	0.11	B8_med	0.00	-0.06	0.01	-0.12	B8_med	0.01	-0.12	0.03	-0.17	B8_med	0.00	0.05
B8_min	0.01	0.08	0.01	0.10	B8_min	0.01	-0.08	0.01	-0.10	B8_min	0.01	-0.12	0.00	-0.04	B8_min	0.00	0.01
B8_sd	0.00	0.07	0.00	0.03	B8_sd	0.00	0.06	0.00	0.04	B8_sd	0.00	0.01	0.02	-0.15	B8_sd	0.00	0.05
B8_var	0.00	0.05	0.00	0.01	B8_var	0.00	0.04	0.00	0.02	B8_var	0.00	-0.01	0.03	-0.16	B8_var	0.00	0.04
B8a_max	0.04	0.19	0.04	0.21	B8a_max	0.00	0.00	0.00	-0.03	B8a_max	0.00	-0.07	0.01	-0.12	B8a_max	0.01	0.10
B8a_mean	0.03	0.16	0.02	0.15	B8a_mean	0.00	-0.04	0.01	-0.08	B8a_mean	0.01	-0.10	0.02	-0.14	B8a_mean	0.00	0.07
B8a_med	0.02	0.15	0.02	0.14	B8a_med	0.00	-0.04	0.01	-0.09	B8a_med	0.01	-0.11	0.02	-0.16	B8a_med	0.00	0.06
B8a_min	0.01	0.08	0.01	0.11	B8a_min	0.00	-0.07	0.01	-0.09	B8a_min	0.01	-0.12	0.00	-0.04	B8a_min	0.00	0.02
B8a_sd	0.01	0.08	0.00	0.06	B8a_sd	0.00	0.07	0.00	0.06	B8a_sd	0.00	0.03	0.01	-0.12	B8a_sd	0.00	0.06
B8a_var	0.00	0.06	0.00	0.05	B8a_var	0.00	0.05	0.00	0.04	B8a_var	0.00	0.02	0.01	-0.12	B8a_var	0.00	0.05
B11_max	0.03	-0.16	0.11	-0.33	B11_max	0.02	-0.16	0.06	-0.25	B11_max	0.06	-0.24	0.07	-0.26	B11_max	0.02	-0.15
B11_mean	0.02	-0.12	0.09	-0.30	B11_mean	0.02	-0.15	0.07	-0.27	B11_mean	0.05	-0.23	0.07	-0.27	B11_mean	0.01	-0.12
B11_med	0.02	-0.13	0.11	-0.33	B11_med	0.02	-0.15	0.08	-0.28	B11_med	0.05	-0.23	0.09	-0.30	B11_med	0.02	-0.13
B11_min	0.00	-0.07	0.01	-0.11	B11_min	0.01	-0.12	0.03	-0.17	B11_min	0.04	-0.19	0.01	-0.08	B11_min	0.01	-0.08
B11_sd	0.02	-0.14	0.09	-0.29	B11_sd	0.00	-0.05	0.01	-0.10	B11_sd	0.00	-0.06	0.05	-0.22	B11_sd	0.01	-0.10
B11_var	0.02	-0.13	0.08	-0.29	B11_var	0.00	-0.06	0.02	-0.12	B11_var	0.00	-0.07	0.07	-0.26	B11_var	0.01	-0.10
B12_max	0.07	-0.26	0.21	-0.46	B12_max	0.04	-0.20	0.10	-0.31	B12_max	0.07	-0.26	0.09	-0.30	B12_max	0.05	-0.22
B12_mean	0.05	-0.23	0.20	-0.45	B12_mean	0.04	-0.19	0.12	-0.34	B12_mean	0.06	-0.25	0.10	-0.31	B12_mean	0.04	-0.20
B12_med	0.05	-0.23	0.22	-0.47	B12_med	0.04	-0.19	0.12	-0.35	B12_med	0.06	-0.25	0.11	-0.33	B12_med	0.04	-0.20
B12_min	0.02	-0.14	0.05	-0.22	B12_min	0.02	-0.15	0.05	-0.23	B12_min	0.05	-0.22	0.02	-0.13	B12_min	0.02	-0.14
B12_sd	0.05	-0.23	0.18	-0.42	B12_sd	0.02	-0.12	0.04	-0.21	B12_sd	0.02	-0.14	0.08	-0.28	B12_sd	0.03	-0.18
B12_var	0.04	-0.19	0.14	-0.38	B12_var	0.01	-0.12	0.05	-0.22	B12_var	0.02	-0.13	0.10	-0.32	B12_var	0.02	-0.16
DVI_max	0.05	0.22	0.06	0.06	DVI_max	0.00	0.01	0.00	0.03	DVI_max	0.00	-0.05	0.01	-0.12	DVI_max	0.01	0.11
DVI_mean	0.05	0.22	0.05	0.24	DVI_mean	0.00	-0.01	0.00	0.01	DVI_mean	0.00	-0.06	0.00	-0.08	DVI_mean	0.01	0.11
DVI_med	0.05	0.22	0.06	0.23	DVI_med	0.00	0.00	0.00	-0.02	DVI_med	0.00	-0.05	0.01	-0.07	DVI_med	0.01	0.11
DVI_min	0.02	0.13	0.03	0.24	DVI_min	0.00	-0.04	0.00	-0.02	DVI_min	0.01	-0.07	0.00	-0.08	DVI_min	0.00	0.05
DVI_sd	0.01	0.09	0.01	0.17	DVI_sd	0.00	0.06	0.00	-0.05	DVI_sd	0.00	-0.01	0.01	-0.01	DVI_sd	0.00	0.07
DVI_var	0.01	0.07	0.00	0.08	DVI_var	0.00	0.04	0.00	0.06	DVI_var	0.00	-0.02	0.02	-0.12	DVI_var	0.00	0.05
EVI_max	0.09	0.30	0.19	0.44	EVI_max	0.04	0.20	0.08	0.28	EVI_max	0.03	0.19	0.01	0.10	EVI_max	0.06	0.24
EVI_mean	0.16	0.40	0.36	0.60	EVI_mean	0.05	0.21	0.09	0.30	EVI_mean	0.04	0.20	0.04	0.20	EVI_mean	0.09	0.30
EVI_med	0.16	0.40	0.36	0.60	EVI_med	0.04	0.21	0.09	0.31	EVI_med	0.04	0.19	0.05	0.22	EVI_med	0.09	0.29
EVI_min	0.12	0.35	0.23	0.48	EVI_min	0.03	0.16	0.04	0.21	EVI_min	0.03	0.17	0.02	0.15	EVI_min	0.06	0.25
EVI_sd	0.01	-0.09	0.01	-0.10	EVI_sd	0.00	0.02	0.00	0.04	EVI_sd	0.00	-0.01	0.00	-0.07	EVI_sd	0.00	-0.05
EVI_var	0.06	-0.24	0.13	-0.36	EVI_var	0.01	-0.11	0.03	-0.17	EVI_var	0.02	-0.14	0.08	-0.27	EVI_var	0.03	-0.18
EVIRE1_max	0.02	0.15	0.04	0.20	EVIRE1_max	0.02	0.15	0.03	0.17	EVIRE1_max	0.01	0.12	0.00	-0.01	EVIRE1_max	0.02	0.13
EVIRE1_mean	0.14	0.37	0.31	0.55	EVIRE1_mean	0.05	0.22	0.09	0.29	EVIRE1_mean	0.04	0.20	0.03	0.17	EVIRE1_mean	0.08	0.29
EVIRE1_med	0.15	0.39	0.34	0.58	EVIRE1_med	0.05	0.22	0.09	0.29	EVIRE1_med	0.04	0.19	0.04	0.19	EVIRE1_med	0.09	0.30
EVIRE1_min	0.06	0.25	0.14	0.38	EVIRE1_min	0.01	0.09	0.02	0.15	EVIRE1_min	0.01	0.11	0.02	0.13	EVIRE1_min	0.03	0.17
EVIRE1_sd	0.00	0.04	0.00	0.04	EVIRE1_sd	0.01	0.11	0.01	0.11	EVIRE1_sd	0.01	0.07	0.00	-0.07	EVIRE1_sd	0.00	0.06
EVIRE1_var	0.00	-0.01	0.00	-0.04	EVIRE1_var	0.00	0.06	0.00	0.05	EVIRE1_var	0.00	0.03	0.01	-0.09	EVIRE1_var	0.00	0.01
GNDVI_max	0.06	0.25	0.17	0.41	GNDVI_max	0.04	0.19	0.08	0.29	GNDVI_max	0.03	0.18	0.02	0.14	GNDVI_max	0.04	0.20

L

GNDVI_mean	0.13	0.36	0.32	0.57	GNDVI_mean	0.04	0.21	0.11	0.33	GNDVI_mean	0.04	0.20	0.07	0.27	GNDVI_mean	0.08	0.27
GNDVI_med	0.12	0.35	0.32	0.56	GNDVI_med	0.04	0.20	0.11	0.33	GNDVI_med	0.04	0.19	0.08	0.28	GNDVI_med	0.07	0.27
GNDVI_min	0.09	0.30	0.19	0.44	GNDVI_min	0.02	0.15	0.05	0.22	GNDVI_min	0.02	0.16	0.03	0.18	GNDVI_min	0.05	0.23
GNDVI_sd	0.02	-0.15	0.04	-0.20	GNDVI_sd	0.00	-0.03	0.00	-0.03	GNDVI_sd	0.00	-0.05	0.01	-0.11	GNDVI_sd	0.01	-0.11
GNDVI_var	0.03	-0.16	0.04	-0.21	GNDVI_var	0.00	-0.06	0.00	-0.06	GNDVI_var	0.01	-0.08	0.02	-0.13	GNDVI_var	0.02	-0.13
MSAVI_max	0.09	0.30	0.21	0.46	MSAVI_max	0.04	0.21	0.10	0.32	MSAVI_max	0.04	0.19	0.03	0.18	MSAVI_max	0.06	0.24
MSAVI_mean	0.14	0.37	0.34	0.58	MSAVI_mean	0.05	0.22	0.11	0.34	MSAVI_mean	0.04	0.21	0.08	0.27	MSAVI_mean	0.08	0.29
MSAVI_med	0.12	0.35	0.32	0.57	MSAVI_med	0.04	0.21	0.12	0.34	MSAVI_med	0.04	0.19	0.08	0.29	MSAVI_med	0.07	0.27
MSAVI_min	0.13	0.36	0.25	0.50	MSAVI_min	0.04	0.19	0.07	0.26	MSAVI_min	0.04	0.21	0.04	0.21	MSAVI_min	0.08	0.28
MSAVI_sd	0.09	-0.29	0.14	-0.38	MSAVI_sd	0.02	-0.13	0.02	-0.14	MSAVI_sd	0.03	-0.17	0.03	-0.16	MSAVI_sd	0.05	-0.22
MSAVI_var	0.07	-0.27	0.12	-0.34	MSAVI_var	0.02	-0.15	0.02	-0.15	MSAVI_var	0.03	-0.18	0.03	-0.18	MSAVI_var	0.05	-0.22
MSAVI2_max	0.08	0.28	0.21	0.45	MSAVI2_max	0.04	0.20	0.10	0.32	MSAVI2_max	0.04	0.19	0.04	0.21	MSAVI2_max	0.06	0.24
MSAVI2_mean	0.12	0.35	0.31	0.56	MSAVI2_mean	0.05	0.21	0.12	0.35	MSAVI2_mean	0.04	0.21	0.09	0.31	MSAVI2_mean	0.08	0.28
MSAVI2_med	0.11	0.33	0.30	0.54	MSAVI2_med	0.04	0.20	0.12	0.35	MSAVI2_med	0.04	0.19	0.10	0.31	MSAVI2_med	0.07	0.26
MSAVI2_min	0.06	0.24	0.15	0.38	MSAVI2_min	0.02	0.15	0.06	0.25	MSAVI2_min	0.04	0.19	0.04	0.20	MSAVI2_min	0.04	0.19
MSAVI2_sd	0.04	-0.19	0.08	-0.29	MSAVI2_sd	0.01	-0.11	0.02	-0.15	MSAVI2_sd	0.03	-0.16	0.03	-0.17	MSAVI2_sd	0.02	-0.15
MSAVI2_var	0.03	-0.18	0.07	-0.26	MSAVI2_var	0.01	-0.11	0.02	-0.15	MSAVI2_var	0.03	-0.17	0.03	-0.16	MSAVI2_var	0.02	-0.15
MSI_max	0.08	0.28	0.17	0.42	MSI_max	0.02	0.16	0.06	0.24	MSI_max	0.03	0.16	0.04	0.19	MSI_max	0.05	0.22
MSI_mean	0.13	0.36	0.27	0.52	MSI_mean	0.02	0.15	0.05	0.22	MSI_mean	0.03	0.18	0.03	0.17	MSI_mean	0.06	0.25
MSI_med	0.12	0.35	0.26	0.51	MSI_med	0.02	0.14	0.05	0.22	MSI_med	0.03	0.17	0.03	0.17	MSI_med	0.06	0.25
MSI_min	0.15	0.39	0.28	0.53	MSI_min	0.02	0.13	0.03	0.17	MSI_min	0.04	0.20	0.02	0.14	MSI_min	0.07	0.26
MSI_sd	0.10	-0.32	0.17	-0.41	MSI_sd	0.00	-0.05	0.00	-0.05	MSI_sd	0.02	-0.15	0.00	-0.06	MSI_sd	0.03	-0.18
MSI_var	0.08	-0.29	0.13	-0.37	MSI_var	0.01	-0.08	0.00	-0.07	MSI_var	0.03	-0.17	0.01	-0.12	MSI_var	0.03	-0.18
NDII5_max	0.13	-0.36	0.25	-0.50	NDII5_max	0.01	-0.11	0.03	-0.16	NDII5_max	0.03	-0.17	0.02	-0.14	NDII5_max	0.05	-0.23
NDII5_mean	0.11	-0.32	0.23	-0.48	NDII5_mean	0.01	-0.10	0.03	-0.16	NDII5_mean	0.02	-0.14	0.01	-0.12	NDII5_mean	0.04	-0.20
NDII5_med	0.10	-0.31	0.22	-0.47	NDII5_med	0.01	-0.09	0.03	-0.16	NDII5_med	0.02	-0.13	0.01	-0.12	NDII5_med	0.04	-0.19
NDII5_min	0.07	-0.26	0.14	-0.38	NDII5_min	0.01	-0.10	0.03	-0.16	NDII5_min	0.02	-0.13	0.01	-0.07	NDII5_min	0.03	-0.17
NDII5_sd	0.05	-0.23	0.09	-0.31	NDII5_sd	0.00	-0.05	0.00	-0.04	NDII5_sd	0.01	-0.12	0.02	-0.14	NDII5_sd	0.02	-0.15
NDII5_var	0.04	-0.20	0.08	-0.28	NDII5_var	0.00	-0.05	0.00	-0.06	NDII5_var	0.01	-0.11	0.03	-0.16	NDII5_var	0.02	-0.14
NDII7_max	0.14	-0.38	0.31	-0.55	NDII7_max	0.03	-0.16	0.05	-0.23	NDII7_max	0.04	-0.20	0.04	-0.19	NDII7_max	0.07	-0.27
NDII7_mean	0.12	-0.35	0.28	-0.53	NDII7_mean	0.02	-0.15	0.06	-0.24	NDII7_mean	0.03	-0.17	0.03	-0.18	NDII7_mean	0.06	-0.24
NDII7_med	0.11	-0.33	0.27	-0.52	NDII7_med	0.02	-0.14	0.06	-0.24	NDII7_med	0.03	-0.16	0.03	-0.18	NDII7_med	0.05	-0.23
NDII7_min	0.09	-0.30	0.19	-0.44	NDII7_min	0.02	-0.14	0.05	-0.22	NDII7_min	0.03	-0.17	0.02	-0.13	NDII7_min	0.05	-0.21
NDII7_sd	0.09	-0.31	0.19	-0.44	NDII7_sd	0.02	-0.12	0.02	-0.14	NDII7_sd	0.03	-0.17	0.03	-0.18	NDII7_sd	0.05	-0.22
NDII7_var	0.06	-0.25	0.14	-0.38	NDII7_var	0.01	-0.11	0.02	-0.15	NDII7_var	0.02	-0.16	0.05	-0.21	NDII7_var	0.04	-0.19
NDVI_max	0.09	0.30	0.21	0.46	NDVI_max	0.04	0.21	0.10	0.32	NDVI_max	0.04	0.19	0.03	0.18	NDVI_max	0.06	0.24
NDVI_mean	0.14	0.37	0.34	0.58	NDVI_mean	0.05	0.22	0.11	0.34	NDVI_mean	0.04	0.21	0.08	0.27	NDVI_mean	0.08	0.29
NDVI_med	0.12	0.35	0.32	0.57	NDVI_med	0.04	0.21	0.12	0.34	NDVI_med	0.04	0.19	0.08	0.29	NDVI_med	0.07	0.27
NDVI_min	0.13	0.36	0.25	0.50	NDVI_min	0.04	0.19	0.07	0.26	NDVI_min	0.04	0.21	0.04	0.21	NDVI_min	0.08	0.28
NDVI_sd	0.09	-0.29	0.14	-0.38	NDVI_sd	0.02	-0.13	0.02	-0.14	NDVI_sd	0.03	-0.17	0.03	-0.16	NDVI_sd	0.05	-0.22
NDVI_var	0.07	-0.27	0.12	-0.34	NDVI_var	0.02	-0.15	0.02	-0.15	NDVI_var	0.03	-0.18	0.03	-0.18	NDVI_var	0.05	-0.22
NDVI6_max	0.12	0.34	0.26	0.51	NDVI6_max	0.05	0.21	0.08	0.29	NDVI6_max	0.04	0.20	0.02	0.13	NDVI6_max	0.07	0.26
NDVI6_mean	0.16	0.40	0.37	0.61	NDVI6_mean	0.05	0.23	0.11	0.33	NDVI6_mean	0.05	0.22	0.05	0.23	NDVI6_mean	0.09	0.31

NDVI6_med	0.15	0.39	0.36	0.60	NDVI6_med	0.05	0.22	0.11	0.34	NDVI6_med	0.05	0.22	0.06	0.24	NDVI6_med	0.09	0.30
NDVI6_min	0.15	0.39	0.32	0.56	NDVI6_min	0.05	0.23	0.08	0.29	NDVI6_min	0.06	0.24	0.04	0.20	NDVI6_min	0.10	0.31
NDVI6_sd	0.03	-0.17	0.04	-0.21	NDVI6_sd	0.01	-0.07	0.00	-0.06	NDVI6_sd	0.01	-0.11	0.02	-0.13	NDVI6_sd	0.02	-0.14
NDVI6_var	0.03	-0.17	0.05	-0.22	NDVI6_var	0.01	-0.08	0.01	-0.08	NDVI6_var	0.01	-0.11	0.02	-0.15	NDVI6_var	0.02	-0.14
NDVI7_max	0.09	0.29	0.21	0.46	NDVI7_max	0.05	0.21	0.10	0.32	NDVI7_max	0.04	0.20	0.03	0.17	NDVI7_max	0.06	0.25
NDVI7_mean	0.14	0.37	0.35	0.59	NDVI7_mean	0.05	0.23	0.13	0.35	NDVI7_mean	0.05	0.22	0.08	0.28	NDVI7_mean	0.09	0.30
NDVI7_med	0.12	0.35	0.33	0.58	NDVI7_med	0.05	0.22	0.13	0.36	NDVI7_med	0.04	0.21	0.09	0.30	NDVI7_med	0.08	0.28
NDVI7_min	0.13	0.36	0.27	0.52	NDVI7_min	0.04	0.21	0.08	0.28	NDVI7_min	0.05	0.23	0.05	0.23	NDVI7_min	0.08	0.29
NDVI7_sd	0.09	-0.30	0.17	-0.41	NDVI7_sd	0.02	-0.15	0.03	-0.17	NDVI7_sd	0.03	-0.18	0.04	-0.20	NDVI7_sd	0.05	-0.23
NDVI7_var	0.07	-0.27	0.13	-0.36	NDVI7_var	0.03	-0.16	0.03	-0.18	NDVI7_var	0.04	-0.19	0.05	-0.23	NDVI7_var	0.05	-0.22
NDVI8a_max	0.09	0.29	0.21	0.46	NDVI8a_max	0.05	0.21	0.10	0.32	NDVI8a_max	0.04	0.20	0.03	0.16	NDVI8a_max	0.06	0.25
NDVI8a_mean	0.14	0.37	0.35	0.59	NDVI8a_mean	0.05	0.23	0.13	0.36	NDVI8a_mean	0.05	0.22	0.08	0.28	NDVI8a_mean	0.09	0.29
NDVI8a_med	0.12	0.35	0.33	0.58	NDVI8a_med	0.05	0.22	0.13	0.36	NDVI8a_med	0.04	0.20	0.09	0.30	NDVI8a_med	0.08	0.28
NDVI8a_min	0.12	0.35	0.26	0.51	NDVI8a_min	0.04	0.21	0.08	0.28	NDVI8a_min	0.05	0.22	0.05	0.22	NDVI8a_min	0.08	0.28
NDVI8a_sd	0.09	-0.29	0.16	-0.40	NDVI8a_sd	0.02	-0.15	0.03	-0.17	NDVI8a_sd	0.03	-0.18	0.04	-0.20	NDVI8a_sd	0.05	-0.23
NDVI8a_var	0.06	-0.25	0.12	-0.35	NDVI8a_var	0.02	-0.16	0.03	-0.18	NDVI8a_var	0.04	-0.19	0.05	-0.22	NDVI8a_var	0.05	-0.21
NDWI_max	0.09	-0.30	0.19	-0.44	NDWI_max	0.02	-0.15	0.05	-0.22	NDWI_max	0.02	-0.16	0.03	-0.18	NDWI_max	0.05	-0.23
NDWI_mean	0.13	-0.36	0.32	-0.57	NDWI_mean	0.04	-0.21	0.11	-0.33	NDWI_mean	0.04	-0.20	0.07	-0.27	NDWI_mean	0.08	-0.27
NDWI_med	0.12	-0.35	0.32	-0.56	NDWI_med	0.04	-0.20	0.11	-0.33	NDWI_med	0.04	-0.19	0.08	-0.28	NDWI_med	0.07	-0.27
NDWI_min	0.06	-0.25	0.17	-0.41	NDWI_min	0.04	-0.19	0.08	-0.29	NDWI_min	0.03	-0.18	0.02	-0.14	NDWI_min	0.04	-0.20
NDWI_sd	0.02	-0.15	0.04	-0.20	NDWI_sd	0.00	-0.03	0.00	-0.03	NDWI_sd	0.00	-0.05	0.01	-0.11	NDWI_sd	0.01	-0.11
NDWI_var	0.03	-0.16	0.04	-0.21	NDWI_var	0.00	-0.06	0.00	-0.06	NDWI_var	0.01	-0.08	0.02	-0.13	NDWI_var	0.02	-0.13
NLVI_max	0.00	0.06	0.01	0.08	NLVI_max	0.01	0.12	0.02	0.12	NLVI_max	0.01	0.09	0.00	-0.04	NLVI_max	0.01	0.07
NLVI_mean	0.11	0.33	0.27	0.52	NLVI_mean	0.07	0.26	0.11	0.33	NLVI_mean	0.06	0.24	0.03	0.17	NLVI_mean	0.08	0.28
NLVI_med	0.16	0.41	0.41	0.64	NLVI_med	0.07	0.27	0.14	0.38	NLVI_med	0.07	0.27	0.07	0.26	NLVI_med	0.11	0.33
NLVI_min	0.11	0.33	0.22	0.47	NLVI_min	0.03	0.17	0.05	0.22	NLVI_min	0.04	0.21	0.03	0.18	NLVI_min	0.06	0.24
NLVI_sd	0.00	0.01	0.00	0.00	NLVI_sd	0.01	0.08	0.01	0.08	NLVI_sd	0.00	0.05	0.01	-0.08	NLVI_sd	0.00	0.03
NLVI_var	0.00	-0.02	0.00	-0.05	NLVI_var	0.00	0.05	0.00	0.03	NLVI_var	0.00	0.02	0.01	-0.09	NLVI_var	0.00	0.00
PSRI_max	0.12	-0.35	0.22	-0.47	PSRI_max	0.03	-0.17	0.05	-0.22	PSRI_max	0.05	-0.22	0.05	-0.22	PSRI_max	0.08	-0.27
PSRI_mean	0.08	-0.29	0.18	-0.42	PSRI_mean	0.04	-0.19	0.08	-0.28	PSRI_mean	0.04	-0.19	0.06	-0.25	PSRI_mean	0.06	-0.25
PSRI_med	0.04	-0.20	0.11	-0.33	PSRI_med	0.02	-0.14	0.06	-0.25	PSRI_med	0.02	-0.13	0.06	-0.24	PSRI_med	0.03	-0.18
PSRI_min	0.09	-0.30	0.14	-0.37	PSRI_min	0.06	-0.24	0.09	-0.29	PSRI_min	0.05	-0.23	0.01	-0.11	PSRI_min	0.08	-0.28
PSRI_sd	0.04	-0.19	0.08	-0.28	PSRI_sd	0.00	-0.04	0.00	-0.06	PSRI_sd	0.01	-0.09	0.03	-0.17	PSRI_sd	0.01	-0.12
PSRI_var	0.04	-0.21	0.09	-0.30	PSRI_var	0.00	-0.07	0.01	-0.10	PSRI_var	0.01	-0.11	0.04	-0.21	PSRI_var	0.02	-0.15
RVI_max	0.00	0.01	0.00	0.05	RVI_max	0.00	0.03	0.01	0.09	RVI_max	0.00	0.01	0.02	0.14	RVI_max	0.00	0.02
RVI_mean	0.01	0.11	0.03	0.17	RVI_mean	0.02	0.12	0.04	0.20	RVI_mean	0.02	0.13	0.05	0.23	RVI_mean	0.01	0.12
RVI_med	0.01	0.07	0.01	0.11	RVI_med	0.01	0.09	0.03	0.16	RVI_med	0.01	0.07	0.05	0.21	RVI_med	0.01	0.07
RVI_min	0.02	0.14	0.04	0.20	RVI_min	0.02	0.14	0.04	0.19	RVI_min	0.02	0.15	0.03	0.18	RVI_min	0.02	0.15
RVI_sd	0.02	-0.14	0.04	-0.20	RVI_sd	0.02	-0.14	0.04	-0.19	RVI_sd	0.02	-0.15	0.04	-0.20	RVI_sd	0.02	-0.15
RVI_var	0.01	-0.11	0.03	-0.16	RVI_var	0.01	-0.12	0.03	-0.16	RVI_var	0.02	-0.14	0.02	-0.15	RVI_var	0.01	-0.12
S2REP_max	0.00	-0.03	0.00	-0.05	S2REP_max	0.00	0.01	0.00	0.00	S2REP_max	0.00	-0.03	0.00	-0.04	S2REP_max	0.00	-0.01
S2REP_mean	0.02	0.15	0.03	0.16	S2REP_mean	0.00	0.00	0.00	-0.01	S2REP_mean	0.00	0.00	0.00	-0.05	S2REP_mean	0.00	0.06
S2REP_med	0.05	0.23	0.07	0.26	S2REP_med	0.00	0.04	0.00	0.02	S2REP_med	0.00	0.07	0.01	-0.07	S2REP_med	0.01	0.12

S2REP_min	0.00	0.06	0.01	0.08	S2REP_min	0.00	-0.03	0.00	-0.04	S2REP_min	0.00	-0.02	0.00	0.04	S2REP_min	0.00	0.01
S2REP_sd	0.00	-0.06	0.01	-0.09	S2REP_sd	0.00	0.03	0.00	0.02	S2REP_sd	0.00	-0.01	0.00	-0.05	S2REP_sd	0.00	-0.01
S2REP_var	0.00	-0.03	0.00	-0.04	S2REP_var	0.00	0.01	0.00	0.01	S2REP_var	0.00	-0.02	0.00	-0.01	S2REP_var	0.00	-0.01
SAVI_max	0.09	0.30	0.21	0.46	SAVI_max	0.04	0.21	0.10	0.32	SAVI_max	0.04	0.19	0.03	0.18	SAVI_max	0.06	0.24
SAVI_mean	0.14	0.37	0.34	0.58	SAVI_mean	0.05	0.22	0.11	0.34	SAVI_mean	0.04	0.21	0.08	0.27	SAVI_mean	0.08	0.29
SAVI_med	0.12	0.35	0.32	0.57	SAVI_med	0.04	0.21	0.12	0.34	SAVI_med	0.04	0.19	0.08	0.29	SAVI_med	0.07	0.27
SAVI_min	0.13	0.36	0.25	0.50	SAVI_min	0.04	0.19	0.07	0.26	SAVI_min	0.04	0.21	0.04	0.21	SAVI_min	0.08	0.28
SAVI_sd	0.09	-0.29	0.14	-0.38	SAVI_sd	0.02	-0.13	0.02	-0.14	SAVI_sd	0.03	-0.17	0.03	-0.16	SAVI_sd	0.05	-0.22
SAVI_var	0.07	-0.27	0.12	-0.34	SAVI_var	0.02	-0.15	0.02	-0.15	SAVI_var	0.03	-0.18	0.03	-0.18	SAVI_var	0.05	-0.22
TCB_max	0.00	-0.08	0.02	-0.18	TCB_max	0.02	-0.04	0.04	-0.09	TCB_max	0.04	-0.06	0.07	-0.25	TCB_max	0.01	-0.06
TCB_mean	0.00	-0.03	0.03	-0.12	TCB_mean	0.03	-0.13	0.08	-0.21	TCB_mean	0.05	-0.20	0.09	-0.26	TCB_mean	0.01	-0.08
TCB_med	0.00	-0.02	0.04	-0.17	TCB_med	0.03	-0.16	0.09	-0.28	TCB_med	0.05	-0.23	0.11	-0.29	TCB_med	0.01	-0.08
TCB_min	0.00	-0.03	0.00	-0.20	TCB_min	0.01	-0.16	0.03	-0.30	TCB_min	0.03	-0.23	0.01	-0.33	TCB_min	0.00	-0.09
TCB_sd	0.00	0.00	0.03	-0.03	TCB_sd	0.00	-0.12	0.00	-0.17	TCB_sd	0.00	-0.17	0.05	-0.09	TCB_sd	0.00	-0.05
TCB_var	0.01	-0.07	0.03	-0.16	TCB_var	0.00	-0.02	0.01	-0.06	TCB_var	0.00	-0.04	0.06	-0.23	TCB_var	0.00	-0.05
TCW_max	0.01	0.10	0.03	0.16	TCW_max	0.01	0.09	0.02	0.15	TCW_max	0.03	0.17	0.01	0.08	TCW_max	0.01	0.08
TCW_mean	0.04	0.21	0.16	0.40	TCW_mean	0.02	0.14	0.07	0.26	TCW_mean	0.05	0.22	0.06	0.24	TCW_mean	0.03	0.16
TCW_med	0.04	0.20	0.17	0.41	TCW_med	0.02	0.13	0.07	0.26	TCW_med	0.04	0.21	0.06	0.25	TCW_med	0.02	0.16
TCW_min	0.07	0.27	0.22	0.47	TCW_min	0.03	0.18	0.07	0.27	TCW_min	0.07	0.26	0.06	0.25	TCW_min	0.05	0.22
TCW_sd	0.05	-0.22	0.17	-0.41	TCW_sd	0.02	-0.14	0.05	-0.22	TCW_sd	0.02	-0.15	0.08	-0.28	TCW_sd	0.03	-0.18
TCW_var	0.06	-0.25	0.20	-0.45	TCW_var	0.02	-0.13	0.04	-0.20	TCW_var	0.02	-0.16	0.06	-0.25	TCW_var	0.04	-0.19
VH146_max	0.00	0.06	0.00	0.05	VH146_max	0.01	0.07	0.00	0.04	VH146_max	0.01	0.08	0.01	0.08	VH146_max	0.00	0.06
VH146_mean	0.00	0.06	0.00	0.04	VH146_mean	0.01	0.08	0.00	0.04	VH146_mean	0.01	0.08	0.01	0.08	VH146_mean	0.01	0.07
VH146_med	0.00	0.07	0.00	0.04	VH146_med	0.01	0.08	0.00	0.04	VH146_med	0.01	0.08	0.01	0.08	VH146_med	0.01	0.07
VH146_min	0.00	0.07	0.00	0.04	VH146_min	0.01	0.08	0.00	0.04	VH146_min	0.01	0.08	0.00	0.07	VH146_min	0.01	0.08
VH146_sd	0.00	0.02	0.00	0.05	VH146_sd	0.00	0.05	0.00	0.02	VH146_sd	0.00	0.04	0.00	0.06	VH146_sd	0.00	0.02
VH146_var	0.00	0.01	0.00	0.02	VH146_var	0.00	0.07	0.00	0.02	VH146_var	0.00	0.04	0.00	0.06	VH146_var	0.00	0.03
VH22_max	0.01	0.11	0.03	0.18	VH22_max	0.01	0.11	0.02	0.14	VH22_max	0.02	0.14	0.01	0.10	VH22_max	0.01	0.10
VH22_mean	0.02	0.12	0.04	0.20	VH22_mean	0.01	0.12	0.03	0.16	VH22_mean	0.02	0.15	0.01	0.12	VH22_mean	0.01	0.11
VH22_med	0.02	0.13	0.04	0.20	VH22_med	0.02	0.12	0.02	0.16	VH22_med	0.02	0.15	0.01	0.11	VH22_med	0.01	0.11
VH22_min	0.02	0.12	0.05	0.21	VH22_min	0.01	0.12	0.03	0.17	VH22_min	0.02	0.15	0.02	0.14	VH22_min	0.01	0.11
VH22_sd	0.00	0.06	0.00	0.07	VH22_sd	0.00	0.06	0.00	0.06	VH22_sd	0.00	0.06	0.00	0.02	VH22_sd	0.00	0.06
VH22_var	0.00	0.05	0.00	0.05	VH22_var	0.00	0.07	0.00	0.05	VH22_var	0.00	0.07	0.00	0.01	VH22_var	0.00	0.06
VH44_max	0.01	0.09	0.02	0.14	VH44_max	0.01	0.08	0.01	0.11	VH44_max	0.01	0.09	0.01	0.11	VH44_max	0.01	0.10
VH44_mean	0.02	0.13	0.03	0.17	VH44_mean	0.01	0.11	0.01	0.12	VH44_mean	0.01	0.12	0.01	0.11	VH44_mean	0.02	0.13
VH44_med	0.02	0.13	0.03	0.18	VH44_med	0.01	0.11	0.01	0.12	VH44_med	0.01	0.12	0.01	0.11	VH44_med	0.02	0.14
VH44_min	0.02	0.13	0.03	0.16	VH44_min	0.01	0.12	0.01	0.12	VH44_min	0.02	0.13	0.01	0.10	VH44_min	0.02	0.14
VH44_sd	0.00	0.02	0.01	0.07	VH44_sd	0.00	0.01	0.00	0.06	VH44_sd	0.00	0.02	0.00	0.07	VH44_sd	0.00	0.02
VH44_var	0.00	0.03	0.00	0.06	VH44_var	0.00	0.03	0.00	0.06	VH44_var	0.00	0.04	0.00	0.06	VH44_var	0.00	0.05
VH95_max	0.00	-0.01	0.00	0.06	VH95_max	0.00	-0.01	0.00	0.03	VH95_max	0.00	-0.01	0.00	0.02	VH95_max	0.00	-0.03
VH95_mean	0.00	0.00	0.01	0.08	VH95_mean	0.00	-0.01	0.00	0.05	VH95_mean	0.00	0.00	0.00	0.04	VH95_mean	0.00	-0.02
VH95_med	0.00	0.00	0.01	0.08	VH95_med	0.00	-0.01	0.00	0.05	VH95_med	0.00	-0.01	0.00	0.05	VH95_med	0.00	-0.02
VH95_min	0.00	0.02	0.01	0.11	VH95_min	0.00	0.01	0.00	0.07	VH95_min	0.00	0.02	0.00	0.05	VH95_min	0.00	0.00

VH95_sd	0.00	-0.06	0.00	-0.04	VH95_sd	0.00	-0.07	0.00	-0.04	VH95_sd	0.00	-0.06	0.00	0.00	VH95_sd	0.01	-0.08
VH95_var	0.01	-0.07	0.00	-0.06	VH95_var	0.00	-0.07	0.00	-0.04	VH95_var	0.00	-0.06	0.00	0.00	VH95_var	0.01	-0.08
VV146_max	0.00	0.01	0.00	0.07	VV146_max	0.00	0.04	0.00	0.06	VV146_max	0.00	0.06	0.02	0.13	VV146_max	0.00	0.01
VV146_mean	0.00	0.02	0.01	0.08	VV146_mean	0.00	0.05	0.01	0.07	VV146_mean	0.00	0.07	0.02	0.14	VV146_mean	0.00	0.02
VV146_med	0.00	0.02	0.01	0.08	VV146_med	0.00	0.05	0.01	0.07	VV146_med	0.00	0.07	0.02	0.14	VV146_med	0.00	0.02
VV146_min	0.00	0.02	0.00	0.07	VV146_min	0.00	0.05	0.01	0.07	VV146_min	0.00	0.07	0.02	0.14	VV146_min	0.00	0.02
VV146_sd	0.00	0.00	0.00	0.06	VV146_sd	0.00	0.01	0.00	0.02	VV146_sd	0.00	0.03	0.01	0.08	VV146_sd	0.00	-0.02
VV146_var	0.00	0.00	0.00	0.03	VV146_var	0.00	0.04	0.00	0.02	VV146_var	0.00	0.04	0.00	0.07	VV146_var	0.00	0.00
VV22_max	0.01	0.10	0.00	0.06	VV22_max	0.01	0.09	0.00	0.04	VV22_max	0.01	0.12	0.00	0.06	VV22_max	0.01	0.09
VV22_mean	0.01	0.12	0.01	0.09	VV22_mean	0.01	0.09	0.00	0.05	VV22_mean	0.02	0.13	0.01	0.07	VV22_mean	0.01	0.09
VV22_med	0.01	0.12	0.01	0.09	VV22_med	0.01	0.09	0.00	0.05	VV22_med	0.02	0.14	0.01	0.07	VV22_med	0.01	0.10
VV22_min	0.01	0.12	0.01	0.10	VV22_min	0.01	0.08	0.00	0.05	VV22_min	0.02	0.13	0.00	0.07	VV22_min	0.01	0.08
VV22_sd	0.00	0.05	0.00	-0.01	VV22_sd	0.00	0.06	0.00	0.02	VV22_sd	0.00	0.06	0.00	0.03	VV22_sd	0.00	0.06
VV22_var	0.00	0.05	0.00	-0.01	VV22_var	0.00	0.07	0.00	0.02	VV22_var	0.00	0.06	0.00	0.02	VV22_var	0.00	0.06
VV44_max	0.00	0.05	0.03	0.16	VV44_max	0.00	0.05	0.01	0.12	VV44_max	0.01	0.07	0.02	0.15	VV44_max	0.00	0.04
VV44_mean	0.01	0.08	0.03	0.19	VV44_mean	0.01	0.07	0.02	0.14	VV44_mean	0.01	0.10	0.03	0.17	VV44_mean	0.01	0.07
VV44_med	0.01	0.09	0.04	0.19	VV44_med	0.01	0.08	0.02	0.15	VV44_med	0.01	0.10	0.03	0.16	VV44_med	0.01	0.08
VV44_min	0.01	0.10	0.04	0.20	VV44_min	0.01	0.08	0.02	0.15	VV44_min	0.01	0.11	0.03	0.16	VV44_min	0.01	0.09
VV44_sd	0.00	-0.03	0.00	0.06	VV44_sd	0.00	-0.01	0.00	0.05	VV44_sd	0.00	0.00	0.01	0.09	VV44_sd	0.00	-0.04
VV44_var	0.00	-0.03	0.00	0.02	VV44_var	0.00	0.00	0.00	0.04	VV44_var	0.00	0.02	0.01	0.07	VV44_var	0.00	-0.03
VV95_max	0.00	-0.04	0.00	-0.07	VV95_max	0.00	-0.05	0.01	-0.08	VV95_max	0.00	-0.06	0.00	-0.02	VV95_max	0.00	-0.05
VV95_mean	0.00	-0.01	0.00	-0.03	VV95_mean	0.00	-0.02	0.00	-0.05	VV95_mean	0.00	-0.02	0.00	0.01	VV95_mean	0.00	-0.02
VV95_med	0.00	-0.01	0.00	-0.02	VV95_med	0.00	-0.02	0.00	-0.04	VV95_med	0.00	-0.02	0.00	0.02	VV95_med	0.00	-0.02
VV95_min	0.00	0.00	0.00	-0.01	VV95_min	0.00	-0.01	0.00	-0.04	VV95_min	0.00	0.00	0.00	0.03	VV95_min	0.00	-0.01
VV95_sd	0.01	-0.10	0.02	-0.14	VV95_sd	0.01	-0.10	0.01	-0.11	VV95_sd	0.01	-0.11	0.00	-0.05	VV95_sd	0.01	-0.10
VV95_var	0.01	-0.10	0.02	-0.14	VV95_var	0.01	-0.09	0.01	-0.10	VV95_var	0.01	-0.10	0.00	-0.05	VV95_var	0.01	-0.09
GLCM_VH146_con	0.00	0.04	0.00	-0.01	GLCM_VH146_con	0.01	0.11	0.00	0.05	GLCM_VH146_con	0.00	0.05	0.00	0.05	GLCM_VH146_con	0.01	0.10
GLCM_VH146_cor	0.00	0.05	0.00	0.01	GLCM_VH146_cor	0.00	0.01	0.00	0.00	GLCM_VH146_cor	0.00	0.01	0.00	-0.03	GLCM_VH146_cor	0.00	0.02
GLCM_VH146_dis	0.00	0.02	0.00	-0.06	GLCM_VH146_dis	0.02	0.14	0.01	0.08	GLCM_VH146_dis	0.01	0.09	0.01	0.07	GLCM_VH146_dis	0.01	0.11
GLCM_VH146_eng	0.00	0.04	0.00	0.06	GLCM_VH146_eng	0.00	-0.07	0.01	-0.08	GLCM_VH146_eng	0.00	-0.04	0.00	-0.06	GLCM_VH146_eng	0.00	-0.03
GLCM_VH146_ent	0.00	-0.03	0.00	-0.06	GLCM_VH146_ent	0.01	0.07	0.01	0.09	GLCM_VH146_ent	0.00	0.05	0.00	0.06	GLCM_VH146_ent	0.00	0.03
GLCM_VH146_homo	0.00	0.00	0.00	0.02	GLCM_VH146_homo	0.02	-0.13	0.01	-0.12	GLCM_VH146_homo	0.01	-0.09	0.01	-0.11	GLCM_VH146_homo	0.01	-0.08
GLCM_VH146_mean	0.01	0.09	0.00	0.06	GLCM_VH146_mean	0.01	0.10	0.00	0.05	GLCM_VH146_mean	0.01	0.10	0.01	0.09	GLCM_VH146_mean	0.01	0.11
GLCM_VH146_sd	0.00	0.03	0.00	-0.06	GLCM_VH146_sd	0.03	0.16	0.01	0.09	GLCM_VH146_sd	0.01	0.10	0.00	0.07	GLCM_VH146_sd	0.02	0.12
GLCM_VH146_sec	0.00	0.04	0.00	0.06	GLCM_VH146_sec	0.00	-0.06	0.01	-0.08	GLCM_VH146_sec	0.00	-0.04	0.00	-0.05	GLCM_VH146_sec	0.00	-0.02
GLCM_VH22_con	0.00	-0.01	0.00	-0.03	GLCM_VH22_con	0.01	0.08	0.01	0.10	GLCM_VH22_con	0.00	0.06	0.00	0.05	GLCM_VH22_con	0.00	0.03
GLCM_VH22_cor	0.00	0.03	0.00	0.01	GLCM_VH22_cor	0.00	-0.05	0.00	-0.06	GLCM_VH22_cor	0.00	-0.06	0.00	-0.04	GLCM_VH22_cor	0.00	0.00
GLCM_VH22_dis	0.00	-0.01	0.00	-0.03	GLCM_VH22_dis	0.02	0.12	0.02	0.15	GLCM_VH22_dis	0.01	0.10	0.01	0.08	GLCM_VH22_dis	0.00	0.05
GLCM_VH22_eng	0.00	-0.04	0.00	-0.06	GLCM_VH22_eng	0.02	-0.15	0.04	-0.20	GLCM_VH22_eng	0.01	-0.11	0.02	-0.15	GLCM_VH22_eng	0.01	-0.09
GLCM_VH22_ent	0.00	0.04	0.00	0.05	GLCM_VH22_ent	0.02	0.16	0.04	0.20	GLCM_VH22_ent	0.01	0.12	0.02	0.15	GLCM_VH22_ent	0.01	0.09
GLCM_VH22_homo	0.00	-0.02	0.00	-0.01	GLCM_VH22_homo	0.02	-0.15	0.03	-0.18	GLCM_VH22_homo	0.02	-0.13	0.01	-0.09	GLCM_VH22_homo	0.01	-0.09
GLCM_VH22_mean	0.02	0.13	0.05	0.23	GLCM_VH22_mean	0.02	0.13	0.03	0.18	GLCM_VH22_mean	0.02	0.14	0.02	0.13	GLCM_VH22_mean	0.01	0.11
GLCM_VH22_sd	0.00	0.00	0.00	-0.03	GLCM_VH22_sd	0.02	0.13	0.03	0.16	GLCM_VH22_sd	0.01	0.10	0.01	0.07	GLCM_VH22_sd	0.00	0.06

GLCM_VH22_sec	0.00	-0.05	0.00	-0.06	GLCM_VH22_sec	0.02	-0.15	0.04	-0.19	GLCM_VH22_sec	0.01	-0.11	0.02	-0.15	GLCM_VH22_sec	0.01	-0.09
GLCM_VH44_con	0.00	0.03	0.00	-0.05	GLCM_VH44_con	0.01	0.10	0.00	0.04	GLCM_VH44_con	0.01	0.07	0.00	0.04	GLCM_VH44_con	0.02	0.13
GLCM_VH44_cor	0.01	0.07	0.00	0.05	GLCM_VH44_cor	0.00	0.04	0.00	0.03	GLCM_VH44_cor	0.00	0.04	0.00	-0.02	GLCM_VH44_cor	0.00	0.05
GLCM_VH44_dis	0.00	0.03	0.01	-0.08	GLCM_VH44_dis	0.02	0.14	0.00	0.06	GLCM_VH44_dis	0.01	0.10	0.00	0.06	GLCM_VH44_dis	0.02	0.14
GLCM_VH44_eng	0.00	-0.02	0.00	0.02	GLCM_VH44_eng	0.03	-0.17	0.02	-0.15	GLCM_VH44_eng	0.01	-0.11	0.02	-0.13	GLCM_VH44_eng	0.01	-0.12
GLCM_VH44_ent	0.00	0.02	0.00	-0.02	GLCM_VH44_ent	0.03	0.18	0.02	0.16	GLCM_VH44_ent	0.01	0.12	0.02	0.13	GLCM_VH44_ent	0.02	0.12
GLCM_VH44_homo	0.00	-0.03	0.00	0.05	GLCM_VH44_homo	0.02	-0.15	0.01	-0.09	GLCM_VH44_homo	0.01	-0.09	0.01	-0.07	GLCM_VH44_homo	0.01	-0.11
GLCM_VH44_mean	0.03	0.16	0.04	0.19	GLCM_VH44_mean	0.02	0.14	0.02	0.15	GLCM_VH44_mean	0.02	0.15	0.02	0.13	GLCM_VH44_mean	0.03	0.17
GLCM_VH44_sd	0.00	0.05	0.01	-0.08	GLCM_VH44_sd	0.03	0.17	0.01	0.08	GLCM_VH44_sd	0.01	0.12	0.00	0.06	GLCM_VH44_sd	0.02	0.16
GLCM_VH44_sec	0.00	-0.02	0.00	0.02	GLCM_VH44_sec	0.03	-0.17	0.02	-0.15	GLCM_VH44_sec	0.01	-0.11	0.02	-0.13	GLCM_VH44_sec	0.01	-0.11
GLCM_VH95_con	0.00	-0.04	0.00	-0.07	GLCM_VH95_con	0.00	0.03	0.00	0.01	GLCM_VH95_con	0.00	0.01	0.00	-0.04	GLCM_VH95_con	0.00	-0.01
GLCM_VH95_cor	0.00	0.02	0.00	-0.02	GLCM_VH95_cor	0.00	-0.01	0.00	-0.05	GLCM_VH95_cor	0.00	-0.03	0.00	-0.03	GLCM_VH95_cor	0.00	0.01
GLCM_VH95_dis	0.00	-0.06	0.01	-0.09	GLCM_VH95_dis	0.00	0.03	0.00	0.02	GLCM_VH95_dis	0.00	0.01	0.00	-0.02	GLCM_VH95_dis	0.00	-0.03
GLCM_VH95_eng	0.00	0.00	0.00	-0.02	GLCM_VH95_eng	0.01	-0.10	0.02	-0.12	GLCM_VH95_eng	0.00	-0.04	0.01	-0.08	GLCM_VH95_eng	0.00	-0.04
GLCM_VH95_ent	0.00	0.00	0.00	0.02	GLCM_VH95_ent	0.01	0.10	0.01	0.12	GLCM_VH95_ent	0.00	0.04	0.01	0.08	GLCM_VH95_ent	0.00	0.04
GLCM_VH95_homo	0.00	0.02	0.00	0.02	GLCM_VH95_homo	0.01	-0.07	0.01	-0.11	GLCM_VH95_homo	0.00	-0.03	0.00	-0.04	GLCM_VH95_homo	0.00	-0.02
GLCM_VH95_mean	0.00	-0.02	0.01	0.10	GLCM_VH95_mean	0.00	-0.01	0.00	0.07	GLCM_VH95_mean	0.00	0.00	0.00	0.06	GLCM_VH95_mean	0.00	-0.03
GLCM_VH95_sd	0.00	-0.05	0.01	-0.09	GLCM_VH95_sd	0.00	0.05	0.00	0.03	GLCM_VH95_sd	0.00	0.02	0.00	-0.02	GLCM_VH95_sd	0.00	-0.01
GLCM_VH95_sec	0.00	0.00	0.00	-0.02	GLCM_VH95_sec	0.01	-0.10	0.02	-0.12	GLCM_VH95_sec	0.00	-0.04	0.01	-0.08	GLCM_VH95_sec	0.00	-0.04
GLCM_VV146_con	0.00	0.03	0.00	-0.02	GLCM_VV146_con	0.01	0.09	0.00	0.04	GLCM_VV146_con	0.00	0.04	0.00	0.05	GLCM_VV146_con	0.01	0.08
GLCM_VV146_cor	0.00	0.06	0.00	0.04	GLCM_VV146_cor	0.00	0.03	0.00	0.01	GLCM_VV146_cor	0.01	0.08	0.00	-0.01	GLCM_VV146_cor	0.00	0.03
GLCM_VV146_dis	0.00	0.01	0.01	-0.08	GLCM_VV146_dis	0.01	0.12	0.00	0.05	GLCM_VV146_dis	0.00	0.06	0.00	0.06	GLCM_VV146_dis	0.01	0.09
GLCM_VV146_eng	0.00	-0.02	0.00	0.07	GLCM_VV146_eng	0.02	-0.16	0.01	-0.10	GLCM_VV146_eng	0.02	-0.13	0.01	-0.10	GLCM_VV146_eng	0.01	-0.10
GLCM_VV146_ent	0.00	0.02	0.01	-0.07	GLCM_VV146_ent	0.02	0.16	0.01	0.10	GLCM_VV146_ent	0.02	0.13	0.01	0.09	GLCM_VV146_ent	0.01	0.11
GLCM_VV146_homo	0.00	0.02	0.01	0.09	GLCM_VV146_homo	0.01	-0.10	0.00	-0.06	GLCM_VV146_homo	0.00	-0.05	0.00	-0.06	GLCM_VV146_homo	0.00	-0.07
GLCM_VV146_mean	0.00	0.06	0.01	0.11	GLCM_VV146_mean	0.01	0.09	0.01	0.11	GLCM_VV146_mean	0.01	0.11	0.03	0.16	GLCM_VV146_mean	0.00	0.06
GLCM_VV146_sd	0.00	0.03	0.01	-0.07	GLCM_VV146_sd	0.02	0.15	0.00	0.06	GLCM_VV146_sd	0.01	0.09	0.00	0.06	GLCM_VV146_sd	0.01	0.11
GLCM_VV146_sec	0.00	-0.01	0.00	0.06	GLCM_VV146_sec	0.02	-0.15	0.01	-0.11	GLCM_VV146_sec	0.02	-0.13	0.01	-0.11	GLCM_VV146_sec	0.01	-0.10
GLCM_VV22_con	0.00	-0.02	0.00	-0.07	GLCM_VV22_con	0.00	0.06	0.00	0.05	GLCM_VV22_con	0.00	0.04	0.00	0.02	GLCM_VV22_con	0.00	0.01
GLCM_VV22_cor	0.00	0.03	0.00	-0.02	GLCM_VV22_cor	0.00	-0.04	0.01	-0.07	GLCM_VV22_cor	0.00	-0.06	0.00	-0.06	GLCM_VV22_cor	0.00	0.01
GLCM_VV22_dis	0.00	-0.03	0.01	-0.07	GLCM_VV22_dis	0.01	0.09	0.01	0.10	GLCM_VV22_dis	0.00	0.06	0.00	0.04	GLCM_VV22_dis	0.00	0.02
GLCM_VV22_eng	0.00	-0.03	0.00	0.01	GLCM_VV22_eng	0.02	-0.13	0.03	-0.17	GLCM_VV22_eng	0.01	-0.08	0.01	-0.08	GLCM_VV22_eng	0.01	-0.09
GLCM_VV22_ent	0.00	0.03	0.00	-0.01	GLCM_VV22_ent	0.02	0.13	0.03	0.17	GLCM_VV22_ent	0.01	0.08	0.01	0.08	GLCM_VV22_ent	0.01	0.09
GLCM_VV22_homo	0.00	0.00	0.00	0.02	GLCM_VV22_homo	0.02	-0.14	0.03	-0.18	GLCM_VV22_homo	0.01	-0.11	0.01	-0.11	GLCM_VV22_homo	0.00	-0.07
GLCM_VV22_mean	0.02	0.13	0.01	0.12	GLCM_VV22_mean	0.01	0.11	0.01	0.08	GLCM_VV22_mean	0.02	0.15	0.01	0.10	GLCM_VV22_mean	0.01	0.11
GLCM_VV22_sd	0.00	-0.03	0.01	-0.08	GLCM_VV22_sd	0.01	0.09	0.01	0.10	GLCM_VV22_sd	0.00	0.06	0.00	0.04	GLCM_VV22_sd	0.00	0.02
GLCM_VV22_sec	0.00	-0.02	0.00	0.00	GLCM_VV22_sec	0.02	-0.13	0.03	-0.17	GLCM_VV22_sec	0.01	-0.07	0.01	-0.09	GLCM_VV22_sec	0.01	-0.09
GLCM_VV44_con	0.00	0.01	0.01	-0.09	GLCM_VV44_con	0.00	0.07	0.00	0.01	GLCM_VV44_con	0.00	0.05	0.00	0.04	GLCM_VV44_con	0.01	0.09
GLCM_VV44_cor	0.01	0.08	0.00	0.04	GLCM_VV44_cor	0.00	0.02	0.00	0.01	GLCM_VV44_cor	0.00	0.03	0.00	-0.02	GLCM_VV44_cor	0.00	0.04
GLCM_VV44_dis	0.00	-0.01	0.01	-0.12	GLCM_VV44_dis	0.01	0.10	0.00	0.04	GLCM_VV44_dis	0.01	0.07	0.00	0.06	GLCM_VV44_dis	0.01	0.09
GLCM_VV44_eng	0.00	-0.01	0.01	0.08	GLCM_VV44_eng	0.03	-0.17	0.02	-0.12	GLCM_VV44_eng	0.02	-0.14	0.02	-0.13	GLCM_VV44_eng	0.01	-0.11
GLCM_VV44_ent	0.00	0.01	0.01	-0.09	GLCM_VV44_ent	0.03	0.17	0.01	0.12	GLCM_VV44_ent	0.02	0.14	0.01	0.12	GLCM_VV44_ent	0.01	0.11
GLCM_VV44_homo	0.00	0.02	0.01	0.09	GLCM_VV44_homo	0.02	-0.14	0.01	-0.09	GLCM_VV44_homo	0.01	-0.09	0.01	-0.09	GLCM_VV44_homo	0.01	-0.08

LV

GLCM_VV44_mean	0.01	0.11	0.04	0.20	GLCM_VV44_mean	0.01	0.10	0.03	0.17	GLCM_VV44_mean	0.02	0.13	0.03	0.18	GLCM_VV44_mean	0.01	0.10
GLCM_VV44_sd	0.00	0.00	0.01	-0.12	GLCM_VV44_sd	0.02	0.12	0.00	0.05	GLCM_VV44_sd	0.01	0.09	0.00	0.06	GLCM_VV44_sd	0.01	0.11
GLCM_VV44_sec	0.00	-0.01	0.01	0.07	GLCM_VV44_sec	0.03	-0.17	0.02	-0.13	GLCM_VV44_sec	0.02	-0.14	0.02	-0.13	GLCM_VV44_sec	0.01	-0.10
GLCM_VV95_con	0.00	-0.04	0.00	-0.07	GLCM_VV95_con	0.00	0.02	0.00	0.01	GLCM_VV95_con	0.00	0.00	0.00	-0.02	GLCM_VV95_con	0.00	-0.02
GLCM_VV95_cor	0.00	0.03	0.00	-0.02	GLCM_VV95_cor	0.00	-0.02	0.00	-0.04	GLCM_VV95_cor	0.00	-0.04	0.00	-0.02	GLCM_VV95_cor	0.00	0.01
GLCM_VV95_dis	0.00	-0.04	0.00	-0.07	GLCM_VV95_dis	0.00	0.02	0.00	0.01	GLCM_VV95_dis	0.00	0.00	0.00	-0.02	GLCM_VV95_dis	0.00	-0.02
GLCM_VV95_eng	0.00	0.02	0.00	0.02	GLCM_VV95_eng	0.01	-0.09	0.01	-0.10	GLCM_VV95_eng	0.00	-0.02	0.01	-0.08	GLCM_VV95_eng	0.00	-0.04
GLCM_VV95_ent	0.00	-0.02	0.00	-0.02	GLCM_VV95_ent	0.01	0.09	0.01	0.11	GLCM_VV95_ent	0.00	0.02	0.01	0.09	GLCM_VV95_ent	0.00	0.04
GLCM_VV95_homo	0.00	0.06	0.00	0.05	GLCM_VV95_homo	0.01	-0.08	0.01	-0.08	GLCM_VV95_homo	0.00	-0.05	0.00	-0.05	GLCM_VV95_homo	0.00	-0.01
GLCM_VV95_mean	0.00	-0.03	0.00	-0.02	GLCM_VV95_mean	0.00	-0.02	0.00	-0.04	GLCM_VV95_mean	0.00	-0.01	0.00	0.03	GLCM_VV95_mean	0.00	-0.04
GLCM_VV95_sd	0.00	-0.07	0.01	-0.11	GLCM_VV95_sd	0.00	0.04	0.00	0.01	GLCM_VV95_sd	0.00	0.01	0.00	-0.01	GLCM_VV95_sd	0.00	-0.02
GLCM_VV95_sec	0.00	0.02	0.00	0.02	GLCM_VV95_sec	0.01	-0.08	0.01	-0.10	GLCM_VV95_sec	0.00	-0.02	0.01	-0.08	GLCM_VV95_sec	0.00	-0.04

C. Regression

i. Mean Vegetation Height – Cross-validation with GEDI Data

Table 35: Calculating the R², RMSE and MAE values between all ten regressions based on the RH50 GEDI data and the selected GEDI validation plots.

Validation of RH50 regression with GEDI RH50 data															
Regression	Validation data	All bands			4 Orbits			Top 10			PC			NC		
		R^2	RMSE (m)	MAE (m)	R^2	RMSE (m)	MAE (m)	R^2	RMSE (m)	MAE (m)	R^2	RMSE (m)	MAE (m)	R^2	RMSE (m)	MAE (m)
RH50 1	GEDI plots val1	0.28	6.37	5.13	0.28	6.37	5.24	0.24	6.57	5.21	0.22	6.62	5.26	0.26	5.20	5.20
RH50 2	GEDI plots val2	0.32	6.63	5.30	0.30	6.67	5.39	0.26	6.94	5.52	0.25	6.96	5.54	0.29	5.49	5.49
RH50 3	GEDI plots val3	0.28	6.60	5.53	0.29	6.62	5.71	0.24	6.83	5.84	0.24	6.84	5.84	0.24	5.76	5.76
RH50 4	GEDI plots val4	0.36	6.37	5.11	0.35	6.46	5.18	0.36	6.53	5.20	0.36	6.53	5.20	0.36	5.21	5.21
RH50 5	GEDI plots val5	0.30	6.45	5.28	0.32	6.37	5.06	0.25	6.65	5.22	0.25	6.67	5.24	0.29	5.21	5.21
RH50 6	GEDI plots val6	0.41	6.04	4.67	0.32	6.35	4.95	0.27	6.53	5.20	0.28	6.47	5.14	0.24	5.20	5.20
RH50 7	GEDI plots val7	0.36	6.02	4.76	0.32	6.13	4.87	0.28	6.32	5.06	0.27	6.35	5.07	0.29	4.96	4.96
RH50 8	GEDI plots val8	0.26	6.51	4.99	0.27	6.50	4.93	0.26	6.51	4.94	0.26	6.53	4.95	0.26	4.99	4.99
RH50 9	GEDI plots val9	0.24	6.36	4.83	0.24	6.35	4.85	0.20	6.51	4.89	0.19	6.54	4.91	0.22	4.76	4.76
RH50 10	GEDI plots val10	0.29	6.30	4.95	0.26	6.42	4.94	0.29	6.33	4.89	0.28	6.36	4.89	0.29	4.94	4.94
All regressions	mean	0.31	6.36	5.05	0.30	6.42	5.11	0.26	6.57	5.20	0.26	6.59	5.20	0.27	5.17	5.17

ii. Max Vegetation Height – Cross-validation with GEDI Data

Table 36: Calculating the R², RMSE and MAE values between all ten regressions based on the RH100 GEDI data and the selected GEDI validation plots.

Validation of RH100 regression with GEDI RH100 data															
Regression	Validation data	All bands			4 Orbits			Top 10			PC			NC		
		R^2	RMSE (m)	MAE (m)	R^2	RMSE (m)	MAE (m)	R^2	RMSE (m)	MAE (m)	R^2	RMSE (m)	MAE (m)	R^2	RMSE (m)	MAE (m)
RH100 1	GEDI plots val1	0.19	7.75	5.92	0.17	7.84	6.03	0.10	8.14	6.42	0.07	8.32	6.27	0.12	8.07	6.67
RH100 2	GEDI plots val2	0.11	8.30	6.90	0.13	8.22	6.49	0.04	8.64	7.06	0.09	8.35	7.00	0.06	8.52	6.74
RH100 3	GEDI plots val3	0.28	7.51	6.09	0.26	7.65	6.16	0.17	8.02	6.31	0.12	8.26	6.31	0.18	7.99	6.54
RH100 4	GEDI plots val4	0.11	8.36	6.31	0.10	8.41	6.44	0.06	8.60	6.82	0.08	8.47	6.78	0.06	8.54	6.76
RH100 5	GEDI plots val5	0.40	6.90	5.75	0.37	7.06	5.91	0.28	7.50	6.25	0.23	7.66	6.20	0.29	7.71	6.23
RH100 6	GEDI plots val6	0.26	7.82	6.33	0.19	8.14	6.61	0.15	8.33	6.80	0.08	8.40	6.85	0.16	8.33	6.87
RH100 7	GEDI plots val7	0.34	7.37	5.79	0.31	7.60	6.03	0.23	7.90	6.22	0.20	8.07	6.50	0.19	8.21	6.42
RH100 8	GEDI plots val8	0.24	7.62	6.09	0.23	7.72	6.26	0.26	7.75	6.24	0.13	8.19	6.52	0.17	8.09	6.62
RH100 9	GEDI plots val9	0.25	7.40	6.09	0.22	7.54	6.10	0.22	7.63	6.23	0.08	8.23	6.47	0.13	7.99	6.61
RH100 10	GEDI plots val10	0.52	6.31	5.34	0.31	7.30	6.19	0.26	7.47	6.33	0.15	7.91	6.61	0.17	7.98	6.68
All regressions	mean	0.27	7.51	6.06	0.23	7.75	6.22	0.18	7.98	6.47	0.12	8.17	6.55	0.15	8.15	6.61

iii. Foliage Height Diversity

Table 37: Calculating the R², RMSE and MAE values between all ten regressions based on the FHD GEDI data and the selected GEDI validation plots.

Validation of FHD regression with GEDI FHD data															
Regression	Validation data	All bands			4 Orbits			Top 10			PC			NC		
		R^2	RMSE	MAE	R^2	RMSE	MAE	R^2	RMSE	MAE	R^2	RMSE	MAE	R^2	RMSE	MAE
RH100 1	GEDI plots val1	0.29	0.25	0.19	0.29	0.25	0.19	0.21	0.27	0.19	0.16	0.27	0.20	0.18	0.27	0.20
RH100 2	GEDI plots val2	0.26	0.26	0.19	0.21	0.26	0.19	0.17	0.27	0.20	0.16	0.27	0.20	0.16	0.27	0.20
RH100 3	GEDI plots val3	0.06	0.45	0.39	0.07	0.44	0.39	0.05	0.44	0.38	0.10	0.44	0.39	0.05	0.44	0.38
RH100 4	GEDI plots val4	0.05	0.45	0.38	0.04	0.45	0.38	0.01	0.48	0.41	0.02	0.44	0.38	0.00	0.49	0.42
RH100 5	GEDI plots val5	0.08	0.45	0.38	0.10	0.45	0.39	0.16	0.43	0.37	0.02	0.47	0.42	0.13	0.43	0.37
RH100 6	GEDI plots val6	0.04	0.45	0.38	0.05	0.44	0.38	0.00	0.45	0.39	0.00	0.45	0.40	0.00	0.45	0.40
RH100 7	GEDI plots val7	0.06	0.48	0.43	0.05	0.46	0.41	0.02	0.46	0.41	0.01	0.45	0.40	0.02	0.45	0.40
RH100 8	GEDI plots val8	0.15	0.43	0.38	0.11	0.44	0.39	0.11	0.44	0.39	0.05	0.44	0.39	0.08	0.45	0.40
RH100 9	GEDI plots val9	0.42	0.22	0.17	0.40	0.22	0.18	0.39	0.22	0.18	0.24	0.24	0.20	0.37	0.22	0.19
RH100 10	GEDI plots val10	0.31	0.21	0.17	0.32	0.21	0.17	0.34	0.21	0.17	0.27	0.22	0.17	0.33	0.22	0.17
All regressions	mean	0.17	0.36	0.31	0.16	0.36	0.31	0.14	0.37	0.31	0.10	0.37	0.32	0.13	0.37	0.31

iv. Aboveground Biomass Density

Table 38: Calculating the R², RMSE and MAE values between all ten regressions based on the AGBD GEDI data and the selected GEDI validation plots.

Validation of AGBD regression with GEDI AGBD data															
Regression	Validation data	All bands			4 Orbits			Top 10			PC			NC		
		R^2	RMSE (Mg/ha)	MAE (Mg/ha)	R^2	RMSE (Mg/ha)	MAE (Mg/ha)	R^2	RMSE (Mg/ha)	MAE (Mg/ha)	R^2	RMSE (Mg/ha)	MAE (Mg/ha)	R^2	RMSE (Mg/ha)	MAE (Mg/ha)
RH100 1	GEDI plots val1	0.20	89.26	70.11	0.17	90.76	72.51	0.06	97.06	75.79	-	-	-	0.12	93.23	74.15
RH100 2	GEDI plots val2	0.29	86.94	67.87	0.38	84.15	65.70	0.23	91.09	72.46	-	-	-	0.33	86.63	67.22
RH100 3	GEDI plots val3	0.38	82.73	64.07	0.26	89.16	70.48	0.16	94.61	76.50	-	-	-	0.23	91.21	72.93
RH100 4	GEDI plots val4	0.29	85.93	66.59	0.25	88.24	65.93	0.15	93.67	72.05	-	-	-	0.24	89.00	67.04
RH100 5	GEDI plots val5	0.32	87.89	66.61	0.21	93.50	68.70	0.11	98.53	71.99	-	-	-	0.25	92.35	67.65
RH100 6	GEDI plots val6	0.31	91.99	68.28	0.24	96.42	72.29	0.18	99.87	74.23	-	-	-	0.27	96.82	71.37
RH100 7	GEDI plots val7	0.15	93.16	72.86	0.16	92.66	73.09	0.11	94.80	74.09	-	-	-	0.13	94.41	74.74
RH100 8	GEDI plots val8	0.31	87.16	70.12	0.30	88.34	70.12	0.18	94.80	76.12	-	-	-	0.20	93.53	74.82
RH100 9	GEDI plots val9	0.23	91.66	69.36	0.28	88.97	67.39	0.25	91.38	69.73	-	-	-	0.27	90.50	67.80
RH100 10	GEDI plots val10	0.23	84.40	69.18	0.17	88.02	71.32	0.13	89.85	72.95	-	-	-	0.19	87.09	69.10
All regressions	mean	0.27	88.11	68.51	0.24	90.02	69.75	0.16	94.57	73.59	-	-	-	0.22	91.48	70.68

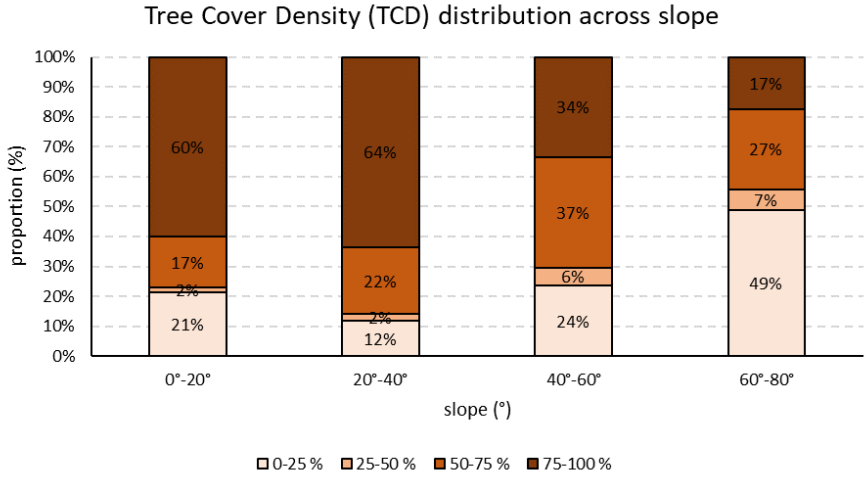

Figure 49: Tree Cover Density (%) distribution across different slope inclinations in percent.

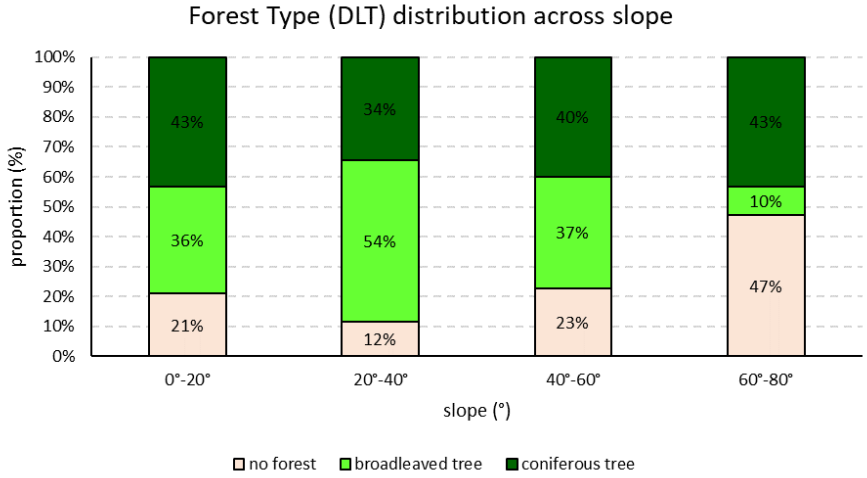

Figure 50: Dominant Leafe Type (DLT) distribution across different slope inclinations in percent.